ATMOSPHERIC PHYSICS

A STUDY OF F-REGION TRAVELLING IONOSPHERIC DISTURBANCES

A thesis
submitted in partial fulfilment
of the requirements for the Degree
of
Doctor of Philosophy in Physics
in the
University of Canterbury

by
Justin Cooper

University of Canterbury
1980

PHYSICAL
SCIENCES
LIBRARY
THESIS
copy 2

ABSTRACT

A Fast-Fourier-Transform method has been used to calculate a series of one-dimensional ground diffraction patterns which arise from point-source illumination of a moving sinusoidal reflector. Correlation analysis was performed on the set of ground patterns to investigate the relationship between the derived pattern drift velocity and random velocity, and the velocity of the moving reflector.

Application of the correlation analysis of Briggs, Phillips and Shinn (1950) to the complex temporal correlations of the ground patterns between spaced receivers gave a true velocity value which agreed with that of the reflector. The derived random velocity was negligible, as desired for a correct description of unchanging reflector shape.

The true velocity obtained from the spatial amplitude correlations using the spatial correlation method of Briggs (1968a) was found to agree closely with the ground velocity of the single specular reflection point on the sinusoidal surface. An undesirable feature was a high value of estimated random velocity. The amplitude temporal correlations and complex spatial correlations gave no useful information.

Synoptic ionograms taken at 15-minute intervals at Christchurch, New Zealand, indicated the presence of a medium-scale travelling ionospheric disturbance on 19th February, 1978. The phase velocity $v_{\phi h}$ = 117 (±10) m. sec^{-1}, horizontal wavelength λ_h = 560 (±90) km, and period T = 80-90 minutes.

Phase-path data for an altitude of 200 km on the same

day show a series of harmonics of a 90-minute fundamental in their maximum entropy power spectra. The harmonics of the phase range arose from movement of a specular reflecting point on a quasi-sinusoidal surface. The existence of several wave cycles of similar frequency in the data and the presence of moderately high magnetic activity allows the auroral electrojet as a possible source for the disturbance observed. No Doppler shifting of gravity-wave frequency arising from the presence of neutral winds was observed.

ACKNOWLEDGMENTS

Many people have contributed ideas and assistance to this author. It is a pleasure to thank the following people in particular.

Professor A.G. McLellan for providing the opportunity and facilities to do the work.

Dr. G.J. Fraser, this author's supervisor, for suggesting the project and for his advice, assistance, and interest throughout.

Mr. R.S. Unwin, Officer-in-charge of the Geophysical Observatory, Physics and Engineering Laboratory, D.S.I.R., for the access to ISIS, ionogram, and Atmospheric-Explorer Satellite data, and for the interest he has taken in the project.

Dr. C.H. Cummack of the Geophysical Observatory for his continuing interest in the work, and for many valuable discussions and freely-given advice.

Dr. R.T.G. Bennett for his assistance and advice, and for his help as assistant supervisor while Dr. Fraser was on leave; and Dr. H.A. von Biel for many clarifying discussions and assistance.

Mr. J. de Voil for the long hours he has given to maintenance of the 4.57 MHz transmitter.

Mrs. M. Boswell and Mrs. M. Sewell for typing the thesis with great care and skill. It is a great pleasure to thank Mrs. Boswell in particular for the care and time she gave to the typing when little time was available to do it.

Mr. L.C. Hunter for the many graphs and diagrams he photographed for this thesis. It is a particular pleasure to thank him for the care, time and effort he gave to their preparation at a time when he had many photographic commitments.

Mr. M.P. Lynn, who built the phase receivers and track-and-hold system at Birdlings Flat. Without the receivers, the phase height results could not have been obtained.

My employer, Wormald Vigilant Ltd., who kindly gave this author four months leave of absence to allow completion of the thesis.

Ms Phillipa Maclean and Mrs. J.A. van der Borch for their lettering of graphs and diagrams, and Mr. M. Gill of the Geophysical Observatory for the ionogram photographs.

INTRODUCTION

This investigation is a study of the short-period atmospheric oscillations observed in the ionospheric F-region known as Travelling Ionospheric Disturbances.

Two distinct nomenclatures are used to describe the earth's upper atmosphere: the first being a description of the ledges and layers of ionization present and the second describing the atmosphere in terms of its temperature structure.

The presence of ionization in the atmosphere begins at 50-60 km altitude, corresponding to the base of the D-ledge, and continues as a significant constituent of the atmosphere until the plasmapause is reached at altitude 20,000 km. The ionization concentration is not uniform in altitude, but instead has a ledged or layered structure. The identifiable regions are the *D-region* from 60-90 km; the *E-layer* from 90-140 km with electron content maximum at 100-110 km; and the *F-region* above 140 km. In the daytime the F-region is divided into an F1-ledge, and an F2-layer whose altitude of maximum ionization can range from 200-275 km. The whole region of ionized atmosphere is termed the *ionosphere*.

The nomenclature in terms of atmospheric temperature defines the troposphere as the region from the ground to the temperature minimum at 20 km. At altitudes above 20 km or so the atmosphere temperature rises again, defining the stratosphere region of the atmosphere. A temperature maximum at 55 km defines the stratopause, or top of the stratosphere. The mesosphere, from 55 to 80 km, defines a region of falling atmospheric temperature.

Above the top of the mesosphere at 80 km - the

mesopause - lies the thermosphere, within which there is initially a very sharp increase of temperature with altitude which falls off to a steady value at about 200 km or so. The thermosphere is a region of the neutral atmosphere in the same altitude range as the ionospheric F-region, and the terms are often used interchangably in the literature.

Changes in the upper atmosphere and ionosphere occur over a great range of time-scales: from the eleven-year scale of sunspot-dependent phenomena, through yearly, seasonal, and diurnal changes, down to the three-minute period acoustic waves at times observed to be present. The study in this thesis is of the travelling wavelike perturbations observed in the F-region known as Travelling Ionospheric Disturbances. They are explained in terms of internal gravity waves propagating in the upper atmosphere and consist of one or more wave cycles with periods ranging from ten minutes to several hours.

Until the recent advent of direct satellite sampling of F-region constituents, airglow measurements and remote-sensing radio experiments were the only ways to investigate the movements and changes in the middle and upper F-regions. The presence of electrons in the ionosphere causes reflection of pulsed or CW radio waves back to the ground, allowing measurement of electron movements and density changes.

Ionosondes measure the virtual height of radio reflection as a function of radio frequency. Both gross ionospheric changes and smaller-scale perturbations can be observed on the resulting records. The phase-path experiment employs coherent detection to measure phase-changes between the transmitted and reflected radio waves. This is a very

sensitive experiment, for if ionospheric conditions allow a coherent reflection to be obtained path changes of fraction of a radio wavelength can be measured.

The experimental work of this thesis compares the results obtained by measurement of a travelling ionospheric disturbance by ionosonde and phase-path methods. Thus in Chapter 1 a brief survey is made of Travelling Disturbance observations using different techniques, after which an account is given of the explanation of the disturbances in terms of internal gravity waves. Chapter 5 is a presentation and analysis of the experimental results obtained by the present author for this work. Numerical models presented in the literature by other workers are used to account for the measured ionospheric response and wave propagation characteristics, and to present a conjecture about sources of the waves.

Four appendices support the experimental work of Chapter 5. Appendix A describes antenna design and construction for operation at 4.57 MHz. Information on coherent detection and data acquisition methods is given in Appendix B. The spectral analysis methods used in Chapter 5 are assessed in Appendix C, and in Appendix E an account is given of echolocation determination as a method of finding the direction of the travelling disturbance.

The second main line of work in this thesis is a numerical simulation of the spaced-receiver drifts experiment. The most common form of this radio technique involves the measurement of ionospheric reflections at three receivers arranged in a triangle at 100-200 metre spacing.

The concept of the technique is that the movement of a drifting, randomly-changing set of ionospheric electron-density irregularities is being measured. The data reduction technique supplies a true velocity parameter which estimates the overall drift of the irregularities, and a random velocity which indicates the extent of random changes in the ionosphere.

Comparison with other methods of measuring wind velocity indicate that the drift experiment gives satisfactory neutral atmosphere velocity estimates in the D- and E-regions. This does not hold for the F-region, where the interpretation of results is primarily in terms of electrodynamic drifts.

Incoherent-scatter observations and ionogram true-height reductions of the F2 region below the F2 peak show that the isoelectronic contours are quasi-sinusoidal in shape. This makes the random, drifting irregularity model less relevant to the F-region situation, especially as the altitude of the turbopause is below that of the F-region.

This gives the motivation to simulate drifts results that might be expected from a sinusoidal specular reflector. To this end Chapter 2 presents a survey of experimental results and data analysis techniques and attempts to assess the relevance of random-scatter and smooth-reflector models to the results obtained.

Chapter 3 is about the description of ionospheric reflection using a smooth, sine-wave shaped reflector. The existence of a Fourier Transform relationship between the radio electromagnetic field at the reflector and the resulting angular spectrum allows the calculation of the ground diffraction pattern, and this is done numerically by the

Fast Fourier Transform technique. The application of the technique is presented and agreement obtained with the results expected when parallel light is incident on the reflector. Appendix D presents some details of result interpretation.

Then in Chapter 4 the point-source illumination of the reflector is simulated and correlation calculations performed on the resulting ground diffraction patterns. A series of patterns over a one-dimensional ground is obtained as the reflector is moved in time, allowing calculation of both spatial and temporal correlations. Two different methods of data reduction are compared, and the relative merits of their ability to obtain the reflector velocity assessed.

The disappointing aspects of the Fourier Transform method were its considerable memory requirements and high computer expense. For these reasons only a small subset of likely situations could be simulated. The reflector height, wavelength, and amplitude were set to allow the presence of one specular point. Initially the reflector concavity was directly over the transmitter, after which the reflector is moved to a maximum extent of 4% of its wavelength. This is a quite realistic simulation of a single drifts velocity determination, but the expense of the method did not allow calculations to be made for other parts of the reflector wavelength or for other reflector parameters.

Experimental data obtained by other workers indicates that in many cases the specular reflector model is a realistic description, but not exclusively so. Recent

satellite observations have shown that electron-density irregularities of a very wide range of spatial scales exist in the F-region, so the specular reflection concept cannot apply at all times.

CONTENTS

CHAPTER 1

TRAVELLING DISTURBANCES IN THE IONOSPHERIC F-REGION

I. INTRCDUCTION

In this chapter the observational and theoretical work on Travelling Ionospheric Disturbances is briefly noted. Many workers have presented results for the observational or for the theoretical sides of the problem, which are available in the literature. On the observational side, the early pioneering experiments by which travelling disturbances were first noticed as short period changes on the ambient or diurnally changing F-region are noted. Some recent experimental techniques with promise of permitting extensive checks with theory are pointed out.

The isothermal atmosphere model of Hines (1960) is extensively used by many workers to check the parameters of measurements. It allows a clear physical picture of the travelling disturbance phenomenon. More extensive measurements have required the development of more complicated numerical models to allow a closer simulation of the F-region, and such models have been able to give solutions which agree with two current observational classifications of travelling disturbances.

Much work remains to be done on this problem, although perhaps the lines of attack seem fairly clear-cut at this time. Some phase-height observational results are presented in Chapter 5 of this thesis and an attempt is made to check

them with model predictions.

II. OBSERVATIONAL ASPECTS OF TRAVELLING DISTURBANCES.

Travelling disturbances in the ionosphere (or T.I.D's) have been observed for many years. Munro (1950,1953) observed disturbances in the daytime F1 and F2 regions using swept-frequency (h′ f) records and fixed-frequency (h′ t) records. Comparatively large disturbances would perturb an ambient h′ f ionogram record over a time of 30 to 90 minutes. The effects would appear on the trace firstly as a characteristic fall in the critical frequency foF_2 followed by kinks or thickenings in the record trace which would travel down the trace from foF_2 to foE in time. Later work by the Australian group on ionogram traces showed that anomalous cusps present upon or above the ambient record could arise as a result of travelling disturbance activity, (Munro and Heisler, 1956b; Heisler, 1958).

Disturbances large enough to show such effects on ionograms allowed calculation of true height and the change of ionization density with time at fixed true heights. An oscillatory change in ionization density was found: the oscillation at greater heights leading that at smaller heights in time (Munro, 1950). This character of vertical phase change with height is one characteristic of internal waves in a fluid (Hines, 1960) in which terms a theoretical explanation of travelling disturbances was given.

The sizes of travelling disturbances also vary. Munro (1953) used h′(t) records at a single fixed frequency and was able to explain characteristic "X", "Y", or "Z" shaped kinks in the virtual height curve as arising from concavity effects in the reflecting layer. These could occur when the corresponding ionogram showed little activity. Concurrent phase-path experiments (Munro, 1950, 1953) revealed the presence of even smaller quasi-periodic disturbances.

An early general survey on travelling disturbance characteristics was given by Munro (1958). His observations, recorded near Sydney, Australia, on a single radio frequency and for primarily the F2 region, gave speeds of order 100 - 150 $m.sec^{-1}$ with only small seasonal changes between summer and winter. Direction was found to change quite sharply with season from a range centered on 40° East of North in (Southern Hemisphere) winter and to one centered on 120° East of North in summer. He also found diurnal variations: direction tended to become more northerly during the day.

Disturbances have since been observed by many workers using different techniques: one direct comparison of some of the methods was done by Essex (1968). The phase-path method is used for small disturbances in this thesis: the corresponding ionogram records were in the main found to be very calm although some moving kinks could be seen. A powerful method of observing travelling disturbances is the incoherent scatter technique (for example, Thome, 1964). The use of very high frequencies (430 MHz in this example) allows observation of electron density contours above and

below the F-region peak, and there is little magnetoionic deviation. At lower heights, below the F2-region peak, disturbances of period between 20 minutes and several hours may be present. A comparative survey of observational methods is presented in Vasseur et al. (1972).

In recent years direct measurements of electron temperature and ion and neutral composition have been made with experiments on the Atmospheric Explorer C satellite. Reber et al. (1975) observe wavelike structure in electron temperature and in various ionic and neutral species; for example in molecular Nitrogen, Argon, Helium, and in ion density. Nevertheless, Reber et al. (1975) did not positively identify the structures as propagating gravity waves in their paper; they felt that confirmation of that possibility required more data.

III. THEORETICAL ASPECTS OF TRAVELLING DISTURBANCES.

The application of internal gravity waves in a model of atmospheric wavelike motion was started by Hines (1960). The model there taken was of an atmosphere stationary in the absence of waves, and uniform in both temperature and composition. Wave oscillation amplitudes were taken small enough to allow neglect of their second- or higher-order terms in the governing equations - this allows linearization of the governing equations. Wave motion was assumed to occur adiabatically. The only forces included in the equations of motion were those of pressure gradients, gravity and

inertia, and the gravitational field was taken to be constant in both magnitude and direction.

For this model the governing equations are the linearized equations of motion, adiabatic state, and continuous mass conservation. These are Equations (6) and (8) of Hines (1960). Wave solutions to this set of equations arise as

$$\frac{(p-p_0)}{p_0 P} = \frac{\rho-\rho_0}{\rho_0 R} = \frac{U_z}{X} = \frac{U_z}{Z} = A \exp i(\omega t - K_x x - K_z z) .$$

This is Equation (13) of Hines (1960): it relates the relative amplitude variations in pressure and density and the horizontal (U_x) and vertical (U_z) perturbation velocities. The constants P, R, X and Z are complex, and give the amplitude and phase relation of $\frac{p-p_0}{p}$, $\frac{\rho-\rho_0}{\rho}$, and U_z and U_x respectively to that of the wave itself. They are functions of the horizontal and vertical wavenumbers K_x and K_z and of angular frequency ω: themselves related by the dispersion equation given in Equation 14 of Hines (1960).

Hines' analysis leads, for cases where horizontal dissipation is neglected, (thus $K_x = k_x$, real) to two alternative types of waves: surface waves, in which the vertical wavenumber is pure imaginary and which are appropriate to a two-fluid stratified atmosphere with a horizontal boundary present; and internal waves, for which the vertical wavenumber is complex thus allowing a phase change in height.

This property of the internal wave spectrum makes it a possible candidate to explain travelling disturbance oscillations. In fact, such an interpretation is now well accepted. Further analysis (Hines, 1960) shows that the internal wave spectrum itself has two regimes allowing propagation - the so-called acoustic waves with propagation allowed for angular frequencies

$$\omega > \omega_a = \frac{\gamma g}{2C}$$

which have phase speeds greater than the speed of sound C, and the gravity mode for which allowed propagation is for frequencies

$$\omega < \omega_b = \frac{(\gamma-1)^{\frac{1}{2}} g}{C}$$

which have phase speeds less than that of sound, for the atmospheric model considered here. (Hines, 1960).

A dispersion diagram appropriate to an isothermal atmosphere with E-region parameters is given in Hines (1960) Fig.10: a similar one for an F-region isothermal atmosphere at 200 km is given in Yeh and Liu (1974), Fig. 4.

Some results to be presented in Chapter 5 show that in many cases the dominant frequency by eye is very close to - or is at - the Brunt frequency ω_b itself. For such periods, Fig. 4 of Yeh and Liu (1974) shows that energy propagation is upward in a direction only some 20° from the vertical, and phase propagation is downward, some 20° from the horizontal. Energy and phase propagation directions are close

to being at right angles here - the construction of Hines (1960) has been used to obtain these results: the quadrant used is the reflection in the k_x axis of that shown by these authors because energy is travelling upwards. The refractive index dispersion diagram, Fig. 10 of Hines (1960) also shows that for such waves, the horizontal wavelength decreases rather sharply as speed decreases.

Numerical modelling of propagating gravity waves has in recent years been able to obtain quite realistic predictions for the neutral atmosphere variations, in terms of temperature structure and chemical composition. In addition, radio measurements are measurement of electron movement - the competing influences of electron-neutral collisions and of the tendency of charged particles to move down magnetic field lines implies that measurement of the electron motion is not related in a simple way to that of the neutral gas. Such situations have been calculated, among others, by Hooke (1968), and isoionic contours have been determined for model T.I.D.'s with parameters close to those of experiment. This work was extended by Hooke (1970a, 1970b) to apply to the F1 and F2 regions separately. Ionospheric responses have been calculated for various input simulated gravity waves as a function of magnetic inclination and azimuthal direction of propagation. The calculated responses change quite sharply with changes in these parameters, and also considerably between the F1 and F2 regions. Such differences between the F1 and F2 regions arise because

of the need to consider the effects of photochemical processes on the wave dynamics in the F1 region, since ion lifetimes are of the order of a wave period. (Hooke 1970a, 1970b).

Other extensive modelling has been done by Francis (1973a, 1973b, 1974). He has found that the observational classification of travelling disturbances into a "Very Large" category and a "Medium-Scale" category (Georges, 1968) can be explained theoretically. The "Very Large" disturbances are characterized by high phase speeds of 300-800 $m.sec^{-1}$ periods of 30 min - 3 hr, and horizontal wavelengths λ_z of order 1000 km and are associated with magnetic storms (Georges, 1968; Francis, 1975). Francis (1973a) finds gravity wave modes are partially ducted at the level of the temperature incline at the base of the thermosphere (Whitten and Poppoff, 1971, p.311). Such modes are almost surface gravity modes with no vertical phase propagation, but are not completely so because the temperature between 100 and 200 km is steadily rising. A model of a stratified two-fluid system, with a sharp boundary representing a step increase in temperature at one specific height between the lower atmosphere and the thermosphere, does not completely describe the system. The continually increasing temperature gradient gives rise to imperfect ducting and attenuation of the wave; and to vertical changes of phase in the thermosphere as a function of height.

The travelling disturbances observed for this thesis (Chapter 5) seem, from the calm corresponding ionograms, to instead fall into the "Medium-Scale" category, (Georges, 1968). These are characterized by phase speeds of 100-250 $m.sec^{-1}$, periods of 15 min (or the Brunt frequency) to 1 hr or so, and horizontal wavelengths λ_x of several hundred km, (for example, Francis, 1974; Francis, 1975). These also can propagate at long distances from the source (for example, Heisler, 1958) which lead to a belief that they were ducted modes. Francis' (1974) calculations have shown that for the speed range of medium-scale T.I.D.'s, no such strong ducting mechanisms were available. He has instead explained the medium-scale T.I.D.'s in terms of unducted or freely propagating gravity waves: these in turn fall into two families - (1) waves which propagate obliquely upward from the (neutral, lower-atmosphere) source and reach the F-region directly and - (2) waves which propagate from the source to the earth, and thence reach the F-region after the earth reflection (Francis, 1974). The former family of waves has been calculated to appear as a single isolated fluctuation; whereas the latter appear as almost monochromatic wave packets (Francis, 1974). An observational distinction between such periodic and non-periodic disturbances has been made by Titheridge (1968, 1971).

Many of the results given in Chapter 5 for daytime F-region show oscillatory behaviour for several cycles. They would seem to fall into the earth-reflected category of waves.

IV. CONCLUSION

The theory of internal gravity waves is by now well accepted in its ability to explain the Travelling Ionospheric Disturbance phenomenon. The primary need at present appears to be experiments which can measure as many significant parameters as possible - always a difficult task with any remote-sensing experiment - to check for agreement or disagreement with the theory. The various experiments available all measure different quantities. An appreciation of the observational biases of each experiment, with respect to the types, heights, and scales of T.I.D.'s that it will measure, is essential for useful comparison between experiments if agreement between experiment and theory is to be put on a firm basis.

CHAPTER 2

SOME IMPLICATIONS OF PHASE-SCREEN MODELS

I. INTRODUCTION

The models of ionospheric reflection fall into two main classes: in the first of which the reflector is made up of many small-scale random scatterers whose motion, as seen by a spaced-receiver drift experiment, is interpreted as an advective drift of the reflector as a whole combined with random changes within the reflector. The second reflector model is one of a smooth isoelectronic contour, normally taken to be in an otherwise stationary atmosphere, whose movement is that of an atmospheric wave travelling through it. Reflection in this latter case arises from a few distinct specular points (and the Fresnel zones around them) and the effects seen are those of mutual interference between such reflection zones.

The real ionosphere is described by these models to a greater or lesser extent. In this chapter previous experimental work is reviewed and for some occasions the specular model is seen to apply. Methods of treating the data to assist discrimination between the models are noted. Nevertheless, problems remain, in that even for cases where the specular model seems to apply, the velocities that are measured by a radio drifts experiment tend for the E region to be those of the neutral wind, rather than the phase speed of any wave present. A possible resolution of this problem is noted and implications for F-region drifts are discussed.

In Chapters 3 and 4 of this thesis an attempt has been

made to construct a numerical model of a phase screen. Some of the experimental results and methods of treating data suggest points to check in the numerical model.

The use of such models may assist in the interpretation of F-region drift observations. The meaning of these, especially in the presence of a travelling ionospheric disturbance, is still an open question.

II. PREVIOUS WORK ON SPECULAR REFLECTION MODELS

(1) Phase-path and angle-of-arrival techniques

Early work on the focussing of radio waves from a mirror-like ionosphere was done by Whitehead (1956). Using the ordinary-wave echo at 4.2 MHz. from the F-region he observed short-lived increased in the mean amplitude of the echo. Typically these would last for some two minutes or so. By considering a concave mirror-like ionosphere above a transmitter-receiver location he found that

$$A^2 = 1 - \frac{h}{2V^2} \frac{d^2P}{dt^2}$$

where in his notation A is echo amplitude, P is phase path, h is layer height, and V is the horizontal velocity of the reflecting surface. From his data, on one occasion, a plot of A^2 against $\frac{d^2P}{dt^2}$ gave V = 110 $m.sec^{-1}$, but the points about his straight line show scatter, which implies that the model is not perfect.

Landmark (1957) found similar coincidence between concavities in phase path and increases in amplitude for his 2.4 MHz. measurements in the E-region. He found velocities mainly in the 50-90 $m.sec^{-1}$ range, and irregularity extents of

10-40 km. He showed also that the maxima in phase path were most likely to occur through a focussing of the electron density contours, rather than by a reduction of electron density in an absorbing region below the reflector.

Whitehead and Landmark both noted that in the absence of focussing the mean amplitude of the echo would be reasonably constant for an hour or so, with fading of the signal (with typical durations of a few seconds) about the mean value. Landmark found that in some cases of focussing, fading about the (increased) mean value became more rapid. Viewing the focussing process as a phase-modulating screen, diffraction theory predicts (Ratcliffe, 1956) amplitude irregularities for deep screens of horizontal extent $\ell = L/\Delta\phi$. Here, $\Delta\phi$ is the maximum phase deviation and L is the scale of the screen. If the rapid fading arises from this cause then for a reflector moving at constant velocity the small-scale and large-scale durations t and T should be related similarly. For cases of smooth, coherent phase-path change Landmark found that plots of $\Delta\phi/T$ versus $1/t$ gave points reasonably close to the line $\Delta\phi/T = 1/t$, and had this line as a reasonable average. The phase-screen model appeared to give a good explanation for the decrease in time scale of amplitude fading for the phase-path case of one coherent echo.

Landmark also observed conditions of irregular or incoherent phase-path changes, and found a considerable increase in amplitude fading speed associated with such cases. Phase incoherence was found to occur when the ratio of maximum phase-path change ΔP to horizontal irregularity extent D increased beyond a certain value, specifically $\frac{\Delta P}{D} > 0.025$. By

considering the amplitude and phase of the incoherent echo for some five minutes of data, Landmark suggested that the phase incoherence arose from the interference of two specular reflecting points on a concave ionospheric reflector.

Landmark's finding that the rapid fading seemed to move with the larger-scale focussing, for the deep-screen yet phase-coherent case, implies that under these circumstances the drifts experiment would measure the phase speed of any atmospheric wave causing the focussing. An early test of this was done by Jones et al. (1957) who compared the results of (1) close-spaced (one wavelength) antenna measurements, (2) simultaneous observations of changes of amplitude and phase path on one receiver, (3) measurement of group height as a function of time, at one receiver for three transmitters spaced at 200 wavelengths apart, (4) measurement of amplitude as a function of time, for the configuration in (3). Recordings were made on 2.05 MHz for E-region with methods (1) and (2) and on 4.1 MHz for F-region with all four methods. The 200-wavelength spacing for F-region is about 15 km - in the light of later work on F-region waves this is quite a small "large-scale" distance.

Comparison of methods (1) and (2) for the E-layer in the main gave good agreement in velocity magnitudes, which were of order 40-80 $m.sec^{-1}$. The amplitude/phase-path-change method cannot measure direction. The close-spaced antenna results were analysed by the Mitra (1949) method which does not take into account changes in the amplitude pattern as it moves. For these cases the velocity derived from the close-spaced method was high compared to that deduced from the amplitude-and-phase-path method. Comparison of method (4) with method (1) for

F-region gave good agreement for directions deduced, but agreement in velocity magnitudes (of order 50-150 $m.sec^{-1}$) for the individual points was not so close, in contrast to the E-region case. Nevertheless, agreement in magnitude between the two methods generally occurred with agreement in direction between the two methods, and disagreements in magnitude and in direction also occurred together. Closer agreement in volocity magnitude was obtained by Whitehead (1956) in his F-region comparison of Mitra closed-spaced antenna results and amplitude/phase-path velocities. Some changes did occur in the F-region pattern over the 15 km. spacing.

MacDougall (1972), Meeklah et al.(1972), and Brownlie et al. (1973a) have used the ray optics model to relate phase-path changes and angles of arrival, and tested their results with experimental data. MacDougall, using a frequency of 6.3 MHz obtained F2-region phase path and angles of arrival. At times of coherent phase the short-period angles of arrival give the angular position of the reflecting point. For some events, the amplitude increase/phase-path maximum as noted by Whitehead (1956) and Landmark (1957) were obtained: and the angle components moved together along the direction of the wave normal, in the direction opposite to that of the moving ripple - as expected for a slow specular point as in Hines' (1975, unpublished) model. Yet for other events the specular reflection point did not move along a line as the ripple model would predict, but would move erratically within a $4^{o} \times 4^{o}$ square about the slowly-changing mean position. Sometimes it appeared that more than one atmospheric wave were involved, possibly travelling in different directions:

sometimes no clear relation between phase path and angle-of-arrival could be found, even though the phase seemed coherent.

Meeklah et al. (1972) have done a comparison of amplitude drift results, phase-path results, and angle of arrival results, for total reflection from the E-region with a frequency of 2.2 MHz. Their receiving array configuration consisted of three antennas at the corners of an equilateral triangle of side 2λ in length. By measurement of amplitude and phase - similar to the amplitude and phase measurements at Birdling's Flat field station - at the three aerials the three sets of results above were obtained.

The angle of arrival, as for MacDougall's (1972) data, is meaningful only in the presence of one specular point. Otherwise the phases received by the aerials, which arise from the mutual interference of reflections from specular points, will give, of course, one apparent specular point only. The data presented by Meeklah et al. (1972) - all for the phase-coherent case - show rapid movement of the reflecting point in azimuth and zenith. Nevertheless, the rapid fluctuations of azimuth and zenith seemed associated with smoothly varying phase height. There was always a rapid change in azimuth and zenith when the phase path passed through a maximum or a minimum.

If the changes in azimuth and zenith angle arise from specular-point interference, the interference must be such that the phase change at any one aerial is small, otherwise coherent phase could not be obtained. Reddi and Rao (1967, 1968) have observed that often, for E-region echoes, phase

discontinuities in an otherwise coherent trace occur at the same time as amplitude minima in the signal. This is a simple consequence of wave interference (Landmark, 1957).

For one specular reflector, the value of azimuth angle at times of phase path minimum allows the direction of motion to be found (Meeklah et al. (1972)). A reasonably close agreement was found between velocity magnitudes and directions between full correlation, similar fades, and phase height/angle-of-arrival methods on total-reflection E-region data. This was under conditions when experiments could be run: correlation-fades experiments were run some 15 minutes after phase-path experiments, so the times are somewhat different.

Using a multielement fan-pattern transmitting array, a similar reception array at right-angles to the first, and antenna phasing techniques, Brownlie et al. (1973a) effectively had a steerable pencil beam available. This was scanned over $\pm 20^{\circ}$ from vertical in the N-S and E-W directions, at angular increments of 1.28°, by sending one pulse in each beam direction successively, at a P.R.F. of 100 Hz. If the echo for that direction exceeded a certain threshold, an oscilloscope trace was brightened for that position. In this way individual specular points could be distinguished at one time, unlike MacDougall's system which could cope with only one.

Their initial measurements for the system, for sporadic-E and spread-F echoes at 3.84 MHz., often indicate that the ionosphere acts as a distorted mirror with up to five distinct reflection points. They do not state how often these have been found to lie on or close to a straight line, but the data they present in their figure 5 indicates that a two-dimensional

focussing model would be necessary. They state that there is small-scale reflector roughness causing fading of each echo.

Brownlie et al.(1973a) have also modelled expected results relating angle-of-arrival, phase path, and wave velocity for a corrugated reflector. They show that for phase range R and off-vertical angle θ for any one echo, then for a fixed-form corrugated structure with height a function of $t - \frac{x}{u}$,

$$U = \frac{1}{\sin\theta} \frac{dR}{dt}$$

with U the velocity of the structure. If a plot of $(\sin\theta)$ versus $\frac{dR}{dt}$ is made for a given specular point then U can be derived: if the plot is non-linear then dispersion is present in that the corrugated reflector changes form as it moves. They model this with three simulated waves of different velocities, peak amplitudes, and wavelengths added together to form a reflector, and obtain dispersion effects explicitly. Similar effects are seen in the data they present, showing that for some occasions at least, a specular-point model must take the dispersive effects of more than one wave into account.

Brownlie et al. (1973a) propose a form of dispersion analysis which differs from that of Briggs (1968b). The conventional dispersion analysis takes the cross-power spectra between antenna pairs for the returns from three spaced receivers. For a frequency value of significant cross-spectral amplitude, the value of the cross-spectrum phase at the frequency is used to find the time difference for that antenna pair at that frequency. Dispersive motion appears as a change in time difference for an antenna pair as a function in frequency. The set of time differences between pairs is

used to obtain an overall diffraction pattern velocity and direction as functions of frequency.

The basis of this method is that the pattern on the ground is to be considered as a number of sine waves moving with possibly different velocities (Down and Maude, 1968). Guha and Geller (1973) have used the dispersion analysis on their simulated drifts records obtained from their sine-wave reflecting model, and have had some success in resolving the velocities of individual waves when more than one wave is present in the model. Nevertheless, as Briggs (1972) points out, the interpretation of the spectrum of a fading signal arising from the resultant of one or more reflecting points themselves moving on a corrugated reflector is not obvious. As he states:

> "The interpretation rests heavily on the assumption that a given spatial Fourier component in the ground pattern is produced by a wave of equal wavelength in the ionosphere. However, when interference between discrete downcoming waves occurs, this is not the case..."

As an alternative approach, Brownlie et al. (1973a) suggest a Fourier analysis performed on $\frac{dR}{dt}$ and on θ, for a given specular point. Their analysis indicates that this should obtain the motion of the given specular point for each component wave in the screen travelling alone, and thus resolve the different velocities in the screen.

The velocity of the diffraction pattern as a whole for a corrugated but dispersive structure is given in Eq. 33 of Brownlie et al. (1973a). It is the velocity of the amplitude maximum arising from all the specular points together. More

than one specular point is required for a sensible answer: in the absence of dispersion the diffraction pattern velocity is twice that of the reflector. In the presence of dispersion, this is not so. Brownlie et al. (1973a) have modelled a specular reflector with three moving waves each having a different velocity, amplitude and wavelength to the other two. They obtain altering values of diffraction pattern velocity with time, and have found that the largest-wavelength perturbation capable of giving multiple specular reflection points predominates in the determination of mean velocity.

The phase height experiment, and the later beam-swinging techniques, seem to show directly that on at least some occasions, a specular reflector model for H.F. ionospheric echoes is more appropriate than an advective drift model. Moreover, the specular reflector often consists of more than one atmospheric wave, which are independent of each other.

In the following section, some evidence for a specular reflection interference model with its effects on correlation measurements is reviewed.

(2) Correlation techniques

From the previous section, it is clear that H.F. phase measurements on the E- and F-regions of the ionosphere indicate the validity of a specular reflector model at least part of the time. In addition, the work of Brownlie et al. (1973a) shows that in the absence of dispersion, the velocity of the diffraction pattern on the ground is twice that of the reflector. If dispersion is present - there is more than one wave in the reflector, and each has its own amplitude, velocity, and

wavelength - the diffraction pattern velocity will alter rapidly in time.

Felgate and Golley (1971) were able to use the Buckland Park aerial array (Briggs et al. 1969) to obtain amplitude correlation patterns for E-region, night-time F region, and for a very small proportion of D-region observations. The details of this array are described in the literature (for example, Felgate and Golley (1971)) - essentially it allows the ionospheric diffraction pattern to be sampled at 89 points in a square matrix of 91 metres, over a circular area of diameter 1 km. For the work described here the data was displayed on a matrix of filament lamps with the same configuration as the receiving aerials, at a pulse repetition frequency of 50 Hz. The area of the array allowed the recording and observing of some spatial characteristics of the pattern, and the change of the spatial characteristics with time.

Felgate and Golley (1971) divided their observed patterns into six basic types. Their detailed classification will not be repeated here, but for some of their patterns they obtained repeated amplitude maxima, or "fringes", with fringe spacing varying from 400 metres to a distance exceeding the array size. These fringes would move across the array (and hence across the matrix of lamps) with typical velocities of 50-100 $m.sec^{-1}$.

Such fringes certainly suggest the presence of interference maxima between specular reflecting points. For their E-region results Felgate and Golley (1971) obtain a specular point spacing of typically 15 km., and for night-time F-region the

spacing is typically 47 km.

Nevertheless the phase-screen model is not always applicable. For some E-region results random type patterns, incorporating an overall drift and random changes within the pattern, were obtained. This is the type of pattern that the original drifts experiment of Briggs et al (1950) assumed to be present. Felgate and Golley (1971) also note E region patterns which either include some fringes with the random pattern, or have a considerable degree of random change combined with the steady drift. These could possibly include some dispersive phase screens, as the pattern velocities from such cases can appear random.

Felgate and Golley (1971) found the proportion of random patterns to fringe patterns to be very much smaller (over their observing period) for night-time F region, compared to day-time E region. By contrast, the absence of any fringes from the D-region patterns taken indicates that a random-screen model of small, scattering irregularities is more appropriate than the isoionic-contour, specular reflector models applicable at least part of the time in the E- and F- regions.

The extended spatial area of the array also allowed Felgate and Golley (1971) to apply the spatial correlation analysis of Briggs (1968a). In this method, the two-dimensional spatial cross-correlation function $\rho(\xi,\eta,\tau_0)$ between two spatial sets of amplitude results taken at a time interval of τ_0 will, because the pattern is moving, have a maximum at spatial vector displacement $\underline{r}$ from the origin. Briggs (1968a) has shown that the vector velocity $\underline{V}$ of the pattern is:

$$\underline{V} = \frac{\underline{r}}{\tau_0}$$

Felgate and Golley (1971) were able to obtain a spatial pattern velocity every second, but because of scatter in these results used 10-second averages. These were compared with the velocity obtained from the three-receiver drifts method (Briggs et al 1950) over a five-minute record. Thus the latter method assumes that the pattern parameters are statistically stationary during the record time. For some cases the spatial correlation analysis showed that the pattern velocity (magnitude and direction) remained reasonably constant over the three-receiver drifts run, and for such cases the velocities given by the two methods agreed. In other cases there were changes in velocity magnitude and/or direction over the three-receiver run. Then the methods would not agree. As outlined earlier, a dispersive wave system with interfering rays reflected by a specular reflector could cause such velocity changes.

The presence of fringes was found to make the spatial autocorrelation function very elongated in the direction parallel to the fringes, at least for the sporadic-E sample shown by Felgate and Golley (1971). This might be expected for F-region also.

An important assumption of the spaced-receiver drifts experiment is that the spatial and time autocorrelation functions have the same shape (Briggs 1950) (Golley and Rossiter 1970). Spaced-antenna experiments have been conducted by several workers to examine the spatial correlation between spaced aerials, and its dependence upon position and spacing. Brown and Chapman (1972) used eight aerials at various positions along a straight line, with a maximum spacing of 570 metres - about four wavelengths for the frequency they used, which was about 2 MHz.

Measurements were made on E-region.

Brown and Chapman's (1972) aerial configuration allowed determination of the instantaneous spatial correlation (i.e. at a fixed time) along the line of their aerials. In general the spatial correlation value decreases as aerial separation increases. This decrease was found, however, to be comparatively smooth or quite scattered, with respect to aerial spacing. Moreover, for a given aerial spacing, the correlation value was found to depend somewhat on the specific aerial pair taken - that is, on the position of the aerial pair within the diffraction pattern. A high scatter of correlation values for a given aerial spacing implies that the 3-minute record used to obtain the correlation was not statistically stationary. Hines and Rao (1968) have modelled changes in time-shifts between aerials with changes in position of a set of close-spaced antennas and their results are discussed shortly.

Brown and Chapman (1972) confirm the conclusion of Golley and Rossiter (1970) that the estimate of the dimension of the characteristic ellipse improves as the ratio aerial spacing: pattern size is increased. The characteristic ellipse is that introduced by Phillips and Spencer (1955) to take account of ground pattern anisometry. The original full correlation analysis of Briggs et al (1950) assumed an isotropic ground pattern. Golley and Rossiter (1970) find that the optimum aerial spacing is the pattern size. However, Golley and Rossiter (1970) explicitly state, and the regular, quasi-gaussian, non-oscillatory time autocorrelation functions of Brown and Chapman (1972) seem to imply, that conditions where periodic interference patterns were present were avoided in

their studies. In these cases the differing time shifts with antenna-pair position may be due to random changes within the diffraction pattern, and the multi-wave specular reflector model of Hines and Rao (1968) may not apply.

The F-region results of Kelleher (1966b) and of MacDougall (1966) contrast those of Brown and Chapman (1972) and of Golley and Rossiter (1970). For the F-region oscillatory correlations - the "bands" of Felgate and Golley (1971) - were often present.

Kelleher (1966b) has done amplitude measurements on F-region and sporadic-E at 4.85 MHz. He had seven receiving antennas, three of which were at the conventional drifts analysis spacing of 1-2 radio wavelengths at the vertices of an isosceles triangle, and others at greater spacings along the isosceles sides produced: the maximum spacing between a pair being 9 wavelengths. His results often gave oscillatory spatial correlations, but oscillations occurred less often in his time autocorrelations - in contrast to the preliminary results of this thesis for which the time autocorrelation was often oscillatory. In addition the apparent velocities

$$v' = \frac{\xi}{\tau'}$$

(with ξ the aerial separation and τ' the time shift of maximum cross-correlation between the aerials) for receivers along a line often differed. The ratio of ξ to τ' was thus often found to be dependent on aerial separation. Such effects may arise from different velocities and structure sizes in the ionospheric reflector, or possibly from interference effects of one wave.

Kelleher (1966b) also found differences between the shapes of spatial and temporal correlograms, especially for what he called "complex spatial structures" within which several spatial scales were present.

MacDougall (1966) also observed F-region, and classified the F-region patterns which he saw into three main types: (a) the blob pattern, (b) the aligned pattern, and (c) confused and churning patterns. Cases of type (b) appeared as interference fringes moving across the array, with the interference assumed to arise from two or more points on a distorted specular reflecting surface. He found fluctuations in drift direction always to be associated with bursts of amplitude in the received echo - the amplitude bursts similar to those which Landmark (1957) observed to be coincident with phase-path concavities. MacDougall's (1966) simultaneous measurements of drift direction, drift speed, and angle of arrival show generally that sudden changes occur in all three quantities at the same time. The detailed analysis of MacDougall's results will be found in his paper, but his results show that for fringe-like echoes a tilted specular reflector model is more appropriate than a random scatter model.

To this point, the contrasting fading models of random-screen scattering and specular reflection have been noted. Computer simulations of specular reflector models (Guha and Geller, 1972, 1973)(Brownlie et al 1973a) show that for such models, in one dimension, the presence of one moving wave causes similar fade and drifts techniques to give the correct wave velocity (after division by 2 for point-source

velocity correction). If more than one moving wave is present then correlation analysis is unable to give a meaningful velocity. Hines and Rao (1968) have modelled a two-dimensional ionosphere, in which three waves are present at different wavenumbers and directions of horizontal travel. Their ionosphere is illuminated by an incoming plane wave. Three receiver locations are taken, O, X, and Y with the distances OX along the x direction and OY along the y direction small compared to the structure size of the diffraction pattern on the ground.

The time shifts Tx and Ty between the appearance of a maximum at O, and its subsequent appearance at X and Y, change with the position of the receiving triangle OXY within the diffracted pattern. An alternative interpretation of the change of time-shifts Tx and Ty with position is that they could be the time shifts, as a function of time, observed for a receiver triangle in one place. (Hines and Rao, 1968). Inspection of the distributions of time-shifts Tx and Ty presented by Hines and Rao (1968) show that the time-shifts derived from their model do not allow resolution of the three waves present, and do not bear any clear relationship to any of the wave parameters. In particular they point out that for travelling-disturbance measurements, a drifts record is taken over a time period small compared to the wave periods. On this model the values of Tx and Ty would not go over the entire distributions of Tx and Ty illustrated, but might take one or two specific values which, as is seen from Hines and Rao (1968) could be very misleading.

This is directly relevant to the experimental results of

this thesis, in the following way. Some of the phase-height results obtained indicate, for a given record, a range of periods simultaneously present. However, a phase-height experiment cannot define direction (in the one-receiver form used in this thesis) and there is no reason for the waves to be travelling in the same direction. The effects on the time-shifts derived from corresponding drifts results could be as outlined above. The experimental drifts data has not been checked for this effect by the author at this time.

In contrast, other F-region phase-height results obtained for this thesis show a very regular period in the phase - an almost monochromatic spectrum. Under these circumstances - the presence of one wave - the specular point model of Hines and Rao (1968) predicts that both full correlation and similar fades analyses would give the correct values of atmospheric wave phase speed and direction, as results for the "true" velocity $\underline{V}$. Guha and Geller (1973) predict a similar result for their specular-reflector model, after application of the point-source correction.

The drifts experiment has been used by many workers (for example, Kelleher 1966a) to obtain F-region "true" velocities and "true" directions of drift. Although the results obtained gave reasonable velocity values of the F-region, oscillatory correlations and an unknown atmospheric wave spectrum make it difficult to know what is being measured, how to interpret the correlations obtained, and what uncertainties or systematic errors should be given to the results. It is likely that in the majority of cases the fading arises from the motion of a specular reflector - which may itself have some degree of

roughness -- rather than from the advective movement of a "blob" of ionization. Either model may be applicable for some of the time, but the considerable altitude of the F-region above the turbopause together with predominant magnetic control of electron movement (at least in the F_2 region (Hooke, 1970a)) makes it difficult to see in what circumstances an advective "blob" model could apply. The interpretation of F-region drifts is a problem of considerable difficulty at present.

(3) Dispersion techniques

If a specular reflector model is applicable, the possibility arises of the presence of more than one atmospheric wave - as is seen at times for some of the F-region experimental results obtained in this thesis. If, in the phase height results, the radius of curvature at concavities exceeds the height of the wave above the ground, the individual waves can clearly be seen since the presence of only one specular point prevents phase changes due to specular-point interference. The drifts results, for both coherent and non-coherent phase height, have an uncertain interpretation.

The problem, then, is one of resolving components of different spatial scales, amplitudes, and velocities present in the ground diffraction pattern. This leaves open the relation of such components in the ground diffraction pattern, to frequency components in the specular reflector.

One method of attack on this problem is known as Dispersion analysis. A powerful form of this analysis has been given by Briggs (1968b). The Buckland Park aerial array (Briggs et al. 1969), previously mentioned in the section on correlation

results, allows measurement of the complete two-dimensional spatial pattern amplitude over the array area. If this is done at two times t_1 and t_2, there exist (in Briggs' notation) two patterns $F_1(x,y)$ and $F_2(x,y)$ of amplitude taken at times t_1 and t_2. As Briggs (1968b) indicates, there exists a spatial cross-correlation and spatial cross-spectrum between the patterns F_1 and F_2. The spatial cross spectrum is complex - it has an amplitude and a phase. The phase may be denoted by $\Delta\phi_{12}(\nu_1,\nu_2)$ where ν_1 and ν_2 are variables in the two-dimensional wave-number plane.

Briggs (1968b) indicates how the vector velocity $\underline{V}(\nu_1,\nu_2)$ of each Fourier component in the wave-number plane can be determined. These Fourier components are spatial Fourier components of pattern amplitude, with the "frequency" a spatial frequency, or wavenumber. Briggs (1968b) indicates the expected form of the results for dispersive and for advective motion. In addition, because the method is a spatial analysis, waves of the same wavelength but of different directions can be resolved.

Without a large array of aerials, three-receiver analysis must be made. For a given pair of aerials a time cross-correlation of amplitude (for that spacing) exists, from which the complex cross-spectrum between the two time-series can be found. The phase of the cross-spectrum $\Delta\Phi_{12}(f)$ (where subscript 1 and 2 denote individual aerials and their time-series, not complete spatial patterns as before) is the phase difference between the time Fourier components in the two records (Briggs, 1968b). As is outlined by Briggs (1967, unpubl.), this phase-difference as a function of frequency can be converted to a

time-difference as a function of frequency between the appropriate pair of aerials. Use of the time differences between the three pairs of aerials in the three-receiver system gives a velocity magnitude V(f) and velocity direction $\phi(f)$. These are for the time Fourier components of the amplitude, taken over the (assumed statistically stationary) time interval over which the record is taken. The result at any frequency f is thus a kind of average over this time.

If more than one wave with amplitude time frequency component f is present, then all such waves are present in the time spectrum at frequency f and the time shifts hence velocity magnitudes and directions for that frequency become meaningless.

From the viewpoint of the phase screen model a difficulty arises in relating the diffraction pattern changes to those of the moving reflector. For a deep phase screen of wavelength λ_{scr} and phase deviation $\Delta\phi$, then for plane-wave screen illumination the scale of the amplitude pattern is $\ell = \frac{\lambda_{scr}}{\Delta\phi}$ for large $\Delta\phi$ (Ratcliffe, 1956). However the amplitude pattern is not itself sinusoidal. In the case of one moving wave the amplitude pattern will move with the screen for plane wave illumination. The various frequency components present (because the amplitude pattern is not sinusoidal) will all move with the same velocity.

For point source illumination the scale of the amplitude pattern in space is about $\ell = \frac{2\lambda_{scr}}{\Delta\phi}$, provided this exceeds the radio wavelength. Because of the preferred point (or point transmitter) the form of this pattern across space is expected to change as it moves. (Figs. 4-5 and 4-6 of Chapter 4

indicate this spatial change: although the wave example there has parameters unlike those usual for H.F. E- and F- region measurements.) One might conjecture that over a spatial dispersion analysis like Briggs' (1968b) would observe several spatial wavenumber components even for a purely sinusoidal reflecting screen, and these components would move with independent velocities different to that of the screen. By symmetry one expects the velocity variations of all components to be repeated with the period of the atmospheric wave (if a pure sinusoidal reflector model were applicable) but other than this it would be difficult to relate the velocities of the amplitude spatial frequency components to that of the screen.

The relation of time changes of amplitude at a fixed place for point-source illumination, to screen velocity, is even more difficult to see. The wave period seems to be the only period of time over which the amplitude time series would repeat itself. One does not expect the amplitude time series to be statistically stationary in any sense even for one wave - the work of Brownlie et al. (1973a) certainly shows that it is not so in the case of several waves. For F-region waves, the data run over which the time spectrum is obtained would be a small fraction of the wave period (a ratio of 3 minutes to 20 minutes, say). Consecutive data runs would then be expected to have different spectra, just for different time-sections of the same atmospheric wave.

These difficulties are implied in Brigg's (1972) point about the specular points' movement on the corrugated reflector, which was quoted in Part II.1 of this chapter. A particularly

clear picture of such movements and the resulting Doppler interference has been given by Gossard (1967) for very-low-frequency measurements at 90 km. He used phase-coherent detectors at antennas positioned at the vertices of a nearly-isosceles triangle. The length of the isosceles sides was about 18 km. In his paper he discusses two specific two-hour-long sets of 3-receiver phase records. One of these had significant peaks in the average power spectrum from the three receiver sites, but the other had no significant peaks in the power spectrum. For the record with significant peaks, speeds and directions of movement (i.e. vector velocities) were obtained from the cross-spectra for those frequencies with significant peaks in the power spectrum. For this record the vector velocities were different for different frequencies, but for a given frequency component the apparent velocities for the three pairs of aerials were found to fit very well onto a straight line (Briggs, unpubl., 1967). This gives confidence in the vector velocities obtained. By contrast, a cross-correlation analysis gives a vector velocity different from that of any frequency component. Confidence in this velocity is low, as the apparent velocities obtained from the cross-correlations between pairs of aerials do not lie on a straight line.

Gossard (1967) interprets the prominent spectral lines as the result of Doppler interference between discrete reflecting points (or more correctly, the Fresnel zone around each reflecting point). Such spectra cannot simply be related to spectra present in the specular reflector on which the reflector points lie.

Gossard (1967) has also performed a dispersion analysis on the record without significant peaks in its power spectrum. Under these circumstances, the absence of specular points and of their mutual interference might be expected. The cross-spectra of both amplitude and of phase records (separately) were taken, and in spite of the apparent absence of specular components, evidence of dispersive behaviour was still obtained in that different frequency components seemed to move with different speeds and directions. This is not compatible with an advective drift model of ionization motion, but a specular-point phase-modulated-reflector model would also have difficulty in explaining the effects, unless conditions perhaps were such that only one specular point was present for the entire atmospheric wave cycle. This requires the radius of curvature of any concavity to exceed the height of the reflector.

Gossard's (1967) results were taken at local night-time. It is interesting that his results, which show that a specular reflector model may apply on some occasions, contrast with the H.F. measurements of Felgate and Golley (1971) who found evidence for an advective drift model for the D-region. Felgate and Golley (1971) state that they took a very small sample of D-region results: also their results were taken during the day. Thus time, place, and possibly altitude were different: the only common feature of the experiments being that measurements were taken at altitudes below the E-region. Nevertheless, it may be that the long-wavelength experiment of Gossard (1967) would detect the presence of a specular-type reflector at such altitudes, while the short-wavelength experiment of Felgate and Golley (1971) would see smaller-scale

scatterers which "roughen" the specular reflector surface. These might be present at a level below the turbopause: whereas for H.F. E- and F-region results, a lack of turbulent blobs of ionization at these heights would cause the H.F. experiment to see the specular reflector there.

As a practical method of attack on the moving reflector problem, dispersion analysis has an uncertain value. In some cases the attempts of workers to obtain the spectrum of the raw fading signal just gives a noise-like spectrum for the result, and interpretation of, and use of, the spectrum is impossible. This is interesting, given the usual existence of a meaningful signal correlation, which would be the Fourier transform of the spectrum. For H.F. measurements, dispersion analysis seems less practical than a correlation method.

(4) Complex correlation techniques

Pfister (1971) has modified the three-receiver drift experiment by using a receiver with coherent detection, so that phase and amplitude are recorded for three spaced antennas. This allows recording of the full complex correlation (Booker et al. 1950, Ratcliffe, 1956). For an incoming plane wave the complex correlation of the diffracted field does not change with distance from the screen (Ratcliffe, 1956, p.213), and so is identical with that at the screen: but this is not so for point source illumination. In this case, and for source and receiver equidistant from the screen, the structure size on the ground is twice that of the ionosphere (Ratcliffe, 1956, p.247).

From Pfister's (1971) complex auto- and cross-correlations,

power spectra and cross-spectra are obtained. Physical interpretation of a complex correlation and of the complex spectrum derived from it is difficult. Pfister's (1971) equation for a complex spatial cross-spectrum

$$W_\tau(\kappa_x,\kappa_y)\exp\, j\Psi_\tau(\kappa_x,\kappa_y) = \iint \underline{\rho}_\tau(\xi,\eta)\cdot\exp\, j\{\kappa_x\xi + \kappa_y\eta\}\, d\xi d\eta$$

with complex correlation $\underline{\rho}_\tau$ (last line of Pfister (1971), p.1004) is to be compared with Eq.3 of Briggs (1968b). Small difference in notation aside, the only physical difference is that $\rho_\tau(\xi,\eta)$ is the full complex correlation of the complex spatial wave-field over the ground in Pfister's (1971) work; but is the spatial correlation of the amplitude in Brigg's (1968b) work.

Pfister's (1971) interpretation of spectra obtained from a complex correlation is that the wavenumbers κ_x and κ_y give a measure of angular distribution, or angle of arrival; and that time frequencies Ω give a measure of the shift in Doppler frequency. Thus, the problem is one in which a two-dimensional crinkly reflector is at some height above a three-receiver system there will be several individual specular reflectors (and Fresnel zones around them) contributing to the received signal. Each reflection point will have an azimuth θ and zenith angle δ with respect to the direction of a particular pair of antennas, and its wavenumber $\kappa = \frac{2\pi}{\lambda} \sin\delta \cos\theta$ (Pfister, 1971), with λ the radio wavelength. (This arises because the phase difference between the two antennas, if at distance ℓ apart, is $\Delta\phi = \frac{2\pi}{\lambda}\ell \sin\delta\cos\theta$). Each such reflection point will also have a Doppler frequency arising from its movement on the reflector.

If a signal on a two-dimensional ground could be measured over all (two-dimensional) space and time then its correlation function becomes

$$\rho(\xi,\eta,\tau) = \sum_{x,y,t} F(x,y,t)F(x+\xi,y+\eta,t+\tau)$$

for a real signal F, and becomes

$$\underline{\rho}(\xi,\eta,\tau) = \sum_{x,y,t} \underline{F}(x,y,t)\underline{F}^{*}(x+\xi,y+\eta,t+\tau)$$

for a complex signal $\underline{F}$.

For three receivers only, the spatial correlations cannot be taken, so if $(\xi_1,\eta_1)(\xi_2,\eta_2)$ and (ξ_3,η_3) are the three pairs of receiver x and y *displacements* then we have only

$$\rho(\xi_1,\eta_1,\tau) \qquad \rho(\xi_2,\eta_2,\tau) \qquad \rho(\xi_3,\eta_3,\tau)$$

for real or complex ρ.

Spatial homogeneity is unlikely - in fact Hines and Rao (1968) showed that for their wave-system model spatial homogeneit was not obtained, so in addition the correlations depend on position

$$\rho_{12}(\xi_1,\eta_1,\tau) \quad \rho_{23}(\xi_2,\eta_2,\tau) \qquad \rho_{31}(\xi_3,\eta_3,\tau)$$

for real or complex ρ, and this is all that can be measured (excepting autocorrelations) in a three-receiver system.

Consider $\rho_{12}(\xi_1,\eta_1,\tau)$. A spectrum derived from this is

$$\underline{W}_{12}(\xi_1,\eta_1,\Omega) = \int_{\tau} \rho_{12}(\xi_1,\eta_1,\tau)\ \exp(2\pi i\Omega\tau)d\tau \ .$$

For a real correlation ρ the complex amplitude $\underline{W}_{12}$ gives the magnitude and the phase of a sinusoidal frequency component

present in ρ, in turn derived from F. For example, F might be the signal amplitude or signal phase. Its frequency components could arise from a dispersion in the ground diffraction pattern, which in turn arises from some indirect relationship to dispersion present in a reflector or alternativel from interference of specular points (Gossard, 1967).

For a complex correlation ρ the three complex amplitudes $\underline{W}_{12}, \underline{W}_{23}, \underline{W}_{31}$ are interpreted by Pfister (1971) to give the angular direction of each wave component in the Doppler frequency domain: the frequency is now interpreted directly as a Doppler frequency. Such angular directions would be significant only for those Doppler frequency components for which a significant spectrum amplitude existed.

If, now, a spatial correlation analysis as that of Briggs (1968a) is performed, the general correlation $\rho(\xi,\eta,\tau)$ becomes for specific lag τ_1

$$\rho(\xi,\eta,\tau_1)$$

for either real or complex ρ. Time homogeneity is unlikely, and so this is dependent on a specific time t_o at the start of the run, so ρ becomes

$$\rho_{t_o}(\xi,\eta,\tau_1)$$

The spectrum obtained is

$$\underline{W}_{t_o}(\kappa_x,\kappa_y,\tau_1) = \iint \rho_{t_o}(\xi,\eta,\tau_1)\exp[2\pi i(\kappa_x x + \kappa_y y)].d\xi d\eta$$

For a real signal F and real correlation ρ the complex amplitude $\underline{W}_{t_o}$ gives the spatial magnitude and phase of a spatial frequency component present in the diffraction pattern on the

ground, at time t_o. Such a component has a wavenumber κ_x in the x-direction and κ_y in the y-direction. As before, such spatial dispersion in the ground diffraction pattern could have some indirect relationship to that in the ionospheric reflector, or arise from specular-point interference.

For a complex signal $\underline{F}$ and complex correlation $\underline{\rho}$, Pfister (1971) interprets $\underline{W}_{t_o}$ to give the Doppler frequency of each angular component (with significant spectrum magnitude) in the wavenumber plane. The wavenumbers are now interpreted as angular directions.

In Pfister's (1971) view his analysis gives evidence for the predominance of interference effects over dispersive effects in the reflected signals. This might not be immediately apparent from the dispersion analyses of Gossard (1967), Briggs (1967 unpubl., 1968b) and others. Physical interpretation of complex spectra arising from complex signals can perhaps be difficult. The significance of the peaks in his (1971) spectral curves is difficult to assess, and the quality of data usually obtainable from ionospheric experiments could make the use of the method difficult. It may be that the direct beam-scanning experiment of Brownlie et al. (1973a) could give results with an easier interpretation. Nevertheless, a use of the phase-screen model outlined in Chapter 4 could be to examine (in one dimension) such complex spectra.

Ratcliffe (1956, p.239) has also indicated how a time-varying diffraction pattern can be interpreted as arising from interference between Doppler-shifted radiation waves, or angular spectrum components.

Figure 7 of Pfister (1971) shows complex correlation

behaviour similar to complex correlations obtained in this thesis for the F-region. The wide structure (slow fall-off) of the amplitude of the complex correlation and the linear behaviour of the phase of the complex correlation with lag will be noted.

Pfister (1971) interprets such correlations as indications of a wave-like structure. Further features of the experimental complex correlations found for this thesis are discussed in Chapter 4, because there they are used to illustrate some possible uses of a specular-point model. One point from that chapter, which will be anticipated here, is that for F-region experimental results obtained for this thesis the correlation of the amplitude (auto- or cross-) was generally oscillatory, decreasing for lag zero much more rapidly than the amplitude of the complex correlation. It was found that the results, for F-region, of a full correlation analysis using the correlation of the amplitude, and of a full correlation analysis using the amplitude of the complex correlation, gave different values for wind speeds and characteristic ellipse scale size, although ellipse orientation and wind direction would agree somewhat more closely, Pfister (1971) also found larger structure sizes for the E-region for the complex correlation case.

These results have implications in terms of a "randomly phased spectrum". (Ratcliffe, 1956, p.224 and p.228). One requirement for an angular spectrum to be randomly phased, for the case of non-uniform illumination (as for the experimental configuration of a point-source transmitted) is for the mean power to be effectively constant over a distance containing a

large number of irregularities. This would not occur for a wave model, having typical ionospheric heights and wavelengths. A screen which modifies only the phase of an incoming wave, even if randomly, cannot give rise to a randomly phased angular spectrum (Ratcliffe, 1956, p.231). Use of a wave model for interpretation of data means that the relations given by Ratcliffe (1956, p.232) between complex correlation $\rho_f(\xi)$ and correlation of amplitude $\rho_A(\xi)$ for the presence and absence of specular components cannot be used. Thus, although in general

$$\rho_f(\xi) > \rho_A(\xi)$$

for F-region autocorrelations, this cannot be assumed to imply a Rayleigh amplitude probability distribution and the lack of a predominant specular component. It is true that the autocorrelations used here were time autocorrelations at one place, compared to Ratcliffe's autocorrelations across space at one time. For point source illumination of the diffracting screen the two would differ, and it is discussed in Chapter 4 how a specular point model could be used to examine this. Nevertheless, phase-height results using the same data often indicated a coherent echo and hence a predominant single specular component. The relationship between reflector movement and the correlations ρ_t and ρ_A are not obvious for a sinusoidal reflector model.

III. IMPLICATIONS OF MODEL CHOICE FOR SPACED-RECEIVER DRIFT MEASUREMENT

It may seem that measurement of ionospheric movement gives

two clearly different results, depending on the reflector model chosen. An advective drift model might be expected to give the neutral atmosphere velocities U_x and U_y (Hines, 1960) regardless of whether these arise from a wave present in the atmosphere or not. A specular reflector model might give a gravity-wave trace velocity $\underline{v}_\phi$, if the Doppler interference from the various specular points could be unravelled. The point is, that the velocities $U_{x,y}$ and v_ϕ are quite different quantities (Hines, 1960), and if a specular reflector model is applicable then independent measurements of the neutral atmosphere velocity (if possible) would give different results to the radio method.

Müller (1968) has shown that tidal components of the neutral wind agree quite closely for spaced-receiver drifts and meteor winds experiments. This agreement between methods was obtained for both the 12-hour harmonic component and the prevailing wind component. Because drifts results and meteor results were taken for slightly different heights, it was necessary to account for the change in neutral wind velocity, and in tidal component phase, with height; when comparing results from the two methods. Agreement was found both for one specific day studied, and for an average over a month. This seems accepted for the E-region in general. Vincent (1972) found, in comparing averaged velocities obtained from his spaced phase-height E-region total reflection results with those from meteor winds, that some correspondence was obtained. Low data rates from his meteor-winds experiment made a detailed comparison difficult.

The clearest evidence that the drifts experiment measures neutral wind velocities in the lower atmosphere seems to come from the studies of Stubbs (1973) and Stubbs and Vincent (1973). Stubbs (1973) compared partial-reflection D-region drifts, obtained from full correlation analysis using a near-equilateral triangle within the Buckland Park array, with winds determined by the Adelaide meteor wind system. Essentially the same volume of atmosphere was measured in both cases. Three-hour wind averages obtained from the two methods show close agreement in general, and reveal tidal components at 85 - 95 km. quite clearly. Stubbs and Vincent (1973) did a detailed meteor-wind/drifts comparison for July (southern hemisphere winter: which is the period of greatest mesospheric disturbance (Fraser and Vincent, 1970)). This choice of time of year lead to a slightly poorer agreement between the two methods: agreement itself was a function of height and was better at lower altitudes. Nevertheless, the overall result is clear: for the D- and E-regions the drifts experiment measures predominantly neutral atmosphere movement: and tidal effects are clearly seen. The interaction between ionization and neutral atmosphere arises mainly from collisons at these heights.

If the velocity detected by a spaced-receiver drifts experiment were some combination of velocities arising from advective drift movement and wave phase speed, then *if* the gravity waves propagate randomly in all directions an average taken over a period long compared to the longest wave period should give a velocity which agrees with that obtained from meteor drifts (Fraser, 1968). However, the results of Müller (1968) show that agreement between the two methods was

reasonably good even for individual points. It may be that residual differences in velocities between the two methods, apart from those arising from sampling error, could be the smaller-scale wave effects present in the spaced-receiver results superimposed on the prevailing and tidal components. (Hines, 1963). As was previously discussed, the short period of a typical drifts run compared to that of a gravity wave could lead to additional differences arising from non-stationary time series during the drifts run.

The work of Manson et al. (1976), in which intensive (5 minute interval) 3-minute long partial reflection drifts runs were taken over an extended period of time, does seem to indicate that for the height range of 80 km to the E-region considered, the radio drift measures the neutral wind velocity. The neutral wind velocity itself consists of mean flow, tidal, and short-period irregular wind components - the latter taken to arise from gravity waves.

For the F-region no comparable alternative method of neutral atmosphere motion is available. One study which has been made is that of Rees et al. (1973) in which the movement of barium vapour clouds was compared with ionospheric drifts, which were found using the method of Briggs (1968a) using the Buckland Park array. The results of the two methods correspond somewhat, but the time resolution of the chemical trail method did not allow a detailed comparison of the irregular wind component. Again it is unclear what relative significance neutral drift, electrodynamic drift (Ratcliffe, 1972, p.88), and specular-point interference have in the drifts results (see also Hines, 1964).

One theory which may explain the agreement of spaced-receiver drifts and neutral winds for the E-region is the critical-layer hypothesis of Hines (1968a). In this hypothesis atmospheric waves with vector phase velocities such that the *component* of wave phase velocity along the direction of a prevailing wind is equal to the speed of the wind itself, have their vertical amplitudes of oscillation enhanced compared to those of other atmospheric waves. Hines (1968a) shows that the interference pattern imposed on the atmosphere by such waves will appear to move with the wind. From the discussion of a phase-screen model, this does not imply that the ground diffraction pattern would instantaneously appear to do so, bit a long term average would agree closely with the average wind.

It is difficult to estimate how often this might happen for the F-region. What measurements there are for neutral F-region motion (for example, Kent and Wright, 1968) indicate that gravity wave or T.I.D. velocities, and neutral atmosphere winds, have the same order of magnitude. However, it is difficult to tell for what proportion of the time critical layers might be significant for F-region drifts results. Averaged results for the three-receiver drifts experiment seem to show that the diurnal component of East-West drifts that is measured corresponds closely to that predicted as a result of electrodynamic plasma movement (Kent and Wright, 1968). The correspondence of averaged results for North-South drifts is less certain. The effect of a (quasi-sinusoidal, say) travelling disturbance superimposed on the background winds on the drift measurements is an open question at this time.

IV. IONOSPHERIC PROPERTIES IGNORED BY THE MODEL.

The specular reflection models and data noted here all assume free-space propagation to the level of the corrugated reflector. This is just not so: atmospheric ionization starts at some 60 km in altitude and is present to 1000 km or more.

The effect of the ionization and geomagnetic field is to cause magnetoionic splitting of the radio wave into Ordinary and Extraordinary components. Theoretical considerations predict the divergence of the components in the Earth's magnetic meridian plane, with the result that the reflection points for the two components differ in horizontal position and in height. The rays thus do not travel in straight lines to the screen.

This effect has been noticed for many years and was used in the early work on travelling disturbances. Munro and Heisler (1956) obtained disturbance velocities and directions by noting the time differences between similar effects on O- and X-reflections for ionograms and fixed-frequency records. The F2-region phase-path data of Reddi and Rao (1971) in their Fig.1(a) shows a time lag of about a minute between phase trace minima for the two modes.

Heisler and Nelson (1967) assumed a Chapman-like F-layer, and have traced rays for radio-waves vertically incident from the ground to their reflection points. From their Fig. 1 it is clear that the ray paths are not straight. Deviation for frequencies near the critical frequency is particularly large.

The New Zealand Department of Scientific and Industrial Research records ionosonde data at Christchurch. Among other parameters f_0F_2 and f_0F_1 hourly median values are calculated over each month. Figures 2-1 to 2-4 show plots of this data for October 1976, and for January, April and July 1977. Measurements in this thesis were taken mainly from June 1977 to January 1978: the frequency of 4.57 MHz used is seen to lie between f_0F_1 and f_0F_2. 4.57 MHz is a substantial fraction of f_0F_2 and considerable divergence of the rays would be expected.

Heisler and Nelson point out the likely effect on ionospheric data arising from the neglect of refraction effects. In this context the relevant point is that the free-space-travel vertical-incidence assumption of many specular-point or diffraction models - including that in this thesis - does not hold in the case of F-region.

For sporadic-E studies the situation may be different. Here the screen is a sudden and intense increase in ionization density over a very small distance, in contrast to the steady increase in electron density until the reflection level that applies in the F-region. For the sporadic-E measurements taken for this thesis the D and normal-E regions seemed absent on examination of the A-scope. Thus even for 2.40 MHz free-space propagation to the Es diffracting screen (or corrugated reflector) was a safer assumption than for F-layer studies.

V. CONCLUSION

A review has been made of some methods of radio measurement of ionospheric movement, and their possible interpretations.

It has been noted how the spaced-receiver drifts experiment might be affected by wavelike specular reflectors, and yet for the D- and E-regions is able to measure neutral wind velocity. For the F-region interpretation of what the drifts experiment measures is less clear.

The interpretation problems noted in this chapter may be partially solved by the use of a numerical phase screen model. Chapter 4 indicates some possibly useful parameters for any numerical model which is to simulate some of the current problems stated here.

FIG 2-1 f_0F_2 & f_0F_1 MEDIAN VALUES
CHRISTCHURCH, N.Z. OCTOBER, 1976

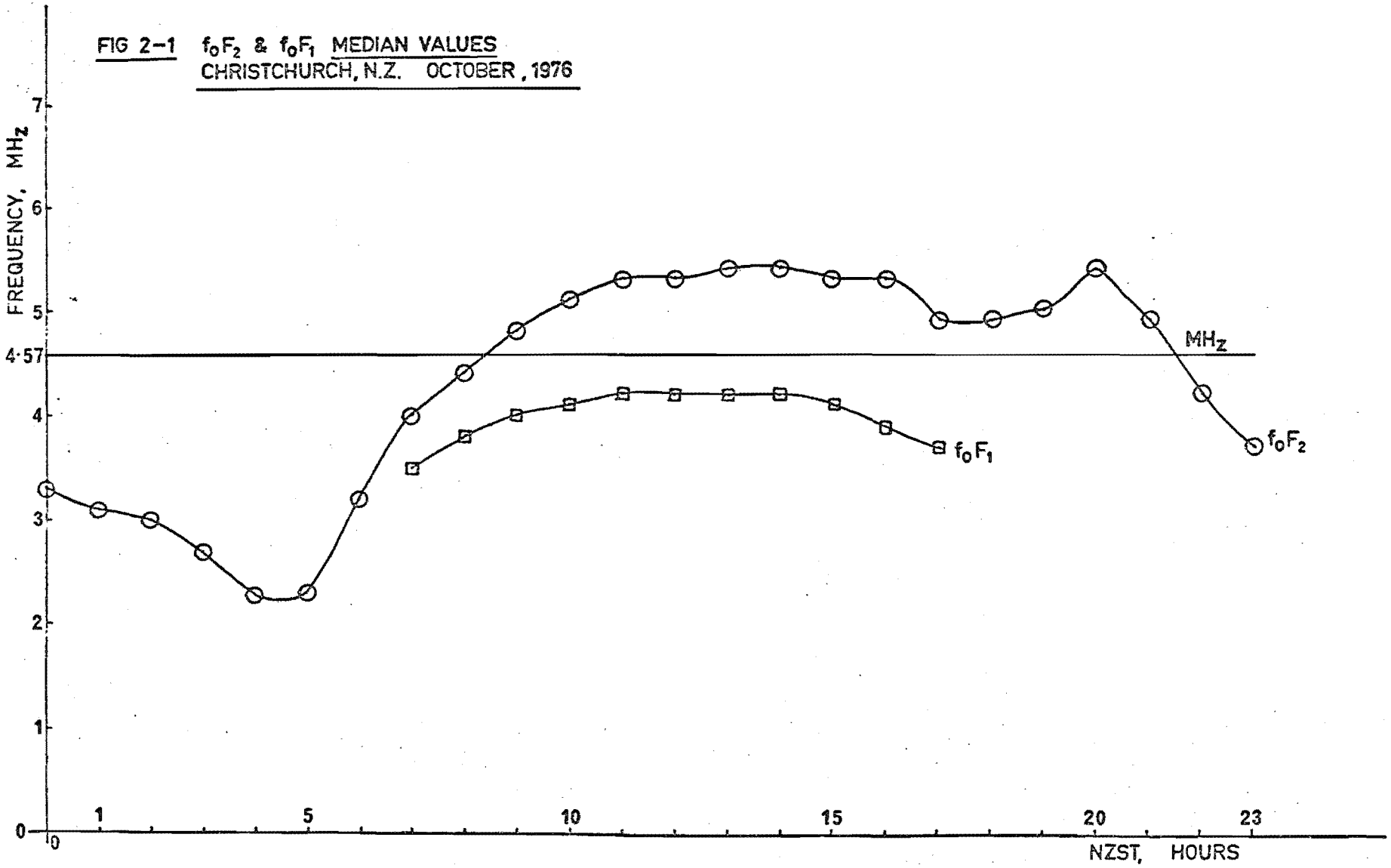

FIG 2–2 f_0F_2 & f_0F_1 MEDIAN VALUES
CHRISTCHURCH, N.Z. JANUARY, 1977

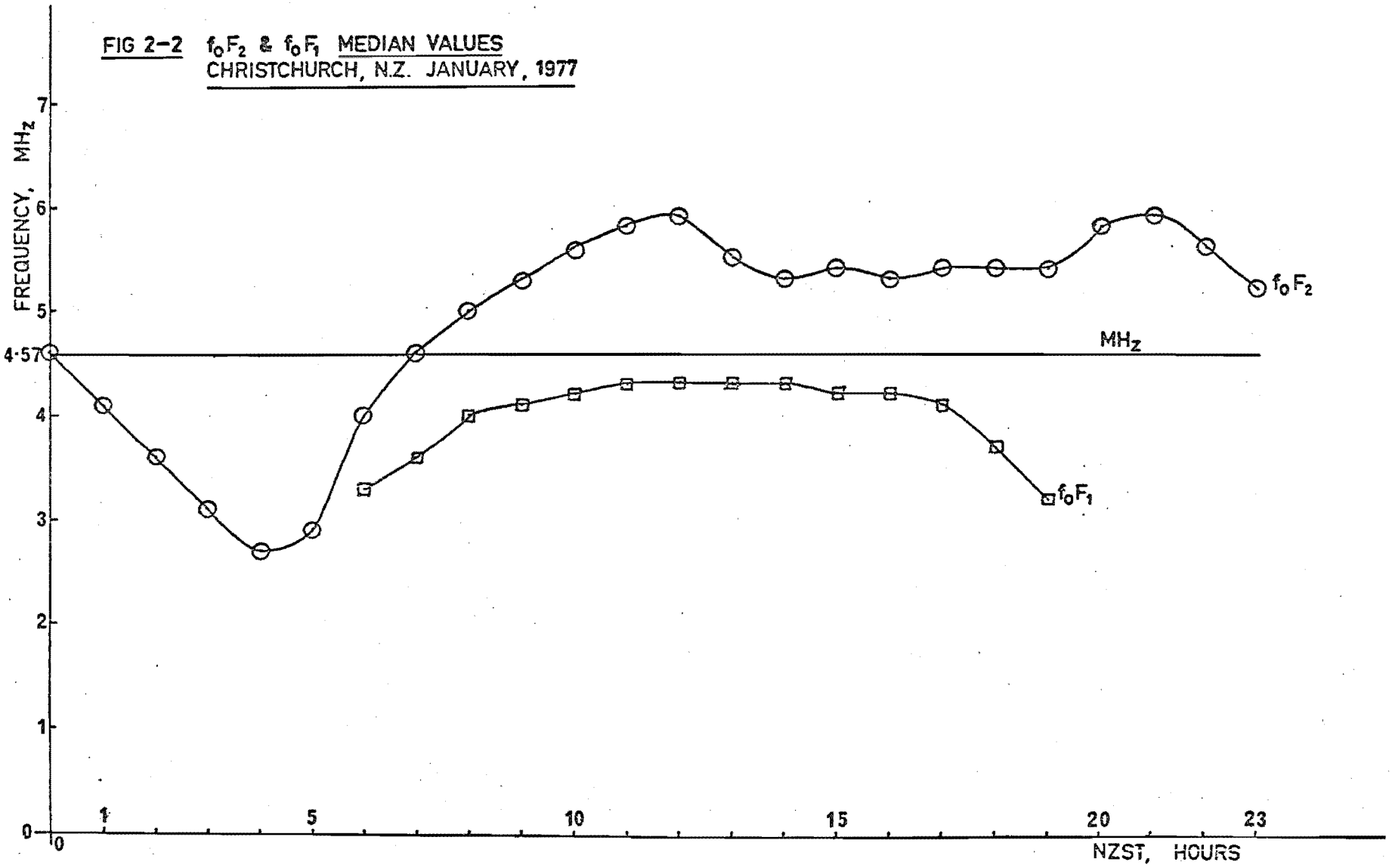

FIG 2-3 f_0F_2 & f_0F_1 MEDIAN VALUES
CHRISTCHURCH, N.Z. APRIL, 1977

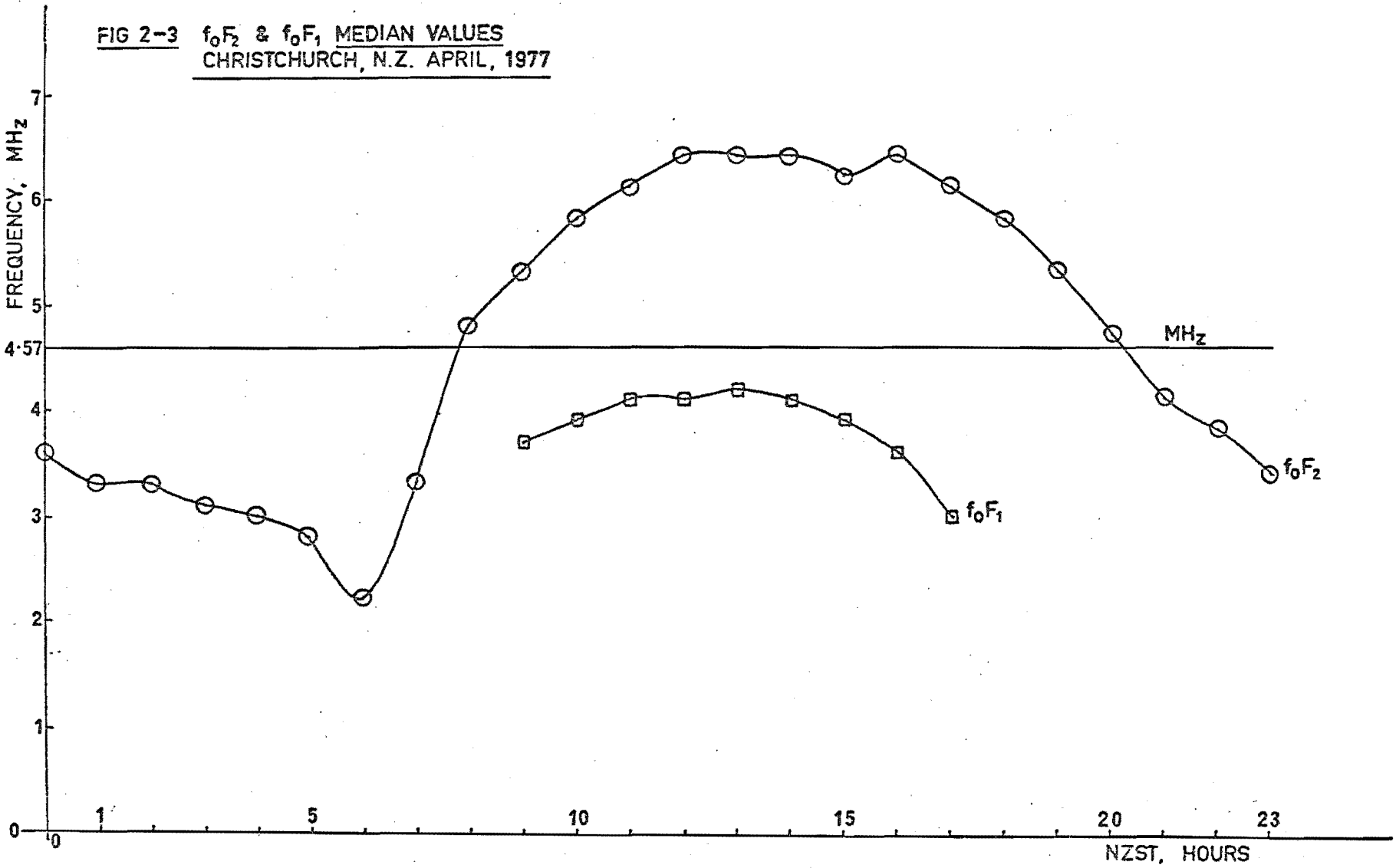

FIG 2-4 f_0F_2 & f_0F_1 MEDIAN VALUES
CHRISTCHURCH, N.Z. JULY, 1977

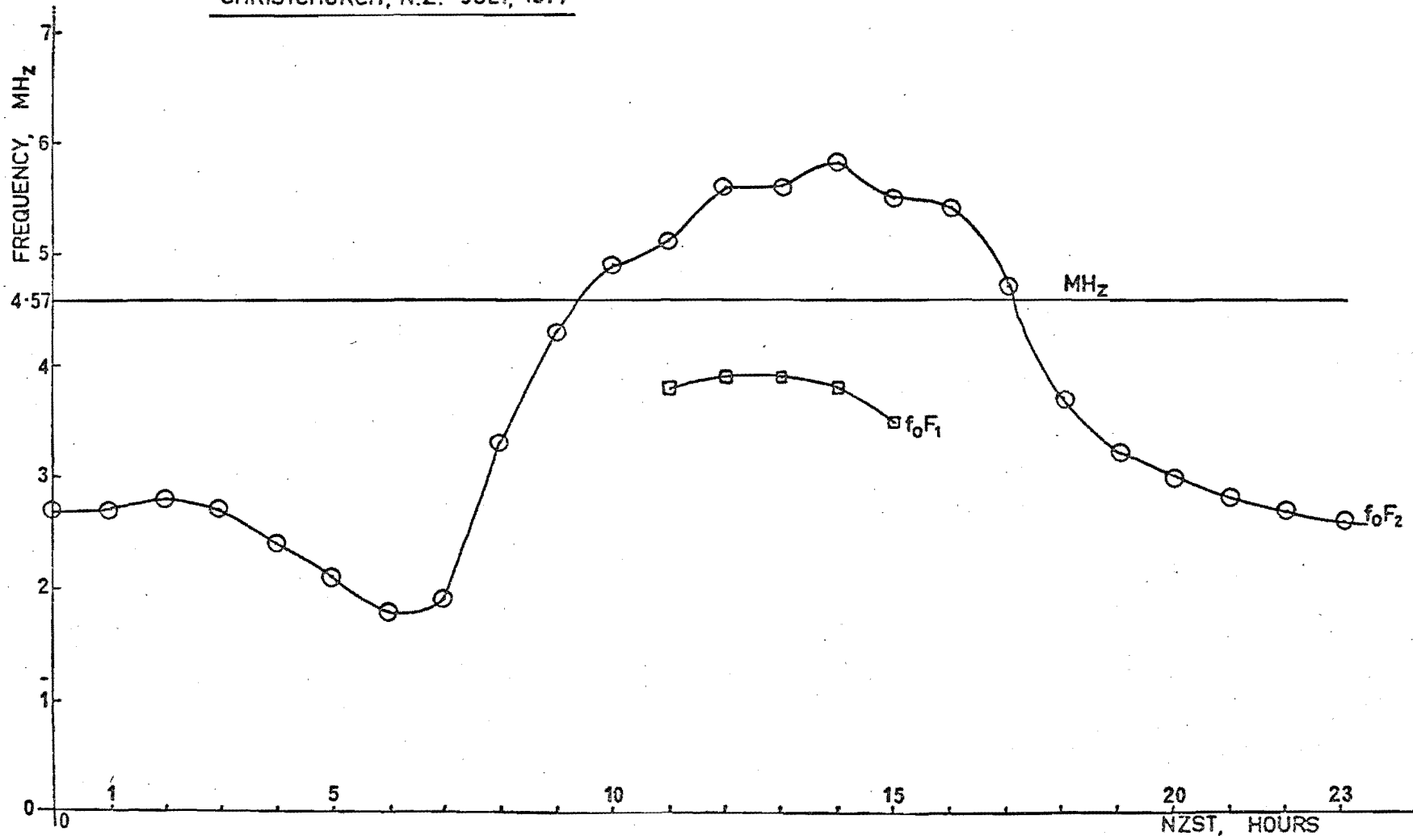

CHAPTER 3

PREPARATION OF NUMERICAL DIFFRACTION CALCULATIONS

I. INTRODUCTION

As discussed in the chapter on the phase-screen model, a possible interpretation of drifts and phase-height results is in terms of a travelling wave perturbing the iso-electronic contours which reflect probing radio waves. The amplitude and phase (with respect to some reference) of the returned echo can be calculated using a ray-optics model, assuming some form for the reflector. This has been done, among others, by Hines (1975, unpubl.): some consequences of his model will be outlined elsewhere in this thesis.

In this chapter we likewise consider a sinusoidal reflector, and again calculate the amplitude and phase of a reflected echo. However, the calculations are done on the basis of Fourier diffraction theory (for example, Ratcliffe, 1956). The parameters of reflectors likely to be physically present in the ionosphere are such that results from a diffraction calculation would approach the ray-optics case. The reason for using a diffraction method is that its Fourier-transform basis allows easy calculation by a Fast-Fourier-transform computer routine. The idea to use this method arose from the work of Buckley (1975) who used a discrete Fourier transform to calculate diffraction patterns.

Work on ionospheric diffraction (for example, Buckley 1975, Whale 1973, Mercier 1962) in general considers random diffracting screens specified by statistical properties. For

example, a phase screen - which modifies only the phase of an incoming wave - is specified by a given phase probability distribution, or phase variance; and by a phase autocorrelation, or phase power spectrum. In contrast, the work here considers a sinusoidal reflector - or phase-modulated diffracting screen - of fixed, definite form. The observation field at given distances from the screen is then found by a Fourier transform diffraction method. Buckley (1975) has briefly considered this definite case, as also have Hargreaves and Hargreaves (1963) using a different numerical method.

In this chapter some standard results on the phase-modulated screen are quoted, mainly from Ratcliffe (1956), for reference. The method of doing the calculations is indicated next; finally some consequences of the theoretical model are shown to be successfully verified in the numerical case. For this last aspect both phase-modulated reflectors and slits are used as diffracting screens.

(1) An Outline of the Fourier Approach

Ratcliffe (1956) has considered a system of uniform phase waves, of common frequency n, each one travelling at its own particular angle θ with the Z axis and with complex amplitude resultant

$$\underline{A}(\theta)d\theta \exp[2\pi i\{X \sin \theta + Z \cos \theta)/\lambda - nt\}]$$

for waves with wavenormals at angles between θ and $\theta+d\theta$. The system is two-dimensional with no Y-variation and the waves are polarized to have either electric or magnetic vector in the X-Z plane.

The X-component of the resultant vector $\underline{A}$ from all the waves is expressed by Ratcliffe's Eq. 1,

$$\underline{f}(x,z)\ \exp(-2\pi int)$$

$$= \int_{\theta=-\pi/2}^{\pi/2} \underline{A}(\theta)\ \cos\theta\ \exp[2\pi i(x \sin\theta + z\cos\theta)]d\theta$$

$$\cdot\ \exp(-2\pi int)$$

with $x = \frac{X}{\lambda}$ and $z = \frac{Z}{\lambda}$.

When the angle is expressed in terms of $S = \sin\theta$ the above becomes (omitting the time factor)

$$\underline{f}(x,z) = \int_{S=-1}^{1} \underline{F}(S)\ \exp\{2\pi i(Sx+Cz)\}dS \qquad C = (1-S^2)^{\frac{1}{2}}$$

and at the plane $z = 0$, including evanescent waves,

$$\underline{f}(x) = \int_{-\infty}^{\infty} \underline{F}(S)\ \exp(2\pi iSx)dS$$

so the complex amplitude component of the angular spectrum is

$$\underline{F}(S) = \int_{-\infty}^{\infty} \underline{f}(x)\ \exp(-2\pi iSx)dS.$$

The summation of the waves in the angular spectrum gives rise to the field distribution $\underline{f}(x)$, and conversely the field distribution at $z = 0$ gives rise to that angular spectrum which is the Fourier transform of the field distribution. The field at an observation plane at z is found from the inverse Fourier transform of the angular spectrum components, each having been shifted in phase by $2\pi iCz$.

II. SCREENS OF DEFINITE FORM

(1) A Summary of Theory

Some standard theoretical results about the phase screen are reproduced for ease of reference.

(a) The Phase-Modulated Diffracting Screen. By definition this is a screen which leaves the incoming amplitude unaltered but alters the phase. If the phase is modulated sinusoidally then (Ratcliffe, 1956, Eq. 17(a)),

$$\underline{f}(x,0) = 1 \cdot \exp\{i\phi_0 + i\Delta\phi \cos\left(\frac{2\pi x}{\lambda_{scr}}\right)\}$$

$$= 1 \cdot \exp\{i\Delta\phi \cos\left(\frac{2\pi x}{\lambda_{scr}}\right)\}$$

where ϕ_0 is the constant change in phase, hereafter ignored; $\Delta\phi$ is the amplitude of the phase deviation, and λ_{scr} is the screen wavelength. Ratcliffe uses d for λ_{scr}.

For small $\Delta\phi$ ($\Delta\phi << 1$)

$$\underline{f}(x,0) \simeq 1 + i\Delta\phi \cos\left(\frac{2\pi x}{\lambda_{scr}}\right)$$

which (Ratcliffe, 1956, P.198) consists of a zero-order component of unit magnitude, and two side components at angles $S = \frac{\pm 1}{\lambda_{scr}}$ with complex amplitudes $\frac{i\Delta\phi}{2}$. The sidebands are in quadrature with the main components, because of the factor i.

For any $\Delta\phi$, small or large,

$$\underline{f}(x,0) = \sum_{n=-\infty}^{\infty} (i)^n J_n(\Delta\phi) \exp\left(\frac{2\pi i n x}{\lambda_{scr}}\right)$$

(where J_n is the Bessel Function of order n).

but $\underline{f}(x,0)$ is periodic and can be expanded as a Fourier series

$$\underline{f}(x,0) = \sum_{n=-\infty}^{\infty} \underline{F}(S_n) \exp(2\pi i S_n x).$$

Comparison of coefficients shows that the Fourier transform $\underline{F}(S)$ of $\underline{f}(x)$ has components

$$\underline{F}(S = \frac{n}{\lambda_{scr}}) = i^n J_n(\Delta\phi)$$

so there are components at spatial frequencies S_n which are multiples of $\frac{1}{\lambda_{scr}}$, whose phases change by $\pi/2$ between each component and the one following it.

Terman (1955, P.589) states that

"a frequency-modulated wave contains sideband components of importance on either side of the carrier wave over a frequency interval approximating the sum of the frequency deviation and the modulating frequency."

This is confirmed by Watson's Table IV (Watson, 1944, P.731) where $J_n(x)$ falls off sharply in magnitude for $n > x+1$. Thus, $J_n(\Delta\phi)$ becomes small when n exceeds $\Delta\phi+1$. For deep screens, $S_{max} \simeq \frac{\Delta\phi+1}{\lambda_{scr}}$, and for shallow screens $S_{max} = \frac{1}{\lambda_{scr}}$, on both sides of the carrier from zero angle in the angular spectrum.

The extent of the angular spectrum from a cosine-phase modulated screen depends on both the spatial period $\frac{1}{\lambda_{scr}}$ and the phase deviation $\Delta\phi$. Reference to Terman (1955, P.593) shows that phase-modulation is just frequency-modulation with the frequency deviation proportional to modulating frequency. Thus, with this in mind, Terman's figures 17-4 (P.591) give an indication of the effect of changes in λ_{scr} and $\Delta\phi$.

For a screen of given wavelength λ_{scr}, increasing the phase deviation $\Delta\phi$ increases the number of significant

sidebands, each a distance $\frac{1}{\lambda_{scr}}$ from the previous sideband. $\underline{F}(S)$ spreads out in spatial frequency, or in angle when interpreted as an angular spectrum.

For a screen of given phase deviation $\Delta\phi$, increasing the screen wavelength λ_{scr} will compress the angular spectrum in spatial frequency, or angle. There is the same number of sidebands $\Delta\phi+1$ on each side of the carrier, but they are closer together, as the spacing $\frac{1}{\lambda_{scr}}$ has decreased.

A sideband at angle $S = \frac{1}{\lambda_{scr}}$ travels with a velocity in the Z-direction of $v = n/C$ which is (Ratcliffe, 1956, P.193)

$$v = v_0\left[1 - \frac{1}{\lambda_{scr}^2}\right]^{-\frac{1}{2}}$$

where velocity is in wavelength units and v_0 is the velocity of the undeviated plane wave - or carrier. The sidebands thus travel at a greater velocity than the carrier. Moreover, the sideband at angle S has a phase difference at (0,z) with respect to the carrier of $\pi z S^2$, where z is the distance of an observation plane parallel to the diffracting screen (Ratcliffe, 1956, P.206). This phase difference is interpreted here as a time lag (Appendix D).

For a shallow ($\Delta\phi < 1$) screen

$$\underline{f}(x,0) = 1 + \frac{i\Delta\phi}{2}\exp\left(\frac{i2\pi x}{\lambda_{scr}}\right) + \frac{i\Delta\phi}{2}\exp\left(\frac{-i2\pi x}{\lambda_{scr}}\right) .$$

The side components gain in phase by $\pi z(\frac{1}{\lambda_{scr}})^2$ over a distance z: they are initially retarded by $\pi/2$ in time with respect to the carrier at the screen. At $z = \frac{1}{2}\lambda_{scr}^2$ the sidebands are in

phase with the carrier. At successive distances of $\frac{\lambda^2_{scr}}{2}$ from the screen the additional distance gain of $\frac{\pi}{2}$ in phase causes successive amplitude modulation, phase modulation, amplitude modulation, across the observation plane at distances $z_1 = \frac{\lambda^2_{scr}}{2}$, $z_2 = \frac{2\lambda^2_{scr}}{2}$, $z_3 = \frac{3\lambda^2_{scr}}{2}$. (These differences in phasing from Ratcliffe arise from the interpretation of positive $\Delta\phi$ - see Appendix D).

For deep screens ($\Delta\phi \geq 1$) there are many sideband components at multiples of $S = \frac{1}{\lambda_{scr}}$ to $S_{max} = \frac{\Delta\phi+1}{\lambda_{scr}}$. Each component is retarded in phase by $\frac{\pi}{2}$ over the previous one: and also travels with increasing speed. Each sideband component at angle nS combines with the main wave at successive distances $z = \frac{\lambda^2_{scr}}{2n^2}$ to give amplitude modulation, phase modulation, with spatial period $\frac{\lambda_{scr}}{n}$. The Fresnel pattern at all distances contains variations of structure smaller than the wavelength of the screen (Ratcliffe, 1956, P.210). The smallest-scale structure seen would be $\frac{\lambda_{scr}}{(\Delta\phi+1)}$ for a screen of phase-depth ϕ, unless the angle $S_{max} = \frac{\Delta\phi+1}{\lambda_{scr}}$ of the sideband exceeds $\frac{\pi}{2}$ radians (in which case $\sin(S_{max})$ is imaginary and the disturbance is evanescent.) In that case structure away from the screen has scale at submultiples $\frac{\lambda_{scr}}{n}$ of the screen for increasing n until $\frac{\lambda_{scr}}{n} < \lambda$, the probing wavelength.

If components of two spatial periods are present in the screen, say λ_{1scr} and λ_{2scr}, the angular spectrum will generally contain intermodulation components at angles $S = \frac{m}{\lambda_{1scr}} \pm \frac{n}{\lambda_{2scr}}$ in addition to those at $S = \frac{m}{\lambda_{1scr}}$ and $S = \frac{n}{\lambda_{2scr}}$. (Ratcliffe, 1956, P.200). However, for a shallow screen, where the total phase deviation arising from the two components together is less than 0.25 radian, the angular

spectrum is the sum of the separate (and first-order only) angular components (Ratcliffe, 1956, P.200).

III. THE NUMERICAL MODELLING OF DIFFRACTION

Following Ratcliffe (1956, Eq. 5) we have

$$\underline{F}(S) = \int_{-\infty}^{\infty} \underline{f}(x) \exp(-2\pi i S x)$$

where $\underline{F}(S)$ is the angular spectrum of screen $\underline{f}(x)$: $S = \sin\theta$ where θ is the angle between the screen normal, and the direction of propagation of the plane-wave component: and x is the distance along the screen in units of a radio wavelength. The observation field (Ratcliffe, 1956, Eq. 43) is

$$\underline{f}(x,z) = \int_{-\infty}^{\infty} \underline{F}(S) \exp\{2\pi i (Sx+Cz)\} dX$$

where $C = (1-S^2)^{\frac{1}{2}} = \cos\theta$ and z is the distance in wavelength units between the screen and an observation plane parallel to it.

Numerical work is done by use of the discrete Fourier transform. The screen $\underline{f}(x)$ is represented by N discrete points $\underline{f}(x_0)$, $\underline{f}(x_1),\ldots,\underline{f}(x_{N-1})$ and the I.D.F.T. (inverse discrete Fourier transform) is applied to obtain a digitized $\underline{F}(S_0)$, $\underline{F}(S_1),\ldots,\underline{F}(S_N)$. After multiplication by the phase z factor a D.F.T. is applied to obtain $\underline{f}(x,z)$.

A choice of Δx implies one of ΔS hence ΔC. Since $C_k = k\Delta C$ the user value of Δx becomes important.

(1) The Prevention of Aliasing

The sampling of the screen waveform must be taken sufficiently frequently within a cycle to prevent aliasing. If aliasing is allowed to occur, there will be additional angular spectrum components present which really arise from further replicas of the (periodic) discrete Fourier transform. The inclusion of these in the calculation makes the observation fields incorrect.

For the phase screen the maximum frequency at which a significant spectral component occurs is

$$S_{max} = \frac{\Delta\phi+1}{\lambda_{scr}}$$

and to avoid aliasing

$$S_{max} < \frac{0.5}{\Delta x}$$

hence

$$\frac{\Delta\phi+1}{\lambda_{scr}} = \frac{0.5}{\Delta x} \qquad \text{or} \qquad \Delta x < \frac{0.5\ \lambda_{scr}}{(\Delta\phi+1)}$$

To avoid leakage problems, this author fixes λ_{scr} by specifying the sample spacing Δx, and an integral number of cycles of the screen present within the N points of the screen. Hence,

$$\lambda_{scr} = \frac{N\Delta x}{\text{Number of cycles}}$$

or

$$\text{Number of cycles} < \frac{0.5N}{(\Delta\phi+1)}$$

for the screen, given its maximum phase deviation $\Delta\phi$ and number of points N.

IV SOME NUMERICAL RESULTS

Calculations of angular spectra and diffracted observation fields have been made using a Fourier Transform method.

Fig. 3-1 shows the principal model taken: a plane wave is incident on a sinusoidal reflector and results in an outgoing diffracted wave. Also shown are the angular spectrum components for the shallow and deep-screen case.

The thin slit is considered briefly and Fourier Transform results compared with those from the Cornu spiral.

(1) The phase screen.

Fig. 3-2 shows phase screens, of depths $\Delta\phi$ = 0.1, 1.0, 3.0 and 10.0. ($\Delta\phi$ is represented by $\Delta\theta$ on the plot headings). As discussed in Appendix D, positive ϕ represents a phase delay with respect to $\phi = 0$ for the probing radio waves of form $\cos(kZ - \omega t + \phi)$ used here. Thus Fig. 3-2 represents the physical form of the reflector, and also the values ϕ used in the simulation.

Fig. 3-3 shows the spreading of the angular spectrum in spatial frequency or angle as the phase depth $\Delta\phi$ increases: significant spectrum components to at least the $(\Delta\phi+1)^{th}$ order can be seen in each case.

(a) Alteration of Observation-plane Distance z.

This leads to the effects of focussing, where the amplitude is maximum at certain distance z for fixed $\Delta\phi$ and λ_{scr}: and

diffracted observation field at distances $n\frac{\lambda_{scr}}{2}$.

For a general reflector y = y(x) in geometrical optics, the radius of curvature is (Love and Rainville, 1967, p.188)

$$\rho(x) = \frac{[1+\{y'(x)\}^2]^{3/2}}{|y''(x)|} \quad .$$

A phase ϕ is a metre distance of $k^{-1}\phi$, or a radio-wavelength distance $\frac{\phi}{2\pi}$. Thus a phase curve $\Delta\phi \cos(\frac{2\pi x}{\lambda_{scr}})$ becomes, in radio-wavelengths units,

$$y(x) = \frac{\Delta\phi}{4\pi} \cos(\frac{2\pi x}{\lambda_{scr}})$$

for a mirror-like reflection screen, because, in travelling to the point y(x) on the screen and back, the path difference is twice y(x).

The radius of curvature of the physical reflector y(x) is at x=0

$$\rho(x=0) = \frac{\lambda_{scr}^2}{\pi \cdot \Delta\phi}$$

and for incoming plane waves the focal point is half this distance,

$$z_F = \frac{\lambda_{scr}^2}{2\pi \cdot \Delta\phi} \quad .$$

From a diffraction viewpoint, a deep phase screen has many sidebands (for example, see the angular spectrum for $\Delta\phi$ = 10 in Fig. 3-3), each of which, for order n, causes alternate amplitude and phase modulation at successive distances $\frac{\lambda_{scr}^2}{2n^2}$. The sideband amplitudes $J_n(\Delta\phi)$ are often comparable in magnitude for many n - as Fig. 3-3 shows, there

increases - that is, not until n exceeds $\Delta\phi$. A diffraction focus arises when the conflicting amplitude variations with distance, arising from the various orders, sum to a maximum for a given distance z.

A phase screen is set up with the following parameters:

Number of points = 1024

Number of cycles within 1024 = 1

$\Delta x = 0.25$

hence $\lambda_{scr} = 1024 \times 0.25 = 256$

with $\Delta\phi = 10.$

The focal distance z_F is expected to occur at

$$z_F = \frac{\lambda_{scr}^2}{2\pi.\Delta\phi} = 1043 \quad .$$

The amplitude of the observation field at x = 0 is calculated for a range of distances z. The maximum amplitude is found to occur at

$$z_M = 1380.$$

Fig. 3-4 shows the amplitudes of the observed fields in space at distances z = 1040, 1085, 1280, 1380 wavelengths. Fig. 3-5 does likewise for the phases. As explained in (1) above, positive phase represents a time lag, and negative phase a time lead. The depth of fading can be seen to increase as the screen-observer distance increases. Complex fading represents the presence of more than one reflecting point in a geometrical-optics model. The distance z = 1380 represents the diffraction focus, at which the deepest fading can be seen. The phase at the origin is also stationary for the greatest spatial extent, at this distance.

shallow, and spreads over a greater distance along the observing plane X.

For a shallow screen, the amplitude field only, phase field only, amplitude field only... are modulated at observer distances $m\frac{\lambda_{scr}^2}{2}$ for integer m (Ratcliffe, 1956, p.208). For the screen wavelength used here, the first such distance is $\lambda_{scr}^2/2 = 32768$: an order of magnitude greater than the distances considered here.

Fig. 3-6 indicates the amplitude and phase results at observer points (x = 0,z) as z is increased through the focussing condition, for parallel light.

It should be noted that the phase values plotted for the observation fields give the phase of $\underline{f}(x,z)$ at time t=0, referred to the diffracting-screen origin (0,0) as phase zero. At fixed time, an undiffracted wave at an observation-plane at distance z will have phase $360z'$ degrees with respect to the screen origin. z' is here the fractional part of distance z: all distances are in wavelength as a unit.

In general, diffracted waves have phase (with respect to the screen origin) a function of x with z as parameter: this will be other than $360^{o}z'$ and is the one here illustrated. It requires the subtraction of $360z'$ degrees to have the observation-plane origin as phase-reference: this point should be noted when comparing the phases of this method with those of Hewish (1951).

None of the figures presented here is affected by this requirement as all the distances are an integral number of wavelengths.

(a) Derivation of the Cornu Spiral. The standard treatment of Fresnel diffraction from a thin slit leads to the Cornu Spiral (for example, Jenkins and White, 1957), from which observation fields at different distances from the slit may be calculated.

A comparison was made with the results of the Fourier Transform method for a slit. The slit used had width 20 wavelengths, and observation distances 50 and 200 wavelengths. Fig. 3-7 shows the results.

It is a known defect of the Huygens-Fresnel theory of diffraction, (from which the Cornu Spiral is derived) that for cylindrical wavefronts, the phase of the resultant diffracted wave is $\pi/4$ radians behind in time from the correct values. This defect is corrected in the Kirchoff theory. The phase results of the Cornu Spiral solution were corrected by $\pi/4$ for comparison with those arising from the Fourier Transform method.

(b) Comparison of results. The phase of the Fourier Transform method agreed with the corrected phase of the Cornu Spiral method. It is indicated in (c) below how the Fourier Transform method incorporates the Kirchoff correction.

Agreement between the two methods was not exact: differences in phase exceeding those in amplitude for the observer distances tried out. Errors in both methods contributed to the differences. The calculation of the Cornu Spiral neglects variation of obliquity factor along the strip-divided wavefront (Jenkins and White, 1957), and also assumes paraxial approximations in that significant distances taken along the wavefront are assumed to be far less than object and image distances. The present image distances of 50 and 200

to hold.

The use of the discrete Fourier Transform implies a replication of the basic waveform: thus a slit becomes physically a grating. Overall, agreement between the two methods improves as (i) the observation field is calculated for distances closer to the slit, and/or as (ii) a larger number of points is taken for the Fourier Transform, keeping the slit at the same width. Tables 3-1 to 3-4 show detailed summaries of the comparison.

The effect of taking a greater number of points in the transform is physically to make coarser the grating caused by the infinite replication of the Fourier Transform. Another viewpoint is that as the number of transform points increases, the angular spectrum is digitized more finely, allowing more accurate calculation of the observation field.

For accurate fields in the non-periodic case, it is seen that it is necessary to take observation points close to the screen, and take a large number of points in the transform.

(c) The angular spectrum solution.

For a one-dimensional screen the diffracted observation-field is

$$\underline{f}(x,z) = \int_{S=-\infty}^{\infty} \underline{F}(S)\ \exp[2\pi i(Sx+Cz)]dS$$

which in the small-angle approximation, with $C = 1 - \frac{1}{2}S^2$, becomes

$$\underline{f}(x,z) = \exp(2\pi iz) \int_{-\infty}^{\infty} \underline{F}(S)\ \exp(-\pi iS^2z)\ \exp(2\pi iSx)dS$$

If $\underline{h}(x) = \exp(-\pi x^2)$ then $\underline{H}(S) = \exp(-\pi S^2)$. (Bracewell, 1965, p.357). Also, by the similarity theorem (Bracewell, 1965, p.101), we have that if $\underline{h}(x)$ has Fourier transform $\underline{H}(S)$, then $\underline{h}(ax)$ has transform $\frac{1}{|a|}\underline{H}(\frac{S}{a})$.

$$\exp(-\pi i z S^2) = \frac{1}{\sqrt{\frac{1}{iz}}} \cdot \exp\left\{ -\pi \cdot \frac{S^2}{\left(\sqrt{\frac{1}{iz}}\right)^2} \right\} \cdot \sqrt{\frac{1}{iz}}$$

$$\Leftrightarrow \sqrt{\frac{1}{iz}} \cdot \exp\left(-\pi \frac{x^2}{iz}\right)$$

$$= \sqrt{\frac{1}{iz}} \cdot \exp\left(\frac{\pi i x^2}{z}\right) \quad .$$

Use of the convolution theorem (Bracewell, 1965, p.108) gives

$$\underline{f}(x,z) = \exp(2\pi i z) \sqrt{\frac{1}{iz}} \int_{x'=-\infty}^{\infty} \exp\left(\frac{\pi i x'^2}{z}\right) \underline{f}(x-x',0)\, dx'$$

This equation has been derived before by Ratcliffe (1956, p.207), but omitting the constant term preceding the integral: and by Buckley (1975, Eq.6).

The constant preceding the integral is made up of three factors:

(i) The $\exp(2\pi i z)$ factor which is the distance phase factor between diffracting screen and observation plane.

(ii) The $\frac{1}{\sqrt{i}} = \exp(-i\pi/4)$ factor which, for the sign convention given in Appendix D, is the $\pi/4$ phase advance necessary to give the field its correct phase.

(iii) The $\frac{1}{\sqrt{z}}$ factor which is the amplitude falloff with distance for a cylindrical wave.

The integral term itself is just a Fresnel integral summation of the complex field contributions arising from the

Table 3-1: Comparison of Cornu Spiral and Fourier Transform Observation fields at distance Z = 50 wavelengths.

Distance along screen wavelengths	Cornu Spiral Fresnel Amplitude	Fourier transform Amplitude, N=256	Fresnel Corrected* Phase, Radians	Fourier transform phase N=256	(Fourier-Fresnel) absolute† difference in amplitude	Percentage†† difference in amplitude	(Fourier-Fresnel) absolute difference in phase	Percentage difference: in phase
0.0	0.84411	0.84672	-0.17239	-0.18458	0.00261	0.31%	-0.01219	7.07%
0.5	0.86932	0.85435	-0.13163	-0.10624	-0.01497	-1.72%	0.02539	-19.29%
1.0	0.93874	0.93851	-0.03378	-0.01912	0.00023	-0.02%	0.01466	-43.40%
1.5	1.02916	1.02519	0.07387	0.03151	-0.00397	-0.39%	-0.04236	-57.34%
2.0	1.10259	1.10264	0.15393	0.18058	0.00005	0.00%	0.02665	17.31%
2.5	1.12884	1.15330	0.18442	0.14572	0.02446	2.17%	-0.03870	-20.98%
3.0	1.11023	1.10338	0.14981	0.14946	-0.00685	-0.62%	-0.00035	-0.23%
3.5	1.08650	1.11263	0.04977	0.08039	0.02613	2.40%	0.03062	61.53%
4.0	1.10211	1.09582	-0.07629	-0.08842	-0.00629	-0.57%	-0.01213	15.90%
4.5	1.15214	1.11747	-0.16549	-0.14901	-0.03467	-0.03%	0.01648	-9.96%
9.5	0.49954	0.57098	-0.04666	0.01693	0.07144	14.30%	0.06359	-136.28%
14.5	0.19884	0.23864	2.01083	1.71229	0.03984	20.02%	-0.29854	-14.85%

* The numbers presented here are the raw phase results with $\frac{\pi}{4}$ subtracted.

† Absolute error as opposed to percentage error: not the absolute magnitude of the error.

†† Percentage error taken as $\frac{\text{(FOURIER-FRESNEL)}}{\text{FRESNEL}} \times \frac{100}{1}$ % .

Table 3-2: Comparison of Cornu Spiral and Fourier Transform Observation Fields at distance Z = 50 wavelengths.

Distance along screen wavelengths	Cornu Spiral Fresnel Amplitude	Fourier Transform amplitude N = 1024	Fresnel Corrected Phase Radians	Fourier Transform Phase N = 1024	(Fourier-Fresnel) absolute difference in amplitude	Percentage Difference: in amplitude	(Fourier-Fresnel absolute difference in phase	Percentage Difference: in phase
0.0	0.84411	0.83708	-0.17239	-0.15167	-0.00703	-8.33%	0.02072	-12.02%
0.5	0.86932	0.86140	-0.13163	-0.12670	-0.00792	-9.11%	0.00493	-3.75%
1.0	0.93874	0.93497	-0.03378	-0.02674	-0.00377	-0.40%	0.00704	-20.84%
1.5	1.02916	1.02503	0.07387	0.06175	-0.00413	-0.40%	-0.01212	-16.41%
2.0	1.10259	1.10743	0.15393	0.14499	0.00484	-0.44%	-0.00894	-5.81%
2.5	1.12884	1.13671	0.18442	0.16857	0.00784	0.70%	-0.01585	-8.59%
3.0	1.11023	1.12714	0.14981	0.15044	0.01691	1.52%	0.00063	0.42%
3.5	1.08650	1.09439	0.04977	0.05572	0.00789	0.73%	0.00595	11.95%
4.0	1.10211	1.09600	-o.07629	-0.05742	-0.00611	0.55%	0.01887	-24.73%
4.5	1.15214	1.13019	-0.16549	-0.16483	-0.02195	-1.91%	0.00066	-0.40%
9.5	0.49954	0.53687	-0.04666	0.00172	0.03733	7.47%	0.04838	-103.69%
14.5	0.19884	0.26056	2.01083	1.81941	0.06212	31.30%	-0.19142	-9.52%

Table 3-3: Comparison of Cornu Spiral and Fourier Transform Observation fields at distance z = 200 wavelengths.

Distance along screen wavelengths	Cornu Spiral Fresnel Amplitude	Fourier transform amplitude, N = 256	Fresnel corrected phase, radians	Fourier transform phase, N = 256	(Fourier-Fresnel) absolute difference in amplitude	Percentage difference: in amplitude	(Fourier-Fresnel) absolute difference in phase	Percentage difference in phase
0.0	1.26519	1.21049	-0.27339	-0.24102	-0.05470	-4.32%	0.03237	-11.84%
1.0	1.24590	1.24632	-0.26487	-0.25197	0.00042	0.03%	0.01290	-4.87%
2.0	1.18966	1.17429	-0.24006	-0.29158	-0.01537	-1.29%	-0.05152	21.46%
3.0	1.10055	1.17537	-0.20121	-0.25387	0.07482	6.80%	-0.05266	26.17%
4.0	0.98560	0.91669	-0.15289	-0.03520	-0.06891	-7.00%	0.11769	-76.98%
5.0	0.85441	0.90662	-0.10282	-0.12635	0.05251	6.15%	-0.02353	22.88%
6.0	0.71908	0.80249	-0.06311	-0.11965	0.08341	11.60%	-0.05654	89.59%
7.0	0.59401	0.56367	-0.05044	-0.11640	-0.03034	-5.11%	-0.06596	130.77%
8.0	0.49581	0.44002	-0.07925	0.14047	-0.05579	-11.25%	0.06122	-77.25%
9.0	0.43831	0.51771	-0.13790	-0.14322	0.07940	18.12%	-0.00532	3.86%
19.0	0.15151	0.23416	2.02190	1.51580	0.08265	54.55%	-0.50610	-25.03%
29.0	0.07464	0.06180	0.51790	-1.17189	-0.01284	-17.20%	-1.68979	-326.28%

Table 3-4: Comparison of Cornu Spiral and Fourier Transform Observation fields at distance z=200 wavelengths.

Distance along screen, wavelengths	Cornu Spiral Fresnel amplitude	Fourier transform amplitude N = 1024	Fresnel corrected phase, radians.	Fourier transform phase, N = 1024	(Fourier-Fresnel) absolute difference in amplitude	Percentage difference in amplitude	(Fourier-Fresnel) absolute difference in phase	Percentag difference in phase
0.0	1.26519	1.25512	-0.27339	-0.26684	-0.01007	-0.76%	0.00655	-2.40%
1.0	1.24590	1.24145	-0.26487	-0.26750	-0.00445	-0.36%	-0.00263	0.99%
2.0	1.18966	1.19558	-0.24006	-0.25550	0.00592	0.50%	-0.01544	6.43%
3.0	1.10055	1.11021	-0.20121	-0.21129	0.00966	0.88%	-0.01008	5.01%
4.0	0.98560	0.99018	-0.15289	-0.14391	0.00458	0.46%	0.00898	-5.87%
5.0	0.85441	0.85358	-0.10282	-0.08931	-0.00083	-0.10%	0.01351	-13.14%
6.0	0.71908	0.72237	-0.06311	-0.07035	0.00329	0.46%	-0.00724	11.47%
7.0	0.59401	0.60960	-0.05044	-0.06928	0.01559	2.62%	-0.01884	37.35%
8.0	0.49581	0.51368	-0.07925	-0.06821	0.01787	3.60%	0.01104	-13.93%
9.0	0.43831	0.43962	-0.13790	-0.09825	0.00131	0.30%	0.03965	-28.75%
19.0	0.15151	0.15537	2.02190	2.07380	0.00386	2.55%	0.05190	2.57%
29.0	0.07464	0.09386	0.51790	0.55905	0.01922	25.75%	0.04115	7.95%

This form of the integral assumes that $(x - x') << z$, and the obliquity factor is not present. This implies that the angular spectrum method gives an accurate diffraction solution only for small angles of diffraction.

It is clear why the phase of the slit case is found to have the correct value. Of course, for experimental measurements on phase-height where a phase screen model for the reflector might be applicable, the absolute phase cannot be measured. Only changes in phase can be recorded. Thus the ability of the angular spectrum method to include the phase correction is of no experimental importance.

(3) The complex correlations of the diffracted fields

The complex correlation $\rho(f)$ for a complex function $\underline{f}(x)$ is (Ratcliffe, 1956, p.210)

$$\rho(\xi) = \frac{\int_{-\infty}^{\infty} \underline{f}(x)\,\underline{f}^*(x+\xi)\,dx}{\int_{-\infty}^{\infty} \underline{f}(x)\,f^*(x)\,dx}$$

for lag ξ and zero mean value for $\underline{f}(x)$.

Digitally, the calculations of correlation are made by taking the discrete correlation

$$\rho(LAG) = \frac{1}{N-|LAG|} \sum_{I=0}^{N-|LAG|} \underline{f}(I + |LAG|).\underline{f}^*(I) \qquad LAG < 0$$

$$\rho(LAG) = \frac{1}{N-LAG} \sum_{I=0}^{N-LAG} \underline{f}(I)\cdot\underline{f}^*(I + LAG) \qquad LAG > 0$$

for the values of function $\underline{f}$ digitized at spacing $I.\Delta x$ for $I = 0, 1, 2, \ldots, N$. Finally the normalized correlation value at $x = LAG.\Delta x$ is found from

$$\rho(\text{LAG}) = \frac{\rho(\text{LAG})}{\rho(\text{LAG} = 0)}$$

(a) Comparison with Hewish's results for the phase screen.

Hewish (1951) has found an expression for the complex autocorrelation function $\rho(\xi)$. His $\kappa = \frac{1}{\lambda_{scr}}$, and with his a and b,

$$a = \Delta\phi(\cos 2\pi\kappa\xi - 1)$$

$$b = \Delta\phi \sin 2\pi\kappa\xi$$

he finds

$$\rho(\xi) = J_0(\sqrt{a^2+b^2})$$

(Hewish's original equation (4) has been corrected to the above expression in Hewish (1952)).

A calculation of this expression was made for $\Delta\phi=10$, $\lambda_{scr} = 12.8$, $\Delta x = 0.25$ (hence also the step in lag ξ) and for a maximum lag of $50\Delta x$. The complex autocorrelation for the same conditions was also calculated directly.

The correlations themselves are not graphed here, but the curves of the complex autocorrelation derived form the two methods were very similar in shape and values. There were some discrepancies between individual values for a given lag - these were less than 10% of either autocorrelation value.

The form of the complex autocorrelation, and its change with increase in $\Delta\phi$, can be seen in Hewish (1951, Fig.2).

For an incoming plane wave the spatial complex correlation function should not vary with distance (Ratcliffe, 1956, p.213). For the phase screen, this was found to be true also for the discrete correlation.

(b) Complex correlation for the slit case. In contrast to results for the phase screen, the discrete complex correlation was found to change with distance from the screen. It would take the correct form (that of a triangle wave) at the screen, but as distance increased the correlation function of the diffracted field tended to spread - fall off more slowly - with increasing spatial lag.

This effect did not depend on the number of points N in the transform. Although the diffracted field changed slightly with N, its correlation was found to be very little affected. Thus it is distance from the diffracting screen which causes the changes and not screen extent.

The reason for this is unknown. Because the slit is not of ionospheric importance, the point was not investigated. Nevertheless, it could be important in this way: the phase screen illuminated by a point source becomes a non-sinusoidal diffracting screen. Correlations obtained from fields derived by the Fourier transform method may then be inaccurate in value.

V. PERIODIC AND NON-PERIODIC SCREENS

For a waveform with an integral number of cycles within the N points of the Discrete Transform, the infinite replication implied by use of the Discrete Fourier Transform effectively creates an infinite sinusoid whose spectrum is a spike at one frequency. For this reason, the diffraction-pattern method used here is successful with sinusoidal phase screens illuminated by parallel light. The absence of "edge diffraction" problems has also been noted by Buckley (1975) for this case. The complex correlation was also found not to change with observer

distance, as expected.

For non-periodic waveforms, the waveform replication must be taken into account. Edge diffraction effects occur and increasing numbers of transform points N are needed to overcome or mitigate these. The slit, of course, is of no ionospheric importance: but the effect is important also for sinusoidal phase screens illuminated by a point source. It will be seen in Chapter 4 that edge diffraction effects become of importance, and can affect the calculation of correlations.

In the periodic case, the prediction of theory (mainly Ratcliffe, 1956) have been reproduced, which allows confidence in the method in this case. In Chapter 4, it will be seen that some care needs to be taken to obtain results of sufficient quality.

FIG 3-1 DIFFRACTION MODEL OF REFLECTING SCREEN

PHASE SCREEN :

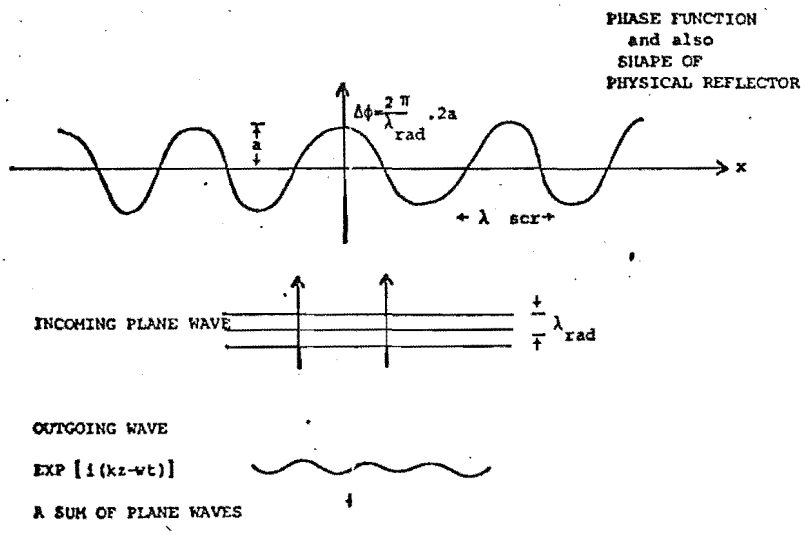

ANGULAR SPECTRUM :

SHALLOW SCREEN : $F(S) = 1.\ \delta(S-0) + i\left(\frac{\Delta\phi}{2}\ \delta(S-S_o) + \frac{\Delta\phi}{2}\ \delta(S+S_o)\right)$

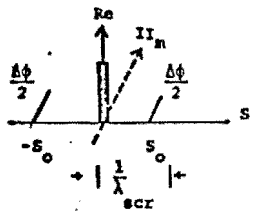

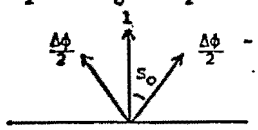

- in quadrature with 1

DEEP SCREEN : $F(S_n) = J_n(\Delta\phi).i^n.\ \delta(S-S_n)$

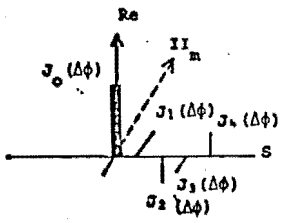

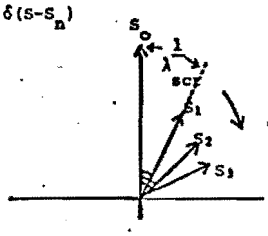

phase retardation of $\frac{\pi}{2}$ at screen wo preceding component.

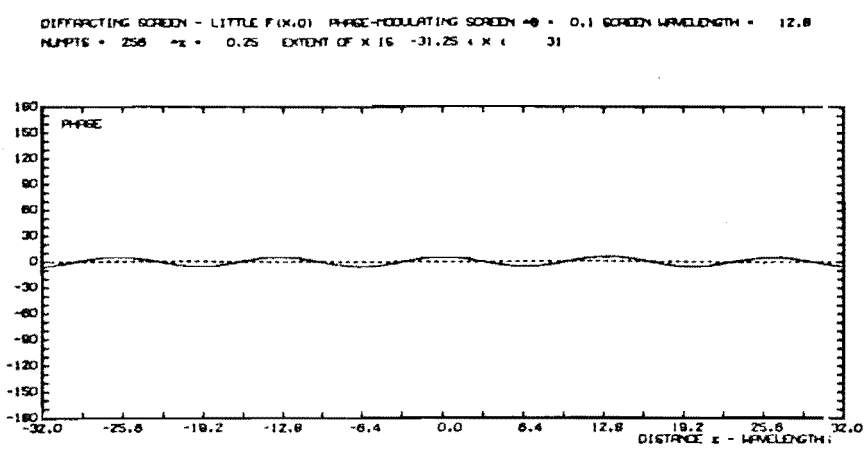

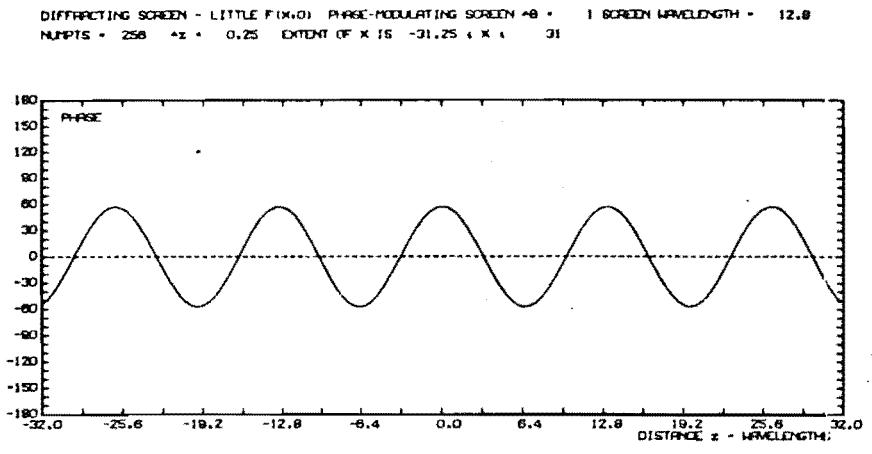

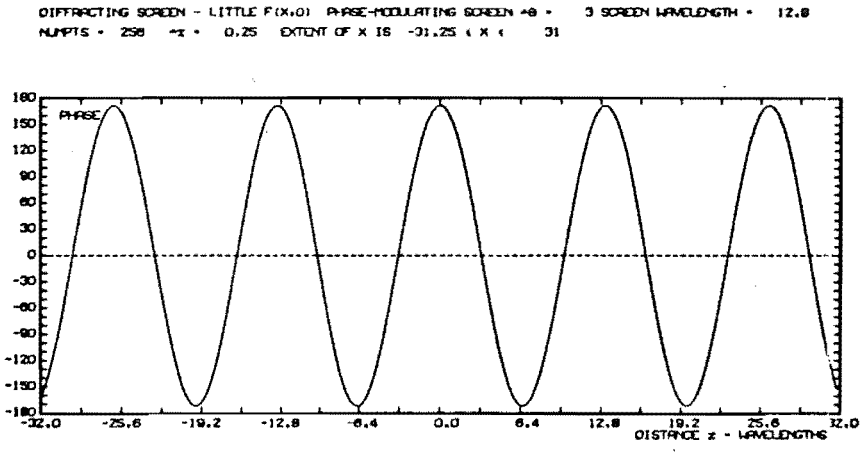

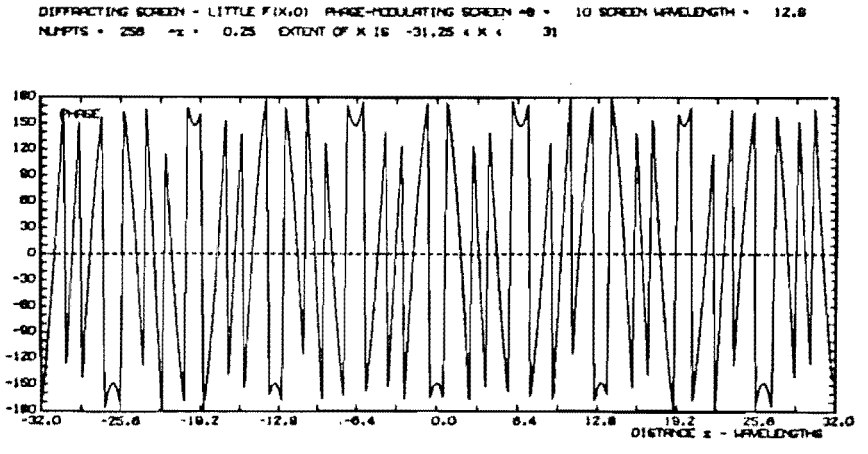

FIG.3–2 PHASE SCREENS.

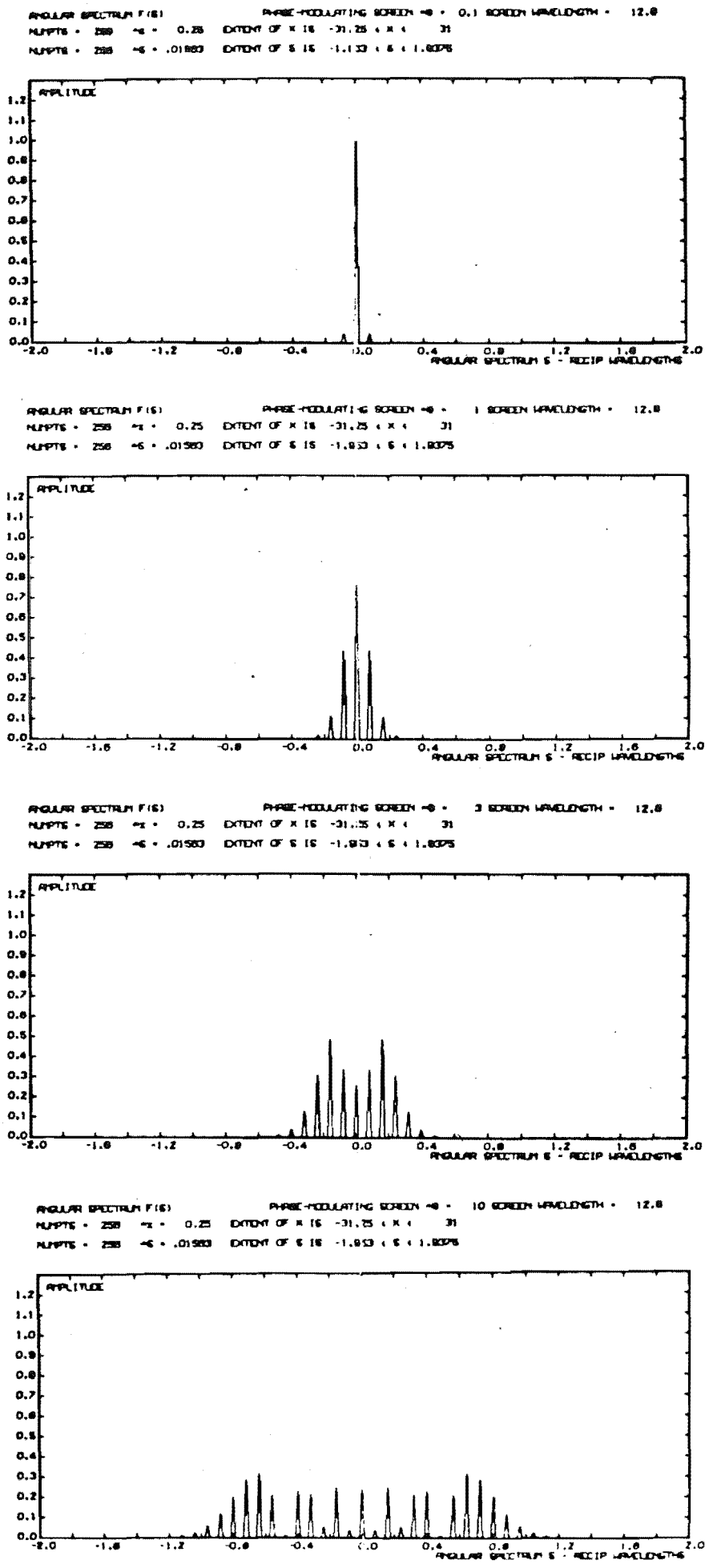

FIG.3–3. ANGULAR SPECTRA, ABSOLUTE VALUES.

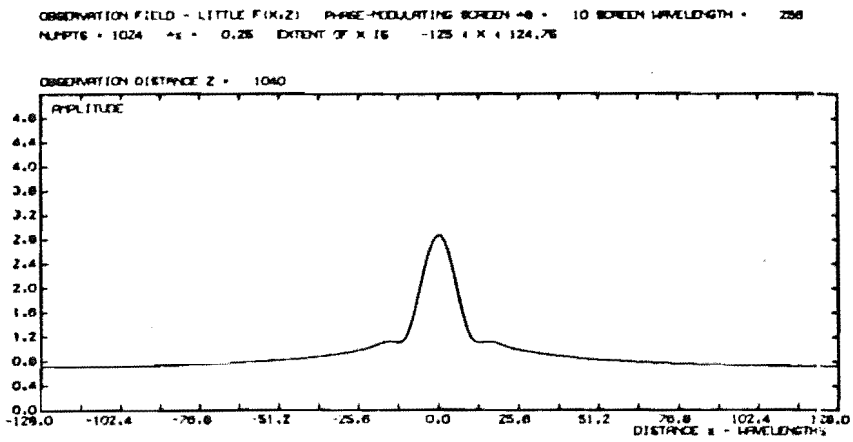

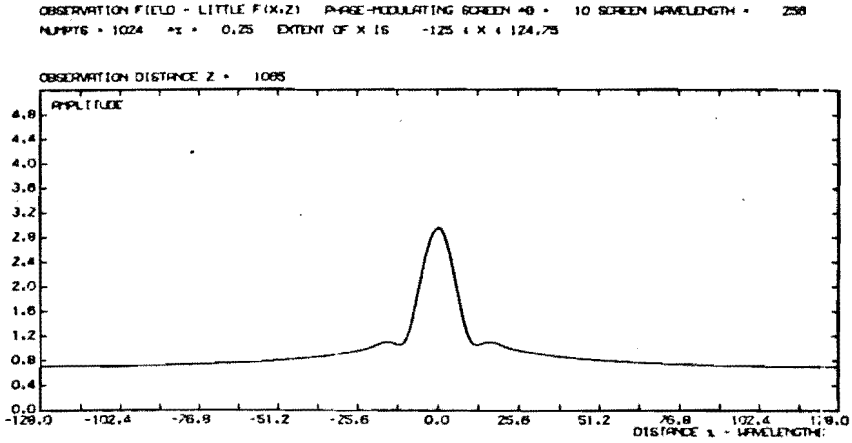

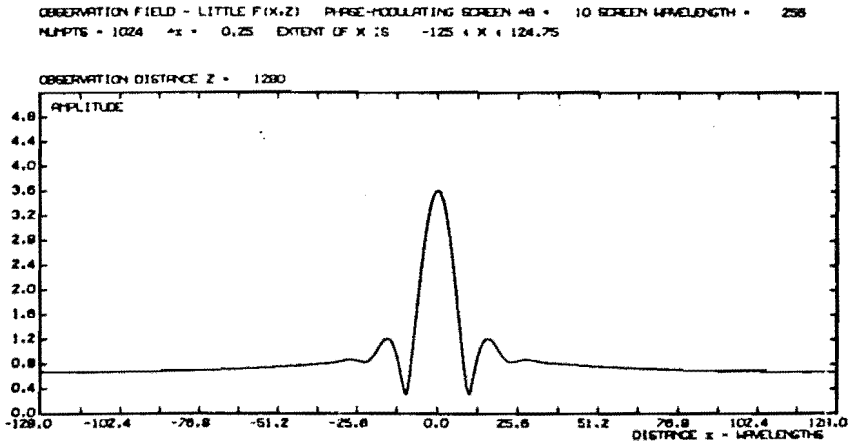

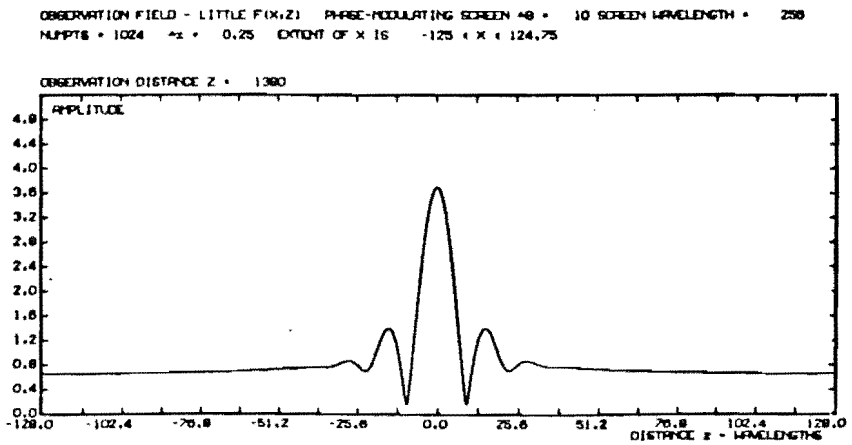

FIG 3-4 FOCUSSING-AMPLITUDE

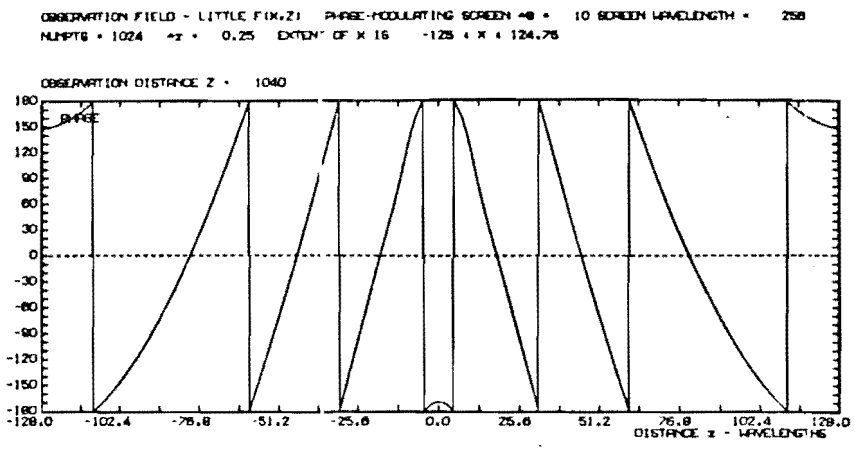

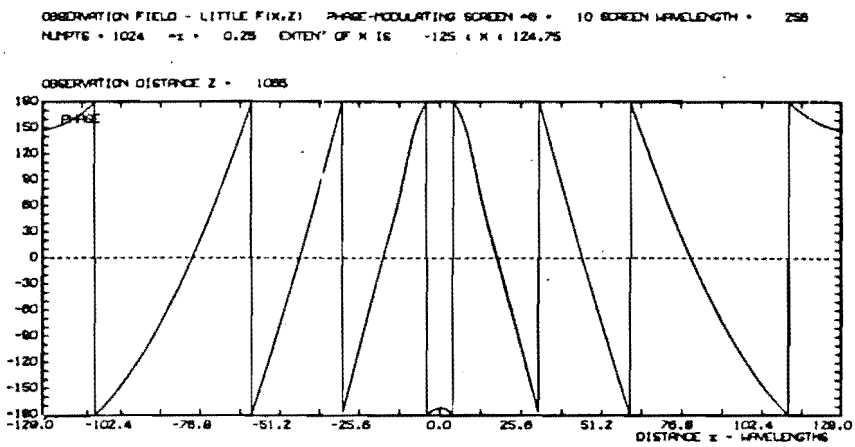

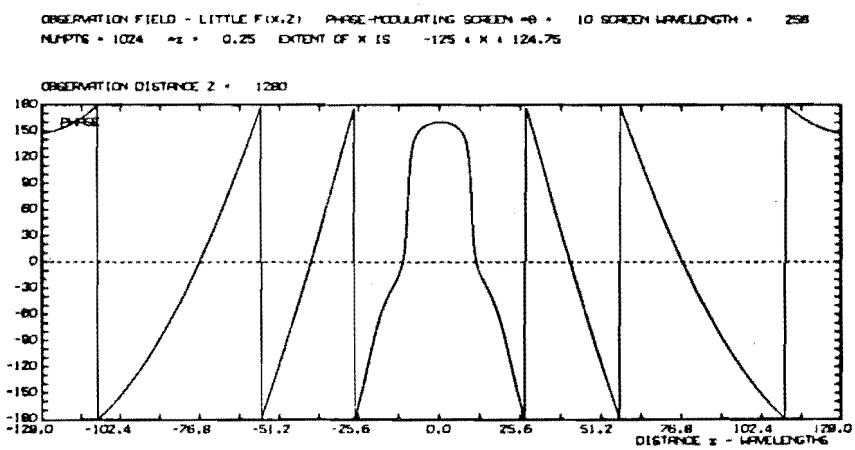

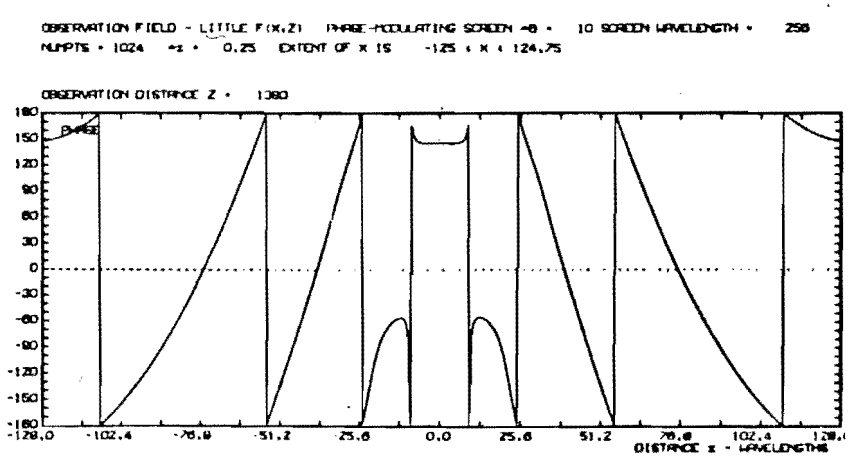

FIG 3-5 FOCUSSING-PHASE

FIG 3-6 FOCUSSING WITH DISTANCE FROM THE SCREEN

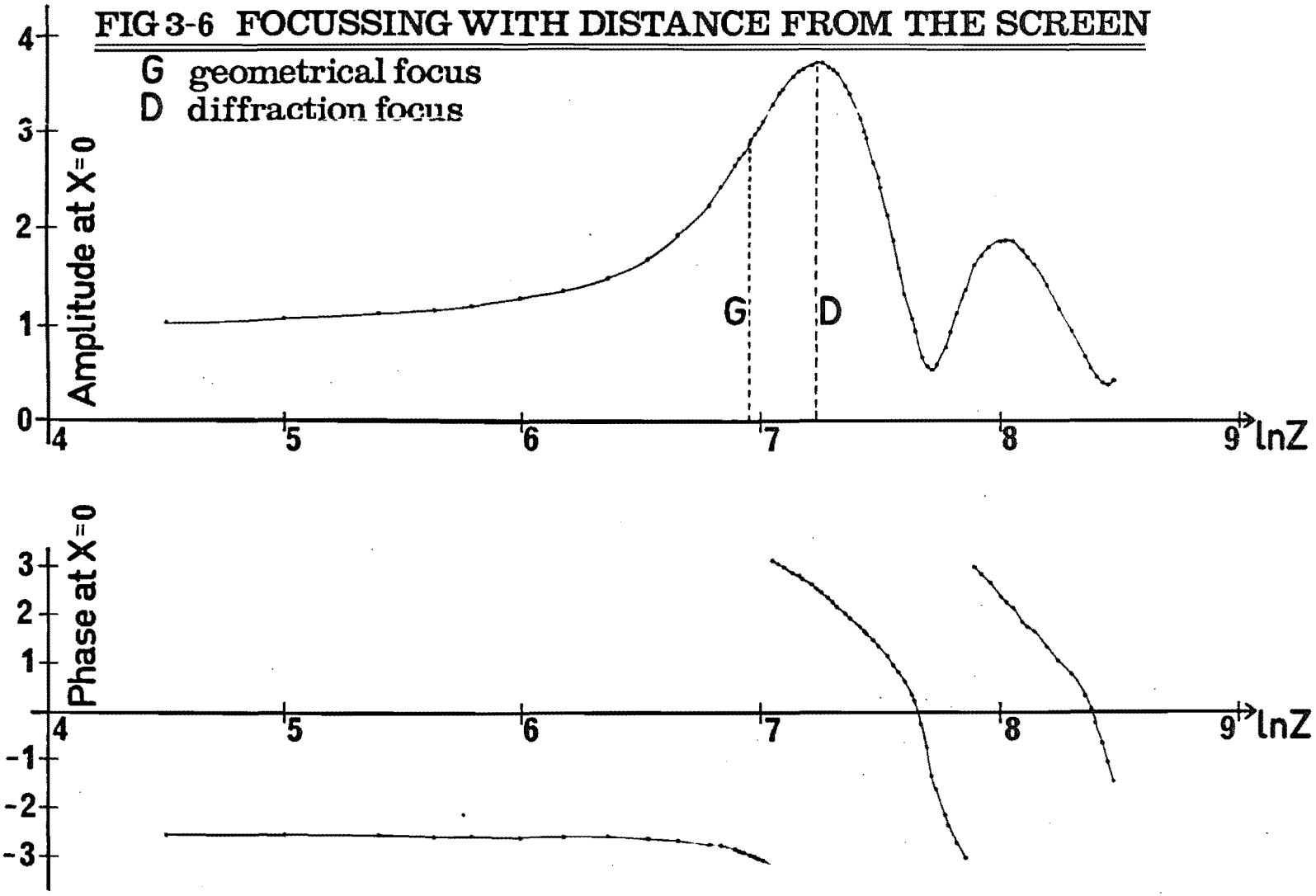

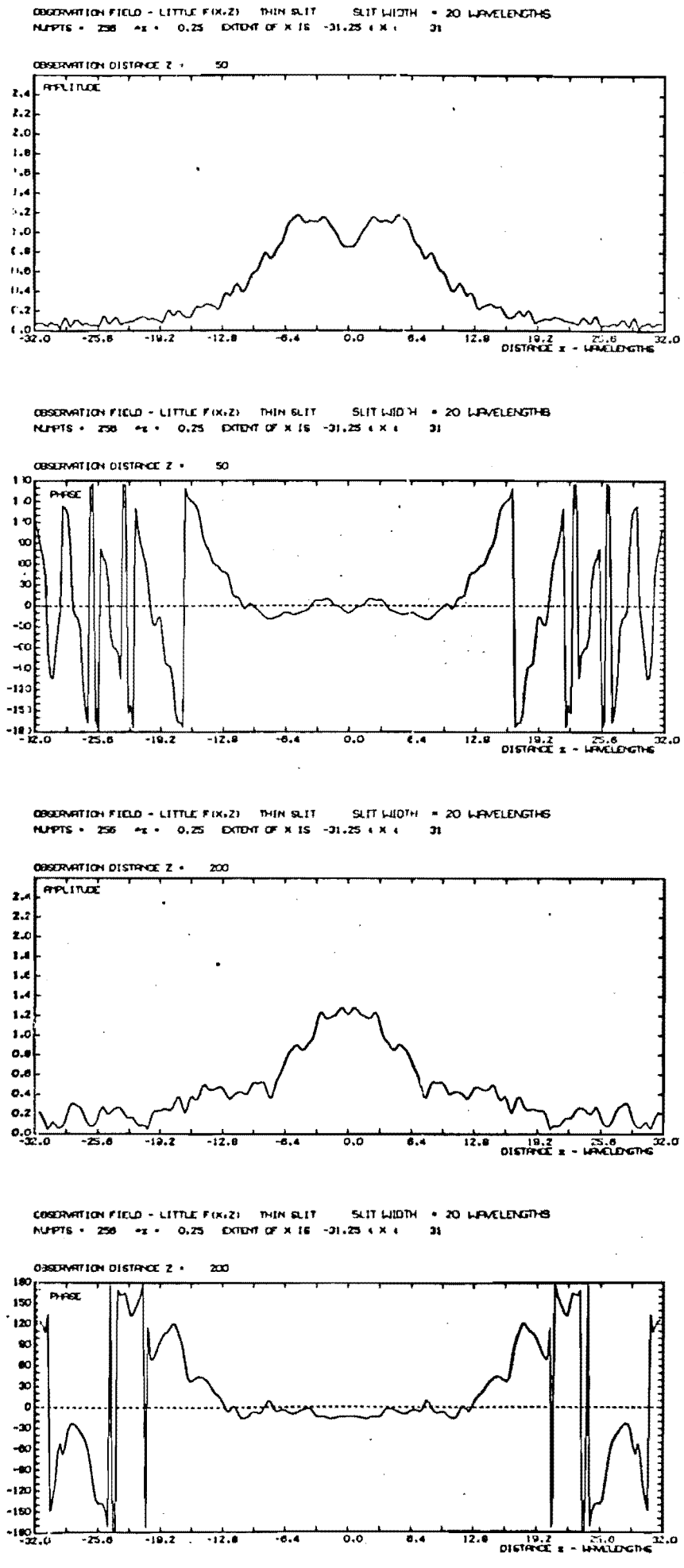

FIG 3-7 FRESNEL DIFFRACTION-THIN SLIT

CHAPTER 4

A DRIFTS EXPERIMENT SIMULATION

I. INTRODUCTION

In this chapter, the Fourier Transform method is used to find the observation fields, or ground patterns, arising from point-source illumination of a sinusoidal reflector.

An indication is given of how the parallel-light model of chapter 3 is extended to point-source illumination. Some feature of, and errors in, the method are noted. The point-source effect of the ground pattern moving at twice the speed of the reflector is successfully reproduced.

A reflector is simulated to be sinusoidal in shape, with wavelength and amplitude parameters typical of the quasi-sinusoidal isoionic contours generated by a gravity wave at low altitudes in the F-region. Eighty shifts of the reflector, by a constant amount each time, generated a timeseries of eighty points for each one of a large number of spatially-separated receivers. This information allows the calculation and comparison of spatial and temporal correlation, to see if the reflector velocity could be accurately calculated.

Differences in the velocity information given by the spatial and temporal correlations are indicated. Differences are also found in the velocity information given by complex and amplitude correlations .

II. SIMULATION OF POINT-SOURCE ILLUMINATION

1. Method of calculation:

Chapter 3 considered the illumination of a diffracting screen with parallel light. Simulation of the experimental situation is now done by locating a point transmitter at the observation-plane origin (0,z).

The transmitter is taken to emit a spherical wavefront, which becomes a circular wavefront when only one ground dimension is considered. Thus the phase-modulating screen is represented by a set of complex numbers, at a resolution Δx along the screen linear dimension x. Inclusion of the spherical wavefront is done by multiplication of each screen value $\underline{f}(x,0)$ by the factor

$$\frac{1}{(x^2 + x^2)^{\frac{1}{2}}} \cdot \exp\{2\pi i (x^2 + z^2)^{\frac{1}{2}}\}$$

with x and z again in wavelength units. The transform procedure outlined in Chapter 3 gave values for the observed ground pattern $\underline{f}(x,z)$.

2. Convergence of the calculations:

From Chapter 3 it was found that non-periodic diffracting screens gave rise to a "grating" effect due to the replication of the Discrete Fourier Transform. The interference between Fourier Transform replicas caused rapid oscillations of significant amplitude around the gross features of the calculated results. This effect may also be viewed as the result of Gibbs' oscillations arising from the truncation of the input diffraction screen.

Such effects arose with the point-source-transmitter case here. The calculation method required the screen parameters to be rather carefully chosen to obtain satisfactory answers.

For a realistic simulation, the physical parameters of the screen should be similar to those of a F-region gravity wave. Restrictions imposed *by the calculation method* were

(a) that the physical length of the screen should be large compared to the observer-screen distance, and

(b) that the resolution along the ground should be small enough to prevent aliasing of small-scale features in the ground diffraction pattern.

The parameters chosen for the simulation were as given in Table 4-1.

TABLE 4-1 DIFFRACTION SCREEN PARAMETERS

Screen wavelength	λ_{scr} = 4096 λrad = 270 km.
Screen height	h = 3800 λrad = 250 km.
Screen peak phase depth (amplitude)	$\Delta\phi$ = 1000 radians = 10.4 km.
Digital-point spacing	Δx = 2 λrad = 131 metres
Screen length	= 16384 points = 2150 km.

where λrad = 65.6 metres for a frequency of 4.57 MHz.

It will be noted that a very large number - 16384 - of points is required for successful simulation. Computational expenses were, in fact, the major limiting factor in the method's application. A conflict always existed between the requirements of long screen physical length and sufficient ground-plane resolution, and the number of points available

for the simulation. The reflector of Table 4-1 had only one reflecting point present, with resulting coherent phase. Screens with a greater phase depth give rise to a smaller-scale ground structure, requiring an increased resolution to avoid aliasing.

An application of tapers and aerial polar diagrams to the screen of Table 4-1 was tried as an attempt to reduce Gibbs' oscillations. Table 4-2 shows the results. No significant improvement to the results was noted, and for the taper window considerable degradation resulted. However, the screen of Table 4-1 was already satisfactory and it is possible that tapers and polar diagrams could improve a marginal result. This point was not followed up here.

Gibbs' oscillations were always present in the computed results and the most that could be achieved was to reduce their magnitude to a very small level. Confirmation that these oscillations did not arise as small-scale structure resulting from phase-screen depth was simply obtained by comparing the results with those arising from an increased screen depth. The spatial scale of the oscillations, superimposed on the gross results, did not alter. Thus they are true edge-diffraction effects. Additional confirmation of this arose on calculation of the transform with a smaller number of points. The same gross features were present but the amplitude of the very small-scale oscillations increased.

TABLE 4-2 METHODS TO IMPROVE CONVERGENCE

METHOD	FORMULA	RESULTS
1. Polar diagram of Transmitting antenna applied : taking antenna as a single half-wave dipole.	Amplitude $\alpha \frac{(\cos(\frac{\pi}{2}\sin\theta)}{\cos\theta}$ θ is the angle from the normal to the wire.	Negligible difference.
2. Transmitter aerials taken as m-element array at half-wavelength spacing.	Amplitude $\alpha \frac{\sin[m(\frac{\pi}{2}\sin\theta)]}{\sin[\frac{\pi}{2}\sin\theta]}$	Negligible difference, until a 100-element array was taken.
Combined with individual half-wave dipole.	$* \frac{\cos(\frac{\pi}{2}\sin\theta)}{\cos\theta}$	The 100-element array caused very noisy phase results.
3. Hanning window applied to screen.		Negligible difference.
4. Taper window applied to screen (10% taper at each end).		Considerable instability in result.

3. Some numerical results:

Fig. 4-1 and Fig. 4-2 indicate the result for a screen with parameters of Table 4-1, except that the phase depth has been increased to 1500 radians. Geometrically this corresponds to a case of multiple specular-point interference, which is reflected in the deep fading of the amplitude results. The transmitter is, as always, at (x = 0, z = 3800).

The results indicate that the model does reproduce the point-source effect. The concavity centre of the screen has been moved 40 wavelengths (x = 40) to the right of the transmitter: the shift of the amplitude to twice this distance (x = 80) is clearly seen. That the transmitter is a preferred point is seen also from the phase results: as asymmetry in phase behaviour is seen at x = 80 in Fig. 4-2.

Fig. 4-3 and Fig. 4-4 indicate likewise for the screen of phase-depth 1000 radians. The perturbation in the amplitude is very small, but the phase-changes are quite clear and show complete coherence. It is interesting to note that the shift of the phase pattern is 130 wavelengths - not the 80 wavelengths expected for the amplitude-pattern movement arising from the point-source effect - and moreover there is less obvious asymmetry arising from the fixed location of the transmitter.

Ratcliffe (1956, p234) shows that the diffraction pattern at distance z from a source at distance z is

> "similar in shape to, but twice as large as, that which would be produced at a distance ½z if the incident radiation came from infinitely distant point source."

Felgate (1970) has shown that for small angles of diffraction, movement of a general, one-dimensional screen of any form

by a distance ξ_o along the x-axis displaces the ground pattern by $2\xi_o$. This result applies for small angles of diffraction. Thus if the screen is moved by a large amount over a stationary transmitter at (0,z) the field will change in form and the concept of a doubled displacement will lose its meaning

III. THE GENERATION OF MOVING PATTERNS

1. The general method:

A review of the method of ground-pattern calculation recalls that a diffracting (always phase-modulating) screen is simulated by defining its complex value $\underline{f}(x,0)$ for a fixed number of points at spatial resolution Δx. The definition of $\underline{f}(x,0)$ includes the effect of illumination by a point-source at distance z.

The ground diffraction pattern $\underline{f}(x,z)$ is found, with values defined at a chosen number of points at spatial resolution Δx. For the simulation here, the complex amplitudes at 16384 receivers along the x-axis were found. Thus the spatial correlation of the field may be found.

If now the screen is moved by an integral number of points (at spacing Δx) a new spatial field $\underline{f}(x,z)$ may be found. Because the transmitter remains at the same point (x = 0,z) the form of the spatial field will change. Repeated movement of the screen will generate a complex-valued timeseries at each of the 16384 receivers present in the calculation. This allows the determination of time auto-correlations, and time cross-correlations between pairs of receivers.

2. Generation parameters:

The screen of Table 4-1 was chosen for this simulation, and was moved by its minimum resolution $\Delta x = 2\lambda rad$ each time, to allow the generation of 80 patterns. Table 4-3 lists the movement parameters.

TABLE 4-3 MOVING-PATTERN SIMULATION

Number of patterns generated = 80
Movement of screen each time = 1.Δx = 2.λrad = 131 metres
Total movement of screen = 160.λrad = 10.5km = (3.9%)λscr

It will be noted that for typical velocities of 100 $m.sec^{-1}$, the simulation gives about one minute's data, with points spaced about one second in time.

IV. THE DETERMINATION OF CORRELATIONS

1. Correlations available from the model:

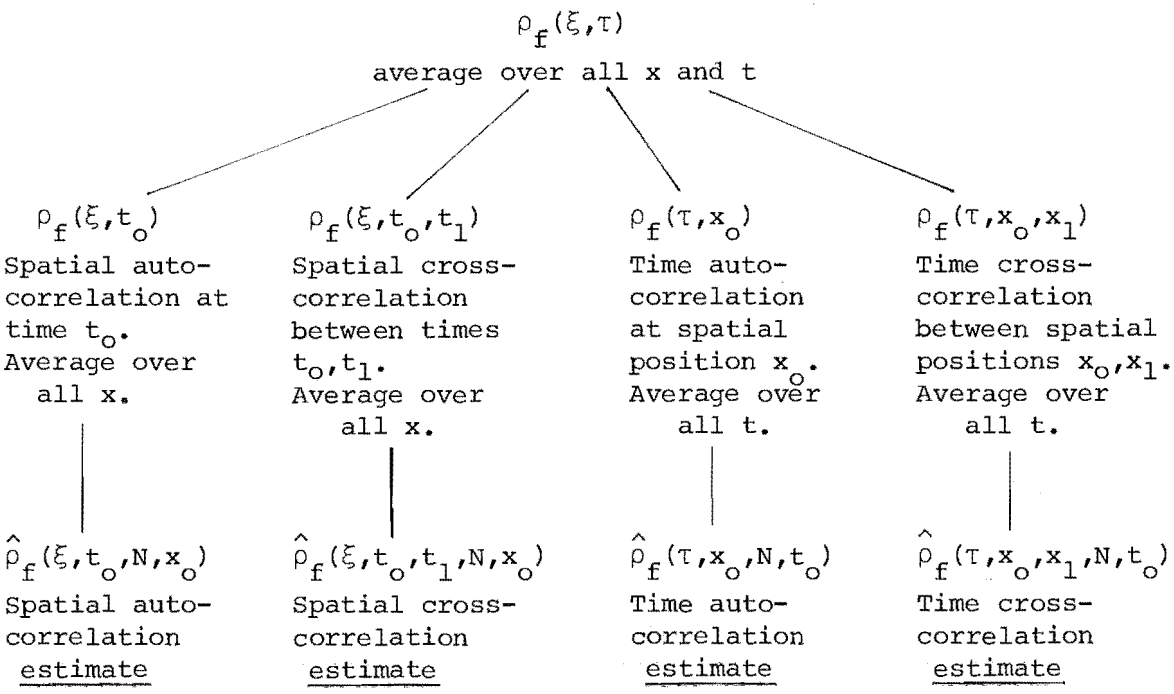

N is the finite number of ground-diffraction-pattern points taken for the correlation estimate: x_o is the data segment start for spatial correlations, and t_o that for time correlations. ρ_f is the full complex correlation of the ground pattern $\underline{f}(s,z,t)$.

The correlation estimates $\hat{\rho}$ are those obtainable from the model. Table 4-4 indicates some comments on the different $\hat{\rho}$'s. A similar scheme applies to the correlations of amplitude ρ_A and the correlations of phase ρ_ϕ.

TABLE 4.4 PROPERTIES OF THE CORRELATION ESTIMATES

CORRELATION	COMMENTS
$\hat{\rho}_f(\xi,t_o,N,x_o)$	This is the spatial autocorrelation over ground x of the field $\underline{f}(x,z,t_o)$ It is available at different times t_o, as the screen is moved. It may be calculated for different segments of the ground line x, using N points starting at $x - x_o$ It will be statistically reliable, as the number of (receiver) points in $\underline{f}(x,z)$ is very large compared to the largest lag value required.
$\hat{\rho}_f(\xi,t_o,t_1,N,x_o)$	This is the spatial cross-correlation over ground x of two different fields, $\underline{f}(x,z,t_o)$ and $\underline{f}(x,z,t_1)$
$\hat{\rho}_f(\tau,x_o,N,t_o)$	This is the time autocorrelation over time t of the field $\underline{f}(x_o,z,t)$. It is available at different places (receivers) x_o. It may be calculated for different segments of time, using N points starting at $t = t_o$. For the present model, the correlation at log values ≥ 16 will not be very reliable, as with only 80 times available a log of 16 is 20% of the data length.
$\hat{\rho}_f(\tau,x_o,x_1,N,t_o)$	This is the time cross-correlation over time t of two different timeseries: $\underline{f}(x_1,z,t)$ with $f(x_2,z,t)$ The short length of the timeseries will not allow a reliable estimate of maximum cross-correlation position; if the receiver separation is so large as to make the appropriate lag value exceed, or be a substantial proportion of, the timeseries length.

(2) The correlation analysis of moving patterns:

The correlation analysis of Briggs, Phillips and Shinn (1950) and Phillips and Spenser (1955) allows the determination of speed and direction parameters of a moving random pattern, together with a measure of the random change in the pattern as opposed to the steady drift in the pattern.

The velocity parameters are obtained normally by measurement of the ground pattern at three spaced receivers over a period of 1-3 minutes. Computation of the time autocorrelations of the amplitudes at the three receivers and of the time cross-correlations between pairs of receivers permits, subject to certain assumptions, an estimate to be made of speed, direction, and pattern-randomness parameters.

Another approach (Briggs, 1968a) to the determination of pattern speed, direction, and random change is to use of the spatial auto- and cross-correlations. This method requires the presence of a large array of receivers spaced over the ground, to permit measurement of the pattern at many spatial points.

In previous sections of this chapter, a moving reflector model has been developed and ground patterns ("observation fields") calculated. Such ground patterns will maintain their general form as the reflector moves, but will change form in detail as a result of the point-source illumination. The correlation analysis - in one ground dimension - is here applied to these ground patterns to obtain velocity and randomness parameters for them.

The approach to the correlation analysis of a one-dimensional ground pattern is here presented briefly: it follows that of Briggs (1968a) and is presented to indicate

the later treatment of the generated patterns.

Let A(x,t) be a random (amplitude) function moving at velocity V along the X-axis and changing in form as it moves (Figure 4-5). Following Briggs (1968a), it is apparent that an observer in the co-ordinate system $0'x_v$ moving with velocity V along the X-axis will see charges arising only from

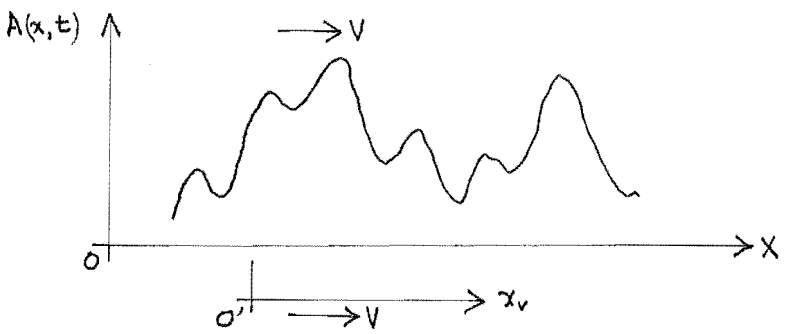

FIGURE 4-5 A DRIFTING RANDOMLY-CHANGING PATTERN

random changes in the pattern. This observer can make observations at spaced points and separated times; and obtain the "space-time" correlation of the "stationary" pattern, as

$$\rho(\xi_v,\tau) = \langle\{A(x_v,t) - \langle A\rangle\}\{A(x_v+\xi_v,t+\tau) - \langle A\rangle\}\rangle$$

assuming unit variance for A.

It is assumed (as in Briggs, Phillips, and Shinn, 1950) that the contours of $\rho(\xi_v,\tau)$ = constant are similar concentric ellipses centered on the origin. Close to the origin any function of two variables will have elliptical contours: the assumption made here is that the constant-correlation contours remain elliptical for low values of correlation far from the origin. Briggs (1968a) notes also that the assumption of elliptical contours also includes the assumption that the spatial and temporal correlation functions have the same shape.

With elliptical contours for $\rho(\xi_v,\tau)$ the functional form is

$$\frac{\xi_v^2}{d^2} + \frac{\tau^2}{\tau_c} = \text{constant}$$

where d is a characteristic length and τ_c a characteristic time scale. From this, a measure of pattern randomness may be obtained: it is the *random velocity* V_c given by

$$V_c = \frac{d}{\tau_c}$$

and is the ratio of space shift to time shift producing the same value of correlation.

A stationary observer will observe time-changes that arise from two causes: those from the steady pattern drift and those from the pattern random changes (Briggs, 1968a).

The patterns generated by the moving reflector model are analysed, to see what values of steady drift V and random velocity V_c are obtainable from the correlation alanysis. These values will be compared with the velocity of the moving screen.

(3) Spatial correlation results:

(a) The determination of spatial correlations. From the description of the method given previously, it will be recalled that a ground pattern measured at 16384 receivers is obtained for each calculation. This allows the calculation of a spatial auto-correlation function. Movement of the reflector and calculation of the ground pattern allows another spatial auto-correlation function to be found: moreover a spatial cross-correlation function between the two ground patterns may be found.

The discrete spatial correlations are calculated over 240 points. This is equivalent to 31.5 km at λ_{rad} = 65.6 m. It will be noted that this takes the spatial correlations over a far longer distance than that of the Buckland Park

aerial array at Adelaide, Australia. The normalization used was $\frac{1}{240-|\tau|}$.

Both complex and amplitude correlations are taken, to examine the difference in results.

(b) Analysis of the spatial correlations. The analysis follows that of Briggs (1968a). The spatial cross-correlation between two ground patterns, measured at times separated by a time interval Δt, will have a maximum for some space shift ξ'. From the assumption of elliptical contours of correlation, it may be shown (Briggs, 1968a) that the true velocity V is

$$V = \frac{\xi'}{\Delta t} \quad .$$

The maximum value of cross-correlation $\rho_m = \rho(\xi', \Delta t)$ will in general be less than unity since the ground pattern changes as it moves. If ξ_m is the value of ξ for which the spatial autocorrelation function has value ρ_m, then it may be shown that the random velocity V_c is

$$V_c = \frac{\xi_m}{\Delta t} \quad .$$

(c) Amplitude spatial correlation results. Fig. 4-6 indicates the correlation for an unshifted screen (with the concavity over the transmitter) and for a screen shifted by 394 m: three spatial resolution distances. Fig. 4-7 does likewise for an unshifted screen and for one shifted by 2495 m: nineteen resolution distances.

The auto-correlations near lag zero exhibit a very small-scale oscillation. This is thought to arise from the Gibbs' oscillation. For small screen movements, the presence of these oscillations made velocity estimations unreliable.

However, Table 4-5 indicates the cross-correlation peak to fall sharply in value as time progresses and the screen is moved by a greater amount.

TABLE 4-5 AMPLITUDE SPATIAL CORRELATION PARAMETERS

Screen displacement, metres	Pattern half-displacement, metres	Cross-correlation maximum ρ_{max}
131 ($1\Delta x$)	-	.964
394 ($3\Delta x$)	-	.943
1050 ($5\Delta x$)	-	.877
2495 ($19\Delta x$)	1575	.699

Where no pattern half-displacement is shown, it could not be reliably estimated. The spatial (and lag) resolution Δx = 131 metres at a radio frequency of 4.57 MHz. If the moving refelctor is taken to move with velocity 131 $m.sec^{-1}$, then

$$V_{true} = \frac{1575 \text{ metres}}{19 \text{ seconds}} = 83 \quad m.sec^{-1}$$

and

$$V_c = \frac{2232 \text{ metres}}{19 \text{ seconds}} = 117 \quad m.sec^{-1}$$

as the auto-correlation of the unshifted reflector has value .699 at Lag 2232 metres. The point source effect requires the "true" velocity of the pattern to be divided by two to obtain V_{true}: the pattern velocity V is twice V_{true} and

$$\frac{V_c}{V} = .71 \ .$$

It is apparent that the "true" velocity obtained bears little relation to that of the reflector and that there would seem to

be a considerable random component. However, the sinusoidal reflector model of Hines (1975, unpublished) considers the signal returned from a sinusoidal reflector illuminated from a point source. The (single) specular point moves on the reflecting surface as the reflector moves, and its velocity is (Hines, 1975, unpublished).

$$V^* = \frac{V}{(1 + \frac{1}{S})}$$

where $S = a\,k^2h$ with a reflector peak amplitude, h the height, and $k = \frac{2\pi}{\lambda_{scr}}$ with λ_{scr} the reflector wavelength. The velocity of the projection of the specular point on the ground for the case here is $V^* = 77\ m.sec^{-1}$.

From this case it appears possible that V_{true} may be a better measure of the specular point ground velocity, than that of the reflector velocity. The expense of the method precluded a check of this point for other cases.

(d) Complex spatial correlation results. Fig. 4-8 indicates the complex spatial correlation result for an unshifted screen, and for one shifted by 394 m. (Fig. 4-9 does likewise for a screen shift of 1050 metres.) No simple relation to the amplitude auto-correlations is apparent: this is to be expected as the signal from a reflector is not randomly phased. A shape similar to $\frac{\sin x}{x}$ can be seen: this was seen to widen with screens of smaller peak amplitude (or phase drift) and narrow at greater peak amplitude. The spatial auto-correlations scale here is about 1 km which is twise the scale $\frac{2\lambda_{scr}}{\Delta\phi} = 540$ m expected from the point-source effect.

It was of interest to deduce a V_{true} from the complex spatial cross-correlation peak. The results are quite different

from those for the amplitude correlations and are given in Table 4-6 below.

TABLE 4-6 COMPLEX SPATIAL CORRELATION PARAMETERS

Screen displacement, metres	Pattern half-displacement, metres	Cross-correlation maximum ρ_{max}	V_{true} $m.sec^{-1}$	V_c $m.sec^{-1}$
131 (1Δx)	230	1.0	230	0
394 (3Δx)	706	1.0	235	0
1050 (8Δx)	1888	.99	236	0
1838 (14Δx)	3249	.99	232	4.7
2495 (19Δx)	4400	.95	231	8.3

V_{true} is again half the pattern velocity V, to allow for the point-source effect. It is seen that although the values are very stable over time, they bear no relation to the reflector of specular-point volocity. At large shifts a "random" velocity component is present, but in comparison to those obtained for the amplitude correlations, the value is very small.

Fig. 4-8 indicates little change in complex spatial auto-correlation between shifted screens; moreover the complex spatial cross-correlation peak value remains very close to unity until large reflector movements are reached. If the complex correlation is understood as the *vector* sum of lagged products, then by the Fourier-Transform shift theorem one expects the effect of a screen shift to be predominantly changes in phase rather than in amplitude. This in fact

THE LIBRARY
UNIVERSITY OF CANTERBURY
CHRISTCHURCH, N.Z.

is what is seen.

Use of the complex spatial cross-correlation to obtain a "true" pattern velocity gave a poor result for the case taken.

(4) Temporal correlation results.

(a) The determination of temporal correlations. For each determination of a ground pattern, an amplitude-and-phase ground pattern value is obtained for each of 16384 receivers. Repeated movement of the ground pattern generates a separate timeseries at each receiver. From these the time auto-correlations at each receiver and the time cross-correlations between receivers may be found.

Eighty patterns were generated, giving a timeseries at each receiver of eighty points. This is a rather short length for correlation analysis, but computational expenses forbade longer timeseries. In general correlation values for absolute lag values greater than 16 were not taken as very reliable. The normalization $\frac{1}{N-|\tau|}$ was used throughout.

(b) Analysis of the temporal correlations. The temporal correlations available were the auto-correlation at each receiver, and the cross-correlation between a given pair of receivers at a known spacing.

It is useful to repeat some pattern velocity definitions from Briggs, Phillips, and Shinn (1950) and Briggs (1968a).

The *true velocity* V of the pattern is that found by an observer moving with the pattern along the ground so as to observe minimum fading. The residual variations arise from random fading, expressed by the *random velocity* V_c parameter.

This is simply the ratio of space shift to time shift producing the same change in correlation for the observer moving with velocity V. Our interest here is to deduce the values of V and V_c from the model correlations.

The *apparent velocity* V' of the pattern is the velocity with which pattern appears to be moving. It is found from the value of the time-lag τ' of maximum cross-correlation between two receivers of known spacing $\Delta\xi$. From the definition,

$$V' = \frac{\Delta\xi}{\tau'} \quad .$$

The final definition is that of the *fading velocity* V'_c. It is the ratio of space shift to time shift producing the same change in the value of correlation. It becomes the random velocity for an observer moving at the drift velocity V. Thus if $\rho(x_o,0) = \rho(0,t_o)$,

$$V'_c = \frac{x_o}{t_o} \quad .$$

The temporal correlations were used to obtain V and V_c. To do this, some relationships between V, V_c, V' and V'_c given in Briggs, Phillips, and Shinn (1950) and Briggs (1968a) are quoted and used to find V and V_c from V' and V'_c.

It is shown in Briggs (1968a) that from the assumption of elliptical contours of correlation, the time-lag τ' for maximum cross-correlation is given by

$$\tau' = \frac{\Delta\xi \cdot V}{(V^2+V_c^{\,2})}$$

from which

$$V' = \frac{\Delta\xi}{\tau} = V + \frac{V_c^{\,2}}{V}$$

or

$$VV' = V^2 + V_c^{\,2}$$

or

$$(V_c')^2 = V^2 + V_c^2$$

(since $(V_c')^2 = VV'$ by Equation (15) of Briggs, Phillips, and Shinn (1950)).

Physically, the fading velocity effect arises from both steady drift and random-change effects, as expected.

V' is found from the cross-correlation maximum. V_c' is found as follows: the cross-correlation $\rho(\Delta\xi,0)$ between the two records gives the effect of a pure space shift $\Delta\xi$. If τ_s is the time-lag of the auto-correlation $\rho(0,\tau)$ such $\rho(0,\tau_s) = \rho(\Delta\xi,0)$, then $\rho(0,\tau_s)$ gives the effect of a pure time-shift producing the same change in correlation as the space shift $\Delta\xi$. So

$$V_c' = \frac{\xi_o}{\tau_s} .$$

Then $$V = \frac{(V_c')^2}{V'}$$

and

$$V_c^2 = (V_c')^2 - V^2 .$$

In this way V' and V_c' are found from the calculated correlations, and V and V_c are derived from them.

(c) Amplitude temporal correlation results. The time spacing between measurements is taken as one second. The reflector movement between calculations, which is $\Delta x = 2\lambda_{rad}$ = 131 metres; becomes a velocity of 131 $m.sec^{-1}$.

Fig. 4-10 indicates the amplitude temporal correlations for a pair of receivers at a spacing of 6565 metres, and Fig. 4-11 the same for spacing 13129 metres. Fig. 4-12 displays the correlations again for a spacing of 6565 metres, but for

receivers located at 6565 and 13129 metres from the transmitter. The changed nature particularly of the cross-correlation between Fig. 4-10 and 4-12 is apparent.

Table 4-7 below indicates the summarized results. The first column shows the receiver pair between which cross-correlations were taken: the receiver separation in metres is also shown.

The lag-position and value of the cross-correlation maxima are shown. In some cases the cross-correlations are rather skewed. For these cases, the lag-position and cross-correlation value of the mid-point between the two zero crossings of the cross-correlation are shown also.

It will be noted that for many cases the cross-correlation maximum is at lag zero. For the cases where it is non-zero, the apparent velocity, V' is found and tabulated in Table 4-7.

The cross-correlation value at lag zero, $\rho(\Delta\xi,0)$ allows the determination of τ_s with $\rho(0,\tau_s) = \rho(\Delta\xi,0)$. V'_c is thus found. The true velocity V and random velocity V_c are found and tabulated in Table 4-7.

The receiver spacings taken are far larger than those used in the conventional spaced-receiver drifts experiment. This arose primarily because no useful result could be obtained for adjacent receivers at 131-metre spacing. Useful results of apparent velocity do not become available until a spacing of 6 km is reached.

Theoretical analyses (e.g., Felgate, 1970) have indicated that a diffracting screen or reflector movement by a certain amount x will result in the movement of the pattern on the ground by 2x. The failure of the method used here to confirm this most probably from the low spatial (and so time)

resolution employed, and the use of very short timeseries implying the presence of fewer than two fades.

Table 4-7 does indicate, however, that for larger receiver spacings the cross-correlation maximum value for amplitudes does fall off as receiver spacing is increased. This indicates a change of form of the ground diffraction pattern as the reflector moves, because the transmitter remains as a preferred point. Indicated also is the fact that the velocities deduced bear little relation to (twice) that of the reflector, and moreover even for identical receiver spacing the values depend upon the location of the receiver pair along the ground. The imaginary values of V_c indicate that the assumption of elliptical contours for the correlation $\rho(\xi,\tau)$ is not valid for this case.

TABLE 4-7 AMPLITUDE TEMPORAL CORRELATION PARAMETERS

Receiver Pair	Receiver Separation, metres	Position of maximum lag seconds	Cross-Correlation maximum ρ_{max}	Apparent Velocity V' $m.sec^{-1}$	Random Velocity V_c $m.sec^{-1}$	Drift Velocity V $m.sec^{-1}$	Lag of zero-midpoint seconds	Cross-Correlation value at midpoint
0 5	656	0	.992	-	-	-	0	.992
0 10	1313	0	.989	-	-	-	1	.965
0 20	2626	0	.986	-	-	-	1	.946
0 50	6565	0	.868	-	-	-	7	.848
0 100	13129	41	.705	320.2	0.0 Im	320.2 404.3	-	-
50 100	6565	30	.50	218.8	Im Im	247.7 287.0	-	-
100 150	6565	6	.82	1094.2	Im 54.6	1456.7 520.4	-	-
150 200	6565	0	.97	-	-	-	2	.938

1. The left-hand subcolumns of V and V_c give values arising for use of the auto-correlation at the first receiver.

   The right-hand subcolumn values arise from use of the auto-correlation at the second receiver.

2. The designation "Im" for V_c indicate that $V^2 > (V'_c)^2$, so that V_c^2 became negative.

(d) Complex temporal correlation results. Fig. 4-13 indicates the comples temporal correlation for a receiver spacing of 2626 metres: Fig. 4-14 for a receiver spacing of 6565 metres. Table 4-8 shows the summarized results.

TABLE 4-8 COMPLEX TEMPORAL CORRELATION PARAMETERS

Receiver Pair		Receiver Separation, metres	Position of maximum lag seconds	Cross-Correlation Maximum ρ_{max}	Apparent pattern velocity V, $m.sec^{-1}$	Random Velocity V_c, $m.sec^{-1}$	Pattern Drift Velocity V, $m.sec^{-1}$
0	5	656	2.5	.96	262	0	262
0	10	1313	5.0	1.00	262	0	262
0	20	2626	10.0	1.01	262	0	262
0	50	6565	25.0	1.03	262	0	262
0	100	13129	50.0	1.09	262	0	262
50	100	656	25.0	1.04	262	0	262
100	150	656	25.0	1.03	262	0	262
150	200	656	25.0	1.01	262	0	262

For all cases the deduced true velocity $V_{True} = 131\ m.sec^{-1}$. This in fact is the speed of the reflector. The point-source effect is clearly operative here. No decrease of the cross-correlation peak value below unity is observed: values greater than unity arise from the use of normalization $\frac{1}{N-|\tau|}$.

It will be noted also that the speed obtained does not depend on the spatial position of the receiver pair in the array.

V. CONCLUSIONS

The determination of spatial and temporal correlations from ground diffraction patterns resulting from point-source illumination of a moving sinusoidal reflector has enabled the calculation of ground-pattern velocity parameters by several different methods. These have been compared with each other, and with the true velocity of the reflector.

The spatial correlations were calculated over a ground distance of 31.5 km. Calculation over a shorter distance, such as one comparable with the diameter of the Buckland Park aerial array, would have required the use of only ten points in the correlation calculation. The complex correlation magnitude was found to have about the right scale $\ell = \frac{2\lambda_{scr}}{\Delta\phi}$ expected to arise from the point-source effect; and gave very consistent apparent velocities which, however, bore no obvious relationship to the reflector velocity.

Because the angular spectrum is not randomly phased, no straightforward connection exists between spatial complex and amplitude correlation. The velocity results arising from the amplitude correlations include a substantial random velocity component, reflecting the change in form of the pattern as it moves. For the one case analysed, the "true" velocity bore little relation to that of the reflector, although it was close to the ground velocity of the (single) specular reflection point present. It is not known whether this is true in general.

The spatial correlation analysis of Briggs (1968a) was designed to find the velocities of random patterns, so that the unsatisfactory results arising here for a reflector movement of 3.9% of its total wavelength is not

surprising. The sinusoidal reflector model is not a complete description of the diffraction process. This is illustrated by the F-region correlation data of Kelleher (1966b) who often obtained oscillatory amplitude spatial correlations but steadily-decreasing temporal correlations - features not reproduced by the model correlations here.

Large-scale ground diffraction patterns of the type discussed here are only one type - albeit the predominant type from the F-region - of ground diffraction pattern possible. Other types of patterns measured over space using the Buckland Park aerial array (Felgate and Golley, 1971) are the random patterns anticipated by the analysis methods of Briggs, Phillips, and Shinn (1950), and fringe patterns arising from the interference of more than one specular reflection point on the reflector.

The temporal correlations were found from a rather short timeseries of eighty points. The reflector was shifted by the minimum resolution distance Δx (=131 metres at 4.57 MHz), so with time interval taken as one second, the reflector velocity becomes 131 $m.sec^{-1}$.

The amplitude auto-correlations were found to fall to 0.5 in about 10 seconds. The receiver spacings used for the determination of cross-correlations exceed those normally used for the close-spaced antenna drift experiment by a factor of about 50. The differences in auto-correlations between the spaced receivers reflect the change in form of the pattern as the reflector moves.

The apparent velocity values for the pattern movement could not be determined until a receiver spacing of 6 km was reached. This disagrees with theoretical results and

is most probably a result of comparatively poor spatial resolution, of short timeseries, and of a small number of fades. Even where results are available, the apparent velocities differ for different receiver spacings, and for different locations of a receiver pair with a given spacing.

These results contrast with those of Guha and Geller (1973) who found that for one moving sinusoidal reflector, excellent agreement was obtained between the true reflector velocity and (half) the apparent drift velocity. However, several fades were present within the time-scope of their correlations. This contrasts with the case here, where the reflector moves by only 3.9% of its wavelength for the time over which the correlation is taken. The scale of the ground-pattern amplitude is such that only one, incomplete fade is available for correlation, and an accurate velocity determination cannot be expected.

The most interesting result of this chapter is the correct determination of the reflector velocity by the complex temporal correlation. This result was obtained over a reflector shift of only 3.9% of its wavelength. It is not known whether this result is true in general, or whether it would apply over other portions of the wave cycle. All the results of this chapter are empirical numerical results, and a theoretical investigation of this point would be a valuable further investigation.

It must be noted again that correlations arising from experimental data do differ from those predicted by a sinusoidal reflector model. It is thus not a complete description of the reflection process.

The Fourier Transform method used here to calculate

ground patterns is, in principle, very simple. In practice, it was found excellent for calculations with incoming parallel light, but subject to convergence problems otherwise. Restraints on computer memory availability lead to a potential conflict between convergence and resolution requirements. This factor also reduced the number of calculations possible, and hence an examination of correlation behaviour in other parts of the reflector wave cycle.

With the exception of use of the complex temporal correlation, correlation analysis appears to be unable to give useful velocity estimates for the ground patterns arising from very large-scale structures. An expected feature that is seen is the change in form of the ground pattern as it moves in space, owing to the stationary position of the illuminating transmitter.

FIG 4-1

OBSERVATION FIELD - LITTLE F(X,Z) PHASE-MODULATING SCREEN $\Delta\theta$ = 1500 SCREEN WAVELENGTH = 4096

NUMPTS = 16384 Δx = 2 EXTENT OF X IS -250 < X < 248

OBSERVATION DISTANCE Z = 3800 CURVED WAVEFRONT X SHIFT IS 40

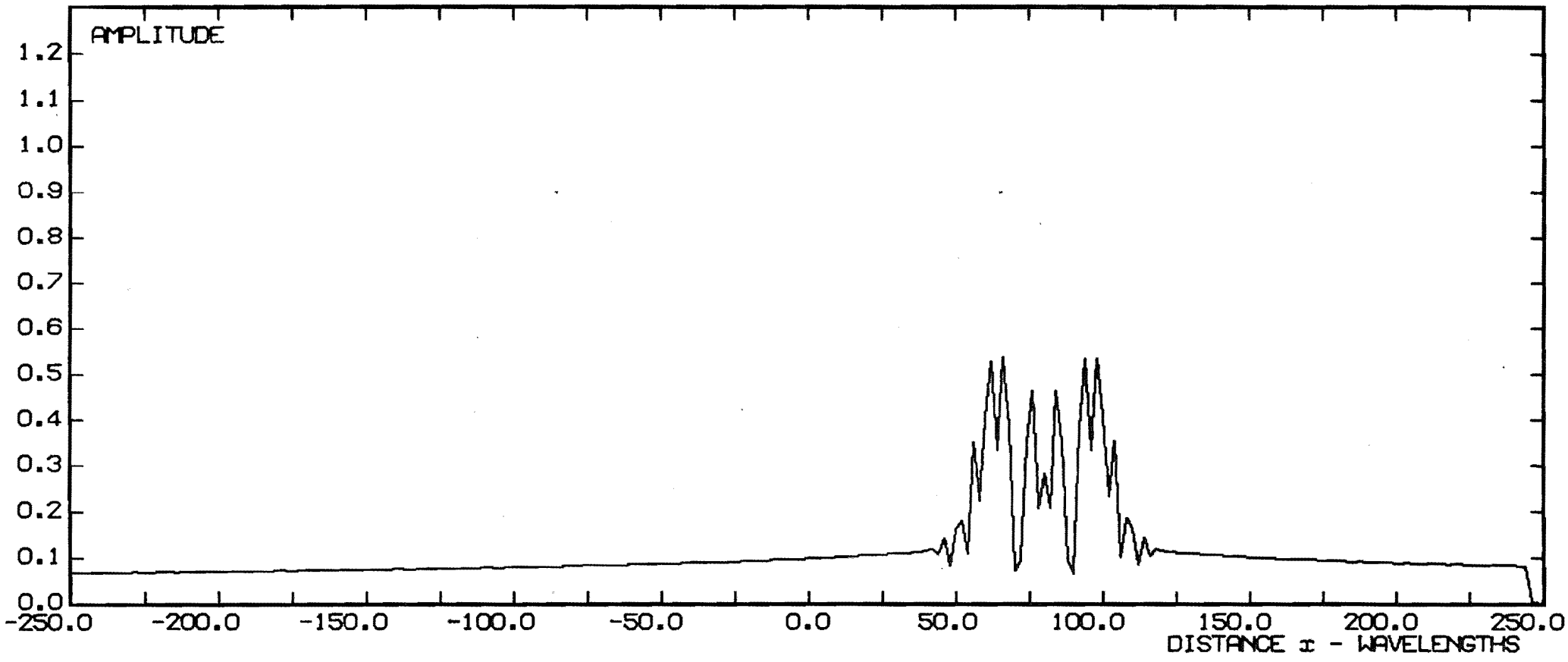

FIG 4-2

OBSERVATION FIELD - LITTLE F(X,Z) PHASE-MODULATING SCREEN $\Delta\theta$ = 1500. SCREEN WAVELENGTH = 4096

NUMPTS = 16384 Δx = 2 EXTENT OF X IS -250 < X < 248

OBSERVATION DISTANCE Z = 3800 CURVED WAVEFRONT X SHIFT IS 40

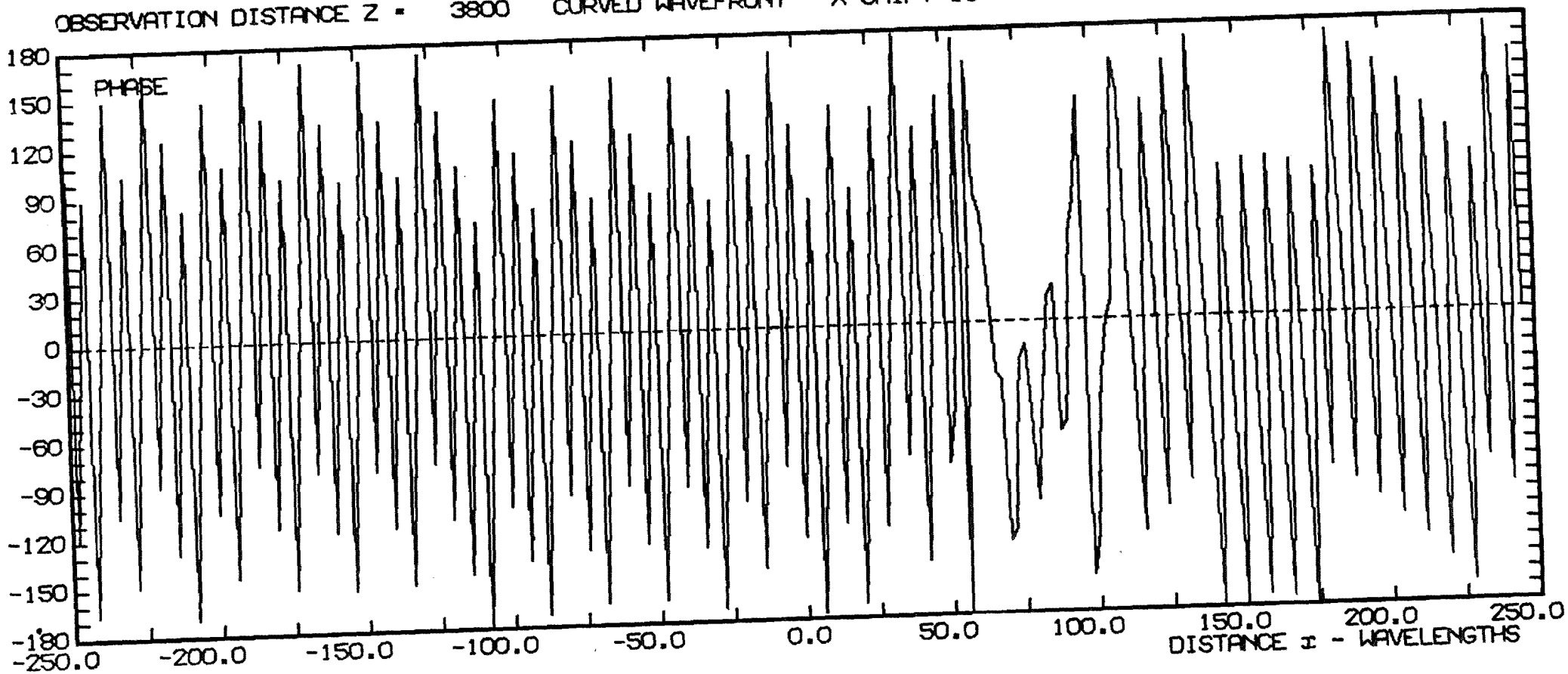

FIG 4-3

OBSERVATION FIELD - LITTLE F(X,Z) PHASE-MODULATING SCREEN ΔΘ = 1000 SCREEN WAVELENGTH = 4096
NUMPTS = 16384 Δx = 2 EXTENT OF X IS -250 < X < 248

OBSERVATION DISTANCE Z = 3800 CURVED WAVEFRONT

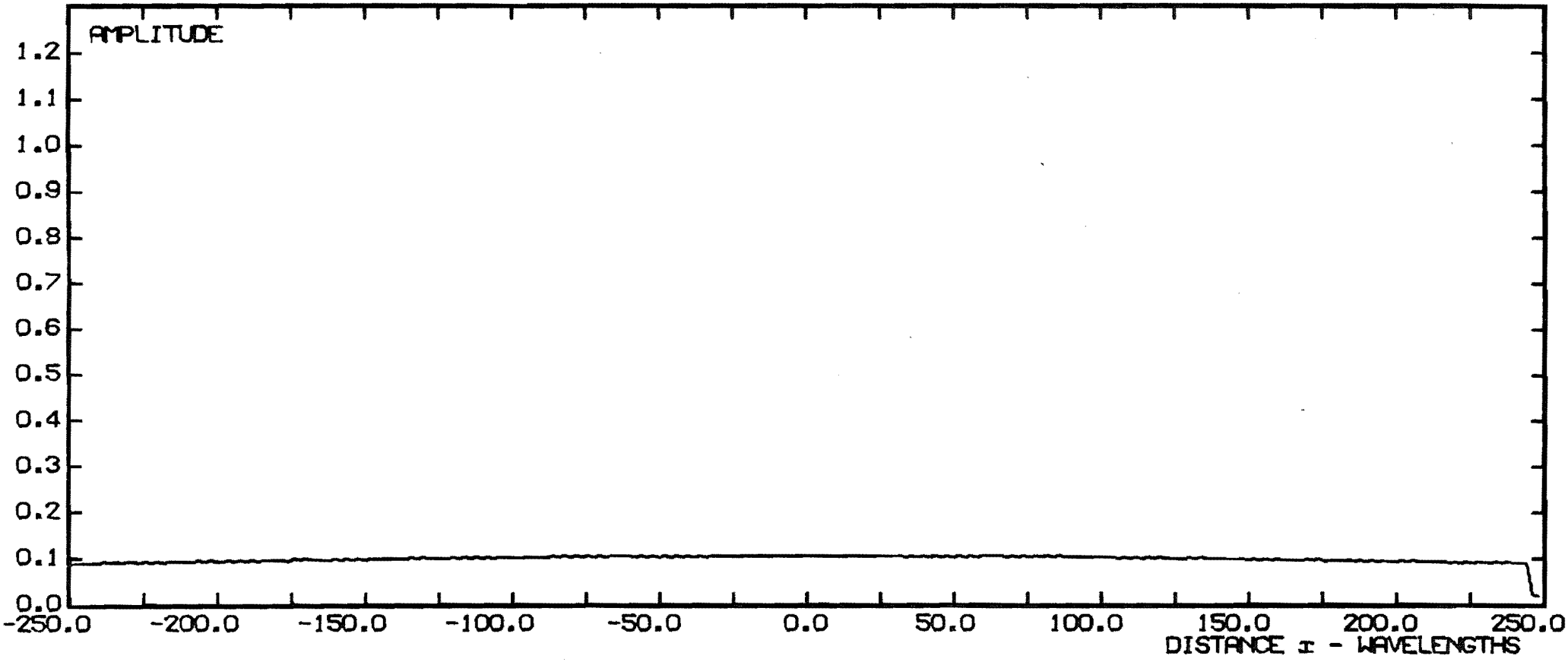

FIG 4-4

OBSERVATION FIELD - LITTLE F(X,Z) PHASE-MODULATING SCREEN $\Delta\theta$ = 1000 SCREEN WAVELENGTH = 4096

NUMPTS = 16384 Δx = 2 EXTENT OF X IS -250 < X < 248

OBSERVATION DISTANCE Z = 3800 CURVED WAVEFRONT X SHIFT IS 40

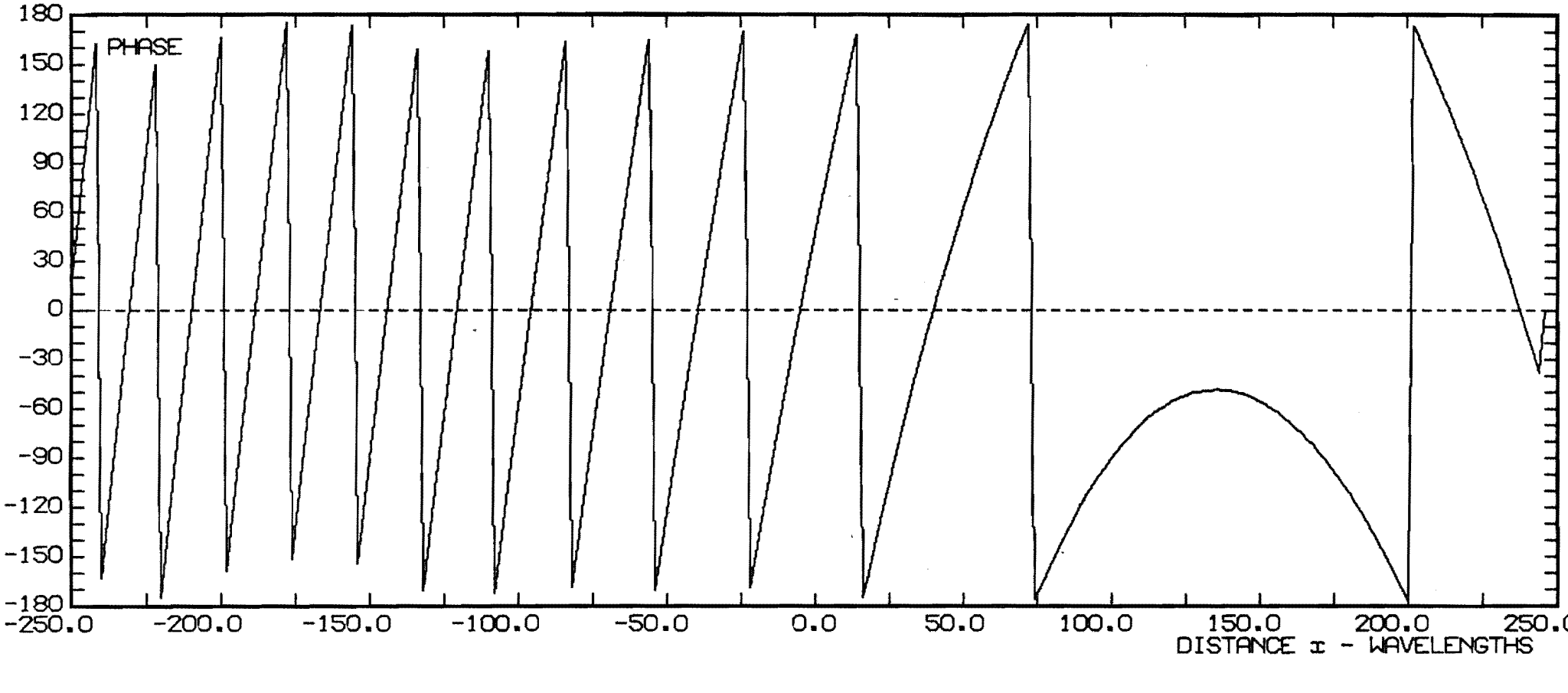

FIG 4-6 AMPLTIUDE SPATIAL CORRELATION - SCREEN SHIFT 394 METRES

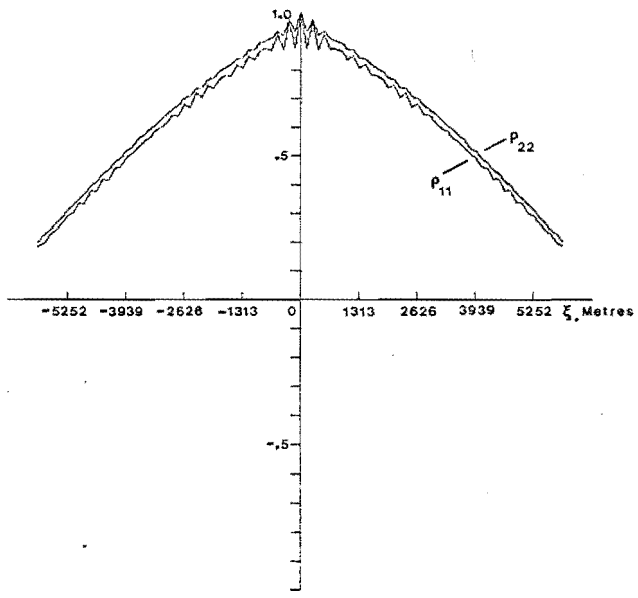

AMPLITUDE AUTOCORRELATION

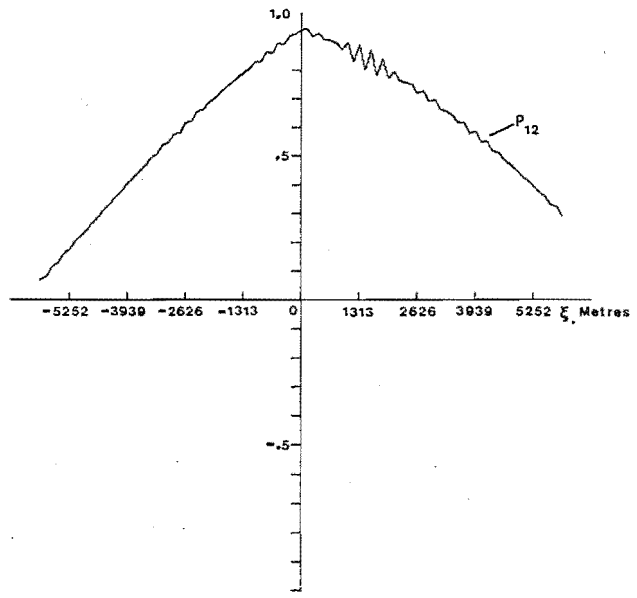

AMPLITUDE CROSSCORRELATION

FIG 4-7 AMPLTIUDE SPATIAL CORRELATION - SCREEN SHIFT 2495 METRES

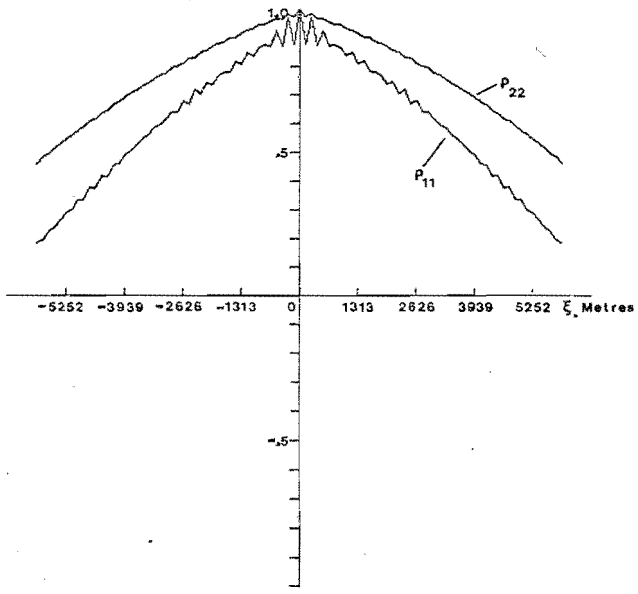

AMPLITUDE AUTOCORRELATION

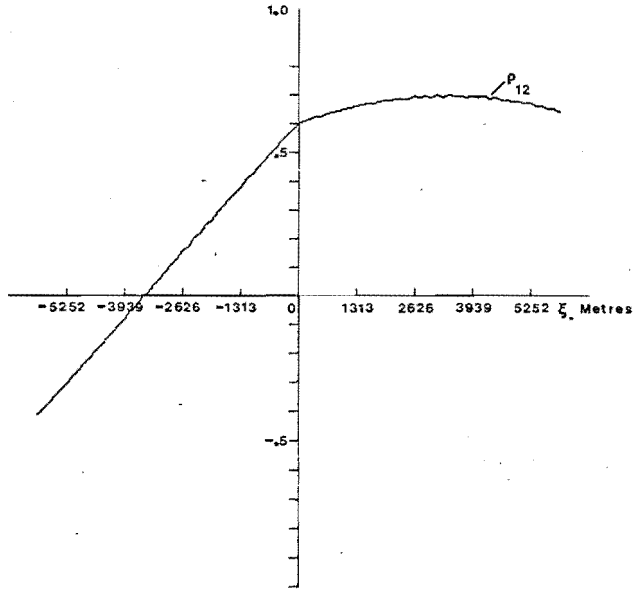

AMPLITUDE CROSSCORRELATION

FIG 4-8 COMPLEX SPATIAL CORRELATION - SCREEN SHIFT 394 METRES

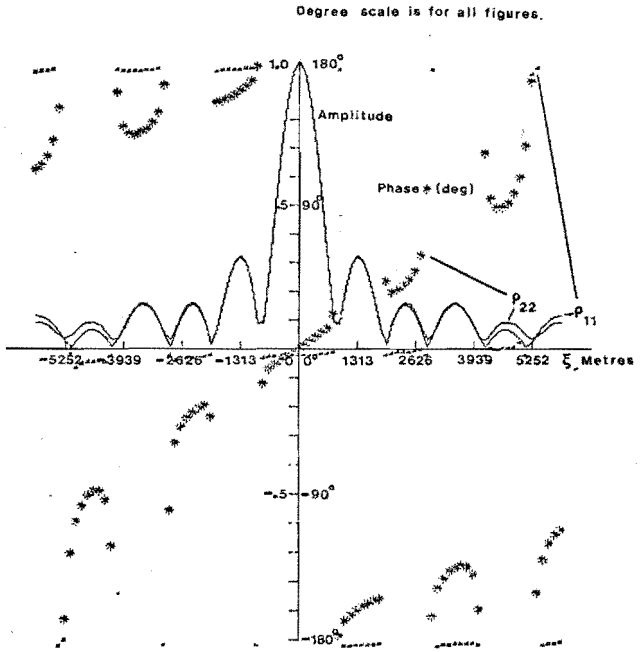

COMPLEX AUTOCORRELATION

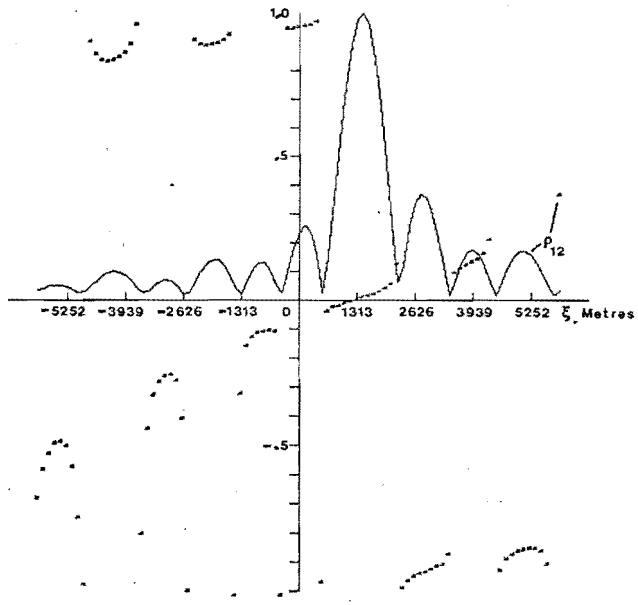

COMPLEX CROSSCORRELATION

FIG 4-9 COMPLEX SPATIAL CORRELATION - SCREEN SHIFT 1050 METRES

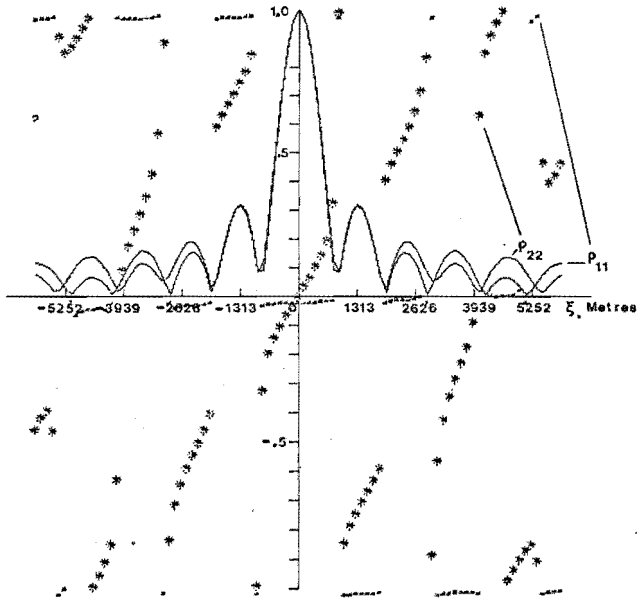

COMPLEX AUTOCORRELATION

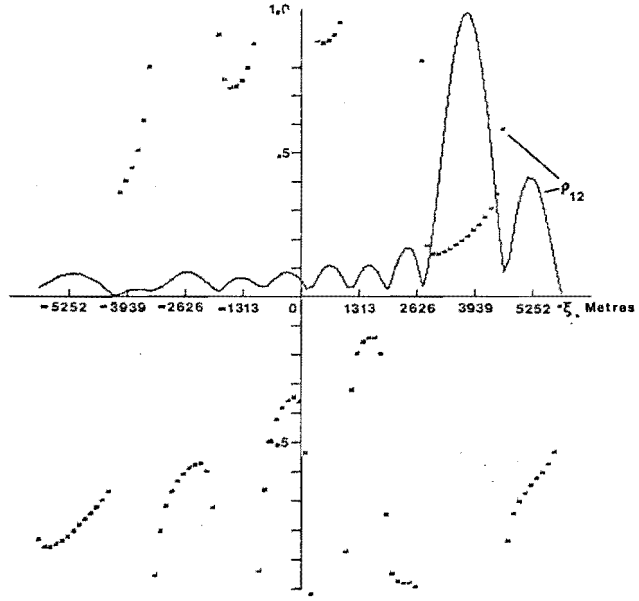

COMPLEX CROSSCORRELATION

FIG 4-10 AMPLITUDE TEMPORAL CORRELATION - RX SPACING 6565 METRES

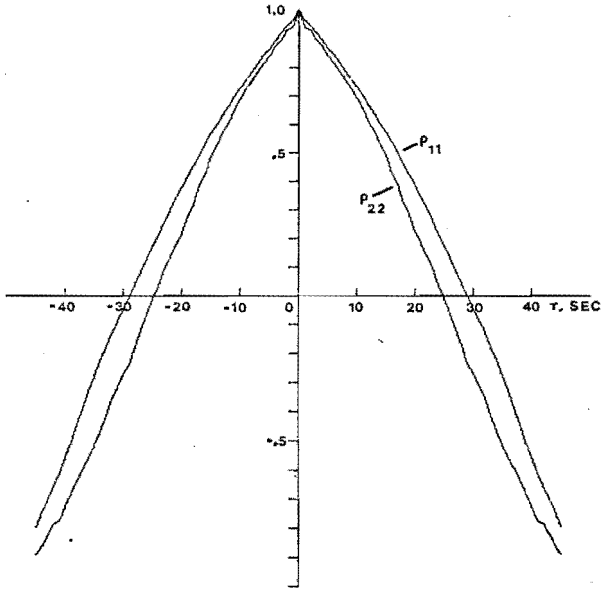

AMPLITUDE AUTOCORRELATION

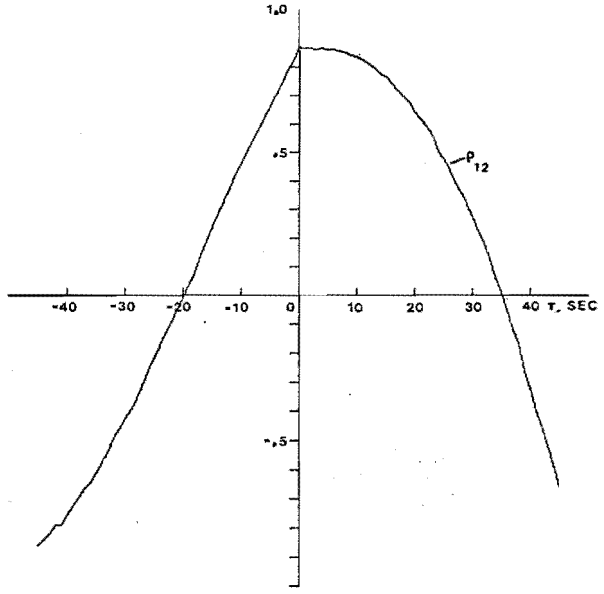

AMPLITUDE CROSSCORRELATION

FIG 4-11 AMPLITUDE TEMPORAL CORRELATION - RX SPACING 13129 METRES

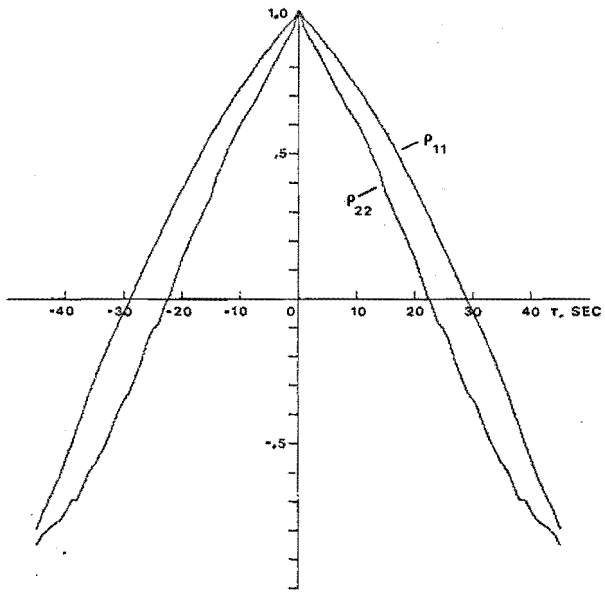

AMPLITUDE AUTOCORRELATION

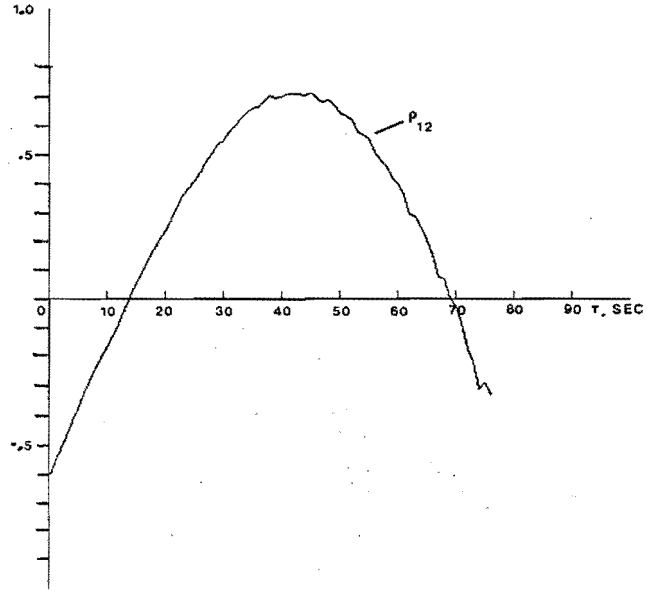

AMPLITUDE CROSSCORRELATION

FIG 4-12 AMPLITUDE TEMPORAL CORRELATION - RX SPACING 6565 METRES

RECEIVER LOCATIONS 6565 & 13129 metres

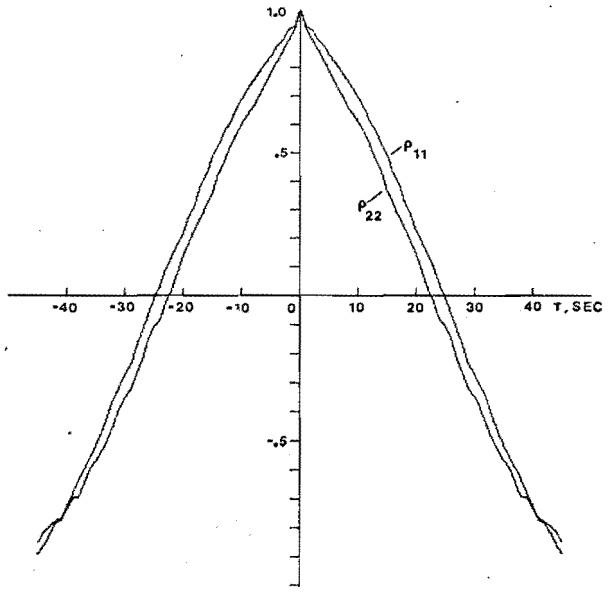

AMPLITUDE AUTOCORRELATION

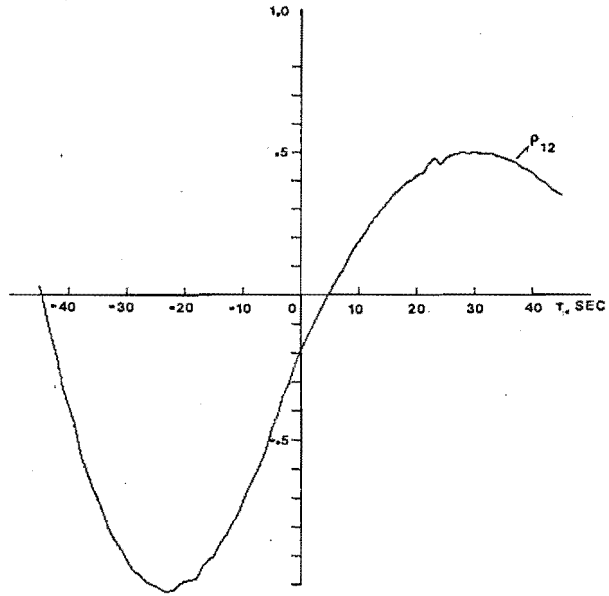

AMPLITUDE CROSSCORRELATION

FIG 4-13 COMPLEX TEMPORAL CORRELATION - RX SPACING 2626 METRES

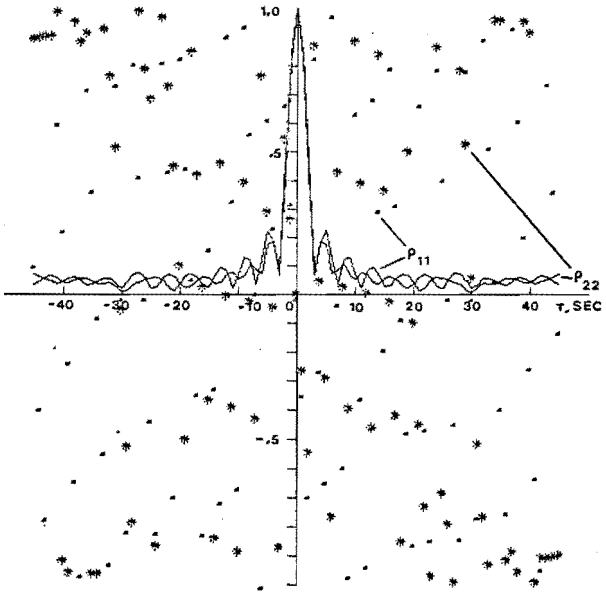

COMPLEX AUTOCORRELATION

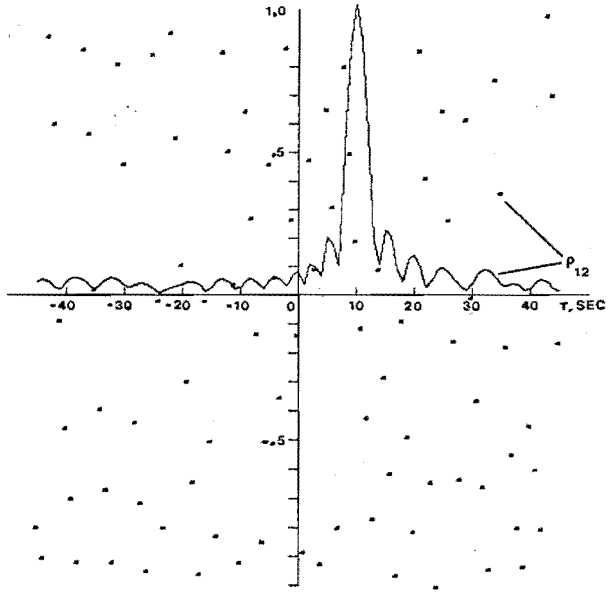

COMPLEX CROSSCORRELATION

FIG 4-14 COMPLEX TEMPORAL CORRELATION - RX SPACING 6565 METRES

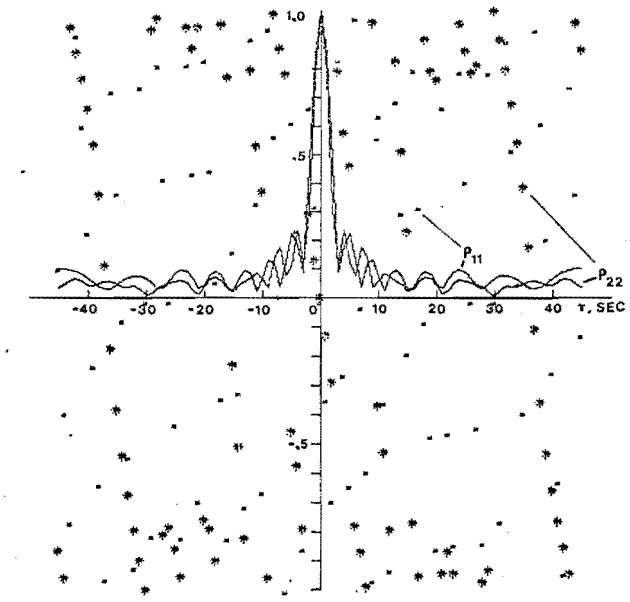

COMPLEX AUTOCORRELATION

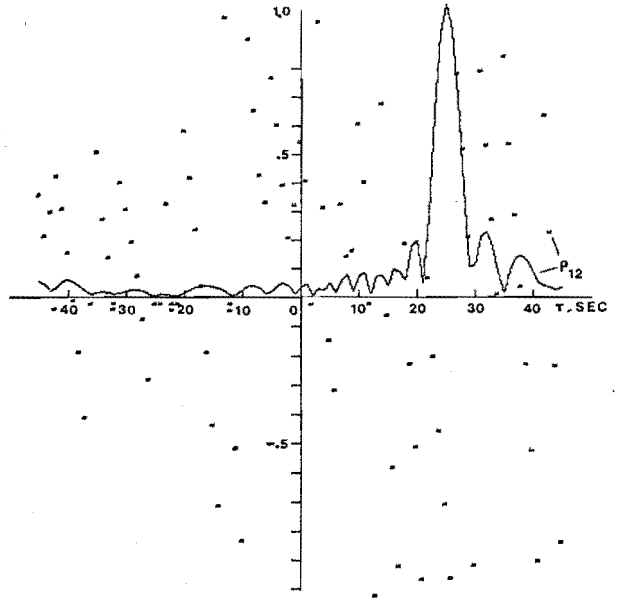

COMPLEX CROSSCORRELATION

CHAPTER 5

PHASE-HEIGHT STUDIES

I. INTRODUCTION

In this chapter the experimental results obtained for this thesis are presented. Measurements were made entirely on the F region. The frequency used for F-region experiments was 4.57 MHz. Details of experimental instrumentation and control can be found in Appendices A and B.

Periods, speeds, and hence horizontal wave phase trace speeds are found and presented. An attempt is made to obtain directions, and a comparison with the predictions of theory is presented.

II. REVIEW OF PREVIOUS WORK

In this section a review of previous phase-height work is made. There is some overlap with the review of chapter 2 on the phase-screen model, but here a phase-screen model interpretation is taken for granted and the main emphasis will be on the periodicities observed.

Findlay (1951, 1953) is the first worker known to this author to have started systematic phase-height work. The technique used in this thesis is different to his: his is outlined in Findlay (1951) and was able to record fringe traces representing the phase-height level on film. An advantage of his method over that used here is that he could record the phase changes in several ionospheric layers at once: provided the lower layers allowed partial transmission of the probing radio wave.

Findlay (1953) interprets minima in phase path as arising from reflections from horizontally-moving clouds of ionization. He is, however, careful to state that:

> ".... there is no direct evidence that the observed movements imply a transport of ionized gas, rather than a movement of an irregularity in the ionization density without actual transport of ionized particles."

By geometry he obtains for the horizontal velocity of a moving cloud

$$\Delta P = \frac{2V^2t^2}{P_0}$$

where P_0 is the minimum value of absolute phase-path P, t is time with zero when $P = P_0$, ΔP is $P - P_0$ the phase-path difference from the minimum, and V the horizontal cloud velocity. His data was found to fit this law quite well and he found velocities predominantly in the range 30-110 $m.sec^{-1}$ for E-region. Direction, of course, could not be found. By considering the velocities and durations of his echoes he found that his echoes scattered energy back to the receiver

within a cone of semi-angle 6^{o}.

Landmark (1957) worked on E-region at 2 MHz and obtained velocities ranging mainly from 40-90 $m.sec^{-1}$. His work on amplitude increases and incoherent phase is described elsewhere in the chapter on the phase-screen model. Work on the F-region was done by McNicol and Thomas (1960). They show film records of Es and F_2 coherent and incoherent phase changes. Some of their data shows magnetionic splitting, with O- and X-ray having different group heights and phase behaviour. This happens because the O- and X-rays are reflected at different places. They also find it difficult to isolate any effect of Es on the F region phase height, because so often the Es causes blanketing of F region.

McNicol and Thomas (1960) made their measurements at Brisbane in Australia. In general, the data they present show a smaller rate of change of phase path with time for the F region than has been obtained by Fooks (1962) or by this author.

Fooks (1962) worked on E- and F-region at 2.4 MHz and 4.0 MHz. He shows some results from both regions. It can be seen that the diurnal changes in F-region phase height, when coherent, are in the order of hundreds of wavelengths. Fook's (1962) displayed daytime F-region data shows periods of about 20 minutes in summer and 12-15 minutes in winter superimposed onto the diurnal changes.

Reddi and Rao (1971) worked on F2 region at 5.6 MHz and took phase-height measurements for both O- and X-modes.

They obtained phase oscillations of periods ranging from 3 to 39 minutes, a predominance of smaller periods over larger ones, and most frequent period at 9 min. This seems rather low for F-region, but although they do not date their data, their paper submission date implies that the data could have been taken any year from 1966 to 1968, at a time of sunspot minimum when the Brunt frequency is lowest. Thus perhaps their 9 minute value is possible for gravity waves. Their data shows oscillation amplitudes of 20 wavelengths or more, superimposed onto a large-scale prenoon phase height decrease and postnoon increase.

Reddi and Rao (1971) note from their results that in general longer-period disturbances have larger phase-path amplitudes, and that disturbance speed decreases as period increases. They obtained their speeds by noting the time delays between phase-path reversals on O- and X-modes. The horizontal separation of O-mode and X-mode reflecting points was calculated from magnetoionic theory and an F-region model, (Reddi and Rao, 1971). Their most frequent value for speed was of order 100 $m.sec^{-1}$.

In this thesis Findlay's (1953) relation between ΔP and t^2, given previously, is used to obtain speeds. The phase-height experiment used in this thesis was set up to measure only one mode for any one run. Examination of ionograms from the Godley Head ionosonde showed that it was the O-mode which was always measured: there was less absorption of this mode so it was used to obtain measurements for long runs.

Reddi and Rao (1971) found, at their location, that some disturbances would appear on the phase path records for one mode and not on those for the other. This is rather surprising, considering that the vertical and horizontal separation of O- and X-mode reflecting points is far less than the expected scales of internal gravity waves (Hines, 1960). Reddi and Rao (1971) found that disturbances which appeared for only one magnetoionic mode generally had smaller periods and amplitudes.

Some of the low periods observed by Reddi and Rao (1971) suggest the possible presence of acoustic waves. In contrast, the work of Tolstoy and Montes (1971) on the F-region seems to confirm the hypothesis that internal gravity waves cause the short-period phase height motions. Their work used three radio frequencies simultaneously: 2.4, 4.8 and 6.0 MHz using the doppler records given by C.W. doppler sounders. They measured the doppler shifts arising from simultaneous C.W. measurements at 2.4, 4.8 and 6.0 MHz (corresponding to true reflection heights of 130, 175 and 240 km) and found the power spectra to show maxima at periods of 10, 12, and 15 minutes respectively. The period of maximum activity increased as height increased.

For any one record taken at any one height, the interesting feature is the peak of activity at a frequency, which may be identified as the Väisäla-Brunt frequency. The amplitude of the spectrum reduced very sharply for higher frequencies, but was still substantial although below

the peak level for frequencies below the Brunt frequency. This implies that the predominant frequency observed in these doppler observations was the Brunt frequency itself.

The reduction of ionograms gave the true heights for the radio frequencies used: a plot of the Brunt frequency against true height was found to be a reasonable fit to a profile of Brunt frequency against height calculated from a model atmosphere. A plot of the square root of the magnitude of the power spectrum peak against height gave reasonable confirmation to the hypothesis that fluctuation amplitude is an exponential function of the height, proportional to exp(z/2H) as predicted by Hines (1960).

Vincent's (1969, 1972) work on phase height in the E region also seemed to confirm the gravity-wave hypothesis as the cause of small-scale motion. His 1969 data showed quasi-sinusoidal phase oscillations of time-scale 5 minutes, which was close to his calculated value of the E-region Brunt frequency (using CIRA data). Power spectra calculated from his 1972 results show a sharp fall-off in the amplitude contributed by periods below the Brunt period which tends to suggest that the phase oscillations arise from gravity waves. This agrees with the work of Tolstoy and Montes (1971), but contrasts with the observations of periods below the Brunt period observed in the F-region by Reddi and Rao (1971). Vincent's (1972) work was done on the Buckland Park array at Adelaide with aerial spacings of 730 m or 910 m. These spacings were large enough to obtain velocity directions

and magnitudes for the coherent-phase case, using time lags of similar phase oscillations between aerials. He obtained velocities predominantly in the range 50-100 $m.sec^{-1}$.

The implications of Vincent's (1972) work on the phase-screen model, and on the comparison of his phase-height results with neutral winds, is discussed elsewhere in the chapter on the phase-screen model.

Schrader and Fraser (1975) obtained spaced-receiver phase-height observations for E region using a frequency of 2.155 MHz and receiver spacing of 2-4 km. They obtain periods of order 5 minutes or so, and speeds ranging from 75-200 $m.sec^{-1}$. They report directions to the northwest in summer and to the southeast in winter.

For the four receivers used by Schrader and Fraser (1975) six time lags (or receiver pairs) are available for the calculation of velocities. In most cases these were found to be consistent among themselves: however for some data this was not so and Schrader and Fraser (1975) attribute this to the simultaneous presence of several atmospheric waves. Another consideration is how long a measured velocity would remain constant. In some cases the velocity would change substantially for sets of data separated by an hour or so - either a new wave is being measured at the later time or the properties of a long-time, continuous wave-train were changing.

With respect to short periods, observations have been made of acoustic waves with a 3-minute period (Georges 1967;

Georges 1968), using a doppler frequency-shift system. Such disturbances are spatially confined to a few hundred km., and the occurrence of severe weather is a necessary but not sufficient condition for their occurrence, (Georges 1968). Although the periods found in the experimental data are rather low, the significant periods are not as low as 3 min. The spatial confinement and absence of severe weather near Birdling's Flat field station at the time of data runs seems to argue against the phase oscillations' arising from this form of acoustic wave. Instead, it is felt that doppler-shifting of wave periods due to F-region winds, and temperature gradients within the F-region may be the cause of the low periods observed, as presented below.

III. THE PHASE HEIGHT EXPERIMENTS RUN

Appendix B outlines the experimental procedure adopted for running phase-height experiments. The frequencies used are stated in the introduction. Data was taken at three aerials spaced at 250 metres apart (Appendix A) spaced in an isosceles triangle (Appendix G). The wide pulsewidths used - 55 μsec at 4.57 MHz and 50 μsec at 2.40 MHz allowed satisfactory phase measurement at the centre of the echo (Appendix B). The failure of the transmitting array to transmit circularly-polarized waves (Appendix A) meant that both modes were received: a check of Godley Head ionograms has shown that O-mode was measured in all cases.

The data was taken at a P.R.F. of 4 sec^{-1}. Velocities are found by Findlay's (1953) method, with some modification using the sine-wave specular reflector model of Hines (1975, unpubl.). The measurements of time-shifts between phase minima at the spaced aerials was attempted, but the small time-shifts involved did not allow success. Vincent (1972) was able to find vector velocities by this method for his E-region phase-height measurements, but he used antenna spacings of 730 and 910 metres. Moreover, the F region structures are larger than the E-region structures in horizontal extent. The method of Reddi and Rao (1971), in which the azimuth of the reflected signal at phase-path minimum is used to give direction, was not employed because the receivers and aerials have not been calibrated for comparative phase (Appendix A).

As part of the synoptic observations programme of the Department of Scientific and Industrial Research, an ionosonde is maintained at Godley Head near Christchurch, 42 km North-East of Birdlings Flat Field Station. Examination of Godley Head ionograms has shown that for 19th February 1978 the run was entirely made in the F_1 region, just below its peak. The result is in contrast to the statistical data presented in Figures 2-1 to 2-4, which imply that for monthly means, 4.57 MHz lies between foF_1 and foF_2. The monthly medians were taken from the D.S.I.R. Ionospheric Data information given by the D.S.I.R. as results of the synoptic observation programme.

Examination of the corresponding ionograms, taken

at 15-minute interval, also showed very calm records. The sensitivity of the phase-height experiment used in this thesis allows the measurement of wave activity when an ionogram would not show any disturbance. For most of the ionogram records corresponding to the runs presented here, there were a few signs of small moving kinks or traces such as those presented as characteristic of medium-scale disturbances by Georges (1968). What activity did appear was seen mainly as moving trace thickenings in the section of ionogram from foF_1 to foE.

IV. INITIAL REDUCTION OF THE DATA

(1) Coherence checking and quadrant tracking.

For all runs the phase data was initially plotted out to check for coherence. Incoherent data was discarded for further analysis in this experiment. Coherent data, for F region especially, was found to pass through many wavelengths between maxima and minima of range. To obtain velocities and wave-oscillation periods the coherent phase must be tracked through as many 2π values as necessary.

This tracking was done using a subroutine written by Dr. G.J. Fraser and adapted slightly by this author. Essentially each raw angle, which was in the range $-\pi$ to $+\pi$ radians, had π added to bring the range to 0 to 2π radians and was then assigned its appropriate quadrant; Q1: $0 - \pi/2$; Q2: $\pi/2 - \pi$; Q3: $\pi - \frac{3\pi}{2}$; and Q4: $\frac{3\pi}{2} - 2\pi$. Differences in phase between adjacent data became quadrant differences. Those involving two quadrants of angle were treated as "phase-jumps" indicating a partially coherent reflection

at that time (Vincent, unpubl., 1967)(Vincent, 1972). The number of jumps was recorded for later printout but no π or 2π term was added or subtracted to the second angle.

Phase differences involving three quadrants involve only those angles in quadrants Q1: $0 - \pi/2$ and in Q4: $\frac{3\pi}{2} - 2\pi$. They are taken to indicate a smooth change into a higher or lower circle. For example, 2π was added to the second angle if the difference between the final and initial angles is negative, since the final angle would be in Q1 and the initial in Q4. The $2n\pi$ terms added to the angles were cumulative, hence tracking was accomplished.

Tests on real data comparing the raw and tracked phase for the coherent case indicated success - oddly enough, the only trouble found was with the calculated phases of the diffraction patterns, where occasionally the tracking would proceed in the wrong direction. These problems seemed to arise when the calculated pattern had a series of phase values rather close to 0 and to 2π. Nothing further was done because the real data seemed to be handled correctly.

The program would, of course, work on either coherent or incoherent data, which is why initial screening was necessary. During a run the ionospheric reflector would become incoherent at times. The program was able to just leave the angles as they were (adding whatever $2n\pi$ term had already been accumulated for the previous coherent stage) and resume tracking when coherence returned. The incoherence would be treated by the program as a section with a high

number of phase jumps. This seemed the physically sensible procedure.

The counting of phase jumps allows the application of the criterion given by Fraser and Vincent (1970) for coherent, partially coherent, and incoherent echoes. One record of the phase-height data files (Appendix B) corresponded to 2.5 minutes of data. On reading the record, the tracking routine would give the number of jumps present in the 2.5 minutes of data. Records with more than six jumps were regarded as incoherent. In practice, it was found that the main cause of phase incoherence was loss of signal and resulting failure of software signal tracking (Appendix B). This occasionally occurred for high absorption of the O-mode signal, and the occurrences are noted in the plots of group height against time (Figure 5.5).

After tracking the data was usually decimated by a factor of ten to give points at 2.5 second spacing. This gave a suitable time spacing for Findlay (1953) velocity determination. Further decimation to a factor of fifty overall was found to give sufficiently close time resolution even at the times of most rapid (but coherent) change, without the burden of unnecessary points. The time spacing was then at 12.8 seconds and the data was filtered, spectrum analysed, and displayed. However, all the original points were required for reliable tracking: decimation prior to tracking caused tracking failure.

(2) Prefiltering of the data.

With the tracked phase now available as a function of time it is of interest to examine the periodicities present. Such periodicities will be superimposed on the large F-region duirnal changes. Both visually and for later spectral analysis, such trends need to be removed, otherwise both bad Fast-Fourier-Transform (FFT) spectra (for example, Brault and White, 1971) and Maximum-Entropy (MEM) spectra (for example, Courtillot et al. 1971) will result. The presence of the trend leaves the time-series non-stationary over the data length, and leakage will contaminate the low-order frequencies in the spectrum.

Behannon and Ness (1966) outline a procedure by which a given filter with a desired gain and phase frequency response can be approximated digitally by a set of discrete weights. The weight values are calculated by a least-squares approximation to the ideal response, and are applied to the time-series by discrete convolution. For the present application a high-pass filter is required for trend removal: the procedure adopted (Behannon and Ness, 1966) is to calculate a low-pass filter first - including a taper to minimize Gibbs oscillations - and move it in the frequency domain to cover the passband required.

The filter used is shown in Fig. 5-1. Its frequency response is plotted in terms of a parameter $p = \frac{S}{S_{Nyq}}$ where S_{Nyq} is the Nyquist frequency $\frac{0.5}{\Delta t}$. For the time spacing here of 12.8 seconds, the filter shown has half-amplitude

response at 43 minutes and 25 seconds.

Fig.5-2 shows the response for the low-frequency range in more detail, and also that of a wider filter which allows more of the trend through. The reciprocal relation between frequency and period means that for this frequency range a small change in cutoff frequency can cause a significant change in cutoff period. A comparison of the effects of the two filters is given below.

Each filtered point $y'(t_i)$ is given by

$$y'(t_i) = \sum_{N=-100}^{100} y(t_i - N\Delta t)W(N\Delta t)$$

V EXPERIMENTAL RESULTS

(1) Daytime F1-region data - 19th February 1978 : 1230-1850.

(a) General Overview

On 19th February 1978 a long run of mainly-coherent phase-path data was obtained between 1230 and 1830. Measurements were taken on the F1 region using a frequency of 4.57 MHz.

Figures 5-4(a) and 5-4(b) show the tracked phase path after pa-sing through the "45-minute" filter. Figure 5-6 shows the original data for half the run until 1542 : Figure 5-7 does likewise for the results of the "90 minute" filter. Figure 5-4 also indicates, for each 2½ minute segment, the criterion C "coherent", P "partially coherent", or I "incoherent" for the phase.

(b) Interpretation of the phase path

For vertical incidence the phase-path P between the transmitter and a reflection point at height h_r is (Budden, 1961)

$$P = \int_0^{hr} \mu dh$$

with phase refractive index μ given by the Appleton-Hartree formula, neglecting collisions (Budden, 1961),

$$\mu^2 = 1 - \frac{X}{1 - \frac{Y_T^2}{2(1-X)} = \left\{\left(\frac{Y_T^2}{2(1-X)}\right)^2 + Y_L^2\right\}^{\frac{1}{2}}}$$

where $X = f_N^2/f^2$; $Y_L = Y\cos\theta$; $Y_T = Y\sin\theta$; $Y = f_H/f$

using f as the transmitted radio frequency, f_N as the plasma

f_H as the gyrofrequency, and θ as the magnetic-field and radio-wave normal directions.

Changes in phase path will arise from changes in the true path, and from ionization concentration changes anywhere along the path. The normal interpretation of phase-path and Doppler measurements (for example, Tolstoy and Montes, 1971) is that the probing radio wave travels in free space until the reflection level, whose movements impose phase variations on the returned echo. This interpretation is justified only if the effects of underlying ionization have a very small or negligible effect on the phase-path changes measured.

For the run discussed here, swept-frequency ionograms taken at the D.S.I.R. Geophysical Observatory Ionosonde located at Godley Head were available at 15-minute intervals. They show the presence of a normal E-region below the F_1 region. (Fig. 5-11 shows three of the ionograms). The effect on phase-path of the E-region presence is calculated below.

Robinson and Dyson (1975) have calculated the effects on phase-path when an electron-density irregularity is superimposed onto a background electron-density profile. Their calculations were made for the effects of changes in irregularity thickness, irregularity intensity, ionization gradient, and probing radio frequency.

The model of Robinson and Dyson (1975) assumes a triangular-shape irregularity superimposed on a straight-line background, as shown in their Fig. 3. The calculations are made for parameters similar to those used in their experiments. Their values are close enough to those used at Christchurch to serve as a guide.

Geophysical Observatory ionospheric data for 19th February,

1978, give 3.70 MHz as the maximum of the hourly values for f_oE. Thus:

$$\text{Maximum value of } f_oE = 3.70 \text{ MHz}$$
$$\text{Corresponding value of } X = (f_oE)^2/f^2$$
$$= (3.70)^2/(4.57)^2$$
$$= 0.66 .$$

If the E-region is treated as an irregularity between the ground and the reflection point in the F_1-region, then the X=0.66 value implies that the presence of the E-region, and fluctuations in it, will have a negligible effect in phase path compared to those measured. This can be seen from their Fig. 4 (change in phase path as a function of irregularity thickness); their Fig. 5 (change in phase path as a function of irregularity intensity); and their Fig. 6 (change in phase path as a function of the background gradient of the ionosphere).

It is concluded that phase path changes observed represent movements in the F_1-region and are little affected by the movements in the E-region.

(b) Wavelike structure of the phase-height curve

References to Fig. 5-4(a) and Fig. 5-4(b) show clear groups of wavelike variation to be seen, especially for the times 1300-1340 hours, 1500-1600 hours, and 1630-1830 hours.

The times 1300-1340 hours and 1630-1830 hours have a period by eye of about 12 minutes. In contrast the 1500-1600 hours time shows waves of a rather larger amplitude and a period of eye of 20 minutes.

It is interesting, although not statistically significant, that data for two other days (12 November, 1977, and 13

November, 1977; not shown here) show a similar enhancement of wave amplitude and period at about the same time. Group-height variations (Fig. 5.5 for 19 February, 1978; not shown for the other data) show the corresponding wavelike group-height variations to be at the bottom of a large trough.

A-scope records for 19 February, 1978, indicate magnetoionic O- and X- mode interference at about 1725 (Fig. 5-5), and this might be taken to be the reason for the enhanced wave amplitude. This is felt to be unlikely; A-scope records for 12 November, 1977, and 13 November, 1977, indicate that magnetoionic mixing took place at different times to the occurrence of the large waves, and instead are indicated on their respective phase records as non-wavelike structures and incoherent features.

The 1500-1600 hours enhancement in wave amplitude and period is thus felt to be real: it is of some concern that very little incoherence arises from the magnetoionic mixing. This indicates the need to keep good A-scope records to trace when mixing occurs.

Examination of less-heavily-filtered versions of the data (Fig. 5-6, Fig. 5-7) still indicates the 12-minute periodicity quite clearly, but also that overall trends and other periodicities are present. The power spectrum analysis, to be discussed later, will give information about these other frequencies.

(C) Stationary-atmosphere parameters

For the purposes of initial interpretation, the atmosphere is assumed to be stationary. Some estimates of temperature and frequency parameters are presented here as a discussion base:

(C1) Isothermal atmosphere

Ionograms for the run of 19th February, 1978, have been reduced by Dr. C.H. Cummack (Geophysical Observatory, DSIR) using the overlapping polynomial method of Titheridge (1968). The ionograms were taken at the Godley Head ionosonde near Christchurch, New Zealand (Lat. 43.6°S, 172.8° E).

A typical scale height of 35 km was obtained. Then, from Hines (1960), for an isothermal atmosphere:

$$\text{Scale Height} \qquad H = \frac{C^2}{\gamma g}$$

and

$$\text{Brunt Frequency} \quad \omega_g = \frac{(\gamma-1)^{\frac{1}{2}} g}{C}$$

with gravitational acceleration $g = 9.2$ m.sec^{-1} and specific-heat $\gamma = 1.40$.

From these, the values

$$\text{Speed of Sound} \quad C = 670 \text{ m.sec}^{-1}$$

and

$$\text{Brunt Period} \quad \tau_g = 12.1 \text{ minutes.}$$

(C2) Temperature-varying atmosphere

For an atmosphere with temperature varying with height, the acoustic cutoff angular frequency ω_a and Brunt frequency ω_B are given by

$$\omega_a^2 = \frac{C^2}{4}\left(\frac{\gamma g}{C^2} - \frac{1}{C^2}\frac{dC^2}{dz}\right)^2 - \frac{C^2}{2}\frac{d}{dz}\left(\frac{\gamma g}{C^2} - \frac{1}{C^2}\frac{dC^2}{dz}\right)$$

$$\omega_B^2 = \frac{(\gamma-1)g^2}{C^2} + \frac{g}{C^2}\frac{dC^2}{dz} .$$

If these are expressed in terms of scale height, ($C^2=\gamma g H$), then:

$$\omega_a^2 = \frac{1}{4}\frac{\gamma g}{H}\left[1 - \left(\frac{dH}{dz}\right)^2 + 2H\frac{d^2H}{dz^2}\right]$$

$$\omega_B^2 = \frac{g}{H}\left[\frac{\gamma-1}{\gamma} + \frac{dH}{dz}\right] \quad .$$

Estimates of values for ω_a^2 and ω_B^2 have been obtained from the 1962 model of Harris and Priester. Reference to Fig. 5-8 shows that at 1400 hours L.T. the true height of reflection for this run was about 180 km. Table 4 of Harris and Priester, applicable to 1400 hours L.T., is used as shown:

TABLE 5-1

Height	Scale Height H	$\left(\frac{dH}{dz}\right)$	$\left(\frac{d^2H}{dz^2}\right)km^{-1}$	$H\frac{d^2H}{dz^2}$
170 km	36.1			
		0.42		
180 km	40.3		-0.004	-0.16
		0.38		
190 km	44.1		-0.004	-0.16
		0.34		
200 km	47.5			

Hence $\omega_a^2 = \frac{1}{4}\frac{\gamma g}{H}\left(1 - 0.16 - 0.32\right) = 4.2 \times 10^{-5}\ sec^{-2}$

ao $\tau_a = 16.2$ minutes.

Also $\omega_B^2 = \frac{g}{H}\left(0.29 - 0.42\right) = 1.59 \times 10^{-4}\ sec^{-2}$

so $\tau_B = 8.3$ minutes.

Again with $g = 9.2\ m.sec^{-2}$ and $\gamma = 1.40$.

The above calculations, and Table 5-1, were prepared by Dr. C.H. Cummack. A similar calculation, by this author, using Table 5 of Harris and Priester (1962) was done for 1800 hours at (Fig. 5-8) 220 km. Collected results are:

TABLE 5-2

TIME, hrs.LT	HEIGHT, Km	τ_a, minutes	τ_B, minutes	τ_g, minutes	C m.sec^{-1}
1400	180	16.2	8.3	12.1	671
1800	220	18.4	8.7	14.4	799

(d) Ionogram data

Routine ionogram soundings at Christchurch at 15-minute spacing are made by the Geophysical Observatory of the Physics and Engineering Laboratory of D.S.I.R. as part of its synoptic observation program. These have been used in (c) above to obtain typical scale heights from which the Brunt period may be calculated.

The ionograms for the run (a typical one of which is shown if Fig. 5-11) are very calm over the entire run. Neither spread-F, nor sporadic-E at the probing frequency of 4.57 MHz, was present at any time during the run. The absence of split traces in the F_2 region indicated the absence of large-scale ionospheric disturbances. However, systematic quasi-periodic changes in layer shape were present: also trace thickenings moving down the trace as time progressed. The latter was one of the first indications of the presence of T.I.D. activity (Munro, 1950). Some complexities and splittings of the trace could be observed at the F_1-peak, which travelled down the F_1-trace in time.

Examination of the trace thickenings of the ionograms was performed by Dr. C.H. Cummack of the Geophysical Observatory. His location of the frequency of a trace thickening or complexity, against time, is shown in Fig. 5-12. He deduces a periodicity of between 1¼ - 1½ hours. For example, looking along the 4 MHz line the presence of a complexity is seen at 1315 hours and

again at 1440 hours, a difference of 85 minutes.

Reference to Fig. 5-12 shows, at 1330 hours, successive phases of the trace complexities to be at frequencies of about 3.7 MHz and 5.2 MHz. True height analysis indicates a separation of approximately 60 km.

The wave characteristics thus are period T = 1½ hours and vertical wavelength λ_z = 60 km.

The successive true heights of 4.57 MHz are of interest. Every 15-minute ionogram from 1230 hours to 1830 hours was reduced to a true height profile using the Titheridge overlapping polynomial method. The reductions were done at the D.S.I.R. Geophysical Observatory. Up to 20 closely-spaced points were taken along a trace, and the true heights at the chosen frequencies were returned.

The true height at 4.57 MHz was found by linear interpolation of the true heights of the adjacent scaled frequency point on each side.

An approximate measure of the oscillation, and overall trend, of the isoelectronic contour at 4.57 MHz is obtained. Fig. 5-8 shows the result. Oscillatory behaviour can be seen, with quasi-period 45 - 60 minutes or so. The peak amplitude of the oscillation is about 4 km until 1400 hrs, while it is about 1 km until about 1500 hrs. The amplitude increases to 2-3 km after 1500 hrs.

With $\tau_a \doteq 17$ minutes and $C \doteq 700$ m.sec^{-1} previously found, and λ_z = 60 km, the asymptotic condition $k_z^2 >> \omega_a^2/C^2$ holds true and the approximate dispersion relation (33) of Hines (1960) may be used (with notation $k_x \rightarrow k_h$ to indicate that the directions in the horizontal plane is unknown):

$$\omega^2 k_z^2 \doteq (\omega_g^2 - \omega^2) k_h^2$$

or

$$\lambda_h^2 = \lambda_B^2 \left(\frac{\tau^2}{\tau_g^2} - 1 \right) \quad .$$

Use of τ = 80 minutes and $\tau_g = \tau_B$ = 8.5 minutes gives

$$\lambda_h = 560 \ (\pm 90) \text{ km}$$

hence

$$k_h = 1.2 \ (\pm 0.2) \times 10^{-2} \text{ km}^{-1} \quad .$$

The error limits arise from the roughness of the estimate: a value of λ_z = 50 km gives λ_h = 470 km. Differing values of τ_g will alter the result also.

The horizontal phase trace speed and vertical phase trace speed are now given by

$$v_{\phi h} = \frac{\omega}{k_h} = 117(\pm 10) \text{ m.sec}^{-1}$$

$$v_{\phi z} = \frac{\omega}{k_z} = 13 \text{ m.sec}^{-1}$$

These are not vector components of the phase velocity, but the velocity of a point of constant phase along the horizontal or the vertical axis (Hines, 1974; Jones, 1976).

In summary, for the wave deduced from ionogram data, the parameters are:

Period T	= 1¼ - 1½ hours
Horizontal wavelength λ_h	= 560 (±90) km
Vertical wavelength λ_z	= 60 (±5) km
Horizontal trace speed $v_{\phi h}$	= 117 (±10) m.sec^{-1}
Vertical trace speed $v_{\phi z}$	= 13 m.sec^{-1}

Peak amplitudes of true height variations:

~ 4 km	1230 - 1400 hrs
~ 1 km	1400 - 1500 hrs.
~ 2-3 km	1500 - 1830 hrs.

An estimate of the minimum vertical wavelength allowed by viscosity can be obtained from the results of Hines (1974, Paper 13: and attached notes). Fig. N1 indicates that at altitude 180 km, the minimum vertical wavelength for waves unquenched by viscosity is about 100 km. On this basis the gravity wave is expected to lose energy through viscosity.

(e) Individual phase-height power spectra

Power spectra of the phase-height variations have been taken to examine the presence and power distribution of periodicities in the data.

The main interest in power spectra is to see how they change in time, and the results arising from series of overlapping power spectra are presented later. In this section an individual power spectrum is considered, and its properties briefly examined.

Most spectra taken for the daytime data of 19th February, 1978, are taken over 128 minutes (600 points) of data. Occasional spectra are taken over 192 minutes (900 points) of data. The data used has been passed through the "90-minute" filter prior to spectral analysis. Reference to Appendix C on spectral analysis methods will indicate that negligible bias in the positions of spectrum peaks is caused by the filtering.

Fig. 5-13 shows log spectra, with the log power amplitude of arbitrary magnitude.

The peak of greatest magnitude is that of period the data length. Overall the spectrum has a number of peaks in it. As discussed in Appendix C, they are felt to be real; and not a result of the use of the MEM method with too great an order

of error-predictor filter.

The first spectrum in Fig. 5-13 also shows a marked dip in response at about 18 minutes period. This will be discussed later in the section on Ionospheric Response.

The regularity of the spectrum peaks could indicate a series of harmonic responses. Table 5-4 indicates the harmonics of 45 minutes. Many of the harmonics of this period are present in the first spectrum of Fig. 5-13. It is interesting to note the 11.25 minute period is quite close to the clear inspection periodicity of 12 minutes.

Taking harmonics of 1½ hours gives the additional periods of 30.0, 18.0, 12.86 and 10.00 minutes. The latter two periods are not present in the data: the 18-minute period corresponds to that of zero ionospheric response: and, in anticipation of the results arising from the overlapping spectra, the 30-minute period is found to be present in later spectra.

It is thus possible that the phase-height spectra observed arise as harmonics of the basic 1½-hour period shown in the ionograms. Harmonics of a basic period have been observed in the incoherent-scatter electron-density data of Yeh, Liu and Hearn (1979). Their Fig. 6 for data of 8th May, 1974, shows spectral peaks which could be harmonics: it appears that three fundamental periods at 40, 31, and 25 minutes are present. The 31-minute period has three harmonic components and the other periods have two.

For a phase height experiment it is possible that harmonics may arise through the detection of phase height changes. The range distance from a transmitter to a reflecting point on even a sinusoidal reflector does not

itself vary sinusoidally. The deviation of the range variation from sinusoidal behaviour becomes greater as the amplitude of the sinusoid increases. Further increase of the sinusoid amplitude leads to the presence of more than one reflecting point, in general with different ranges.

These effects were noted in the work of Munro (1953) who recorded the group-path range for the virtual-height reflection of 5.8 MHz. He noted complexities in the range of the fixed-frequency echo, which at times gave rise to echoes at multiple ranges. The disturbances were classified into "X-", "Y-", and "Z-" types: the X-type arising from multiple specular reflections from a curved reflector.

The departure from sinusoidal behaviour of the range will lead to the presence of harmonics in the power spectrum of its variations. Austin (1969) has considered a sinusoidal reflector at height 100 km and wavelength 63 km, with increasing amplitude values a' of 0.1 km, 0.625 km, 0.95 km, and 2.0 km. The situation is shown in his Fig. 4-3, reproduced here as Fig. 5-15. For low values of a' the phase range is closely sinusoidal and similar to the shape of the reflector, but for increasing reflector amplitude the departure of phase range variation from that of the reflector is more apparent, until eventually Munro's "x-type" complexity is reproduced as a result of the presence of three specular-reflector points.

Table 4-1 of Austin (1969), reproduced here as Table 5-3, gives the harmonic components of the power spectra of the range variations. It is clear that the greater distortion in range leads to increased power in the harmonics.

TABLE 5-3

a′	Harmonic			
	Fundamental	1st	2nd	3rd
0.1	99%	0.21%	0.059%	0.024%
0.625	97%	2.07%	0.28%	0.054%
0.95	96%	3.20%	0.91%	0.18%
2.0	92%	6.40%	1.50%	0.30%

In part (d) above, it was found from ionogram data that for the 19th February, 1978, run considered here, a gravity wave was present with parameters:

$$h_{true} = 180 \text{ km}$$

$$\lambda_h = 560 \text{ km}$$

$$\text{Peak amplitude maximum} = 4 \text{ km}$$

$$\text{Period } T = 80 \text{ minutes} .$$

Range values at a time-interval of 12.80 seconds were calculated on the basis of a sinusoidal model identical to Austin's (1969). The parameters used were those of the wave seen on the ionogram and the resulting spectrum for 2 hours of data is in Fig. 5-15a.

A clear harmonic structure can be seen whose periods are appropriate to a fundamental of 80 minutes. Considerable similarity with the spectra of the experimental data can be seen.

An assessment needs to be made as to whether the real data is one wave at period 80 minutes whose harmonics appear in the phase-height results: or whether other periods are present.

A spectrum for a three-hour length of data taken for 19th February, 1978, is shown in the second panel of Fig. 5-13. For periods less than 15 minutes the positions of

spectrum peaks are fairly stable between the two-hour set and the three-hour set. Additional peaks are present in the three-hour spectrum arising most probably from the increased resolution with greater data length. A change of greater significance occurs for the 40-minute (two-hour spectrum) peak, which is split into two peaks at 50 minutes and 30 minutes for the three-hour spectrum. These could arise as the first two harmonics of an 80 minute oscillation.

In contrast, a three-hour spectrum of ranges arising from the sinusoidal model (not shown) showed very little difference from the two-hour spectrum.

The three-hour spectrum of the 19th February data would not be expected to arise from a stationary timeseries, but the effect of taking a longer length of data is one of improvement of resolution. Broadening of the spectrum peaks arising from non-stationarity of sinusoidal components does not seem to have occurred to any great extent. The non-stationarity of the spectrum could arise from that in the fundamental 80 minute wave, which would be reflected in the behaviour of the harmonics. The assumption of a sinusoidal reflector also is an idealized description - known to be incorrect because the 1345 ionogram shows a double (split) trace at the F_1 peak. Munro and Heisler (1956, Figs. 6 and 7) showed this to arise from a non-sinusoidal reflecting layer. Non-stationarity in the time series would arise from this also.

It is felt by this author that the spectrum peaks in the 19th February data arise mainly from harmonics of a 80 minute wave generated by the phase-height method of measurement. However, it is possible that harmonics

in the atmosphere itself exist due to the gravity wave (Yeh, Liu, and Hearn, 1979). Anticipation of the overlapping-spectrum results, discussed in (g) below, indicates that spectrum characteristics remain quite steady over some hours. One would expect this to arise from several oscillations of an 80-minute wave (which is present in the ionogram data), rather than from a broad spectrum of waves which would be expected to change more rapidly. The experiment cannot tell whether spectrum harmonics arise from harmonics in the range deviation, or in the atmosphere itself, or from a combination of these effects. If wave harmonics were present in the atmosphere itself and were measured by a phase-height experiment, they could, of course, generate their own harmonics in range variation. The data does not allow the verification or reputation of this conjecture.

(f) Ionospheric Response

Radio measurements of thermospheric oscillations measure electron movement, as opposed to neutral atmosphere movement. The response of the ionosphere to an internal gravity wave is highly anisotropic, and depends both on wave parameters and background ionosphere parameters.

Extensive computations of ionospheric response have been made by Hooke, (1968, 1970a, 1970b). His work has indicated a considerable difference in the nature of the response to a given gravity wave between the F_1 and F_2 regions. The F_2-region response is the simpler case, and is used below to give a very rough account of the same

TABLE 5-4 HARMONICS OF 45-MINUTES

Period	Present in Phase-height Spectrum (Fig. 5-13, first panel)	Present in Group Height Spectrum (Fig. 5-14)
45.00	Yes	Yes, if 55-minute peak acceptable
22.50	Yes	Yes
15.00	Probably	Yes
11.25	Yes	Probably
9.00	Yes	No
7.50	Yes	No
6.43	Probably	Probably
5.63	Probably	No
5.00	Yes	Yes
4.50	Yes	Yes
4.09	Yes	No
3.75	Yes	Yes

features of the data spectra. Then brief consideration is given to some features of Hooke's (1970b) results for the F_1 region, and their relation to the F_1 region data treated here.

The basis of Hooke's work is to assume a stationary atmosphere, with movement arising only from the perturbation velocity $\underline{u}$, of a gravity wave. For the F_2 region, changes in ionization concentration are taken to arise solely through ion transport. Production and loss are neglected as the lifetimes of the ions are longer than the wave frequencies of interest. (Hooke, 1970a). The ion transport velocity $\underline{u}_i$ is given by (MacLeod, 1966):

$$\underline{u}_i = \frac{1}{(1+R^2)} \left[R^2 \underline{u} + \underline{R}(\underline{u} \times \underline{l}_B) + (\underline{u} \cdot \underline{l}_B)\underline{l}_B\right]$$

with $R = \frac{\nu_i}{\omega_i}$, the ratio of ion-neutral collision frequency ν_i to ion gyrofrequency ω_i. $\underline{l}_B$ is a unit vector in the direction of the magnetic field. The time-rate of change of electron density, arising solely from the ionization movement, is obtained from the continuity equation.

Equation (7) of Hooke (1970a) then gives the F_2-region electron-density perturbation, as a function of gravity-wave and background ionosphere parameters:

$$\frac{N'_e}{N_{eo}} = \left(\frac{\underline{u} \cdot \underline{l}_B}{\omega}\right) \left\{(\underline{k} \cdot \underline{l}_B + i(\underline{l}_B \cdot \underline{l}_z) \cdot \left[\frac{1}{2H} + \frac{d}{dz}(\ell n\ N_{eo})\right]\right\}$$

where $\underline{k}$ is the total wavenumber of the atmospheric gravity wave, $\underline{l}_z$ is a unit vector vertically upwards, and H is the neutral atmosphere scale height.

Sterling et al. (1971) have simplified this expression, for F_2-peak conditions and for meridionally-travelling transverse gravity waves with $\lambda_z << 4\pi H$. Their equation (4) gives

$$\frac{N'_e}{N_{eo}} = \left(\frac{u\tau_g}{2\lambda}\right)\left(\frac{\tau}{\tau_g}\right) \sin\left[2 \sin^{-1}\left(\frac{\tau_g}{\tau}\right) - 2I\right]$$

where I is the magnetic inclination. (A correction factor of 2 in the denominator, found necessary by Nagpal et al. (1974) has been inserted above).

The quantity

$$\left(\frac{\tau}{\tau_g}\right)\sin\left[2 \sin^{-1}\left(\frac{\tau_g}{\tau}\right) - 2I\right]$$

with $I = -68.9^\circ$ (Roederer et al. 1965) for Christchurch, New Zealand, is plotted in Fig. 5-16. The solid line is for

τ_g = 12.5 minutes, previously found from the measured scale height assuming an isothermal atmosphere. The dashed line is for τ_B = 8.5 minutes in the temperature-varying case.

It will be noted that the Sterling equation (hence Fig. 5-14) allows a zero ionospheric response to neutral-atmosphere waves of a certain period. At the F_2-peak, where $\frac{d}{dz}(\ell n\ N_{eo}) = 0$, this condition arises when $\underline{u}.\underline{l}_B$ is zero: physically the neutral-gas velocity is at right angles to the field lines and has relatively little influence on the ionization movement. Also, the response is almost zero for $\underline{k}.\underline{l}_B = 0$, and for gravity-waves of small vertical wavelength the vertical wavenumber term will exceed the $\frac{1}{2\pi}$ term and the response dip will be quite pronounced.

The latter case applies for equatorward-propagating waves (Hooke, 1970a, Fig. 1). Equation (34) of Hines (1960), which is an approximation to the full dispersion relation (21) in the limit of long periods and short vertical wavelength, is:

$$\omega^2 k_z^2 = \omega_g^2 k_x^2 \quad .$$

Under these circumstances the angle θ of wave-vector $\underline{k}$ to the horizontal is given by

$$\tan\theta = \frac{k_z}{k_x} = \frac{\omega_g}{\omega} = \frac{\tau}{\tau_g}$$

and for $\underline{k}$ to be perpendicular to the magnetic field line, so that $\underline{k}.\underline{l}_B$ is zero, the angle of dip I is $\frac{\pi}{2} - \theta$. Thus for zero response

$$\tan I = \frac{\tau_g}{\tau} \doteq \sin I, \text{ small for long periods}$$

for which comes the zero-response condition $I = \sin^{-1}\left(\frac{\tau_g}{\tau}\right)$.

Although applicable strictly only to long periods, this gives a physical insight into the cause of zero ionospheric response.

For τ_g = 12.5 minutes, zero ionospheric response would be expected for wave period τ = 35 minutes. For τ_B = 8.5 minutes, zero response occurs at τ = 24 minutes. This latter result is closer to the observed power dip at τ = 18 minutes: in fact, the period value for minimum response is sensitive to the value of τ_B used and a value of τ_B = 6.5 minutes gives a zero-response period of 18 minutes.

It must be recalled that the Sterling et al. (1971) equation applies only at the F_2-peak, for meridionally-travelling waves with $\lambda_z << 4\pi H$. The data run of 19th February, 1978, was taken in the F_1-region and azimuthal direction is unknown.

For the data, the ionogram results previously discussed give λ_z = 50 km, so with H = 35 km, $\lambda_z \triangleq 0.11(4\pi H)$. The observed dip in the spectrum at τ = 18 minutes could arise from the zero-response effect. The estimate of τ_B = 8.5 minutes from the ionograms is only an estimate; moreover, wave propagation at other azimuths will also shift the period of zero response (Gupta and Nagpal, 1973).

Examination of the spectra show an increased amplitude of response at longer periods. This might be expected from the theoretical response curve. Two reasons exist to make this an inadequate explanation. First, the theoretical response curve is based on the work of Hooke (1970a) which assumes the same energy density per unit mass for internal gravity waves for all periods. If the differing spectrum periods arise as harmonics of a basic 1½ hour oscillation

(as previously discussed), the energy density would be expected to fall off for higher-order harmonics. Greater activity level at longer periods would also reflect greater energy as well as larger response.

The second inadequacy in the explanation above is that for daytime F_1-region conditions, the work of Hooke (1970b) shows that the expected response does not always increase with period. A response maximum can be reached in the 20-30-minute-period region and then the response decreases as period increases. Hooke's (1970b) Fig.4 indicates this. However, it must be noted that Hooke's (1970b) caculations assumed equal wave energy density for all waves so that even this effect could be overcome if the neutral waves at longer periods had greater energy.

The application of an F_2-peak response calculation to F_1-region data must thus be taken with considerable caution. Within the F_2-region itself, the F_2-peak response can give a reasonable indication of expected response at other F_2-region heights, as illustrated by the incoherent-scatter electron-density data of Yeh, Liu, and Hearn (1979). Their Fig. 6 shows electron density power spectra at three F_2-region altitudes: one at the F_2-peak and one each above and below the peak. All three spectra illustrate the expected spectrum dip: that at the F_2-peak most sharply. This does not justify the extrapolation of F_2-peak results to F_1-region conditions, where the effects of ionization production and loss become significant.

The theory of Hooke (1970b), which applies to the F_1-region, is the appropriate one to apply to the experimental results obtained here. In contrast to the F_2-region, solar

directional control of ionospheric response is considerable in the F_1-region. It turns out that the calculations of Hooke (1970b) were made for Sydney, Australia. His results will be used here as an indication of possibilities; as definite confirmation of,or disagreement with,his results is not possible with the data obtained here.

Reference to Hooke's (1970b) Fig. 3 indicates that the ionospheric response as a function of wave direction has very predominant maxima (sharp directional "tuning") in winter, and hardly any directional tuning in summer (apart from the considerable enhancement in response for waves with an equatorward propagation component over those with a poleward propagation component). For 19th February, 1978, the solar declination is about -12^{o} (Astronomical Ephemeris data): thus a response between the second and third panels of Hooke's Fig. 3 might be expected. It would have two fairly broad peaks, close together in azimuth and not well-resolved, and with amplitudes not much greater than the overall response to all waves with a northward propagation component.

Hooke's Fig. 3 is for a local time of 0800 hours. In general, the peaks in F_1 region response are calculated to follow the sun in azimuthal directions across the sky, and so for the data recorded from 1230-1900 hours L.T. here, a small enhancement in amplitude might be expected for waves travelling in a North-West direction: with preferred direction becoming more westerly as the day progresses.

In fact, with the small peak amplitudes, the only significant factor likely in directional response is the substantial difference in response for Northward/Southward travelling waves.

A further point to be noted from Hooke's Fig. 3 is that for summer conditions, the calculated ionospheric responses including wave-induced ionization production and loss, and neglecting them, are very close. (In Hooke's 1970b paper the solid curves represent the former case and the dashed curves the latter one). As Hooke (1970b) notes, the dashed curves, for computation neglecting wave-induced ionization, correspond closely to the response results of Hooke (1970a) arising solely from dynamical effects in the F_2-region. The major difference between these cases is one of response amplitude: the calculated amplitudes of Hooke (1970b) are less than those of Hooke (1970a) because of an additional ionization loss rate term in the governing equations for the F_1-region response. (Hooke, 1970b, Equations (19) and (20): contrast with Equation (18) for the F_2-region response).

In the light of these results, it is tempting to extrapolate Hooke's results to state that in summer, there is a similarity in ionospheric response between the F_1- and F_2-regions assuming a stationary atmosphere. One might then state that the Sterling et al. (1971) result actually explains the spectrum dips seen for the F_1-region data.

Unfortunately such extrapolation is not justified. It must be noted that Hooke's (1970b) Fig. 3 applies for wave parameters of λ_h = 400 km, λ_z = 200 km, and τ = 26.5 minutes. Reference to other F_1 results of Hooke's (Hooke 1968b) indicate that for parameters λ_h = 100 km, λ_z = 100 km, and τ = 15.3 minutes, then winter response has less directional tuning and is closer to the results neglecting photoionization perturbations than the corresponding summer data (Hooke, 1968b, Fig. 5).

Without exact calculations for the conditions of the data observed, attempted extrapolation of Hooke's published results is really guesswork. One notes that for winter conditions (Hooke, 1970b, Fig. 4), the greatest overall response amplitude is for waves in the 20-minute period region, and the response actually decreases for longer periods. Exact calculation would be needed to find the expected summer response: moreover the energy density per unit mass of the measured waves is most unlikely to be the same at all periods. High energy at greater periods would predominate over a slight decrease in ionospheric response.

An overall assessment of the effects of ionospheric response (assuming for the present a stationary atmosphere) is that for F_1-region data the F_2-response can give an approximate guide to expected response, but that for meaningful comparisons with theoretical F_1-region response, exact calculations using Hooke's theory need to be made.

(g) Overlapping Spectra

An indication of spectrum change with time over the duration of the data run has been obtained by finding the successive spectra of a 128-minute data segment, as it is moved through the data run in time.

Fig. 5-17 shows a set of 76 spectra. The first spectrum is for the 1256-1504 data, and each succeeding spectrum is for a data segment starting and finishing 154 seconds in time after its predecessor. The axis into the page indicates the starting time of day for data input to the labelled spectrum: the spectrum is thus over 128 minutes starting at the labelled time.

Fig. 5-18 is as Fig. 5-17 but indicates spectra from a rear view. For both these figures, the power amplitude scale is linear. The peak whose period is the data length, 2 hours, has been omitted. Fig. 5-19 presents the same information as successive log spectra in time: the whole group of spectra have been rotated towards the observer. Period changes are most easily seen on this figure.

Data input to the spectrum analysis has been filtered by the "90-minute" filter to attenuate, but not remove, trends.

Examination of Fig. 5-19 indicates that successive spectra are mostly regular and stable until 1445 hours, after which the spectra change with time, indicating peak splitting and shifting. This occurs at almost all periods (Fig. 5-19) but can be seen most clearly at the longer periods. Fig. 5-19 does indicate that minor spectrum changes do occur at all times.

One feature which seems predominant over the whole data run is a very steady 8-minute peak, which, on the basis of the ionogram scale-height calculations, corresponds to the Brunt frequency. Features which alter are the 12-minute peak, which splits to 11 and 14 minutes after 1445; and the 30-minute peak, which splits to 22 and 45 minute-peaks after 1445.

The MEM spectral analysis can give false peak splitting and shifts (Fougere et al. 1976). On the basis of the tests and discussion in Appendix C, it is stated that spectrum changes illustrated here are features of the data and not artefacts of the MEM method.

The 18-minute response dip, noticed in the 1256-1504 spectrum and discussed in the context of F_2-region dynamical response (which left aside the question of F_1-region

measurements and associated photochemical effects on ionospheric response) can be seen as a feature of the spectra at 16 minutes period until 1445 or so. After this time, a predominant dip appears at 20 minutes, and a dip in response can also be seen at 13 minutes after 1530 hours. The 18-minute dip between 1230 and 1445 becomes very small between 1410 and 1420.

Other significant changes at 1445 are the behaviour of the 12-minute peak and 30-minute peak. To assess the reality of these effects a test is made for the effect of data length taken, on the resulting spectrum.

Fig. 5-20 shows a comparison of the first fifteen linear spectra arising from data length of 3 hours (192 minutes) and 2 hours (128 minutes) respectively: Fig. 5-21 does the same for log spectra.

For periods of 15 minutes or less, the two cases show spectral peaks broadly in the same positions and with similar stabilities. The 3-hour spectra have improved resolution, illustrated in some peak splitting for the shorter periods. For the 2-hour data, the 18-minute dip of the first two spectra can be seen to become a 16-minute dip subsequently, as discussed before. For the 3-hour data, a steady 18-minute peak, surrounded by steady dips at 15 minutes and 21 minutes, can be seen. The 30-minute peak (initially 40 minutes) of the 2-hour data is resolved into two peaks, of periods 30 minutes and 45 minutes, in the 3-hour data. These latter peaks are quite steady in period over the spectra shown (contrast the 40-minute peak of the first two 2-hr spectra with the 30-minute peak of the remaining spectra) and could be interpreted as confirmation of the 1½-hour layer oscillation

and associated harmonics discussed earlier.

For the spectra shown in the comparison, the spectra for 3 hours length of data seen better resolved and more stable in time over the 2-hour spectra. The 3-hour spectra effectively cover the data from 1300 to 1640, which is the end of the data length taken for the last 3-hour spectrum.

The lengthening of a data sample over which a spectrum is to be found does allow increased resolution of adjacent sinusoidal components. However, broadening of spectrum peaks can occur if the timeseries is non-stationary. The sequence of 2-hour spectra from 1300-1330 starting times indicates that the timeseries is reasonably stationary from 1300 to 1530, so that the main effect of taking 3 hours of data per spectrum will improve resolution, especially at longer periods.

The behaviour and changes of the long-period peaks for the 2-hour spectra thus need to be assessed with some reservation. Thus the split, after 1445, of the 30-minute peak into two peaks of periods 45 minutes and 22 minutes (Fig. 5-19) would indicate a genuine indication of change in spectrum characteristics after that time, but the period values themselves are of some doubt.

Figs. 5-17 and 5-18, the linear plots, show that marked differences occur in the amplitude of the 30-minute (45-minute and 22-minute after 1445) over the data run. For example, the amplitude is low for spectra at starting times 1300 - 1345 hours and again at 1415 - 1500 hours. Between starting times of 1345 - 1415 hours and 1500 - 1545 hours the peaks (at 45 minutes after 1445) have considerable amplitude.

It will be observed also that the higher peaks are generally narrow-band and the lower peaks somewhat broader-

band. For MEM spectra, the estimate of power at a given frequency is given by the area under the spectrum peak, not by the peak amplitude (Ulrych and Bishop 1975). Thus the broad-band activity and narrow-band activity have comparable (with a factor of 2 or 3) powers.

Direct comparison of the "90-minute filtered" data (Fig. 5-7) with the associated spectrum shows fairly regular periodic behaviour until 1400, after which a lesser phase coherence can be seen to cause irregular amplitudes and non-cyclic "periods". Such changes are even more marked after 1445, the time that changes in behaviour are seen in the spectra. The data for the later half of the run is not shown here.

Throughout the duration of the run, the true height rose from 170 km to 240 km steadily (Fig. 5-8), with measurements made on the F_1-region throughout.

(h) The direction of propagation

The phase-path data presented to this point have been obtained using coherent transmission and reception at one antenna. This antenna was one of three placed in a right-angled triangle with a spacing of 250 m along the right-angled sides. Fig. E-1 of Appendix E indicates the arrangement, which is used for an ionospheric drift experiment.

Coherent reception was performed at 4.57 MHz for F-region observations at all three spaced antennas. It was hoped to obtain the direction of propagation by observing the time differences between phase maxima between the aerials. This method has been used by Vincent (1972) in his E-region

observations of phase height: he used antennas at spacings of 730 and 910 metres, and successfully obtained wave directions.

As expected, this approach did not work well with the coherent F-region observations reported here. The F-region structures are larger, and show very little change within the spacing of the antennas here. Any velocities and directions derived were found to have such high errors that the values were meaningless. This was because the time differences between aerials were very small.

This was unfortunate, because the observation of phase maxima at spaced antennas does not depend on the relative phase calibration between the different receiver/feeder/ antenna systems. The existence of a phase maximum, and its time displacements from phase maxima at other aerials, do not depend on obtaining the correct value for the phase at each aerial.

By contrast, another approach was attempted, using the phase of the complex cross-correlation between the antennas. The essentials of the method are that the phase of the complex cross-correlation between two timeseries is the mean phase difference between the signals, with individual phase values present in the mean being weighted according to their relative values (Pfister, 1971; Paul, Wright, and Fedor, 1974). The phase difference is of course averaged over the time over which the correlation was taken. From this the echolocation may be determined. The changes of the echolocation in time give the direction of wave travel.

The two main assumptions behind this approach are: firstly, that what is measured by the correlations is the

same thing measured by the tracked phase height. If the correlations are looking at a much smaller-scale phenomenon then this approach will be invalid. The second assumption is that radio propagation is free space until a sinusoidal perfect reflector is reached, ignoring the effects of radio-wave refraction and underlying variation in electron density A technical assumption is made also: that the absolute phase differences between receiver/feeder/antenna systems are known.

In obtaining absolute values of echolocation position this last assumption is probably the least valid. In contrast to the comparison of phase maxima between antennas, this approach has a very low random error but an unknown systematic error in direction. In spite of this, however, it does allow the observer to see if the echolocation moves primarily along a line (the trace direction of the wave) or whether it moves in a random way.

Fig.5-22 shows a typical complex crosscorrelation. Correlations were not taken over the whole run, but only over about an hour of it. The resulting echolocations are shown in Fig. 5-23. In general, they are located near a line in direction 90^{o} East of North (or 90^{o} West of South).

It will be noted that echolocation for times quite close together are often situated on opposite sides of the origin. This is probably because incoming phase differences are forced within the range -180^{o} to 180^{o}. If a wider range were allowed, more points which are close in time would be close in echolocation, as expected for a large-scale wave.

The result obtained agrees broadly with the statistical data obtained by Munro (1958). His Fig. 6 indicates a

February mean velocity over eight years of data of about 120 $m.sec^{-1}$ directed 120^{o} East of North. Munro's mean value for February is, of course, taken over a very large number of disturbances over many February day and years. Scatter around the mean arose from diurnal, day-to-day, and year-to-year changes, but for February data his Fig. 11 shows the directions to be almost all East of North with an occurrence peak at 120^{o} East of North. Similarly his Fig. 16, for January, 1951-1954, shows the diurnal variation in disturbance direction to be within $\pm 40^{o}$ of 120^{o} East of North between 1300 and 1700 hrs. The point to be made here is that the scatter in Munro's observed data is narrow enough that propagation East of North is a very much preferred direction. The existence of the direction observation here within this scatter range is the significant fact: not the close agreement with the overall mean.

Cowling, Webb, and Yeh (1971) have studied the propagation of internal gravity waves in a horizontally-stratified windy atmosphere. By tracing a gravity-wave group ray through a series of horizontal layers, each with its own wind velocity, they find that three physical processes arising from the interation of the wind with the wave may arise:

(a) *Reflection.* If the wind is blowing strongly against the wave, then a height may exist for which the gravity-wave group ray is reflected from that height and continues to propagate with a downward component towards the ground.

(b) *Critical coupling.* A wind blowing strongly in the wave direction may Doppler-shift the wave frequency to zero, to an observer moving with the wind. The wave is not reflected, nor does it penetrate beyond

the height at which critical coupling occurs; but rather it is absorbed into the wind flow.

(c) *Penetration.* A wind that is not strong enough to cause either reflection or critical coupling of the gravity wave will allow the gravity wave to propagate to greater heights.

In general, the adoption of a model of horizontal wind as a function of altitude and of time imposes restrictions on the periods, speeds, and azimuths of ground-generated gravity waves which may be seen in the F-region. Only waves which have penetrated to the chosen altitude will be observed: others will be either reflected or trapped. Fig. 6 of Cowling, Webb and Yeh (1971) indicates the allowed starting azimuth directions of a 45-minute gravity wave on the ground, which will allow observation at 300 km. The allowed directions are a function of local time of observation.

Yeh, Webb, and Cowling (1972) have fitted Munro's (1958) statistical data to their model. Munro's diurnal variation of observed azimuth with local time of observation was found to correspond to the penetration region allowed by the winds. In addition, the observations were found to correspond with those waves which took minimum time to propagate from the ground to the observation point.

Such wind effects are only one of the selective provesses which apply to gravity-wave propagation into thermospheric heights. The ionization response discussed in (f) above is another selective process, one of ionization response to a given gravity wave and thus relevant to radio observations.

The windy atmosphere model of Cowling, Webb, and Yeh (1971) takes the gravity wave to be generated at the ground. In section (i) below, the auroral electrojet is considered as a possible source mechanism, and this is located at 120 km. It is recognised that the considerations of this

section and that below are inconsistent, and that a combined calculation is really necessary for best comparison with data.

(i) The auroral electrojet as a possible source mechanism.

To this point, the analysis of the phase-height data has been in terms of the wave parameters present at the point of observation over Christchurch. In this section a brief discussion of the auroral electrojet as a possible source mechanism is made, based on model predictions of Francis (1973a, 1973b, 1974).

Since the first observations of TIDs, an observational distinction has been made between "large-scale" and "medium-scale" TIDs. The former group are characterized by very high phase speeds (300 - 1000 $m.sec^{-1}$), large amplitudes, and long (800 - 3000 km) wavelengths, and their occurrence is well correlated by high magnetic activity, as indicated by the planetary magnetic index $K_p > 5$.

The second group of disturbances are characterized by lower (100 - 250 $m.sec^{-1}$) phase speeds, smaller amplitudes, and smaller (100 - 600 km) wavelengths, and are not clearly correlated with magnetic activity. Within this group a further observational distinction has been made between periodic and non-periodic disturbances (Titheridge, 1968, 1971).

Both large- and medium-scale disturbances have been observed to propagate for several thousands of kilometres and this has lead to the hypothesis that a ducting mechanism applied to the wave propagation. This has been confirmed by Francis (1973a) in the case of the large-scale TIDs. If the steep temperature rise at the base of the thermosphere

is modelled as a step function in temperature, the large-scale TIDs may be modelled as surface waves travelling along the temperature interface. The speeds and propagation distances calculated agreed with the results of observations.

The view that medium-scale TIDs were also ducted modes was initially upheld by the work of Friedman (1966) who obtained a discrete spectrum of wave modes, ducted between the mesopause and the earth's surface. Speeds in the correct range for medium-scale TID were obtained and the observations in the F-region arose from leakage from the mesosphere duct.

Later calculations by Francis (1973b) indicated that the discrete modes obtained by Friedman arose because his step-function approximation to the atmospheric temperature gradient was too coarse in altitude. The results of Francis (1973b) indicate that medium-scale TID are freely propagating gravity-wave modes. Observations in the F-region arise because typically only 25% of the wave energy of an upgoing gravity wave is reflected at the thermospheric interface, allowing gravity wave effects to be observed in the F-region. Francis' conclusions were that no strongly ducted modes with phase speeds less than 250 m. sec^{-1} existed, and that the long distances of propagation sometimes observed arise from the refraction of free gravity waves to follow the surface of the earth (Francis, 1972).

The travelling disturbance present in the data for 19th February, 1978, is clearly in the medium-scale class. On the basis of Francis' calculations, it can be expected to propagate as a free gravity-wave mode.

It is now of interest to consider the auroral electrojet as a possible candidate for a source. The

models of Francis (1973a, 1973b) hitherto quoted are propagation models, but he has also modelled the medium-scale disturbances expected to arise from a line source of force, analogous to the action of the auroral electrojet.

The full calculated response consists of a discrete spectrum of high-speed ducted modes (corresponding to the large-scale TID) and a continuous spectrum of freely-propagating waves (corresponding to medium-scale TID).

Francis' (1974) calculations indicate that two families of freely-propagating waves exist. The first family of waves is non-periodic - almost pulse-like - and examples can be seen in Francis (1974, Figures 8 to 12). This family of waves is associated with direct propagation from the source through the atmosphere to the observation point. The second family consists of periodic waves with several cycles present, and these arise when a ground reflection occurs along the gravity-wave ray path between emission from the source and observation at the field point. The calculated results for these cases may be seen in Francis (1974, Figures 3 to 7).

To compare the measured data with either of these cases, consider Fig. 5-19. As previously noted, the over-lapping spectra indicate fairly stable periodic behaviour from 1300 to 1530. When it is recalled that the time of day given is that for the *start* of the two-hour data segment, then stable periodic behaviour could be considered present from 1300 to about 1700.

This period of time includes 3 cycles of an 80-minute wave. It will be recalled also that λ_x = 560 km and period T = 80 minutes.

Fig. 3 of Francis (1974) indicates the horizontal neutral velocity fluctuation $V'_x(x,z,t)$ where x is the ground range from the source, z is the observation altitude (200 km, close to that for the experiment here) and t is the time after the action of the source.

The t = 5 hrs panel of the figure shows a mean horizontal wavelength $\langle\lambda_x\rangle$ = 549 km over a ground range x of 3000 - 5000 km. Fig. 5 (Francis, 1974) indicates a mean period $\langle\tau\rangle$ = 61 minutes at ground range x of 5000 km. About five wave cycles are present.

The wavelengths between the data and the model agree well, and the periods agree with somewhat more discrepancy. The ground range is found by noting that the maximum auroral occurrence occurs in a zone located at about 78°S geomagnetic latitude on the day side (Whitten and Popoff, 1971). With Christchurch at 47.7°S geomagnetic latitude and earth-plus-altitude radius of 6600 km, the ground range from source to observation point becomes 3500 km.

Qualitative agreement exists between the data measured here and Francis' (1974) model.

Examination of magnetic activity indices (Lincoln, 1978) indicates, for 19th February, 1978, the planetary magnetic K_p index to have values 3 and 4- for Universal Time periods 0000 - 0300 and 0300 - 0600 respectively. (It will be recalled that the data run time was 1230 - 1830 N.Z.S.T., which is twelve hours in advance of U.T.) These values indicate moderate worldwide magnetic activity: approaching a value large enough to expect the occurrence of large-scale TID. From the tables (Lincoln, 1978) the K_p index for the run of 1230 - 1830 exceeds the adjacent three-hourly values

on either side of the run.

The presence of moderate K_p does not indicate only auroral-zone activity, as it is a world-wide index obtained from data of many stations. A more specific measure of auroral zone activity is the AE index, which is derived from magnetic measurements at sub-auroral stations (Rostoker, 1972). Unfortunately AE values are not readily obtainable, and are not available at Christchurch for 1978 at present (Mr. P. Gill, DSIR Geophysical Observatory, personal communication), and so no statement can be made about their values for the present data.

The qualitative agreement between the model of Francis (1974) and the data here, together with the magnetic activity level, does allow the auroral electrojet to be a candidate as a source for the wave observed. No more definite statement than this can be made. On the one hand, the model of Francis (1974) assumes an atmosphere stationary in the absence of wave perturbation, and the presence of winds along the propagation path and at the point of observation may affect the calculated response considerably. For the data, the tentative East-West direction obtained in (h) above, if reliable, would rule out the auroral electrojet as a source on the grounds of direction. This discussion has been, therefore, only a statement of a possibility.

(j) The presence of neutral winds.

Davies et al. (1973) have observed spectral maxima in Doppler data at periods under the Brunt period for the height observed. They attribute this effect to a Doppler shift of the observed wave frequency due to a wind at the

height of observation. The intrinsic wave frequency τ and observed wave frequency τ_o are related by

$$\tau_o = \frac{v_\phi - U}{v_\phi} \tau$$

where v_ϕ is the horizontal trace speed of the gravity wave as measured on the ground, and U is the horizontal component of the wind parallel to v_ϕ.

Geisler's (1967, Fig. 4) model is used to obtain neutral wind velocities at 300 km altitude. Taking v_ϕ = 117 m. sec^{-1} at 90^o East of North, Table 5-5 gives Geisler's wind velocities and the values of the factor $\left(\frac{v_\phi - U}{v_\phi}\right)$.

TABLE 5-5 PERIOD DOPPLER SHIFTS

Time	Geisler Model		U, m. sec^{-1}	$\frac{v_\phi - U}{v_\phi}$
	Speed	Direction		
1327 hrs	65 m. sec^{-1}	210^oE of N	65 cos(210^o-90^o= - 33	1.3
1745 hrs	70 m. sec^{-1}	90^oE of N	70 cos(90^o-90^o) = 70	.4

The table shows that for a constant intrinsic wave frequency, the observed wave frequency would be expected to vary by a considerable amount. No sign of any frequency change of such magnitude is illustrated in the log overlapping spectra, Fig. 5-19.

VI CONCLUSIONS

A phase-path run of data was taken at Christchurch on 19th February, 1978, from 1230 - 1830 NZST and spectral analysis was performed on the phase changes. Synoptic ionogram observations at 15-minute spacing were examined for evidence of travelling ionosphere disturbances.

A medium-scale travelling disturbance of several cycles duration was present throughout the run. No major complexities were observed in the traces, but an analysis of kinks and thickenings by Dr. C.H. Cummack of DSIR Geophysical Observatory indicated the presence of a wave with parameters

$T = 1\frac{1}{4} - 1\frac{1}{2}$ hours

$\lambda_h = 560\ (\pm 90)$ km

$\lambda_z = 60\ (\pm 5)$ km

$v_{\phi h} = 117\ (\pm 10)$ m. sec^{-1}

$v_{\phi z} = 13$ m. sec^{-1}

and with peak amplitudes of true height variations of 2 - 4 km.

A phase-path spectrum analysis performed by this author indicated the existence of a number of spectrum peaks, which were harmonically related. The harmonics appeared to be those of a basic 80 - 90 minute wave. On this basis it was concluded that only the one wave - with parameters above - was present and that the other spectrum peaks arose from harmonics in the range variation of the phase path. This conclusion was confirmed by observing that the spectra of 3 hours data indicated more of the expected harmonics. This interpretation assumes free-space propagation until a sinusoidally-shaped reflector is reached, which is an over-simplification of the physical situation; yet a power

spectrum of such a simulation was found to reproduce the data quite well. Phase-path and ionograms seem to be measuring the same wave.

In the power spectra a fairly consistent peak at eight minutes can be seen: it is not possible to tell if this is a high harmonic of 80 minutes or an oscillation at the Brunt frequency for the atmosphere. A minimum in power spectrum response is observed at 18 minutes period, which is reasonably close to that calculated from the ionization-response model of Hooke (1970a).

An examination of overlapping spectra indicated that for most of the run, the spectrum characteristics were very stable in time. It is interesting to note that this spectrum stability existed over a set of data which was very largely incoherent, according to the criterion of Fraser and Vincent (1970). The steady period values and number of cycles of the wave made the auroral electrojet a possible candidate as a source mechanism, when compared with the model predictions of Francis (1974). The moderate magnetic activity, indicated by $K_p \sim 3\text{-}4$, allowed this as a possibility. The stability of the overlapping spectra also indicated that changing winds did not alter the wave periods by Doppler shift to any great extent.

An attempt was made to obtain wave direction by use of the complex autocorrelation phase to obtain the echolocation. The absolute reliability of the measurements is in some doubt, but indications were that propagation was in a direction 90° East of North. This is close to Munro's (1958) mean of statistical data for February for many years of observations.

The observations are a typical example of a medium-scale travelling ionospheric disturbance.

FIG 5-1

PHASE HEIGHT BANDPASS DETRENDING FILTER

TIME SPACING OF POINTS IS 12.8 SECONDS

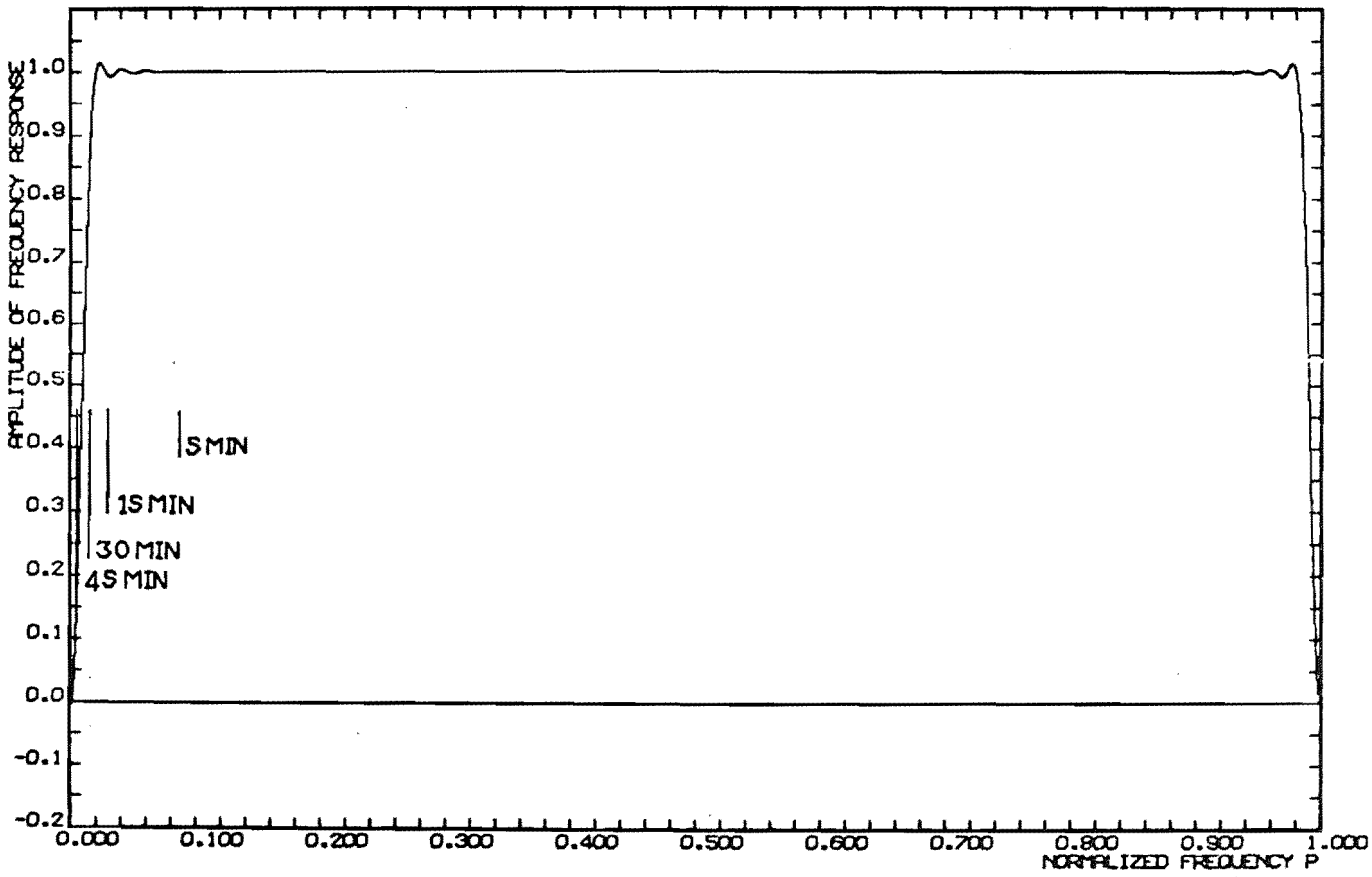

FIG 5-2

COMPARISON OF DATA FILTERS

TIME SPACING 12.8 SECONDS

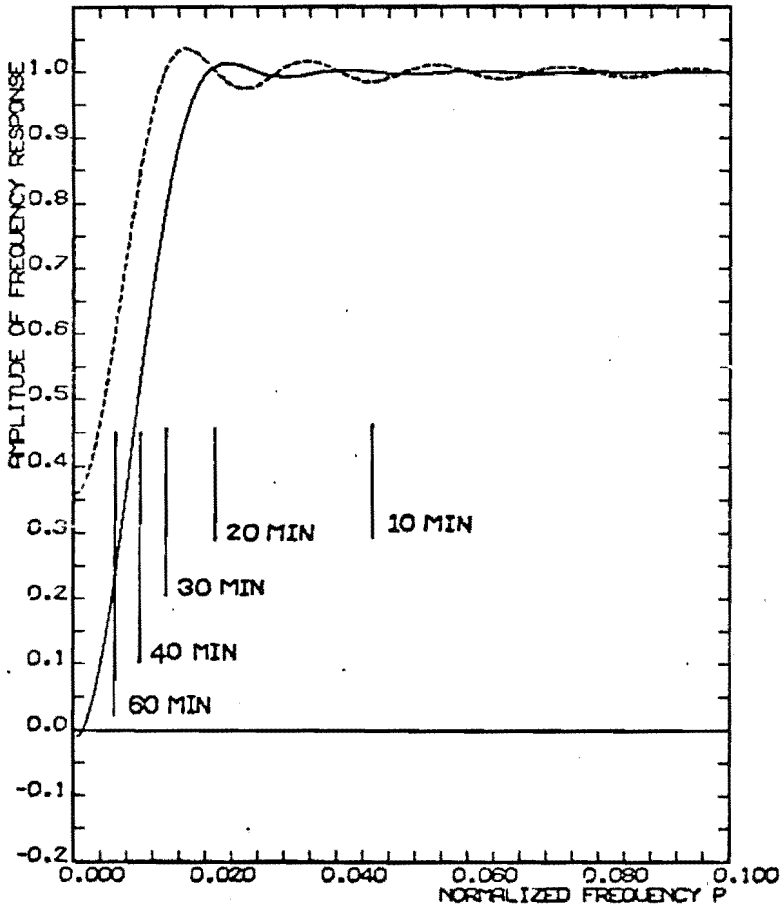

FIG 5-**4a** F1 REGION 19 FEB 1978 AT 1230

ΔT 12.8 SEC FREQ 4.57 MHZ HEIGHT 170 KM

DT0219781230 TRACKED AND FILTERED PHASE

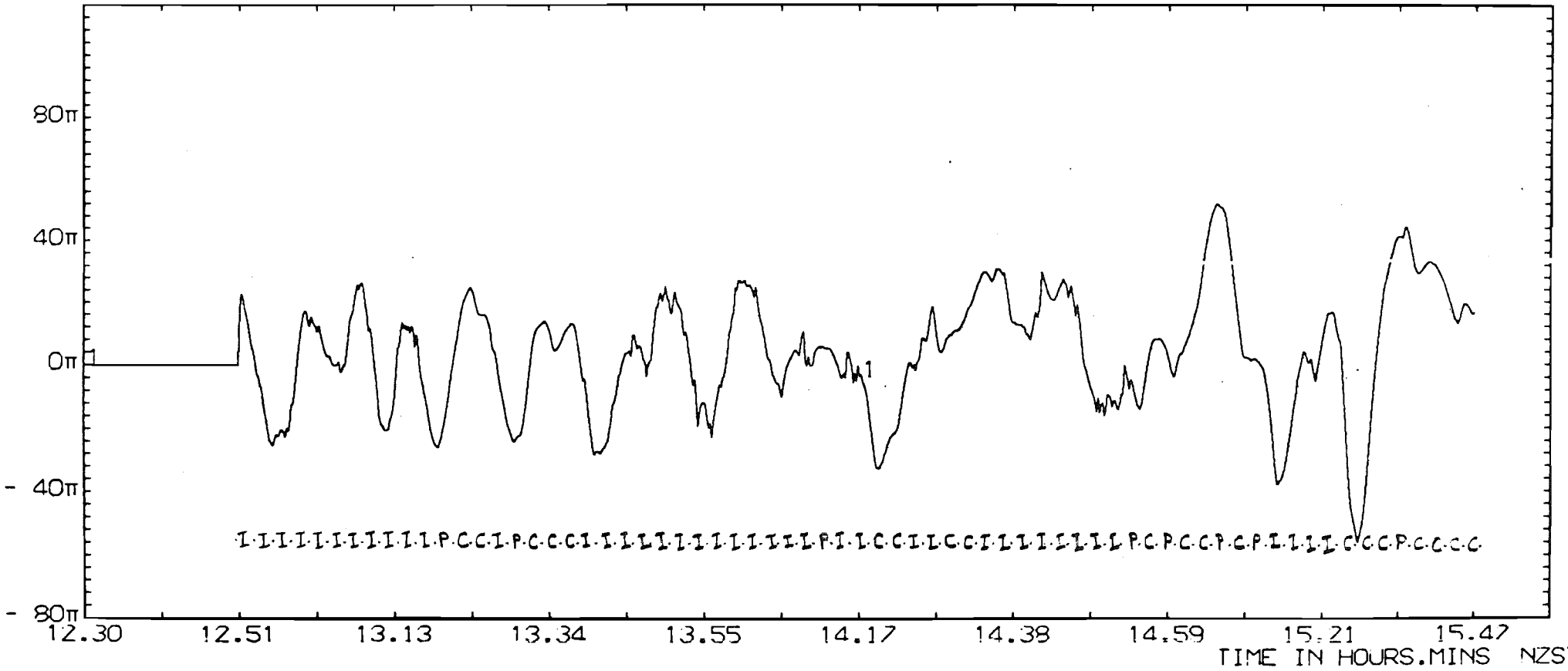

FIG 5-**4b** F1 REGION 19 FEB 1978 AT 1230

ΔT 12.8 SEC FREQ 4.57 MHZ HEIGHT 170 KM

DT0219781230 TRACKED AND FILTERED PHASE

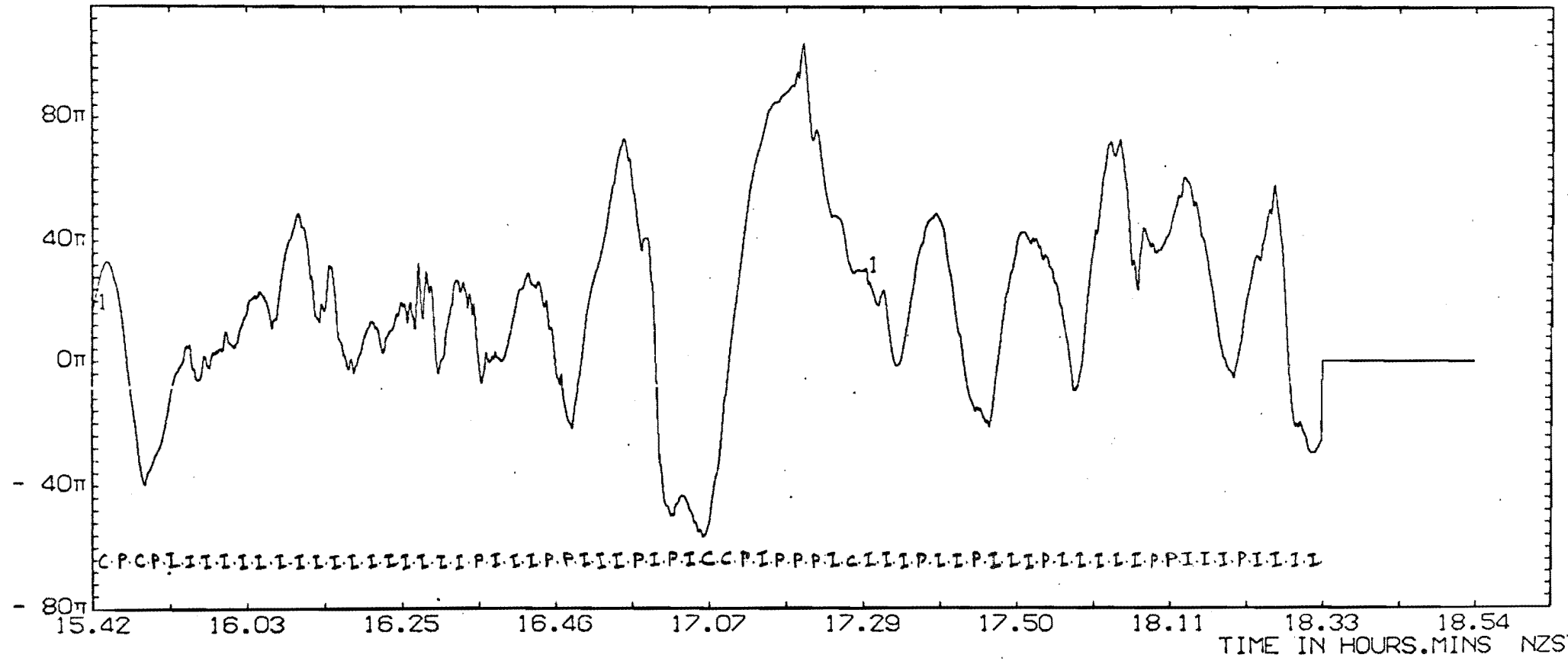

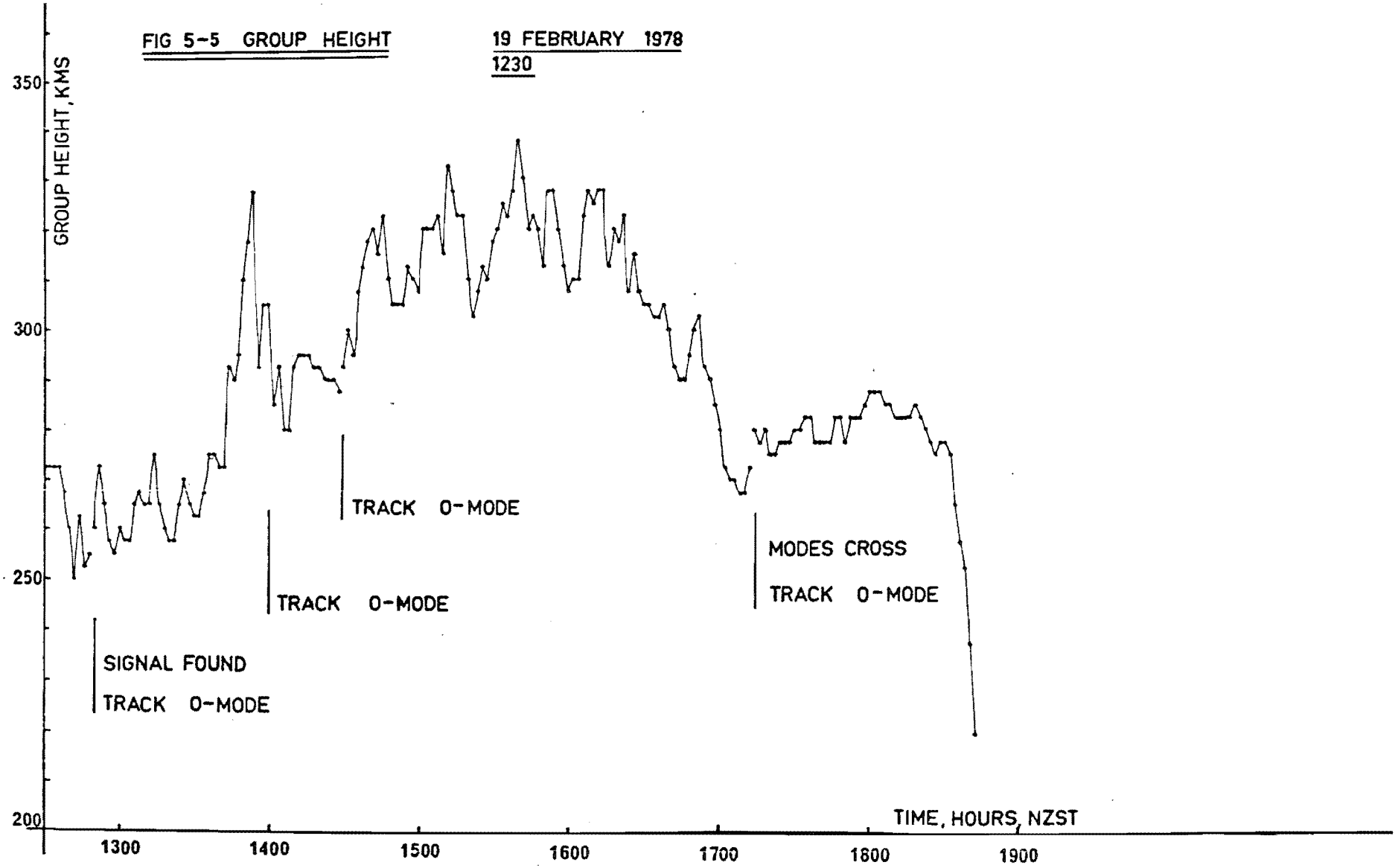
FIG 5-5 GROUP HEIGHT
19 FEBRUARY 1978
1230
GROUP HEIGHT, KMS
350
300
250
200
1300
1400
1500
1600
1700
1800
1900
TIME, HOURS, NZST
SIGNAL FOUND
TRACK O-MODE
TRACK O-MODE
TRACK O-MODE
MODES CROSS
TRACK O-MODE

FIG 5-6 F1 REGION 19 FEB 1978 AT 1230

ΔT 12.8 SEC FREQ 4.57 MHZ HEIGHT 170 KM

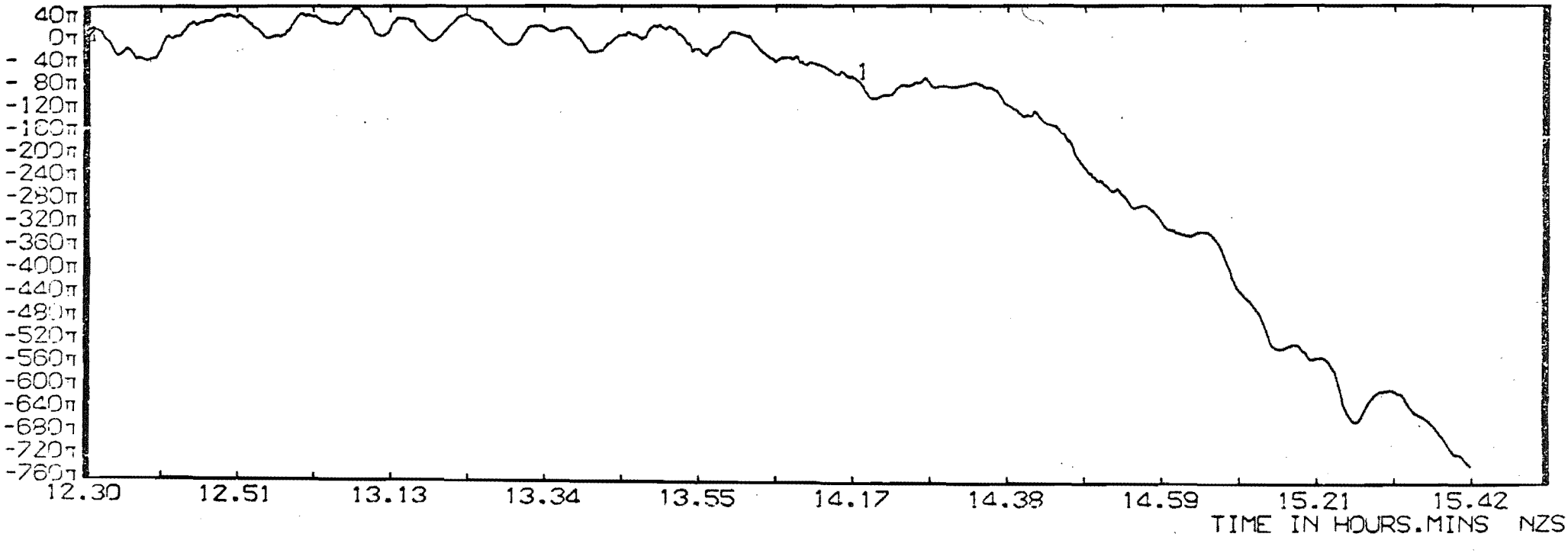

FIG 5-7 F1 REGION 19 FEB 1978 AT 1230

ΔT 12.8 SEC FREQ 4.57 MHZ HEIGHT 170 KM

DT0219781230 TRACKED AND FILTERED PHASE

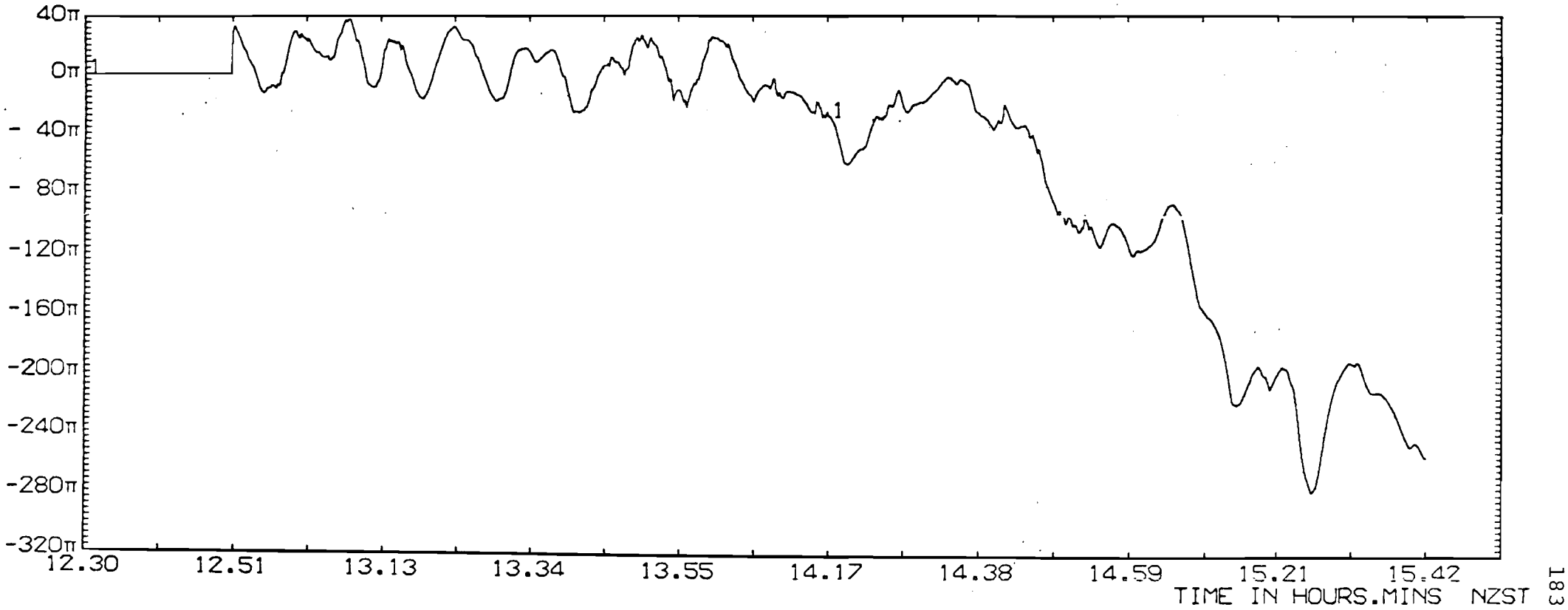

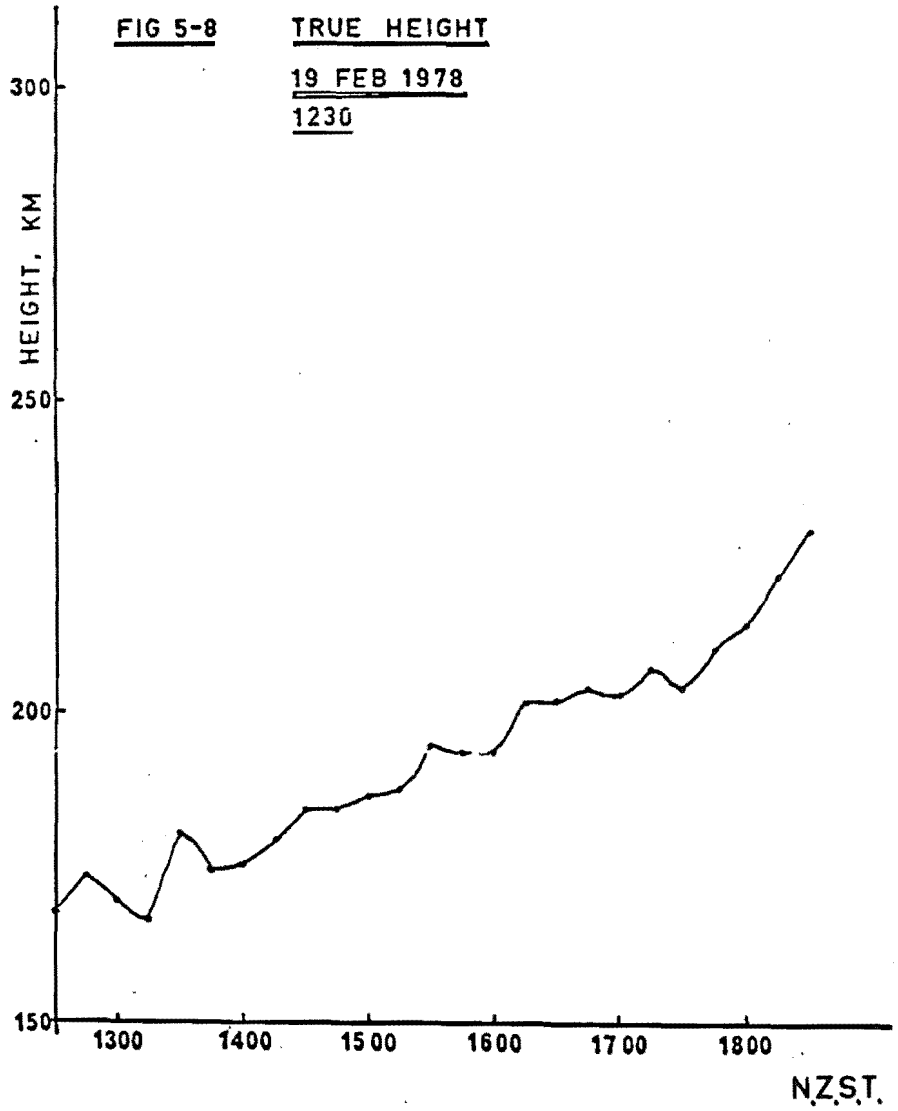
FIG 5-8
TRUE HEIGHT
19 FEB 1978
1230
300
250
200
150
HEIGHT, KM
1300
1400
1500
1600
1700
1800
N.Z.S.T.

FIG 5-9 P v. $\frac{V^2}{h} t^2$ PLOT

19 FEB 1978 at 1327

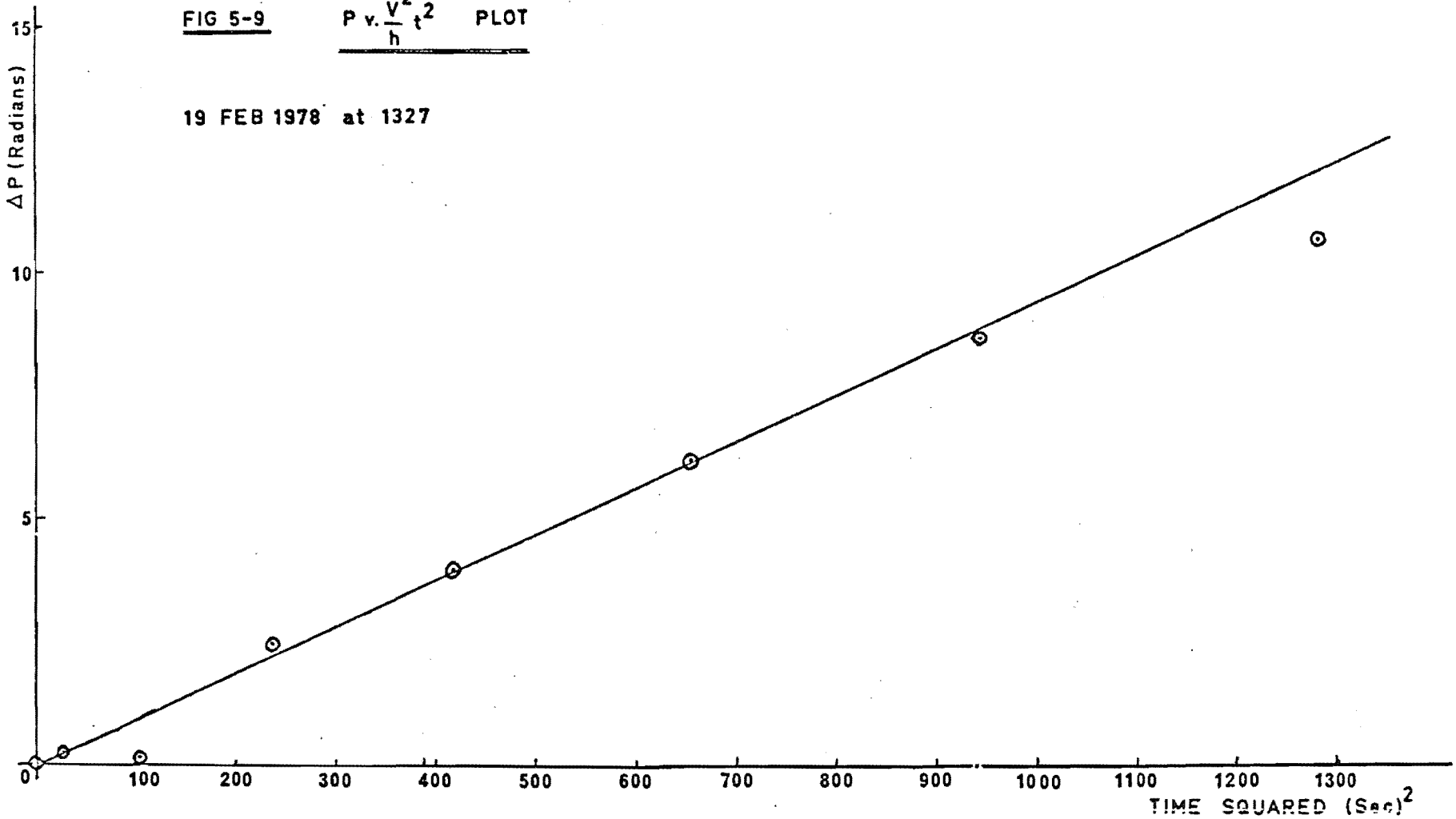

FIG 5-10 19 FEB 1978

RAW PHASE DATA

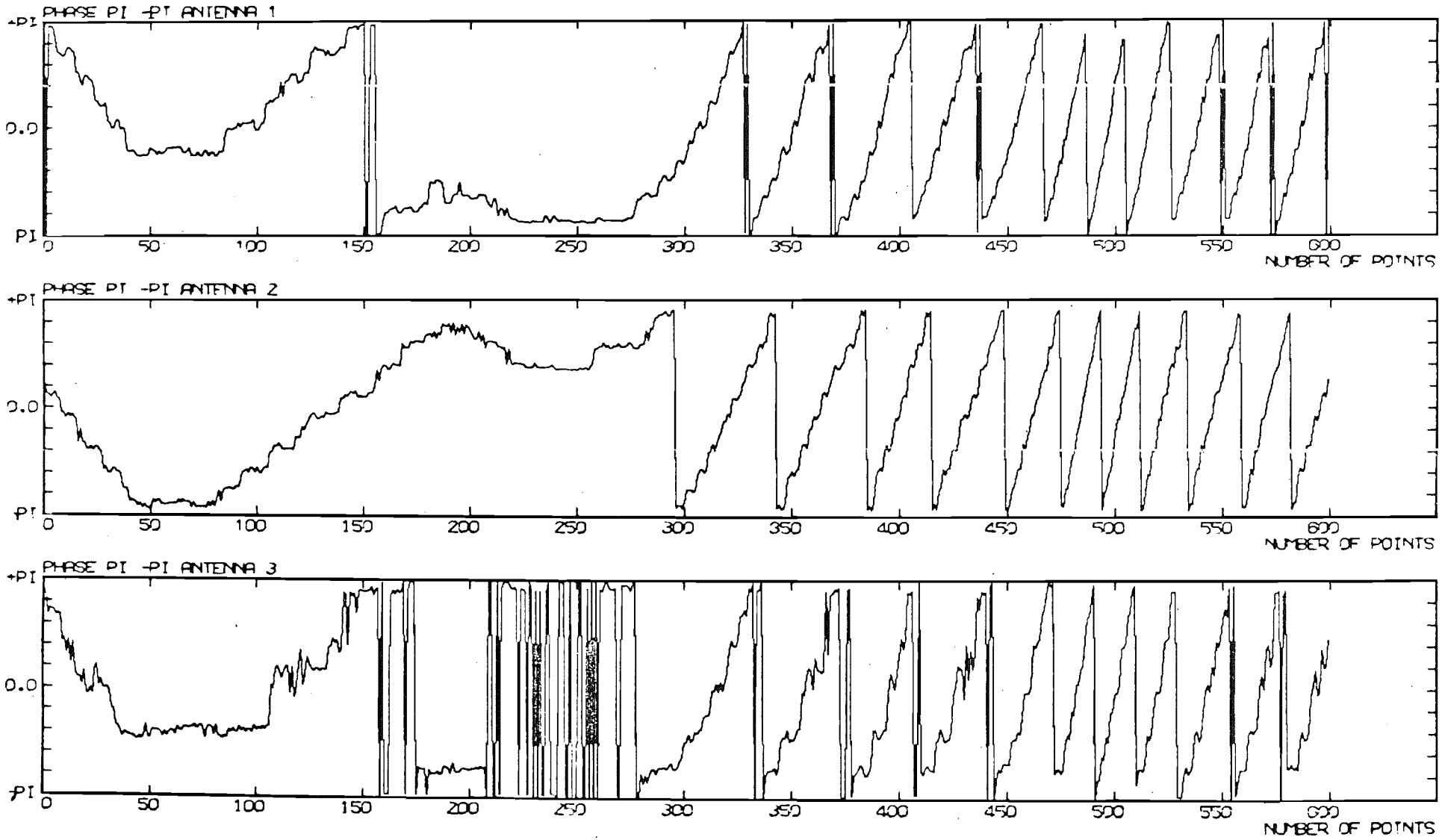

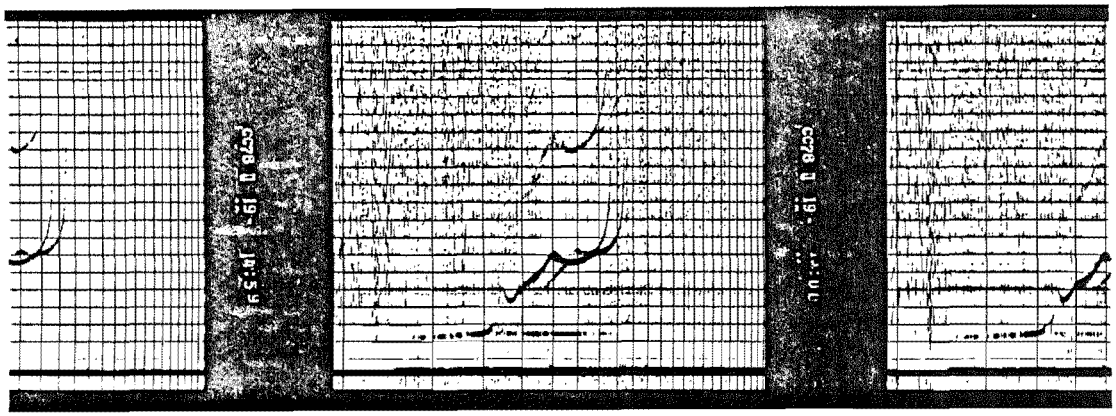

19 FEB. 1978 AT 1500

FIG 5-11

FIG 5-12 (By C.H. Cummack)

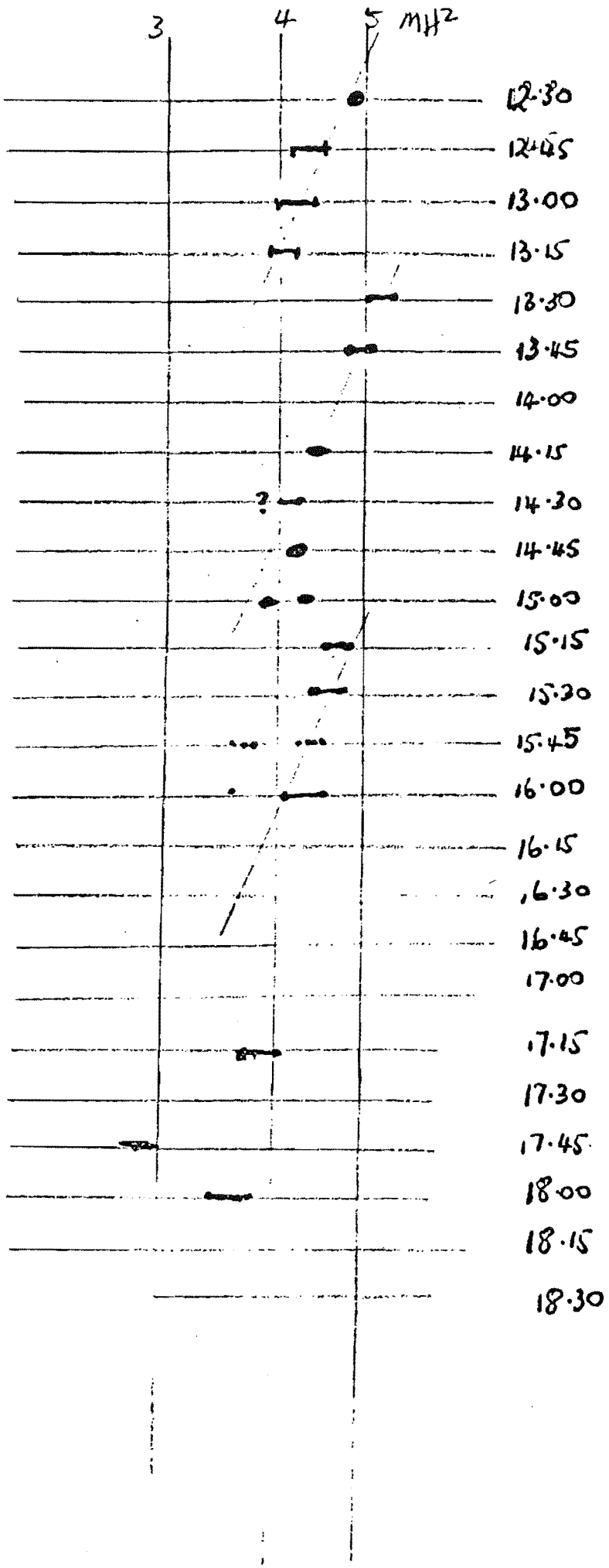

FIG 5-13

LOG MEM SPECTRUM 19 FEB 1978 1256-1504 90-MIN FILTER

600 POINTS LOG FPE 17.84012 ORDER OF PREDICT-ER FILTER 240

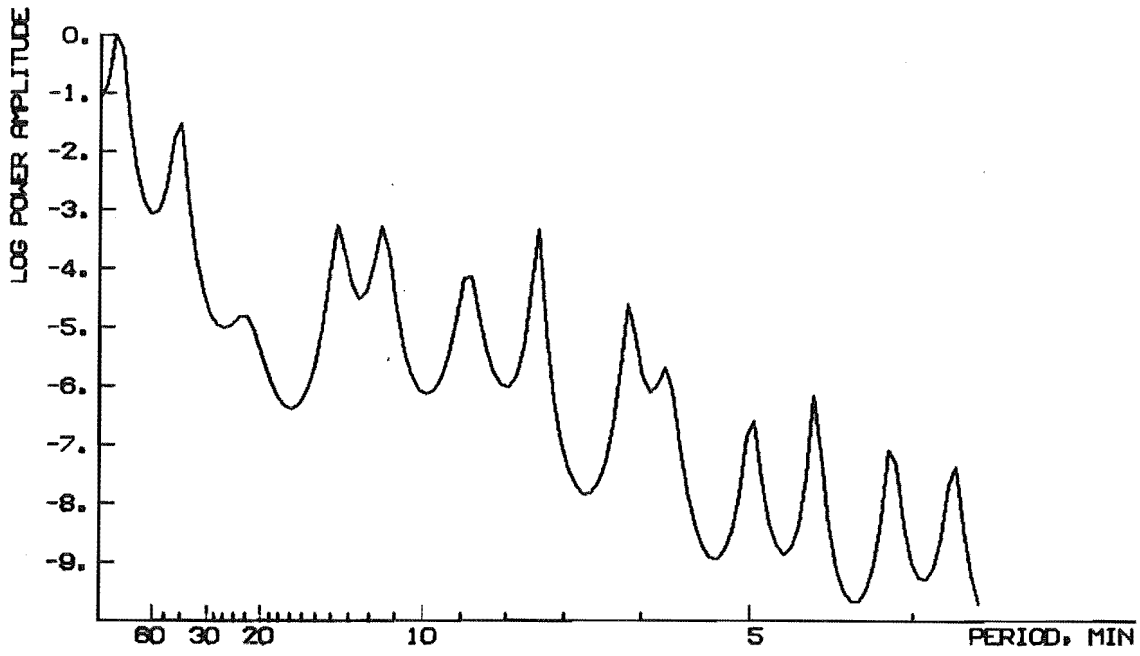

LOG MEM SPECTRUM 19 FEB 1978 1256-1608 90-MIN FILTER

900 POINTS LOG FPE 17.27643 ORDER OF PREDICT-ER FILTER 360

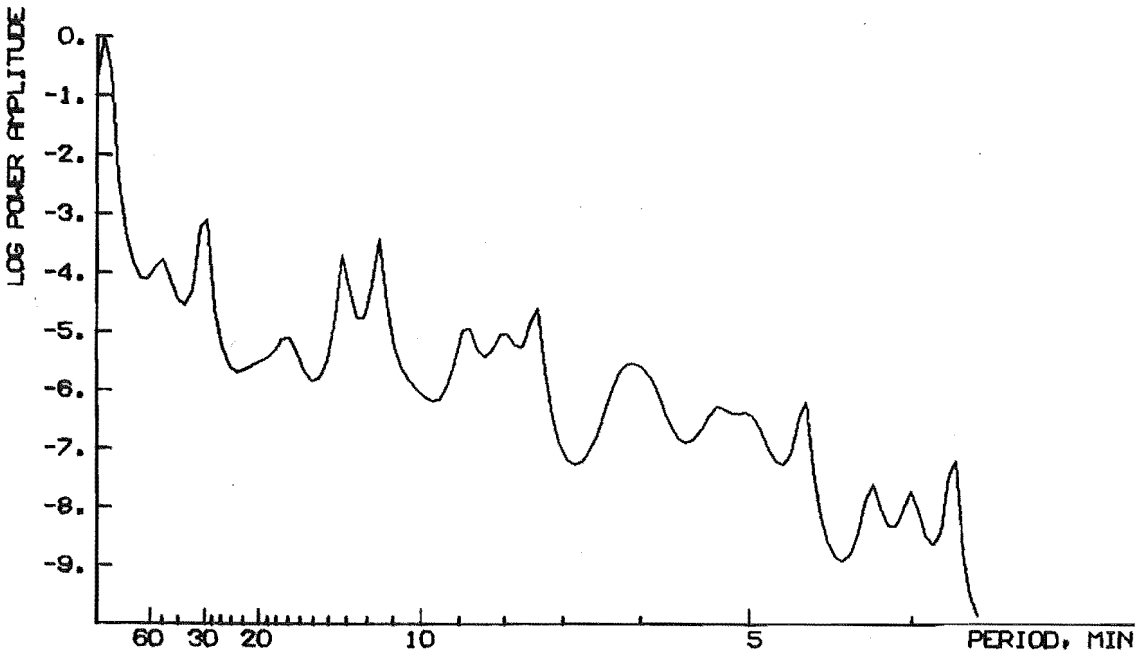

FIG 5-14 GROUP HEIGHT SPECTRUM

LOG MEM SPECTRUM 19 FEB 1978 1300-1500 NO FILTER

240 POINTS LOG FPE 12.77904 ORDER OF PREDICT-ER FILTER 96

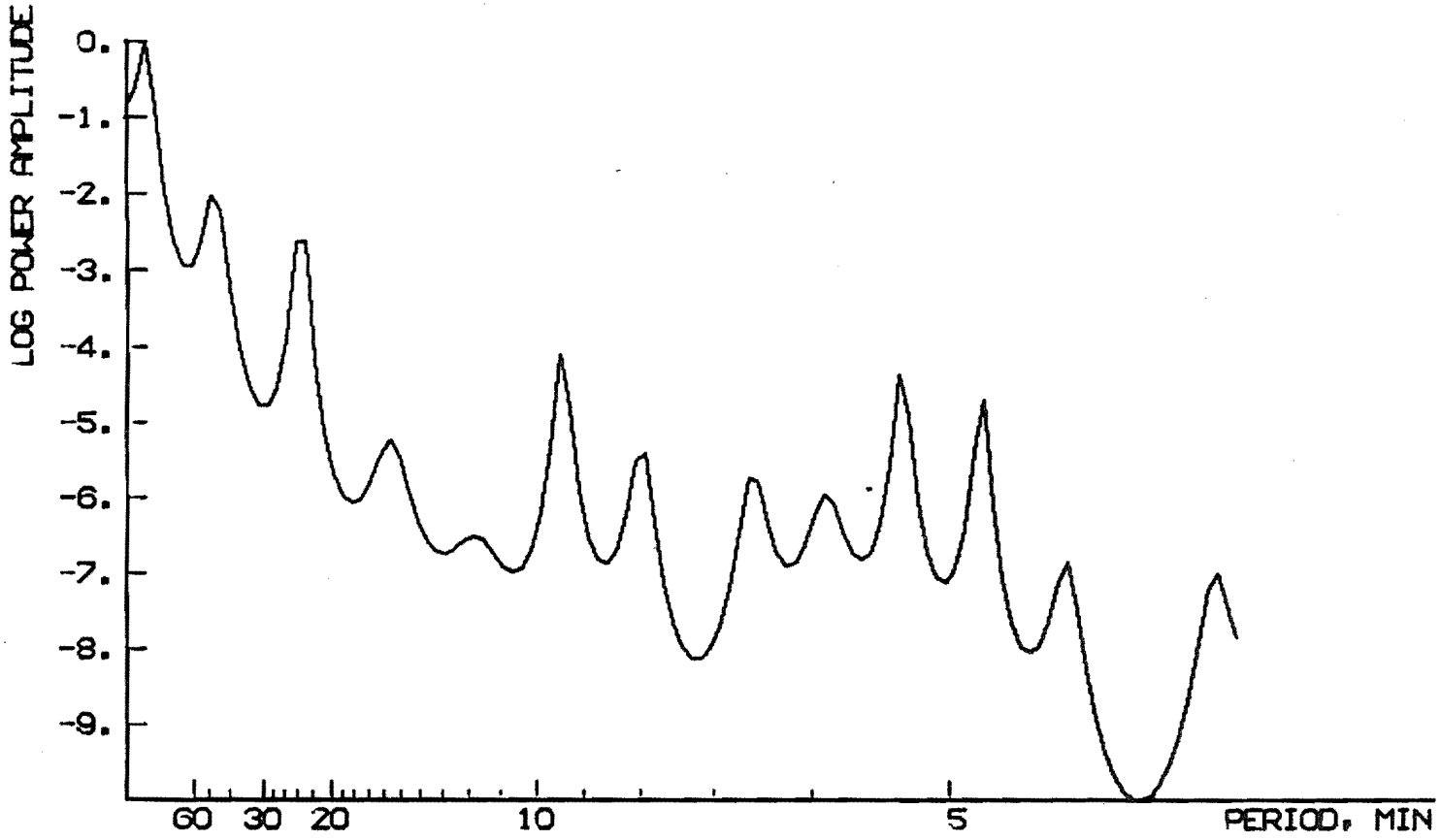

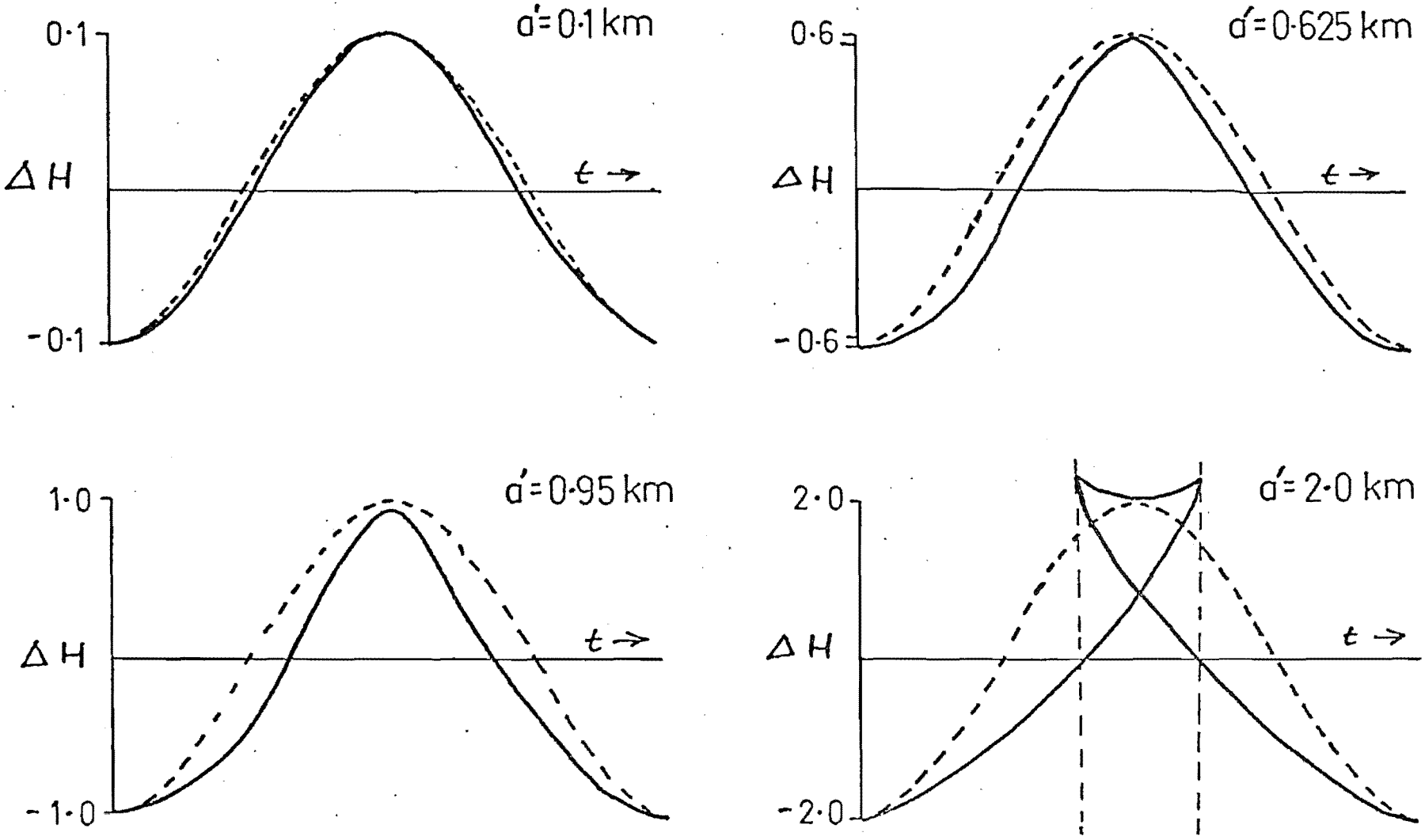

FIG. 5-15 (FROM AUSTIN 1969)
CALCULATED PHASE HEIGHT

FIG 5-15a

LOG MEM SPECTRUM - CRINKLE REFLECTOR

600 POINTS LOG FPE -26.1222 ORDER OF PREDICT-ER FILTER 240

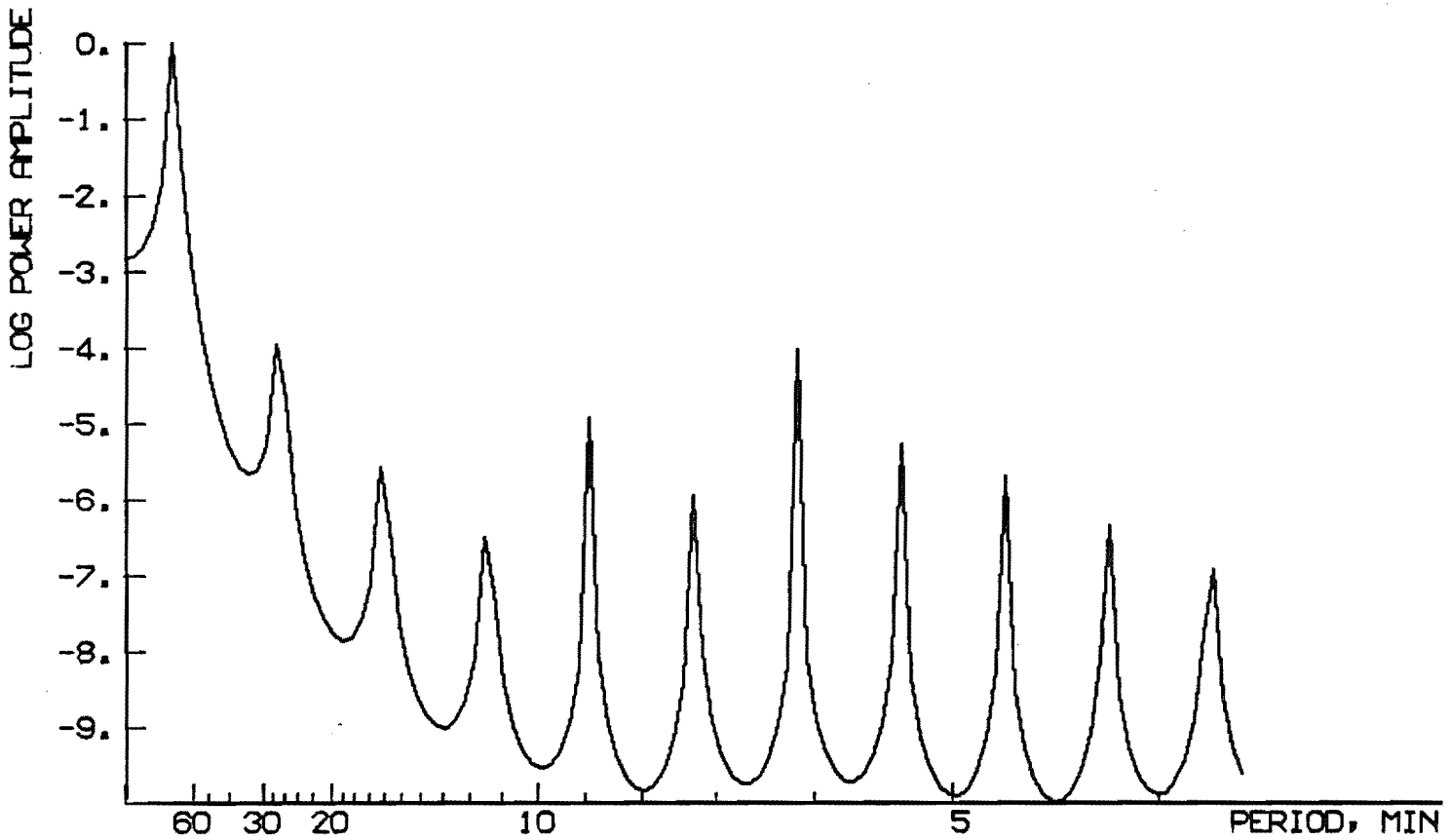

Fig 5-16

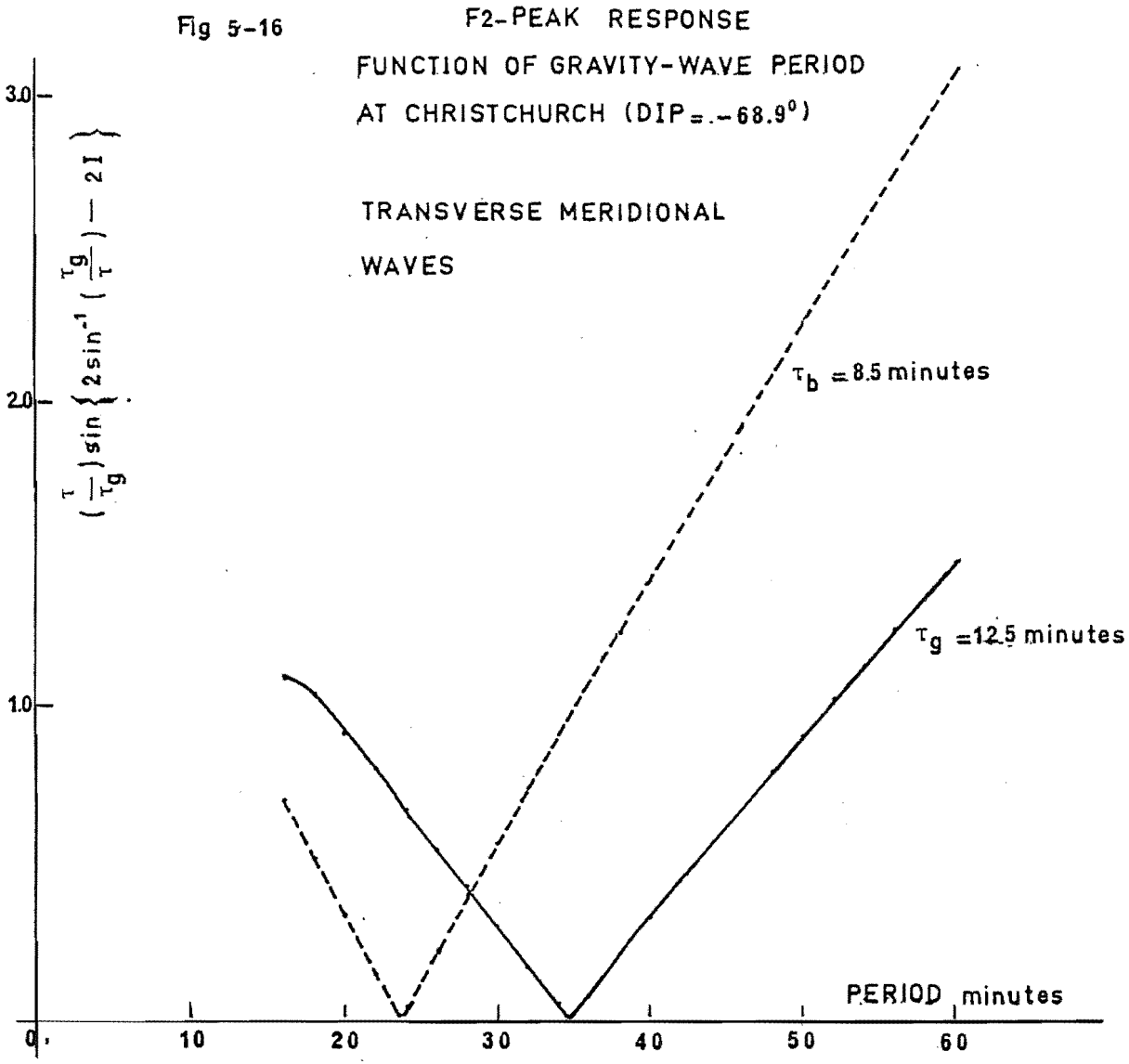
F2-PEAK RESPONSE
FUNCTION OF GRAVITY-WAVE PERIOD
AT CHRISTCHURCH (DIP = -68.9°)
TRANSVERSE MERIDIONAL
WAVES
τ_b = 8.5 minutes
τ_g = 12.5 minutes
$\left(\frac{\tau}{\tau_g}\right) \sin\left\{2\sin^{-1}\left(\frac{\tau_g}{\tau}\right) - 2I\right\}$
3.0
2.0
1.0
0
10
20
30
40
50
60
PERIOD minutes

FIG 5-17

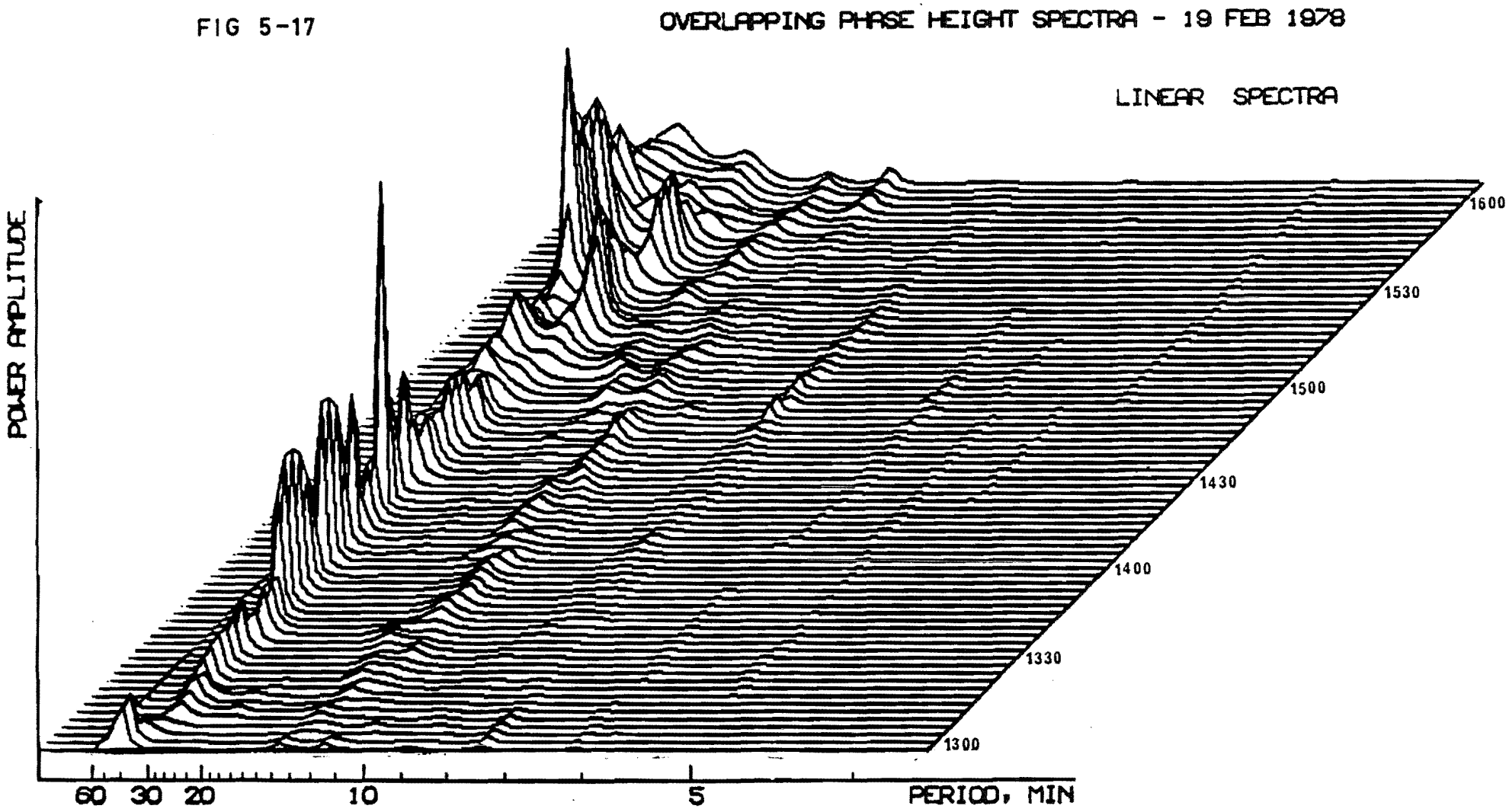
OVERLAPPING PHASE HEIGHT SPECTRA - 19 FEB 1978
LINEAR SPECTRA
POWER AMPLITUDE
1600
1530
1500
1430
1400
1330
1300
60
30
20
10
5
PERIOD, MIN

FIG 5-18

OVERLAPPING PHASE HEIGHT SPECTRA - 19 FEB 1978

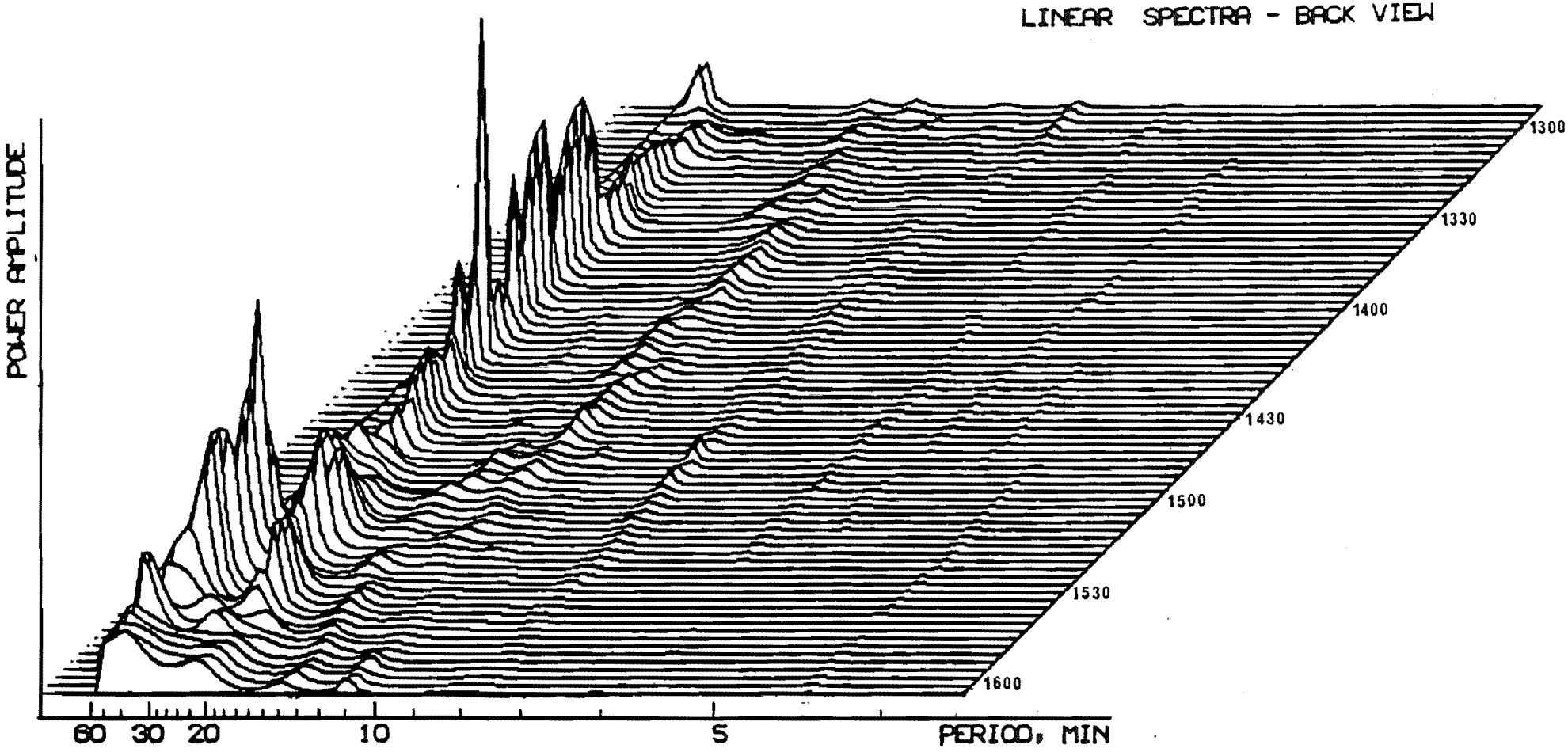

FIG 5-19

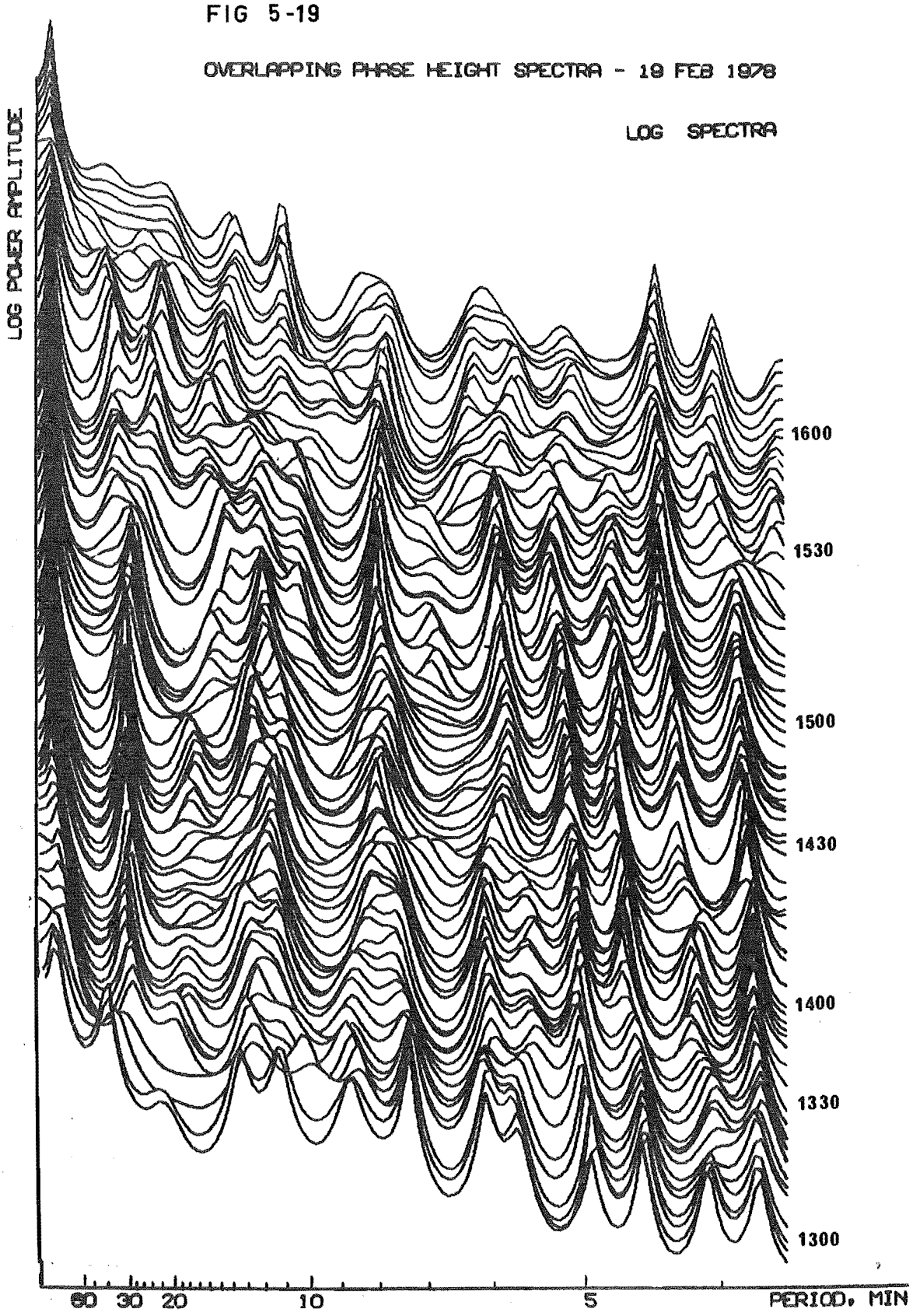
OVERLAPPING PHASE HEIGHT SPECTRA - 19 FEB 1978
LOG SPECTRA
LOG POWER AMPLITUDE
1600
1530
1500
1430
1400
1330
1300
60 30 20 10 5
PERIOD, MIN

FIG 5-20

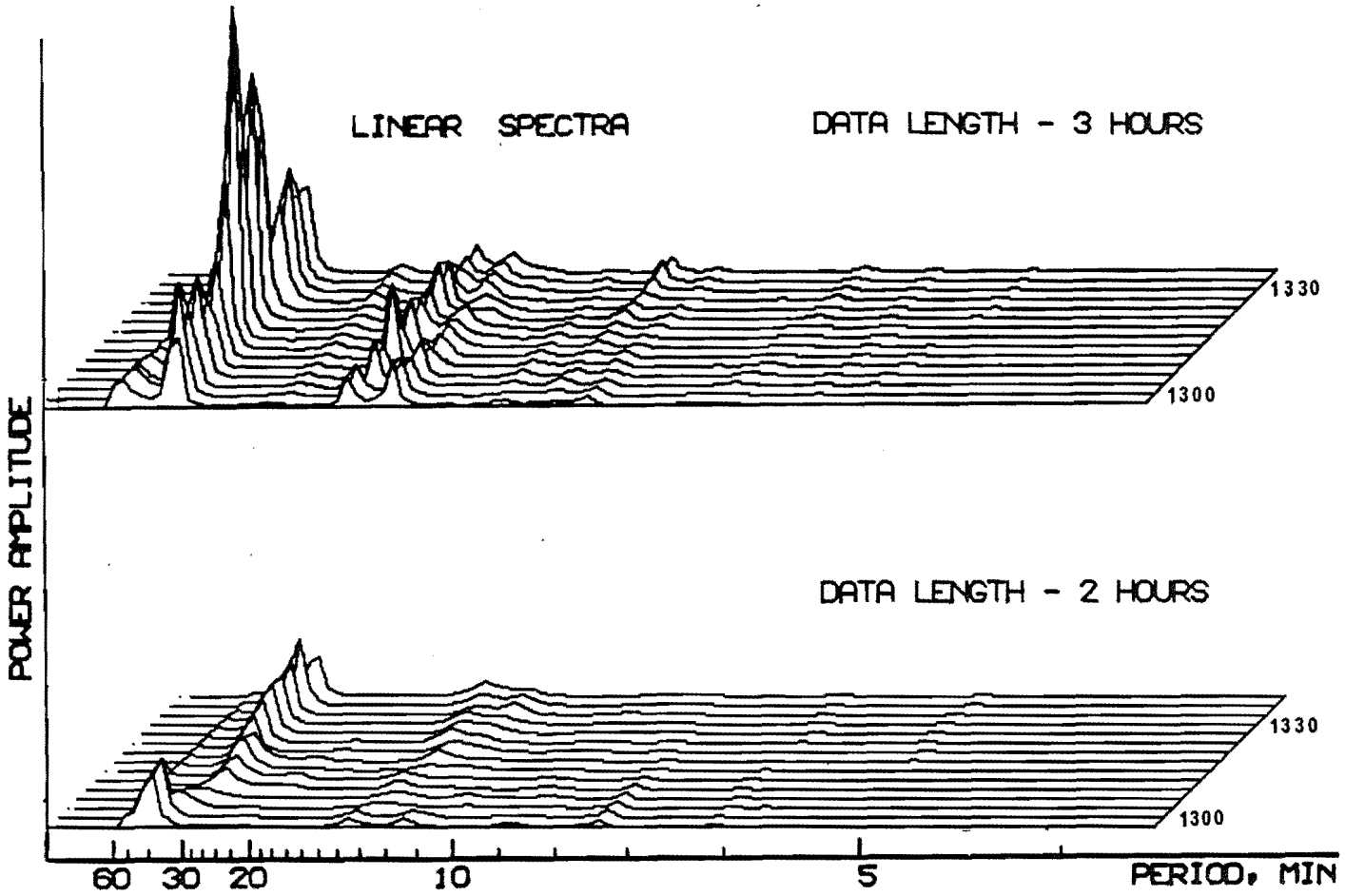
LINEAR SPECTRA
DATA LENGTH - 3 HOURS
1330
1300
DATA LENGTH - 2 HOURS
1330
1300
POWER AMPLITUDE
60
30
20
10
5
PERIOD, MIN

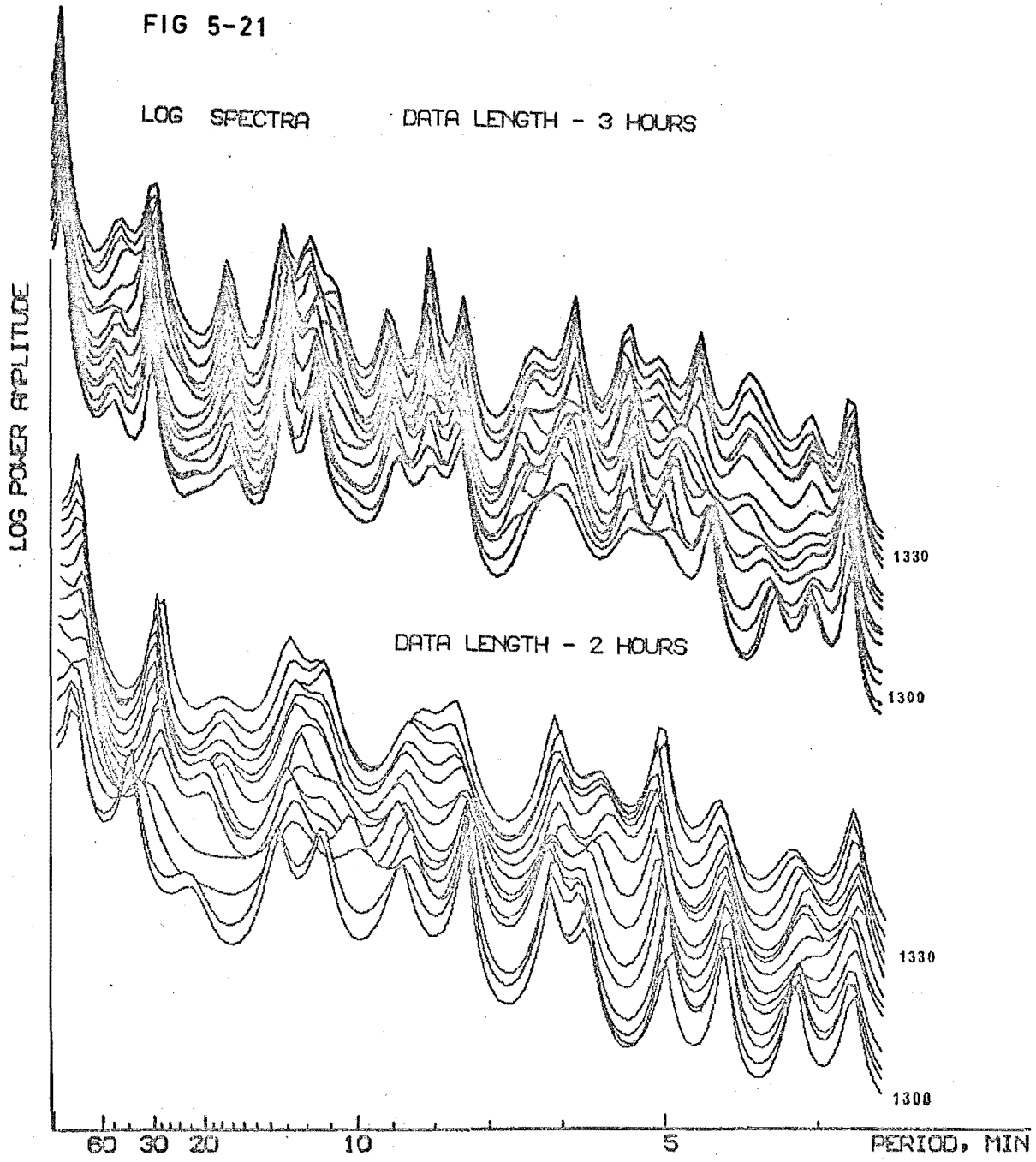
FIG 5-21
LOG SPECTRA
DATA LENGTH - 3 HOURS
LOG POWER AMPLITUDE
1330
1300
DATA LENGTH - 2 HOURS
1330
1300
60 30 20
10
5
PERIOD, MIN

FIG 5-22 COMPLEX CORRELATION - 19 FEB 1978 AT 1300 HOURS

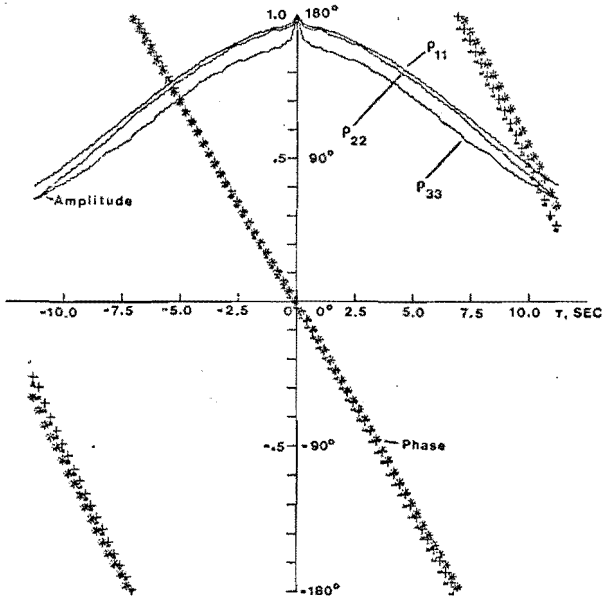

COMPLEX AUTOCORRELATION

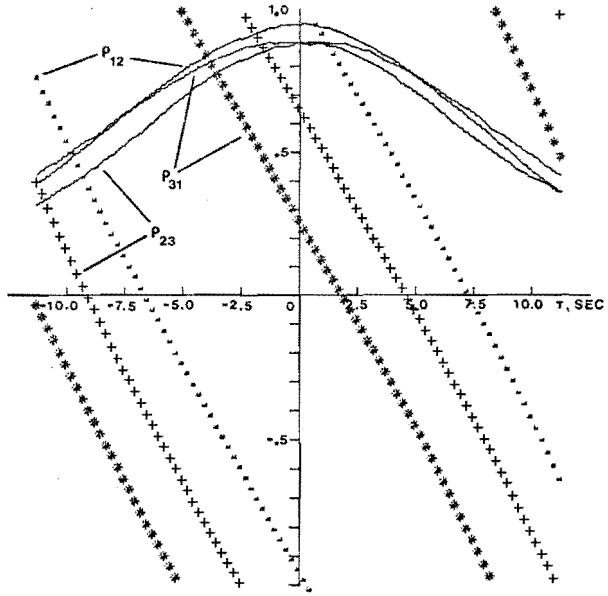

COMPLEX CROSSCORRELATION

FIG 5-23

ECHOLOCATIONS

19 February 1978

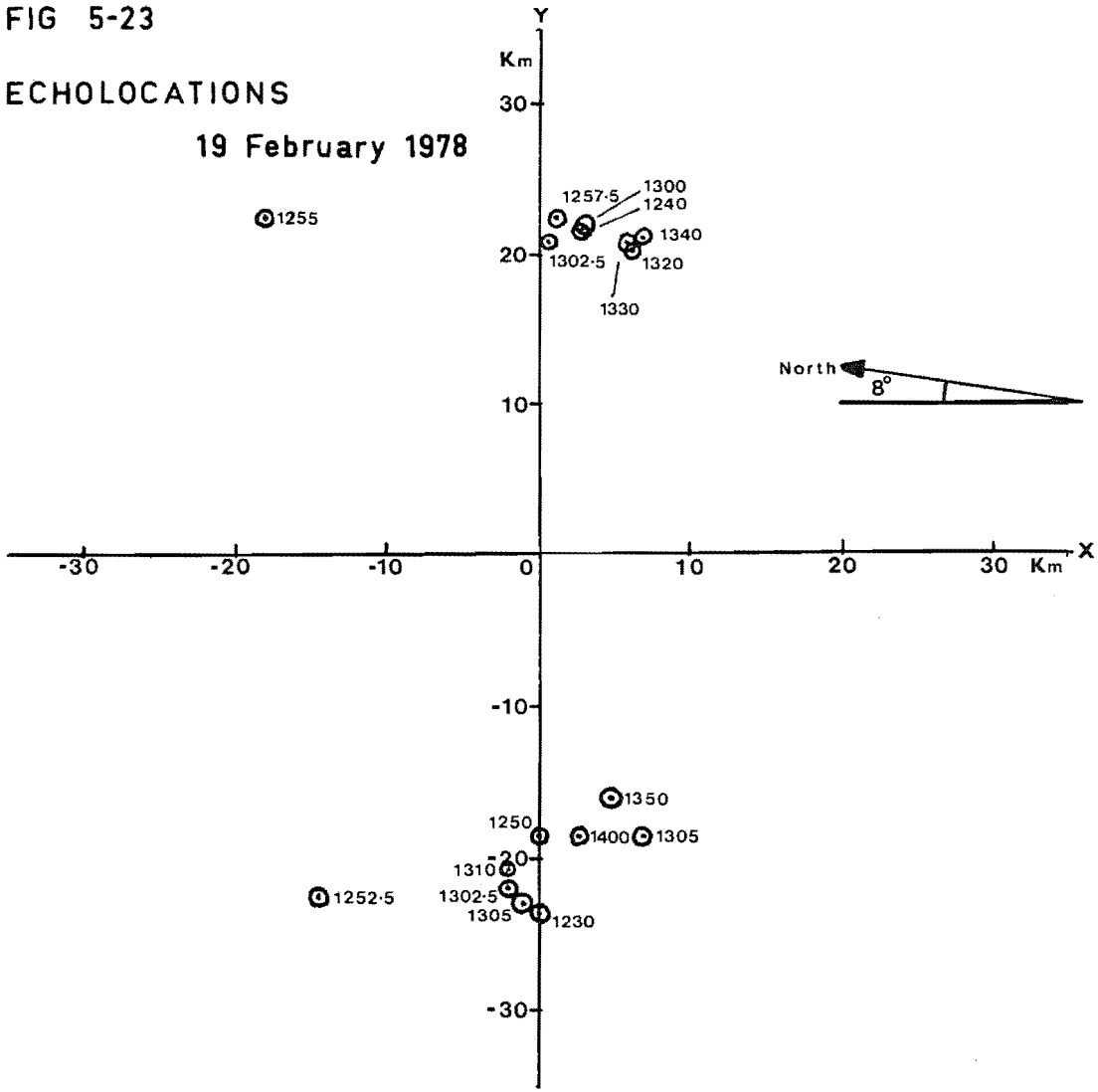

CHAPTER 6

CONCLUSION

Two main themes made up this investigation. A numerical model of a moving sinusoidal reflector illuminated by a point transmitter allowed the calculation of spatial and temporal correlations, and a determination of their relation to reflector velocity. The experimental work involved the measurement of phase-path variations in the F1 region by coherent reception of pulsed transmissions at 4.57 MHz.

The description of a ground diffraction pattern using the concept of an angular spectrum has normally been applied to the scattering of radio-waves from small-scale irregularities in the ionosphere. In principle the description of diffraction by the angular spectrum may be applied to a reflector of any type, and in the work reported here a sinusoidal reflector has been used. The Fourier Transform relationships between the electromagnetic field emerging from the screen, the corresponding angular spectrum and the resulting ground diffraction pattern have allowed the calculation of the ground pattern by Discrete Fourier Transform techniques.

Thus a two-dimensional problem was considered - one vertical dimension up and one horizontal dimension. The ground pattern over this one-dimensional ground was calculated for a sinusoidal reflector illuminated by a point transmitter on the ground. The parameters of the reflector were chosen to approximate those of an F-region gravity wave. Movement of the reflector and determination of the resulting ground patterns allowed spatial and temporal correlations to be

calculated.

Pattern drift velocity and random velocity were calculated using all of spatial and temporal complex and amplitude correlations. The pattern drift velocity derived from the complex time correlations between spaced receivers was found to give the only correct estimate of the reflector velocity; with negligible random velocity as expected for an unchanging reflector shape. The amplitude spatial correlations lead to a drift velocity close to the ground velocity of the specular point on the reflector. A significant random velocity value was also obtained.

No useful estimates for the reflector velocity were obtained from the complex spatial and amplitude temporal correlations. The apparent drift velocities from the latter correlations differed with receiver-pair location, even for pairs with the same spacing. The amplitude temporal correlations are those most often used in close-spaced-receiver drifts experiments, and the differing of apparent velocity with receiver-pair location has been observed experimentally.

The large receiver spacings of the simulation do not allow a complete simulation of close-spaced drift measurements, but the results obtained give an indication of the correlations and velocities found when measurements are made over a period of time which is small compared to the reflector period. Comparison of complex and amplitude temporal correlations from data indicate a similar scale of correlation change with time. This disagrees with the results of the sinusoidal reflector model, indicating that this model is not a full description of radio reflection from the F region.

The second theme of this investigation has involved the

measurement and analysis of phase-path data in the F1 region. The phase path is mainly incoherent, by the criterion of Fraser and Vincent (1970), but tracking the phase through ±360 n degrees has enabled power spectra to be obtained.

Ionogram observations for the day chosen for analysis indicated the presence of a medium-scale Ionospheric Travelling Disturbance of period about 80 minutes, with several cycles present. The power spectra of the phase-path data showed considerable harmonic structure corresponding to a fundamental period of about 80-90 minutes. The questions then arose: did the measured harmonics arise from harmonic components of the atmospheric gravity wave, or from harmonic components in the phase path arising from movement of a specular point on a sinusoidal reflector?

The power spectrum of the phase-path arising from a sinusoidal reflector of amplitude period, and wavelength equal to those of the ionogram wave showed close qualitative similarity to the experimental spectra. Although the group retardation in the experimental radio data has been neglected in this comparison, it was concluded that ionogram and phase-path data are measuring the same wave, and that harmonics seen in the phase-path spectra arise from specular-point movement on a quasi-sinusoidal surface.

Derivation of velocity, amplitude, wavelength, and period values gave results as expected for a medium-scale Travelling Ionospheric Disturbance. Examination of over-lapping power spectra indicated very stable spectrum characteristics, with the exception of the last hour of the data run. A particularly stable spectrum peak was present at the calculated (temperature-varying atmosphere) Brunt

Frequency: however the spectrum peak could have also been a high harmonic of the 80-90 minute fundamental. A spectrum dip at period 18 minutes gave qualitative agreement with the ionization response calculations of Hooke.

The models of Francis have indicated that long-distance propagation of medium-scale Travelling Ionospheric Disturbances is possible by the refraction of freely-propagating gravity waves round the surface of the earth. The presence of several wave cycles and the stability of the spectra indicated the auroral electrojet as a possible source mechanism - a conjecture made more plausible by the presence of moderately high magnetic activity at the time the data was taken.

An attempt to obtain direction using the phase of the complex cross-correlation between the three receiving aerials indicated that the gravity-wave was travelling East-West, or vice versa. This is in close agreement with the statistical data of Munro, but is not a possible result of the auroral electrojet source hypothesis.

No Doppler shift of wave period, as measured by the phase-path data, arising from the presence of neutral winds was detected. The phase-path and ionogram data appeared to be measuring the same wave.

REFERENCES

ANDERSEN, M. On the calculation of filter coefficients for maximum entropy analysis. Geophysics, 39, 1974, 69-72.

A.R.R.L. ANTENNA HANDBOOK, THE. 13th ed. Newington, Connecticut, The American Radio Relay League, Inc., 1974,336p.

BEHANNON, K.W. and NESS, N.F. The design of Numerical Filters for Geomagnetic Data analysis. Washington, National Aeronautics and Space Administration: Report NASA TN D-3341., 1966. 35p.

BEYNON, W.J.G. and WRIGHT, J.C. The analysis of ionospheric drift data in the closely-spaced receiver method. J.atmos.terr.Phys.31, 1969: 593-596.

BLAKE, L.V. Antennas. New York, John Wiley and Sons, Inc., 1966, 415p.

BLAKE, L.V. Transmission lines and waveguides. New York, John Wiley and Sons, Inc., 1969., 315p.

BOOKER, H.G., RATCLIFFE, J.A., and SHINN, D.H. Diffraction from an irregular screen with applications to to ionospheric problems. Phil.Trans.R.Soc.A242, 1950: 579-607.

BORN, M. and WOLF, E. Principles of Optics; electromagnetic theory of propagation, interference, and diffraction of light. 3d.ed. Oxford, Pergamon Press, 1965, 808p.

BRACEWELL, R.N. The Fourier Transform and Its Applications. New York, McGraw-Hill Book Co., 1965, 381p.

BRAULT, J.W. and WHITE, O.R. The Analysis and Restoration of Astronomical Data via the Fast Fourier Transform. Astron.& Astrophys. 13 1971: 169-189.

BRIGGS, B.H. Instruction Manual for ionospheric drift measurements. Adelaide, University of Adelaide. 1967. 38p.

BRIGGS, B.H. On the analysis of moving patterns in geophysics - I. Correlation analysis. J.atmos.terr.Phys. 30, 1968a:1777-1788.

BRIGGS, B.H. On the analysis of moving patterns in geophysics - II. Dispersion analysis. J.atmos.terr.Phys. 30, 1968b: 1789-1794.

BRIGGS, B.H., PHILLIPS, G.J., and SHINN, D.H. The Analysis of Observations on Spaced Receivers of the Fading of Radio Signals. Proc.phys.Soc. 63B, 1950: 106-121.

BRIGGS, B.H. Recent work on Ionospheric Irregularities and Drifts. Geofysiske Publikasjoner 29, 1972: 121-134.

BRIGHAM, E.O. The Fast Fourier Transform. New Jersey, Prentice-Hall Inc., 1974. 252p.

BROWN, G.M. and CHAPMAN, J.W. An investigation of the ground diffraction pattern of radio waves reflected from the ionosphere. J.atmos.terr. Phys. 34, 1972: 1445-1454.

BROWNLIE, G.D., DRYBURGH, L.G., and WHITEHEAD, J.D. Measurement of the velocity of waves in the ionosphere: A comparison of the ray theory approach and diffraction theory. J.atmos.terr.Phys. 35, 1973a: 2147-2162.

BROWNLIE, G.D., DRYBURGH, L.G. and WHITEHEAD, J.D. Measurement of the Dispersion of Waves in the Ionosphere. Nature Phys.Sci. 244, 1973b: 123-124.

BUCKLEY, R. Diffraction by a random phase-changing screen: A numerical experiment. J.atmos.terr.Phys. 37, 1975: 1431-1446.

BUDDEN, K.G. Radio Waves in the Ionosphere. Cambridge, University Press, 1961, 542p.

CHAN, K.L., and VILLARD, O.G. Observation of Large-Scale Traveling Ionospheric Disturbances by Spaced-Path High-Frequency Instantaneous-Frequency Measurements. J. geophys. Res. 67, 1962:973-988.

CHEN, W.Y. and STEGEN, G.R. Experiments with Maximum Entropy Power Spectra of Sinusoids. J.geophys.Res. 79, 1974: 3019-3022.

COOLEY, J.W. and TUKEY, J.W. An Algorithm for the Machine Calculation of Complex Fourier Series. Maths. Compt. 19, 1965: 297-301.

COURTILLOT, V., LE MOUËL, J.L., and MAYAUD, P.N. Maximum Entropy Spectral Analysis of the geomagnetic activity index aa over a 107-year interval. J. geophys.Res. 82, 1977: 2641-2649.

COWLING, D.H., WEBB, H.D. and YEH, K.C. Group Rays of Internal Gravity Waves in a Wind-Stratified Atmosphere. J. Geophys. Res. 76, 1971: 213-220.

DAVIES, K. and JONES, J.E. Evidence for waves and winds in the ionospheric F region. *In* Bowhill, S.A., Jaffe, L.D., and Rycroft, M.J. *Editors.* Space Research XII. Berlin, Akademie-Verlag, 1972, p.1133-1142.

DAVIS, K., JONES, T.B., and WEAVER, P.F. Ionospheric Winds in the F-Region and their effects on the limiting periods of gravity waves. Planet.Space Sci. 21, 1973: 147-149.

DOBBIE, L.G. Calculation of Inductance. *In* Langford-Smith, F. (Ed.) Radiotron Designer's Handbook. 4th ed. Sydney, Wireless Press, 1963, p.429-449.

DOWN, W.H. and MAUDE, A.D. The variation of the shape of cross-correlation curves with receiver separation in spaced receiver ionospheric drift measurements. J.atmos.terr.Phys. 30, 1968: 897-902.

ESSEX, E.A. Comparison of ionospheric gravity wave periods as measured by different experimental techniques. J.atmos.terr.Phys. 37, 1975: 1349-1356.

FELGATE, D.G. On the point source effect in the measurement of ionospheric drifts. J.atmos.terr.Phys. 32, 1970: 241-245.

FELGATE, D.G. and GOLLEY, M.G. Ionospheric irregularities and movements observed with a large aerial array. J.atmos.terr.Phys. 33, 1971: 1353-1369.

FINDLAY, J.W. The phase and group paths of radio waves returned from region E of the ionosphere. J.atmos.terr. Phys. 1, 1951: 353-366.

FINDLAY, J.W. Moving clouds of ionization in region E of the ionosphere. J.atmos.terr.Phys. 3, 1953: 73-78.

FOOKS, G.F. Ionospheric irregularities and the phase paths of radio waves. J.atmos.terr.Phys. 24, 1962: 937-947.

FOUGERE, P.F. A Solution to the Problem of Spontaneous Line Splitting in Maximum Entropy Power Spectrum Analysis. J. geophys. Res. 82, 1977 : 1051-1054.

FOUGERE, P.F., ZAWALICK, E.J., and RADOSKI, H.R. Spontaneous line splitting in maximum entropy power spectrum analysis. Phys. Earth Planet. Inter. 12, 1976: 201-207.

FRASER, G.J. Southern hemisphere mid-altitude winds at heights of 70-100 km. J. atmos. terr. Phys. 30, 1968: 707-719.

FRASER, G.J. and VINCENT, R.A. A study of D-region irregularities. J.atmos.terr.Phys. 32, 1970: 1591-1607.

FRANCIS, S.H. Propagation of internal acoustic-gravity waves around a spherical earth. J. Geophys. Res. 77, 1972: 4221-4226.

FRANCIS, S.H. Acoustic-Gravity Modes and Large-Scale Traveling Disturbances of a Realistic, Dissipative Atmosphere. J.geophys.Res. 78, 1973a: 2278-2301.

FRANCIS, S.H. Lower-Atmosphere Gravity Modes and Their Relation to Medium-Scale Traveling Ionospheric Disturbances. J.geophys.Res. 78, 1973b: 8289-8295.

FRANCIS, S.H. A Theory of Medium Scale Traveling Ionospheric Disturbances. J.geophys.Res. 79, 1974: 5245-5260.

FRANCIS, S.H. Global propagation of atmosphere gravity waves: a review. J.atmos.terr.Phys. 37, 1975: 1011-1054.

GEISLER, J.E. A numerical Study of the wind system in the middle atmosphere. J.atmos.terr.Phys. 29, 1967: 1469-1482

GEORGES, T.M. Evidence for the Influence of Atmospheric Waves on Ionospheric Motions. J.geophys.Res. 72, 1967: 422-425.

GEORGES, T.M. HF Doppler studies of traveling ionospheric disturbances. J.atmos.terr.Phys. 30, 1968: 735-746.

GOLLEY, M.G. and ROSSITER, D.E. Some tests of methods of analysis of ionospheric drift records using an array of 89 aerials. J.atmos.terr.Phys. 32, 1970: 1215-1233.

GOSSARD, E.E. The Apparent Movement of the Spectral Components in Fading Records of Ionospherically Reflected Radio Waves. J.geophys.Res. 72, 1967: 1563-1569.

GUHA, D. and GELLER, M.A. Computer Simulation of the Three-Receiver Drift Experiment. Illinois, University of Illinois, Urbana, Illinois. Aeronomy Report No.50, Aeronomy Laboratory, Department of Electrical Engineering, 1972. 185p.

GUHA, D. and GELLER, M.A. Computer simulation studies of a spaced-receiver drift experiment. J.atmos.terr. Phys. 35, 1973: 1853-1867.

GUPTA, A.B. and NAGPAL, O.P. F-2 Region Ionospheric Response to Atmospheric Gravity Waves. Annls.Géophys 29, 1973: 307-319.

GUPTA, A.B., NAGPAL, O.P., and SETTY, C.S.G.K. Effects of atmospheric temperature gradients and neutral winds on the low cut off period of gravity waves. Annls. Géophys. 29, 1973: 301-305.

HARGREAVES, J.K. and HARGREAVES, S. A numerical Approach to the solution of Radio Diffraction Problems. J. Res. natn. Bur. Stand. 67D, 1963: 685-698.

HARRIS, I. and PRIESTER, W. Time-dependent Structure of the Upper Atmosphere. J.atmos.Sci., 1962: 286-301.

HEISLER, L.H. Anomalies in Ionosonde records due to Travelling Ionospheric Disturbances. Aust. J.Phys. 11, 1958: 79-90.

HEISLER, L.H. and NELSON, G.J. Divergence of radio waves in the ionospheric medium. J.atmos.terr.Phys. 29, 1967: 839-855.

HEWISH, A. The diffraction of radio waves in passing through a phase-changing ionosphere. Proc.R.Soc. A209, 1951: 81-96.

HEWISH, A. The diffraction of galactic radio waves as a method of investigating the irregular structure in the ionosphere. Proc.R.Soc. A214, 1952: 494-514.

HINES, C.O. Internal Atmospheric gravity waves at ionospheric heights. Can.J.Phys. 38, 1960: 1441-1481.

HINES, C.O. Ionization irregularities in the E-region. J. atmos.terr.Phys. 25, 1963: 305-306.

HINES, C.O. Ionospheric movements and irregularities. *In* Odishaw, H. (Ed.) Research in Geophysics - I. Sun, Upper Atmosphere, and Space. Massachusetts, M.I.T. Press, Cambridge, Massachusetts, 1964, p.299-318.

HINES, C.O. Some consequences of gravity-wave critical layers in the upper atmosphere. J.atmos.terr.Phys. 30, 1968: 837-843.

HINES, C.O. and RAO, R.R. Validity of three-station methods of determining ionospheric motions. J.atmos. terr.Phys. 30, 1968: 979-993.

HINES, C.O. Propagation velocities and speeds in ionospheric waves: A review. J. Atmos.terr.Phys. 74, 1974: 1179-1204.

HINES, C.O. The Upper Atmosphere in Motion. Washington, D.C. American Geophysical Union, 1974: 1027 p.

HOOKE, W.H. Ionospheric irregularities produced by internal atmospheric gravity waves. J.atmos. terr.Phys. 30, 1968: 795-823.

HOOKE, W.H. The Response of the F-region ionopshere to Internal Atmospheric Gravity Waves. *In* Georges, T.M. (Editor) Symposium on Acoustic-Gravity Waves in the Atmosphere, Boulder, Colorado, 1968b. Sponsored by the Environmental Science Services Administration and the Advanced Research Project Agency. 437pp.

HOOKE, W.H. The Ionospheric Response to Internal Gravity Waves. 1. The F_2 Region Response J.geophys.Res. 75, 1970a: 5535-5544.

HOOKE, W.H. Ionospheric Response to Internal Gravity Waves. 2. Lower F Region Response. J.geophys.Res. 75, 1970b: 7229-7238.

JENKINS, F.A. and WHITE, H.E. Fundamentals of Optics. 3d ed. New York, McGraw-Hill Book Co., Ltd., 1957, 637p.

JONES, I.L., LANDMARK, B., and SETTY, C.S.G.K. Movements of ionospheric irregularities observed simultaneously by different methods. J.atmos. terr.Phys. 10, 1957: 296-301.

JONES, W.L. Linear Internal Gravity Waves in the Atmosphere. Handbuch der Physik XLIX/5, 1976: 177-216.

KELLEHER, R.F. Some characteristics of the ground diffraction pattern caused by the vertical reflection of radio waves from the ionosphere. J.atmos.terr. Phys. 28, 1966a: 99-102.

KELLEHER, R.F. Some statistical properties of the ground diffraction patterns of vertically reflected radio waves. J.atmos.terr.Phys. 28, 1966b: 213-223.

KENT, G.S. and WRIGHT, R.W.H. Movements of ionospheric irregularities and atmospheric winds. J.atmos. terr.Phys. 30, 1968: 697-691.

KRAUS, J.D. Multi-wire Dipole Antennas. Electronics 13, 1940: 26-27.

KRAUS, J.D. Antennas. New York, McGraw-Hill Book Company, 1950, 553p.

KWA, E. Tide effects on Antenna Impedance. M.Sc. Thesis in preparation. Christchurch, University of Canterbury, 1977.

LACOSS, R.T. Data adaptive spectral analysis methods. Geophysics, 36, 1971: 661-675.

LANDMARK, B. The fading of radio waves reflected from the E layer. J.atmos.terr.Phys. 10, 1957: 288-295.

LINCOLN, J.V. (Editor) Geomagnetic and Solar Data. J.geophys.Res. 83, 1978: 2727.

LOVE, C.E. and RAINVILLE, E.D. Differential and Integral Calculus. 6th ed. New York, MacMillan Co., 579p.

MacDOUGALL, J.W. The interpretation of ionospheric drift measurements. J. atmos. terr. Phys. 28, 1966: 1093-1109.

MacDOUGALL, J.W. F Region travelling disturbances over Jamaica. *In* Bowhill, S.A., Jaffe, L.D., and Rycroft, J.J. *Editors*. Space Research XII. Berlin, Akademie-Verlag, 1972, p.1133-1142.

MacLEAN, T.S.M. Impedance properties of capacitively loaded dipoles. Proc.Instn elect. Engrs. 115, 1968: 1411-1418

MacLEOD, M.A. Sporadic-E theory, 1, Collision-geomagnetic equilibrium. J.Atmos.Sci. 23, 1966: 96-109.

McNICOL, R.W.E. and THOMAS, J.A. Measurements of changes in the phase path of radio waves reflected from the ionosphere at normal incidence. Aust.J.Phys. 13, 1960: 120-131.

MANSON, A.H., GREGORY, J.B., and STEPHENSON, D.G. Gravity waves in the lower atmosphere. J.atmos.terr. Phys. 38, 1976: 143-148.

MEEKLAH, J.S., REES, D.T., and MANSON, A.H. Amplitude and phase measurements of medium-frequency radio-waves reflected from the lower ionosphere - I. E-region. J.atmos.terr.Phys. 34, 1972: 911-925.

MERCIER, R.P. Diffraction by a screen causing large random phase fluctuations. Proc.Camb.Phil.Soc.Math. Phys.Sci. 58, 1962: 382-400.

MITRA, S.N. A radio method of measuring winds in the ionosphere. Proc.Instn elect. Engrs. 96(III), 1949: 441-446.

MULLER, H.G. Simultaneous observations of meteor winds and ionospheric drifts. J.atmos.terr.Phys. 30 1968: 701-706.

MUNRO, G.H. Travelling disturbances in the ionosphere. Proc.R.Soc. A202, 1950: 208-223.

MUNRO, G.H. Reflexions from irregularities in the ionosphere. Proc.R.Soc. A219, 1953: 447-463.

MUNRO, G.H. Travelling Ionospheric Disturbances in the F region. Aust.J.Phys. 11, 1958: 91-112.

MUNRO, G.H. and HEISLER, L.H. Divergence of radio waves in the ionosphere. Aust.J.Phys. 9, 1956: 359-372.

MUNRO, G.H. and HEISLER, L.H. Cusp type anomalies in variable frequency ionospheric records. Aust. J.Phys. 9, 1956b: 343-358.

NAGPAL, O.P., GUPTA, A.B., and SETTY, C.S.G.K. Some studies of atmospheric gravity waves at equatorial and temperate latitudes. Annls Géophys. 29, 1973: 293-300.

NAGPAL, O.P., GUPTA, A.B., and SETTY, C.S.G.K. Some estimates of gravity-wave associated neutral particle velocity perturbations in the F2-region over Delhi. J.atmos.terr.Phys. 36, 1974: 1146-1156.

PAPOULIS, A. The Fourier Integral and its Applications. New York, McGraw-Hill Book Co., Inc., 1962. 318p.

PFISTER, W. The wave-like nature of inhomogeneities in the E-region. J.atmos.terr.Phys. 33, 1971: 999-1025.

PHILLIPS, G.J. and SPENCER M. The Effects of Anisometric Amplitude Patterns in the Measurement of Ionospheric Drifts. Proc.phys.Soc. 68B, 1955: 481-492.

PITTEWAY, M.L.V., WRIGHT, J.W., and FEDOR, L.S. The interpretation of ionospheric radio drift measurements - III. Validation of correlation analysis by computer simulation. J.atmos.terr.Phys. 33, 1971: 635-660.

RADOSKI, H.R., FOUGERE, P.F., and ZAWALICK, E.J. A Comparison of Power Spectral Estimates and Applications of the Maximum Entrophy Method. J.geophys.Res. 80, 1975: 619-625.

RADOSKI, H.R., ZAWALICK, E.J., and FOUGERE, P.F. The Superiority of Maximum Entropy Power Spectrum Techniques Applied to Geomagnetic Micro-pulsations. Phys.Earth Planet. Inter. 12, 1976: 208-216.

RATCLIFFE, J.A. Some aspects of diffraction theory and their application to the ionosphere. Rep.Prog.Phys. 29, 1956: 188-267.

RATCLIFFE, J.A. The Magneto-Ionic Theory and its Applications to the Ionosphere. Cambridge, University Press, 1959. 206p.

RATCLIFFE, J.A. An introduction to the ionosphere and magnetosphere. Cambridge, University of Cambridge Press, 1972. 256p.

REBER, C.A., HEDIN, A.E., PELZ, D.T., POTTER, W.E., and BRACE, L.H. Phase and Amplitude Relationships of Wave Structure Observed in the Lower Thermosphere. J.geophys.Res. 80, 1975: 4576-4580.

REDDI, C.R., and RAO, R.R. Anomalous variations in phase path records. J.atmos.terr.Phys. 29, 1967: 1603-1610.

WHALE, H.A. Diffraction of a plane wave by a random phase screen. J.atmos.terr.Phys. 35, 1973: 263-274.

WHITEHEAD, J.D. The focussing of short radio waves reflected from the ionosphere. J.atmos.terr. Phys. 9, 1956: 269-275.

WHITTEN, R.C. and POPPOFF, I.G. Fundamentals of Aeronomy. New York, John Wiley and Sons, Inc., 1971.

WRIGHT, J.W. and PITTEWAY, M.L.V. Computer Simulation of ionospheric radio drift methods, and their analysis by correlation methods. Radio Sci. (U.S.) 13, 1978: 189-210.

YEH, K.C. and LIU, C.H. Acoustic-Gravity Waves in the Upper Atmosphere. Rev. Geophys. and Space Phys. 12, 1974: 193-216.

YEH, K.C., LIU, C.H., and HEARN, A.L. Propagation of Gravity Wave Spectra in the Thermosphere. J.geophys. Res. 84, 1979: 834-838.

YEH, K.C., WEBB, H.D., and COWLING, D.H. Evidence of Directional Filtering of Travelling Ionospheric Disturbances. Nature Phys. Sci., 235, 1972: 131-132.

APPENDIX A

ANTENNA ARRAY PREPARATION

Previous work in this department on the D- and E-regions has predominantly used a frequency of 2.40 MHz. Over Christchurch, the E-region critical frequency exceeds 2.40 MHz over much of the daytime (D.S.I.R. Ionospheric data for Christchurch) so it was decided to use 4.57 MHz for daytime F-region work.

Because the antennas then available were all 2.40 MHz folded dipoles, either new arrays had to be constructed or the 2.40 MHz arrays adapted. In fact, a new transmitter array was built, and the receiver arrays were adapted. This work is described in this appendix.

I. METHOD OF ANTENNA MEASUREMENT

Since the antennas discussed in this chapter are all about thirty feet above the ground, direct measurement of antenna input impedance would require some means of direct access to that height.

An alternative approach, which is followed throughout this thesis, is to measure the lookin impedance at the bottom end of the antenna feeder and calculate the load - antenna input - impedance that would give rise to it.

Blake (1969, p.61) presents an equation which gives the input impedance at one end of a transmission line of length ℓ, in terms of its characteristic impedance Z_0 and load impedance at the other end Z_L. It is:

$$Z_i = Z_0 \left[\frac{Z_L \cos \beta\ell + jZ_0 \sin \beta\ell}{Z_0 \cos \beta\ell + jZ_L \sin \beta\ell}\right] \qquad \text{(A-1)}$$

with $\beta = \frac{2\pi}{\lambda}$.

This strictly applies only to the lossless-line case: its use is justified by experimental results presented later.

The equation A-1 can be inverted to give Z_L as a function of Z_0 and Z_i. The result is

$$Z_L = Z_0 \left[\frac{Z_i \cos \beta\ell - jZ_0 \sin \beta\ell}{Z_0 \cos \beta\ell - jZ_i \sin \beta\ell}\right] \qquad \text{(A-2)}$$

(1) Experimental Check

Combinations of resistors, capacitors, and inductors had their impedance measured directly and then placed at the end of a twelve-foot length of RG59-U co-axial cable. The input impedance was measured at the other end and compared with that calculated in equation A-1 from the prior direct measurement of the load.

Table A-1 below shows the cable characteristics: Table A-2 compares measured and calculated input impedances.

Table A-1: Characteristics of cable used in experimental comparison

---

Type of Cable: Essex RG59-U coaxial cable

Length of Cable: 12' = 3.658m

Frequency for which zero admittance obtained for a line shorted at the other end: 13.4799 MHz.

Calculated velocity factor: v = .657

At 20.0 MHz, open circuit admittance: .66 mho, -115 pF

closed circuit admittance: .38 mho, +105 pF

Calculated characteristic impedance: 72.4 $e^{j0^{\circ}29'}$ ohms.

Table A-2 shows that the measured input impedance (Z_i) agrees very closely with the input impedance calculated from the load. This is so even where the measured load does not agree with the nominal load, as in the case of 10 KΩ paralleled with 6 μh.

For this reason it is felt justified both to use a loss-less-line equation, and to use its inversion to find antenna impedances at the top of feeder lines. Measurements using nominal 300Ω balanced twinload have also been analyzed this way, although no similar comparison test was performed on that type of lead.

Throughout this thesis, measurements referred to as "antenna" or "remote load" impedances are actually calculated impedances using equation A-2. The "lookin" impedances are directly measured, and may be used to calculate the antenna impedances.

All bridge measurements were carried out on a Wayne Kerr model B601 R.F. bridge, except those for the comparison test for which a Wayne Kerr B801 Admittance bridge was used. The receiver used was an Eddystone model 680X, calibrated in frequency with a Hewlett-Packard 5245L frequency counter. The R.F. source for measurements at Birdling's Flat was a General Radio Co. Type 605A Standard Signal Generator and for the comparison test a Hewlett-Packard 606A signal generator was used.

A listing of the PDP-8 Fortran program to perform the calculations is presented at the end of the appendix.

Table A-2: Comparison of calculated and measured input impedances for a given load impedance.

Nominal load	Measured Load		Measured Input		Calculated Input*		Frequency
	Resistance	Reactance	Resistance	Reactance	Resistance	Reactance	(MHz)
120Ω	134.05	0.17	133.54	-14.16	132.04	-13.63	0.70
	134.41	0.06	123.22	-32.09	122.53	-31.38	1.75
	134.59	0.33	114.84	-40.61	114.15	-39.04	2.40
	145.56	-0.49	75.77	-68.63	82.35	-53.77	4.57
	146.84	-0.58	61.75	-48.54	63.46	-47.60	6.15
120Ω in parallel with a nominal 6μh coil	83.44	76.90	186.79	-23.51	188.33	-17.13	4.57
	104.14	70.24	110.75	-76.36	117.23	-68.48	6.15
10KΩ† in parallel with a nominal 6μh coil	5.71	164.78	89.82	-664.09	71.65	-630.56	4.57
	9.57	224.23	5.79	-166.01	6.04	-172.65	6.15
23Ω	22.25	1.61	98.08	89.74	73.48	92.25	9.00
23Ω in parallel with nominal 6μh coil	22.22	3.11	55.28	73.64	51.85	74.79	7.50
	22.10	2.90	52.91	92.55	76.91	95.03	9.00
23Ω in parallel with nominal 82pF capacitor	22.18	-0.74	72.53	85.37	67.19	88.28	9.00

* calculated from equation A-1.

† results imply a parallel resistor in the region of 4K7 and a parallel inductor of order 6μh.

All results given in terms of series values and in units of ohms. The series values are obtained from the parallel values measured on the B801 bridge.

All antenna impedances measured in this thesis are the complex load impedances presented by the antenna at its point of entry. For all antennas, including the Kraus 3/8λ antenna discussed in the transmission section, this point is the centre-feeding point which is coincident with a current loop (Blake, 1966, P.141). When reactance is tuned out the impedance is just the sum of the radiation resistance and the loss resistance. Unless mutual impedances or driving-point impedances are specifically measured, the quoted impedance is the self-impedance of the antenna, as modified by the effective earth. These were not found to depart very much from free-space values. The antenna wire was hard-drawn copper of .064" diameter.

II. RECEPTION ARRAY

This section dexcribes the adaption of the then current 2.40 MHz folded dipole arrays to allow reception at both 2.40 MHz and 4.57 MHz.

Two main methods of array adaption are discussed: the trap method was chosen finally as the permanent system. Because folded-dipole antennas do not operate well at twice their fundamental frequency (A.R.R.L. Antenna Handbook, 1974, P.106), this type was abandoned in favour of single-wire dipoles.

(1) Damping of the Dipoles with Resistors.

The loss component of the antenna resistance far exceeds the radiative component. Thus matching must be done to a resistance of order 1000 ohms. Power absorbed in this resistor is lost to the receivers, although reactance is damped out quite satisfactorily.

(2) Capacitative Coupling

(a) Results of Maclean. Maclean (1968) has done an experimental and theoretical investigation upon the effects arising on incorporation of capacitors in the arms of a centre-fed dipole. From figure A-1, reproduced from Maclean, it is seen that incorporating capacitors alters the characteristics of antenna impedance - especially those of the reactance - from those of an unloaded dipole of same length.

For a single capacitor in each arm, the main effect over the unloaded case is a movement of the resistance and of the reactance plots up the frequency (or ℓ/λ) axis compared to the unloaded case: there is also some smoothing of the reactance curve against frequency. The limit at one end is the unloaded case - infinite capacitance between the sections being equivalent to a direct connection which makes the dipole of length 2ℓ. As the loading capacitance is decreased the reactance between the sections of length ℓ_1 and ℓ_2 becomes greater. The resistance and reactance curves shift up the frequency or ℓ/λ axis, to the limit of the shortened dipole of length $2\ell_1$.

Mclean did his impedance measurements on a monopole antenna. This (Tai, 1961, P.3-21) has an impedance one-half that of a dipole of corresponding length. He doubled his actual measurements to compare with the theory, which was calculated for a dipole. Reasonable agreement - especially for the resistance case - was obtained. The greatest departures are found where the (complete) dipole length is an integral number of wavelengths.

This close agreement gives confidence in Maclean's results, and suggests similar measurements on the aerials at Birdling's Flat. By experiment Maclean found that the smoothing of resistance and reactance curves against frequency was greater with multiple sectioning and loading. This suggests the possibility of broadbanding the antenna.

(b) Application to Birdling's antennae. Maclean's Figure 11, "Experimental input reactance as a function of frequency", shows that even for triple loading, the change of reactance with frequency is greatest for $0.25 < \ell/\lambda < 0.5$. The curve does not smooth out until ℓ/λ exceeds 0.6.

For the two frequencies of interest, we have

f, MHz	ℓ/λ
2.40	0.25
4.57	0.48

Thus the possibility of broadbanding is not too hopeful.

(c) Experimental Results. An experimental single-wire dipole with an egg insulator half-way along each arm was erected. The antenna was centre-fed through a 1:1 balun. For initial work RG58-U 53Ω coax was used as a feeder: subsequently RG59-U 73Ω coax was employed.

By measuring the remote load impedance for a resistor attached both directly at the end of the coax feeder and through the 1:1 balun, for frequencies between 2 and 5 MHz, the balun was found to transform resistance faithfully and to add a constant 3 ohms of inductive reactance flatly right across the band.

By electrical shorting across the egg insulators the 2.4 MHz dipole is reproduced. Comparison of antenna impedances with Maclean's theoretical results gave satisfactory qualitative agreement: the main departures again in the region where the total dipole length is a multiple of the wavelength.

With some faith in the unloaded case, a value of 47 pF on each arm was tried. Reference to Graph A-1 shows resistance values move up the frequency axis over the unloaded case: the first peak after $\ell/\lambda = 0.2$ is seen to move up from 3.2 MHz in the unloaded case to 4.6 MHz in the C = 47 pF case. Taking "no connection" as a "zero pF" limit, and "direct connection" as an "infinity pF" limit, the resistance-frequency curves are seen to trend from one limit to the other as the loading capacitance rises. The zero pF limit corresponds to an unloaded dipole of length $2\ell_1$, and the infinite pF limit to one of length 2ℓ. C = 47 pF loading lies half-way between the extremes.

The reactance curves, Graph A-2, display the trends even more sharply. As in Maclean's Figure 9, the curves stretch and shift up the frequency axis as C_{load} decreases.

Single loading at C = 47 pF gives a resistance of 75Ω at 2.4 MHz and 630Ω at 4.57 MHz. The reactance at both frequencies is about -300Ω. No one reactive element can tune this out at two different frequencies. Nevertheless, the C = 47 pF curve allows the best opportunity to fit the antenna to the requirement of reception at both 2.4 MHz and 4.57 MHz.

The good agreement between Maclean's results and this author's results for single loading, when frequency is expressed in terms of Maclean's parameter ℓ/λ, gives an idea of

results expected from triple loading. No measurements for this case were performed by this author, Maclean's results (refer to his Figure 11) imply that an inductor whose reactance decreases with frequency would be needed to tune out the antenna reactance.

Operation of the antenna at two frequencies using this method requires broadbanding across the entire band bounded by the two frequencies. At this stage it was felt worth while to attempt to make the antenna suitable for 2.4 MHz and 4.57 MHz alone, so further work was done using tuned traps to compare results with those of capacitative broadbanding.

(3) Tuned-Trap Loading

This technique is well-known in multiband antenna operation (A.R.R.L. Antenna Handbook, 1974, P.182) (Terman, 1943, P.854). The antenna is divided into an inner portion of suitable length for operation at the fundamental at 4.57 MHz, and an outer portion with length such that the inner and outer portions together work at the fundamental at 2.40 MHz. An egg insulator provides mechanical support between the sections.

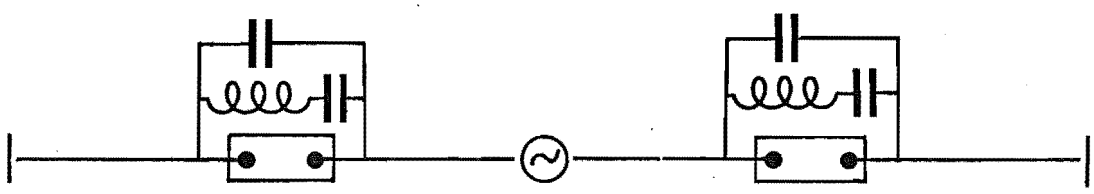

MULTIBAND TRAP ANTENNA

In the trap the series inductor and capacitor are chosen for series resonance at 2.40 MHz. The impedance at the trap point is zero for that frequency and operation at 2.40 MHz is not affected. This combination becomes inductive at 4.57 MHz and the parallel capacitor is chosen for parallel resonance at 4.57 MHz. The outer portion is cut off and the inner portion operates at the fundamental at 4.57 MHz.

(a) Experimental results. A test aerial was erected and had inner and outer parts tuned to length for harmonic operation without traps present. Two test traps were then attached.

Initial results showed that the antenna would tune to resonance at 2.40 MHz, but regardless of length or capacitance adjustment would not tune to resonance below 4.61 MHz in the parallel-resonant case. It turned out that the resistance of the parallel-resonant circuit was too low.

Resistors of various values were substituted for the traps. Graph A-3 shows clearly that for satisfactory antenna resonance tuning at 4.57 MHz a resistance value of 27K or more is required. Below this, the input resistance of the antenna is significantly higher than the theoretical dipole value of 67 ohms; and the zero-reactance point is shifted to a frequency greater than 4.57 MHz.

The resistance presented by a parallel-resonance circuit at resonance is $R_{parr} = Q_0\omega_0 L$ for Q_0 exceeding 10 (Terman, 1943, P.144). Thus L and Q must be such as to make R_{parr} exceed 27K.

(b) Design and construction of weatherproof traps. The formula

$$L = \frac{\mu_0 N^2}{\ell} A$$

for the self-inductance of a solenoid applies only to an internal point for a coil long in comparison with its diameter. For a coil of given inductance to have highest possible Q, the coil length must be half its diameter (Terman, 1943, P.74). The design curves given by Dobbie (1963, P.429) gave a lead to coil design, but specifications were not critical as long as R_{parr} was greater than 27K.

The final version of the traps incorporated an inductor wound on the outside surface of a hollow tufnol rod, of outside diameter $1\frac{1}{8}$", inside diameter $\frac{7}{8}$" and length 2". Dobbie's curves give:

Current sheet inductance for 10 turns per inch = 5 μh.
(coil diameter = $1\frac{1}{8}$")

Required inductance = 62 μh (a convenient value for resonance)

∴ Number of turns = 70

∴ Pitch p $= \frac{2}{70}$

$= .0286.$

For highest Q, d the wire diameter is required to be

$d = 0.7p$

∴ d = .02" or 25 SWG wire.

This suggested data just gives a guide: specifications do not require close compliance with these figures.

The data for the traps as actually built is:

Pitch = .03125

Wire = 25 SWG grade

Unloaded Q = 230-240

For 2.40 MHz resonance, a series capacitor of 80 pF was required. Thus:

$L = 55\mu h$

so by calculation one expects

$R_{parr} = Q_0\omega_0 L = 199K\Omega$

$R_{series} = \omega_0 L/Q_0 = 3.5\Omega.$

By measurement, $R_{parr} = 175K\Omega$ at 4.57 MHz. This well exceeds $27K\Omega$, allowing effective cutoff. The location of the trap from the centre of the antenna is over halfway along the 2.40 MHz-length total dipole arm. This is a relatively high impedance point that would be little affected by the series resistance of the trap. For parallel resonance a capacitance of 25 pF is required in parallel with the (coil - 80 pF) series combination. A $10M\Omega$ bleeder resistor was also placed across this capacitor.

After the wire was placed in the groove the entire tufnol rod was epoxy-resin sealed. Fixed polystyrene capacitors and twisted-pair wires were used for tuning. The entire trap was firmly mounted mechanically within a P.V.C. pipe. The electrical connections were brought out using two brass screws, one in each of two P.V.C. endcaps which were sealed over the ends of the pipe. Two traps were mounted on each antenna, across the egg insulators connecting the antenna segments.

Resonance was now obtained on both 2.40 MHz and 4.57 MHz. Graph A-4 shows the remote load aerial impedances at 2.40 MHz and 4.57 MHz.

Mr G.S. Lees of this department assisted in the design, construction and installation of the traps and aerials.

(4) Array Design

Each array consisted of two broadside parallel in-phase trap dipoles. The antenna spacing within an array is 66 metres and the array spacing is 250 metres. The 75-ohm entry-point impedance is transformed by a balun to 75 ohms unbalanced into a co-axial feeder. At ground level another balun transforms this to 300 ohms balanced to feed 300-ohm open-wire line feeding to the array centre.

At the array centre the open-wire lines leading from the antennas are connected in parallel. The resulting 150 ohms is transformed to 600 ohms using a balanced transformer to feed 600-ohm open wire line leading to the receiving hut. There, a balanced transformer transforms the impedance to 300 ohms which in turn is transformed using a balun to 75 ohms unbalanced for feeding to the receivers.

All impedances quoted are nominal only. Bleeder resistors of value several MΩ were placed across all baluns and transformers until the hut earth was reached.

(5) Some Recent Results on Phase Measurement

Mr E. Kwa of this department has used one reception array to investigate the effects of tidal changes on antenna impedance (Kwa , unpubl., 1977). He used a sensitive chart-recording bridge which he built to make continuous measurements

of the effect of water-table height on array impedance, over periods of two days at a time.

His preliminary results show that the phase of array impedance at 2.40 MHz can change by some 300-700 degrees in phase in four hours or so. The effect oscillates with the tides. It is probable that measurements on 4.57 MHz are of the same order. Ionospheric phase-height changes are usually at least two orders of magnitude greater than this - especially for F region. Although the effects are probably not strictly additive, it is felt that the tidal changes can be counted as a very low-frequency trend and removed with a linear digital filter. Problems may arise for very steady phase-height for E-region.

Comparison of phase between aerial arrays is difficult at these frequencies. It should be stated here that the aerials and arrays have never been calibrated for phase. The array feeders are of unequal length: this alone brings in a phase difference between arrays. Tidal effects would add a slowly-changing component to these differences.

For the phase height and amplitude drifts experiments these effects are probably not important. The phase height uses only one antenna and tidal effects can be filtered out. The amplitude gain of an antenna does depend on the depth of the effective earth, but effects would occur over a much longer time-scale than the usual one minute or three minute average drifts run.

The phase of the complex auto- and cross-correlations would be affected by the tidal changes over the typical four-hour time scale previously mentioned.

III. TRANSMISSION ARRAY

The transmission array available for transmission at 4.57 MHz had been used for 6.15 MHz previously, using half-wave folded dipoles. Operation at a lower frequency requires a longer aerial if folded dipoles are to be used: this was physically difficult because of the post separation of half a 6.15 MHz wavelength.

Preparation of the transmission array thus involved different physical problems to those of the reception array, which were discussed in part II of this appendix. Moreover, peak powers of kilowatt order must be handled by a transmission array. It was decided also to transmit 4.57 MHz in circular polarization.

This section discusses the modification of the 6.15 MHz transmission array to obtain polarized transmission at 4.57 MHz.

(1) Antenna Development

(a) Extension of 6.15 MHz dipoles. Extension in length of the 6.15 MHz folded dipoles for resonance at 4.57 MHz was found satisfactory for an individual aerial. Problems arose when the mutual impedance between extended aerials was found to be significant. It was not mechanically possible to keep adjacent extensions mutually at right angles and out of contact. It is necessary to avoid coupling, as this will destroy the ninety-degree phasing required between pairs of parallel elements to transmit circular polarization. Thus this solution was not available.

(b) Resistive Loading of Antenna. A series damping resistor was placed in the middle of the top lead of the folded dipole. A value of 670 ohms was enough to damp out changes in reactive components at 4.57 MHz, but a constant inductive reactance was always present. If this arrangement had been used, the total input resistance would be the sum of a 300 ohm radiative component and 670 ohm loss component.

(c) Kraus $\frac{3}{8}$-wavelength four-wire antenna. Kraus (1950, P.417) describes a four-wire, open-ended, centre-fed dipole of length $\frac{3}{8}$-wavelength corresponding to design frequency. It has a nominal input impedance of 225 ohms in free space.

For 6.15 MHz, $\frac{\lambda}{2}$ is 24.4 metres. For 4.57 MHz, $\frac{3\lambda}{8}$ is 24.6 metres. Thus it seemed possible to fit a $\frac{3\lambda}{8}$ antenna for 4.57 MHz between poles spaced at a half-wavelength for 6.15 MHz. Moreover, the input impedance is an excellent match for the 220 ohm (nominal 300 ohm) marine-core twinlead used at Birdling's Flat to feed the transmission antennae. In addition, there are no damping resistors to absorb power.

An experimental four-wire antenna was erected on one side of the 6.15 MHz array. Measurements showed resonance at 5.0 MHz. An addition of length was necessary to lower the resonant frequency, so the centre support was pulled down somewhat to accommodate the addition. The arms of the antenna were thus at 30^{o} to the horizontal.

Results are presented in Graph A-5 and Graph A-6 for tuning at 4.62 MHz. Subsequent tuning in length brought resonance to 4.57 MHz.

Kraus (1940) has done standing-wave ratio measurements on a similar antenna at about 14 MHz. He found SWR ratios to change quite sharply as the antenna length increased or decreased from tuned resonance, but SWR ratios remained quite constant over a 0.5 MHz change in frequency when the antenna was at resonant length. This means the antenna may be used to transmit pulses as short as 2 μsec - far below the 55 μsec used here.

(2) Polarization of Transmission and Feeding Network.

To transmit a circularly-polarized electromagnetic wave it is a standard method to cross two half-wave dipoles and feed the antennae in phase quadrature (Kraus, 1950, P.425). With respect to polarization it is equivalent to use two pairs each consisting of two broadside parallel elements arranged to form a square, and have the pairs fed in phase quadrature.

Von Biel (unpubl., 1970, P.61) has developed a four terminal "sine hybrid" network which feeds its two output terminals in quadrature provided they are loaded with the characteristic impedance of the network. It so happens that the inner square formed by the centre antenna feed posts has edges of length that required for a 4.57 MHz transmission-line version of this circuit. Figure A-2 shows the layout. Thus the feeder lines were mounted on these posts; adjacent lines were turned by 180° along their lengths in opposite directions. Coupling between lines appeared very small.

A power relay is wired to switch the phasing of one pair of antennae by 180°. This allows circular polarization of the transmitted wave. Switching between modes was

done on computer command.

Running of the experiment showed that both O- and X-modes were received. This contrasts to the results of Kelleher (1966a) who was able to get F-region drifts results for O- and X-modes separately, using a similar system. The reasons for this may be:

(i) Magnetoionic mixing. At the reflector some energy can be passed from one mode to another (Budden, 1961; Ratcliffe, 1959). Transmission of one mode alone can still give rise to reception of two. Discrimination between modes on reception (for example, von Biel, 1977) is in principle a preferred approach.

(ii) Coupling within the shifting network. von Biel's (1970, unpubl.) phase-shift network was implemented in lumped-component form. The transmission-line version used here would be sensitive to mutual coupling between phase-shifting transmission lines. In addition, the design to "nominal" impedance (which was satisfactory for the reception array) meant that transmission lines and aerial load were not exactly matched. While matching was close enough to allow near-maximum-power-transfer, residual reactance was still found to be present and this lead to unwanted phase shifts.

(iii) Coupling between the aerials. Measurement of mutual impedance between pairs of transmitting antennas (for example, Terman and Pettit, 1952) indicated its presence, and again this gave rise to subsequent phase shifts and hence the transmitted wave was not perfectly circularly polarized.

In practice it was found that the group heights of O-

and X-modes remained apart for a high proportion of any data run. The availability of a moveable receiver gate and software tracking of the F-region signal (Appendix B) made selection of only one of the received modes possible. The echo of greater amplitude was taken for results, and ionograms from the Godley Head ionosonde later checked for mode information.

IV CONCLUSION

A description has been given of the design and construction of the 4.57 MHz antenna arrays used for the results of this thesis. This work was necessary, because the then current experimental system was designed for 2.40 MHz could not be used for daytime F-region work at this location.

FIGURE A-1 ANTENNA CAPACITATIVE COUPLING
- AFTER MACLEAN (1968) -

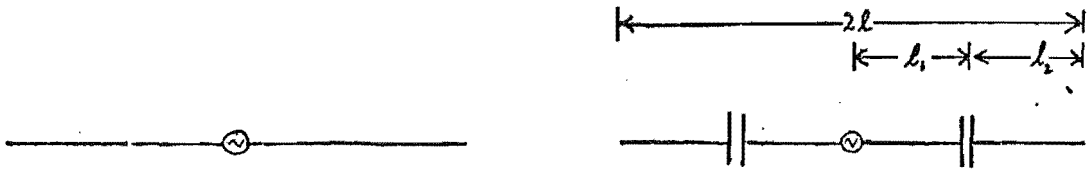

UNLOADED DIPOLE

LOADED DIPOLE

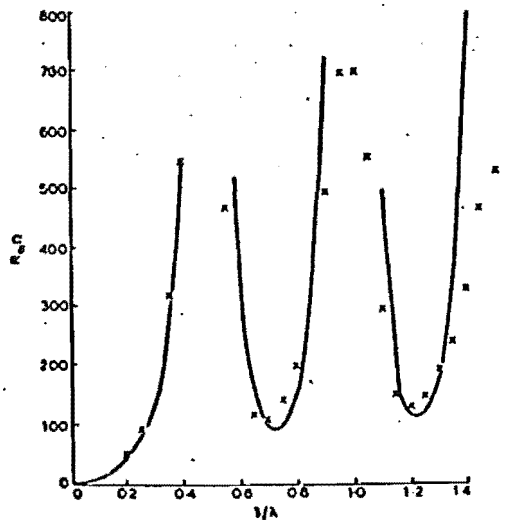

Fig. 4
Input resistance of unloaded dipole as a function of frequency
——— theoretical
× × × × experimental

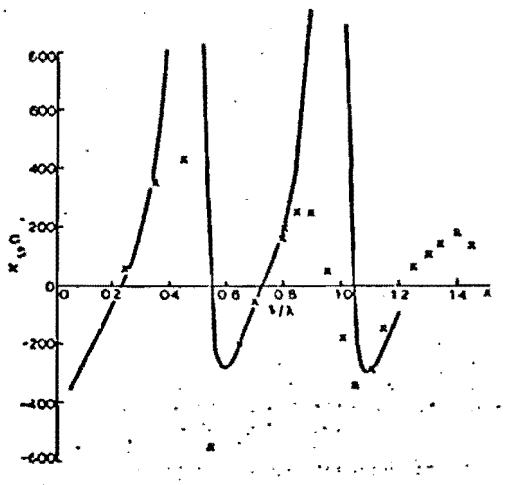

Fig. 5
Input reactance of unloaded dipole as a function of frequency
——— theoretical
× × × × experimental

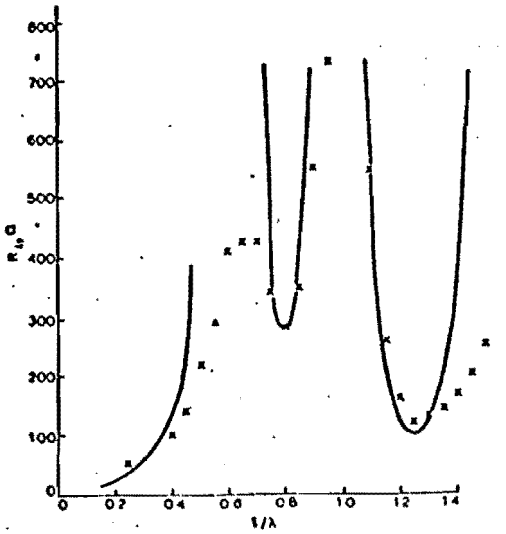

Fig. 6
Input resistance of singly loaded dipole as a function of frequency
——— theoretical (C_1 = 1·3pf)
× × × × experimental

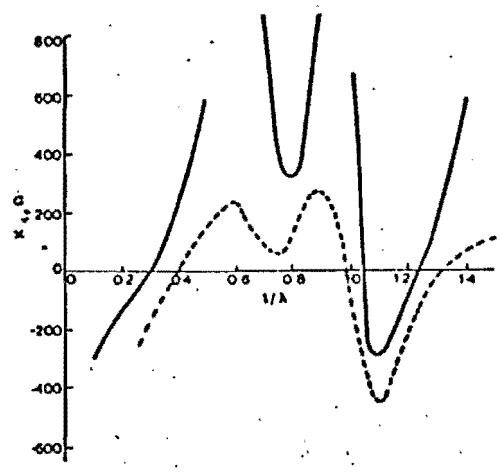

Fig. 8
Input reactance of singly loaded dipole as a function of frequency
——— theoretical (C_1 = 1·3pf)
× × × × experimental

FIGURE A-2

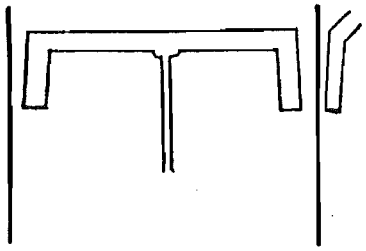

EXTENDED ANTENNA

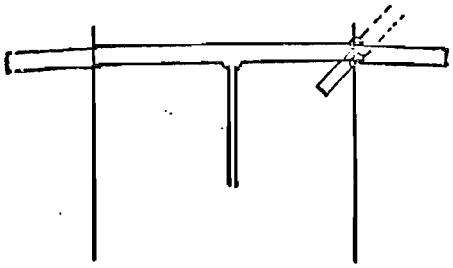

STRETCHED EXTENSION

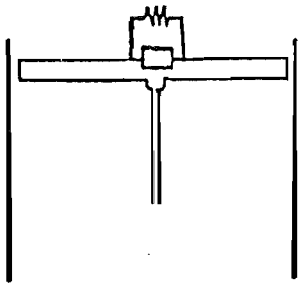

RESISTIVE LOADING

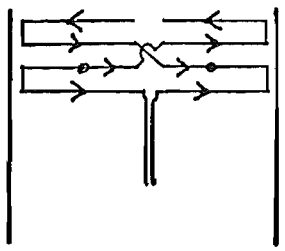

KRAUS $\frac{3}{8}$-λ ANTENNA

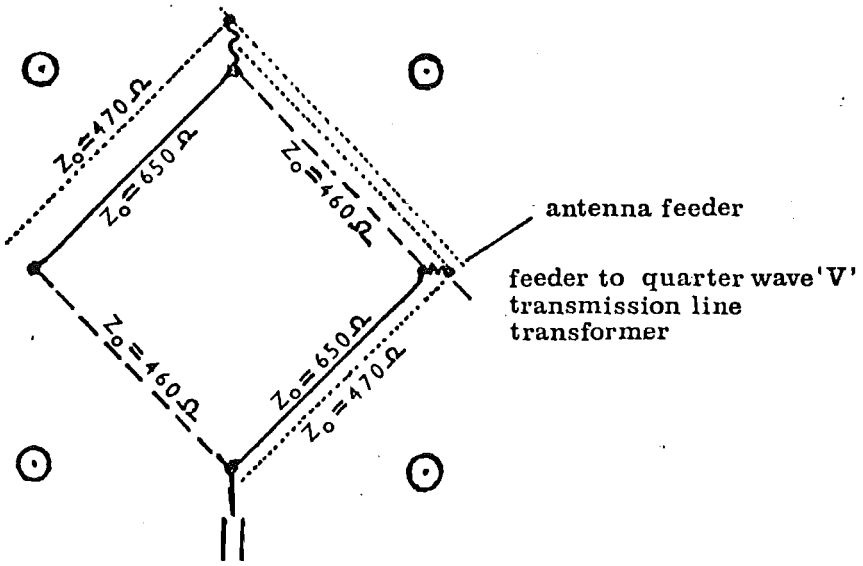

POLARIZATION OF TX ARRAY

GRAPH A-1 SINGLE-WIRE CAPACITOR-LOADED ANTENNA-CENTRE-FED RESISTANCE VERSUS FREQUENCY

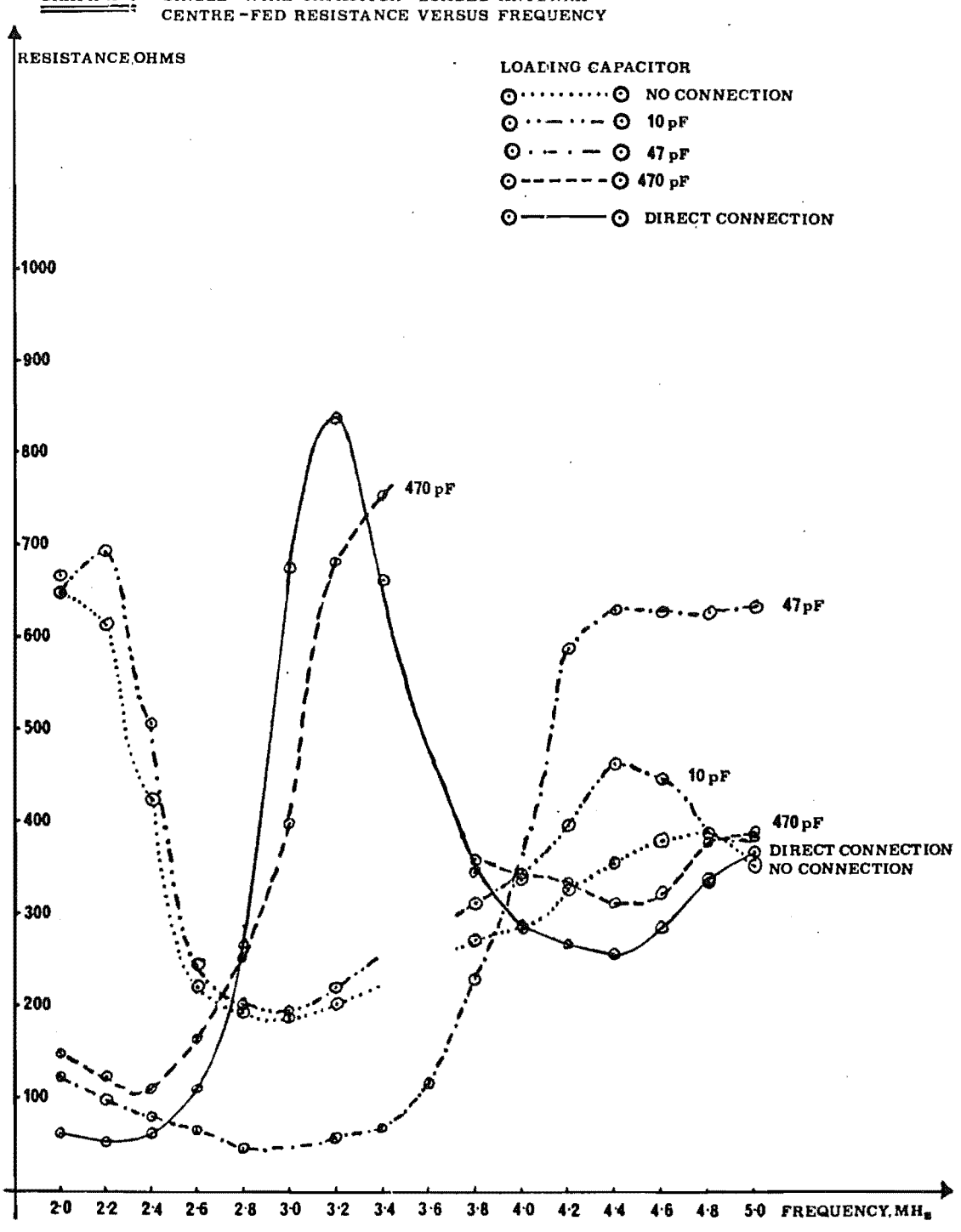

GRAPH A-2 SINGLE-WIRE CAPACITOR-LOADED ANTENNA-
CENTRE-FED REACTANCE VERSUS FREQUENCY

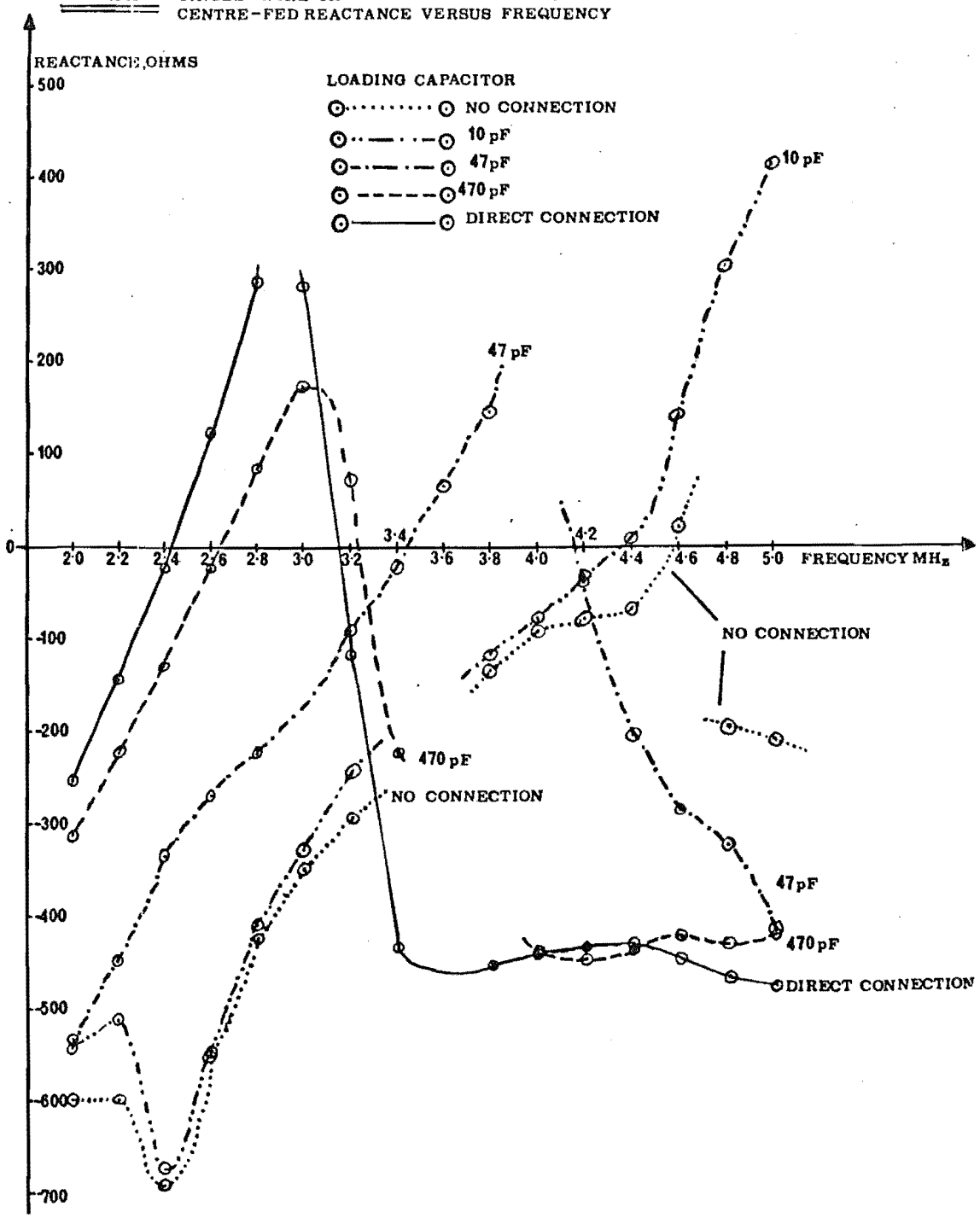

GRAPH A-3 INNER DIPOLE OF LENGTH
OUTER DIPOLE OF LENGTH
EFFECT OF JOINING INNER AND OUTER DIPOLES BY RESISTORS

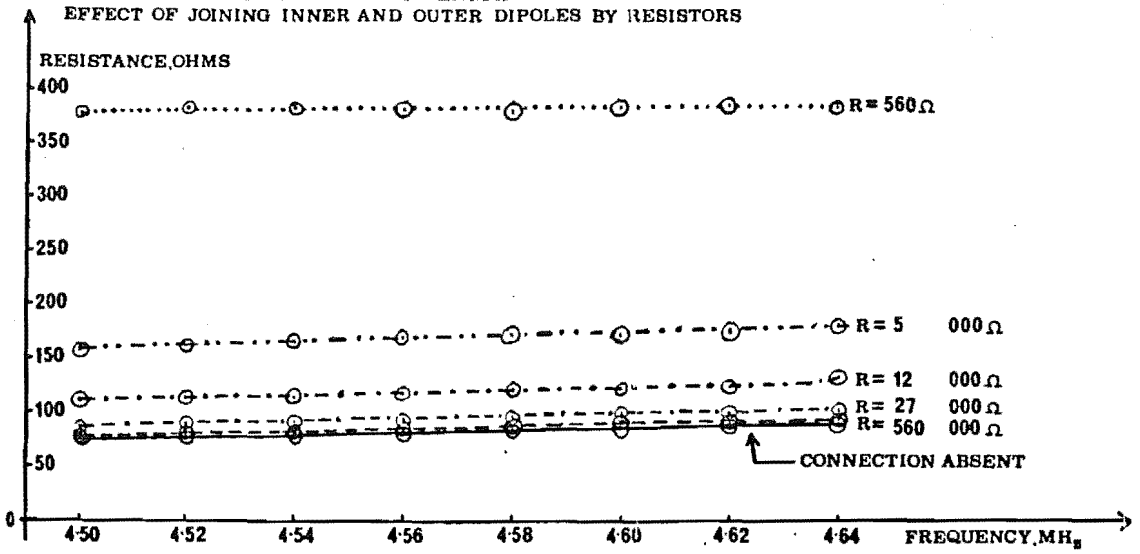

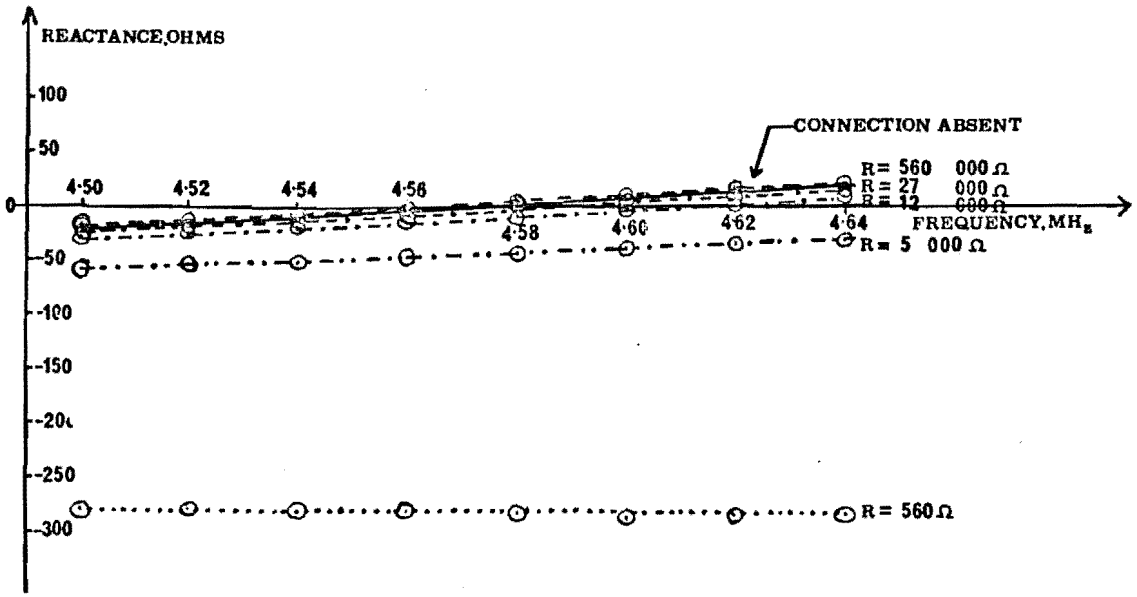

GRAPH A-4 ANTENNA IMPEDANCE WITH TUNED TRAPS

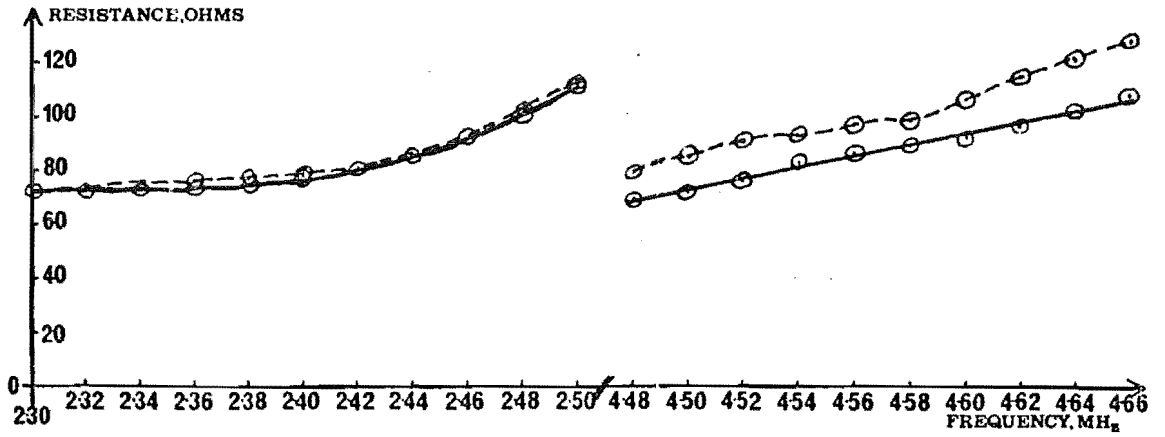

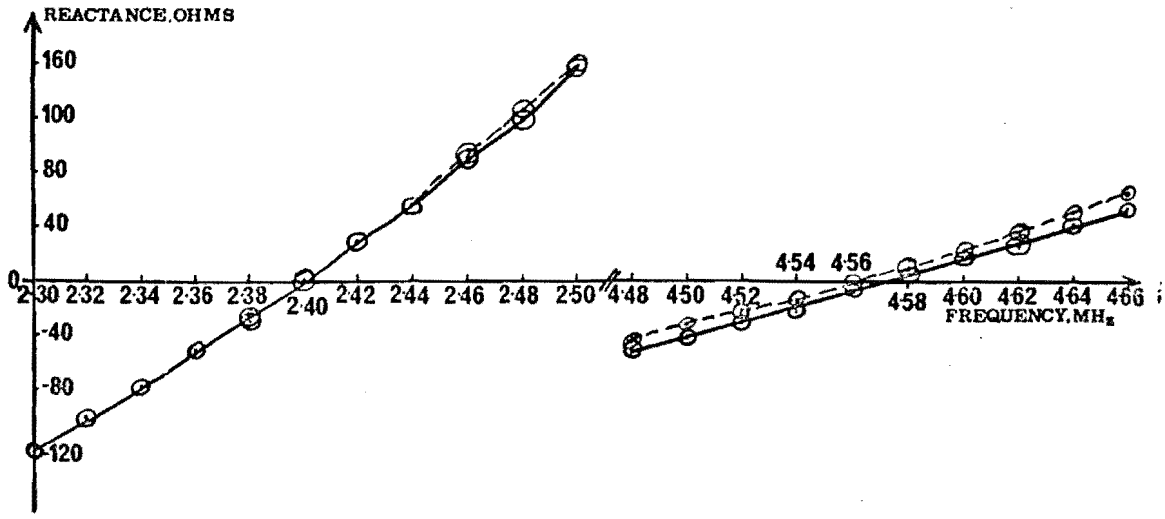

GRAPH A-5 RESISTANCE OF KRAUS ANTENNA

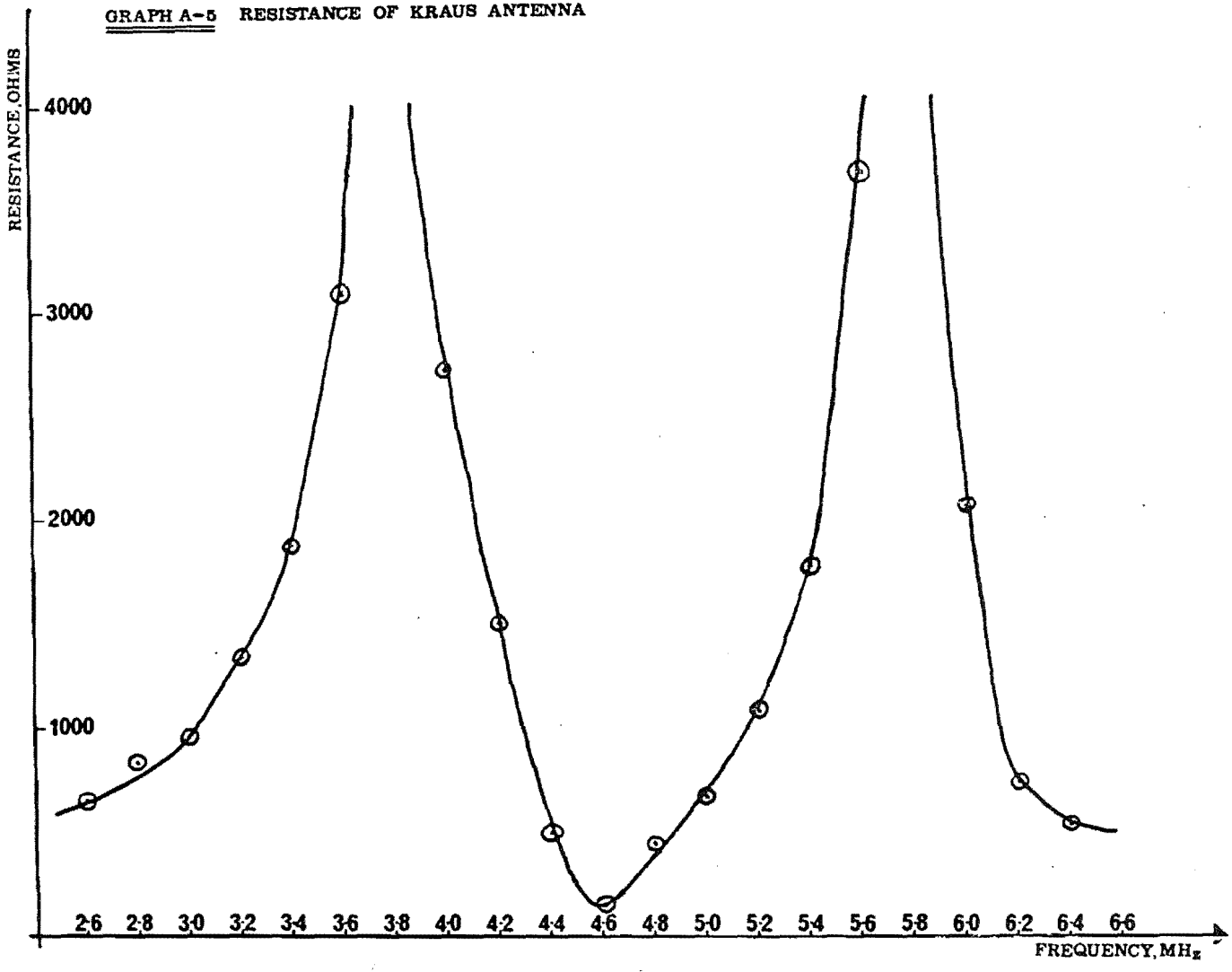

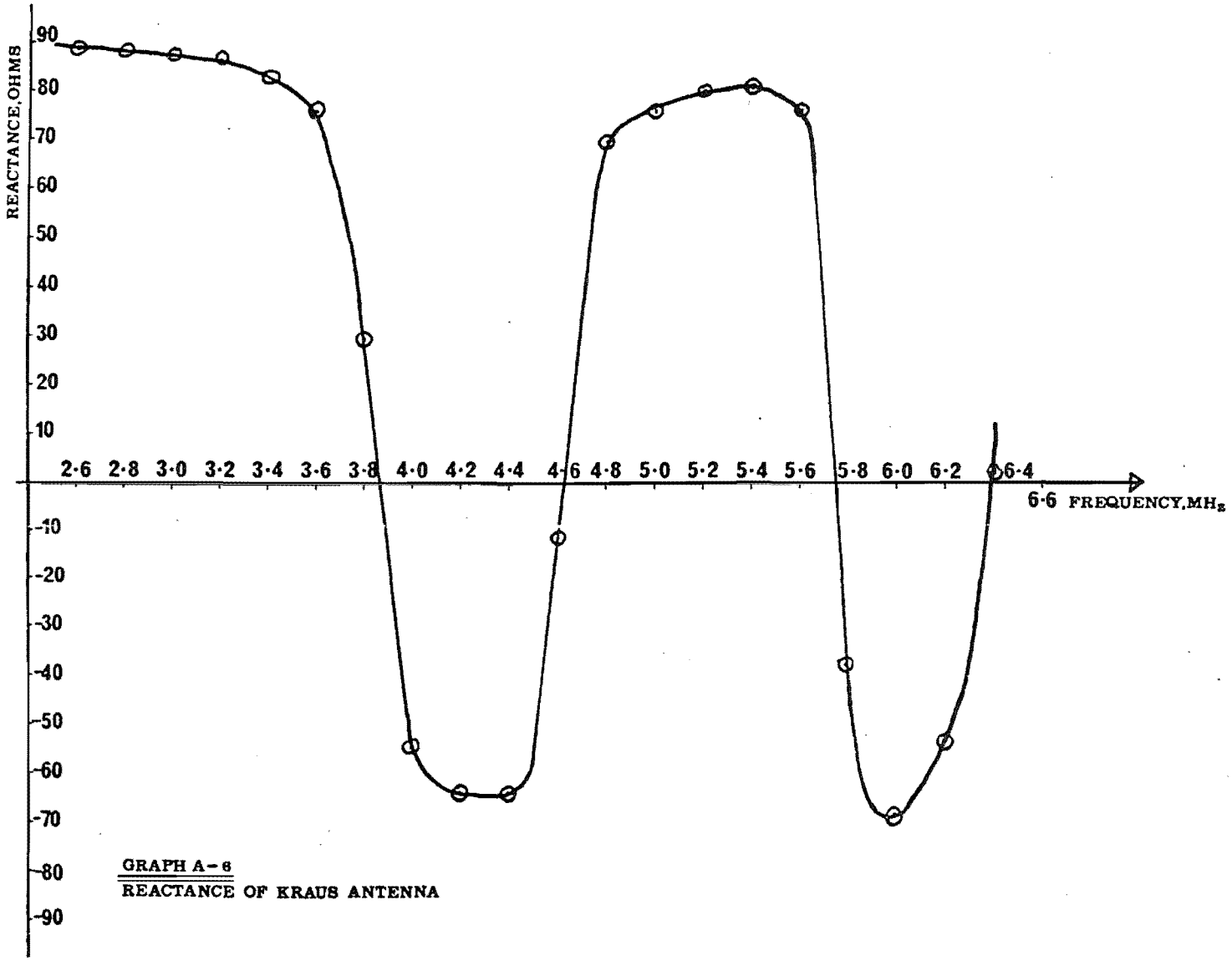

GRAPH A – 6
REACTANCE OF KRAUS ANTENNA

FORTRAN SOURCE LISTING OF IMPD.SV

RETURNS ANTENNA IMPEDANCES

```
C       THIS PROGRAMME WILL READ DIAL VALUES OF COMPLEX IMPEDANCE
C       FROM THE WAYNE KERR BRIDGE.
C
C       FOR THE SWITCH REGISTER GREATER THAN OCTAL 4, THE INPUT
C       VALUES ARE TAKEN TO BE THOSE LOOKING INTO AN ANTENNA
C       TWINLEAD FEEDER OF LENGTH ALENGH, VELOCITY FACTOR VEL,
C       AND INTRINSIC IMPEDANCE Z0.
C       THE VALUES RETURNED ARE THOSE OF COMPLEX ANTENNA IMPEDANCE
C       AT POINT OF ENTRY TO ANTENNA, FOR THE INPUT FREQUENCY.
C
C       FOR THE SWITCH REGISTER LESS THAN OCTAL 4, ONLY
C       THE DIRECT CALCULATION OF LOOKIN IMPEDANCE AS A LOAD IS
C       RETURNED.
C
C       EXCEPT THAT FOR THE SWITCH REGISTER EQUAL TO OCTAL 3,
C       BOTH THE LOOKIN IMPEDANCE AND THE ANTENNA LOAD AT THE
C       END OF THE FEEDER ARE RETURNED.
C
C       TO STOP THE PROGRAMME, PUT OCTAL 4 IN THE SWITCH REGISTER.
C
C       THE OPPORTUNITY TO CHANGE THE SWITCH REGISTER IS AT
C       'PAUSE 400', THEN PRESS 'CONTINUE'.
C
C       IN ALL CASES REAL OR DUMMY CHARACTERISTICS OF THE
C       TWINLEAD FEEDER ARE READ IN FIRST.
C
C       FOR ANOTHER FEEDER RESTART THE PROGRAMME.
C
C       REFERENCE: 'TRANSMISSION LINES AND WAVEGUIDES,' L.V. BLAKE,
C       PUBL. JOHN WILEY & SONS INC., 1969, P. 61.
C
C
C
      DIMENSION Z0(2), ZI(2),ZL(2),ZP(2),ZR(2)
      ZR(1)=0.
      ZR(2)=1.
      RAD=57.2958
      PI=3.1416
      N=0
      READ (1,20)ALENGH,VEL,Z0(1),Z0(2)
   20 FORMAT('FEEDER LENGTH IN METRES IS',F7.3,/'VELOCITY
     * FACTOR IS',F7.3,/'INTRINSIC IMPEDANCE:REAL PART,OHMS
     *'F7.3,/'INTRINSIC IMPEDANCE: IMAGINARY PART!!!,OHMS'
     *,F7.3)
```

```
      WRITE(1,463)
      WRITE(1,464)
      WRITE(1,1)
    1 FORMAT(///)
   17 CONTINUE
      PAUSE 256
      N=IRDSW(0)
      IF(N-4)15,99,15
  463 FORMAT('RESTN. DIAL,KOHM',5X,'MULT',5X,'TERM',5X,'F 7
     *.3,**,F3.1,**,F3.1')
   15 READ(1,2)ZI(1),ZI(2),ZL(1)
  464 FORMAT('CAPN. DIAL,PF',5X,'MULT',5X,'TERM',5X,'F7.3,
     ***,F3.1,**,F3.1')
      READ(1,2)ZL(2),ZP(1),ZP(2)
    2 FORMAT(F7.3,'**',F3.1,'**',F3.1)
      READ(1,3)FREQ
    3 FORMAT('FREQUENCY,MHZ',F6.2)
      A=ZI(2)
      B=ZL(1)
      ZI(1)=ZI(1)*(A*B)
      ZI(1)=ZI(1)*1000.
      A=ZL(2)
      B=(2.*PI)*(FREQ*A)
      B=B/1000000.
      A=1.
      ZL(2)=A/B
  558 FORMAT('ZL(1)=',F15.5,'ZL(2)=',F15.5)
      IF(ZL(2))4,99,5
    5 ZL(2)=-ZL(2)
      A=ZP(1)
      B=ZP(2)
      A=A*B
      A=1./A
      ZL(2)=A*ZL(2)
      GO TO 6
    4 ZL(2)=-ZL(2)
      A=ZP(1)
      B=ZP(2)
      A=A*B
      ZL(2)=A*ZL(2)
    6 ZI(2)=ZL(2)
C   ZL(1) AND ZL(2) ARE RESISTANCE AND REACTANCE RESPECTIVELY.
      A=ZI(1)
      B=ZI(2)
      A=A/B
      A=A*A
      A=1.+A
      B=ZI(1)
      C=B/A
C   SERIES RESISTANCE OBTAINED.
      A=ZI(1)
```

```
      B=ZI(2)
      A=B/A
      A=A*A
      A=1.+A
      B=ZI(2)
      D=B/A
C  SERIES REACTANCE OBTAINED.
      ZI(1)=C
      ZI(2)=D
      IF(N-4)25,26,26
   25 WRITE(1,27)ZI(1),ZI(2)
   27 FORMAT('LOOKIN IMPEDANCE IS',F7.2,'OHMS',',',2X,F7.2,
     *'OHMS')
      C=ZI(1)
      D=ZI(2)
      A=D/C
      A=ATAN(A)
      A=A*RAD
      B=(C*C)+(D*D)
      B=SQRT(B)
      WRITE(1,16)B,A
      IF(N-3)40,26,40
   40 GO TO 24
   26 CONTINUE
      FREQ=300./FREQ
      FREQ=VEL*FREQ
      FREQ=(2.*PI)/FREQ
      FREQ=ALENGH*FREQ
      A=SIN(FREQ)
      B=COS(FREQ)
      CALL MULT(ZR,ZO,ZP)
      DO 12 I=1,2
   12 ZL(I)=(ZI(I)*B)-(ZP(I)*A)
      CALL MULT(ZR,ZI,ZP)
      DO 13 I=1,2
   13 ZP(I)=(ZO(I)*B)-(ZP(I)*A)
      CALL DIVID(ZL,ZP,ZL)
      CALL MULT(ZO,ZL,ZL)
      A=ZL(1)
      B=ZL(2)
      B=B/A
      C=ATAN(B)
      C=C*RAD
      B=ZL(2)
      A=(A*A)+(B*B)
      A=SQRT(A)
      WRITE(1,18)
   18 FORMAT('LOAD IMPEDANCE AT END OF FEEDER GIVEN')
      WRITE(1,14)ZL(1),ZL(2)
      WRITE(1,16)A,C
   14 FORMAT('SERIES RESISTANCE=',F10.2,2X,'SERIES REACTANCE
```

```
  *=',F10.2)
16    FORMAT('MAGNITUDE=',F10.2,'PHASE ANGLE=',F7.1,1X,'DEG
  *REES',//)
24    CONTINUE
      GO TO 17
99    WRITE(1,30)
30    FORMAT('PROGRAMME STOPPED')
      CALL EXIT
      END
```

MULTIPLICATION SUBROUTINE FOR COMPLEX Z

```
      SUBROUTINE MULT(A,B,C)
      DIMENSION A(2),B(2),C(2)
      D=A(1)
      E=A(2)
      F=B(1)
      G=B(2)
      C(1)=(D*F)-(E*G)
      C(2)=(D*G)+(E*F)
      RETURN
      END
```

DIVISION SUBROUTINE FOR COMPLEX Z

```
      SUBROUTINE DIVID(A,B,C)
      DIMENSION A(2),B(2),C(2)
      D=A(1)
      E=A(2)
      F=B(1)
      G=B(2)
      H=((F*F)+(G*G))
      C(1)=((D*F)+(E*G))/H
      C(2)=((E*F)-(D*G))/H
      RETURN
      END
```

APPENDIX B

EQUIPMENT CIRCUITS AND EXPERIMENT PROCEDURE

Reception of signals on 4.57 MHz was done by coherent detection, to allow recording of amplitude and phase.

At the time that the decision was made to build a 4.57 MHz coherent-reception system, there was a coherent-reception system for 2.40 MHz already in existence. In preference to building 4.57 MHz receivers, it was decided to build a set of "front-end" converters to the 2.40 MHz receivers to mix the 4.57 MHz to 2.40 MHz.

The 2.40 MHz receiver and phase-lock system was the responsibility of M.P. Lynn and S.H. Krenek, and is described briefly in I below, both for completeness, and to explain the interfacing of the 4.57 MHz system to it. The 4.57 MHz converter and phase-lock system was the responsibility of this author and is described in II below.

I. THE 2.40 MHz RECEIVER SYSTEM

The general approach to coherent detection adopted here is to have a master phase-reference oscillator at 9.60 MHz from which both the transmitter and the receivers derive reference 2.40 MHz waveforms. This contrasts with the approach of some other experimenters who rely on very stable oscillators at spread locations to have negligible phase drift.

The phase reference oscillator is a 9.60 MHz TTL oscillator. D-type flip flops in SN7474 packages divide this

frequency by four to obtain 2.40 MHz. The division is arranged to give two 2.40 MHz outputs, one (the SINE output) of which is 90° in time behind the other (the COSINE output).

The block diagram of the M.P. Lynn system given here in Figure B-1 shows that selection of COSINE or SINE outputs is done by feeding the separate outputs to separate AND gates. The other input of one AND gate is connected to the Q-output of a D-type flip-flop: the other input of the other AND gate to the $\bar{Q}$ output. The AND gate outputs are tied together and lead to the receivers. Selection of COSINE or SINE is now done by setting the D-input level on the D-type flip-flop and clocking this level to the Q-output. This is done by the station control register of the controlling PDP-8 computer, which is described later.

The local oscillator output is fed in as the modulator input to an LM1496 balanced-modulator package. 2.40 MHz signals received by the aerials are amplified in an R.F. amplifier stage and passed to the modulator carrier input. The 4.80 MHz sideband resulting from the mixing is filtered out, leaving the constant voltage output proportional to A cos ϕ or A sin ϕ, depending on the selection of COSINE or SINE input from the local oscillator. Here, A is the amplitude of the returned echo, and ϕ the phase of the carrier with respect to the 2.40 MHz reference.

After amplification of the detector output by a video amplifier stage, the receiver output voltage is sent to a sample-and-hold system. This was also designed and built by M.P. Lynn. Three identical receivers were built, with the 2.40 MHz COSINE or SINE sent to each. Thus voltage $A_1 \cos \phi_1$ $A_2 \cos \phi_2$, $A_3 \cos \phi_3$ (or $A_1 \sin \phi_1$, $A_1 \sin \phi_2$, $A_1 \sin \phi_3$ if

SINE was selected) were presented to the three sample-and-hold circuits.

The rate of sampling and analogue to digital conversion was controlled by a PDP-8 computer. Details specific to the experiments are described later. For the three receivers, sampling of the echo is started at a chosen delay after a transmitter trigger command. The sampling was done for a chosen number of heights, and the height gating (hence that for the sample-and-hold circuits and A-D converter circuits) was normally 2.5 km.

The transmitter carrier is phase-locked to the receiver local oscillator by use of the 4.8 MHz from which the 2.40 MHz COSINE is derived. This 4.8 MHz waveform is sent through a line-driver to the transmitter. A line-receiver designed and built by S.H. Krenek divided the 4.8 MHz by two to give 2.40 MHz. This was then fed to the 2.40 MHz transmitter to serve as a carrier.

To obtain signal amplitude and phase for the three spaced aerials two transmitter pulses are sent, 10 milliseconds apart. Between pulses the COSINE local oscillator output is replaced by the SINE oscillator output. The six voltage levels

$$A_1 \cos \phi_1 \quad A_2 \cos \phi_2 \quad A_3 \cos \phi_3$$
$$A_1 \sin \phi_1 \quad A_1 \sin \phi_2 \quad A_3 \sin \phi_3$$

give the required A_1, A_2, A_3 and ϕ_1, ϕ_2 and ϕ_3. The 10 millisecond spacing was found short enough for the amplitudes and phases to remain sensibly constant, yet avoid multiple-echo problems. In practice, only intense sporadic-E or night-time F-region would on occasions cause sampling of a high-multiple COSINE with a SINE SIGNAL.

The COSINE-SINE pulse pair was normally triggered, and echoes sampled, every 256 msec.

II THE 4.57 MHz CONVERTER SYSTEM

A similar method of approach to coherent detection was adopted for 4.57 MHz transmission and reception. A master oscillator at 11.54 MHz allowed the derivation of a 4.57 MHz signal to drive the 4.57 MHz transmitter. A 6.97 MHz signal was also derived, to mix with the 4.57 MHz received signal to give 2.40 MHz input to the Lynn receivers. This work was done by the present author, and details are given below.

(a) The phase-locking system. Measurement of amplitude and phase on 4.57 MHz requires the 2.40 MHz arising from the mixing to be phase-locked to the 2.40 MHz reference in some way.

This was done by a method kindly suggested by H.A. von Biel of this department. The method outlined (Fig. B-3) shows that a free-running 11.54 MHz crystal-controlled TTL oscillator is mixed with a 2.40 MHz reference in a LM1496 balanced modulator. The two modulator outputs are separately filtered to give the two sidebands: these are 9.14 MHz (= 2 x 4.57 MHz) and 13.94 MHz (= 2 x 6.97 MHz).

The 9.14 MHz is sent through a line-driver to the transmitter, where a line-receiver restores it to TTL levels and divides it by two. The 4.57 MHz is sent as carrier drive to the 4.57 MHz transmitter. The 13.94 MHz is halved and fed to the converters as 6.97 MHz.

As described elsewhere in this appendix, the 6.97 MHz and 4.57 MHz from the antennas is mixed to give 2.40 MHz. Any drift of the 11.54 MHz crystal does not matter, since with

f_1 = 11.54 MHz and f_2 = 2.40 MHz, then

f_1 mixed with f_2 gives $f_3 = f_1 + f_2$ (13.94 MHz)

and $F_4 = f_1 - f_2$ (9.14 MHz)

If f_1 changes at a rate $\frac{df_1}{dt}$, then

$$\frac{d\left(\frac{f_3}{2}\right)}{dt} = \tfrac{1}{2}\left(\frac{df_1}{dt}\right)$$

and

$$\frac{d\left(\frac{f_4}{2}\right)}{dt} = \tfrac{1}{2}\left(\frac{df_1}{dt}\right)$$

Then $\frac{f_3}{2}$ mixed with $\frac{f_4}{2}$ gives $f_5 = \frac{f_3}{2} + \frac{f_4}{2}$ (11.54 MHz)

and $f_6 = \frac{f_3}{2} - \frac{f_4}{2}$ (2.40 MHz)

and $\frac{df_6}{dt} = \frac{d}{dt}\left(\frac{f_3}{2} - \frac{f_4}{2}\right) = 0$

Both oscillators are in fact TTL square-wave switching waveforms. Their spectra have frequency-components at f_1, $3f_1$, $5f_1$,... and f_2, $3f_2$, $5f_2$,... and the modulation output will have all the sum and difference frequencies $nf_1 \pm mf_2$. However, the amplitude ratio of successive spectral components is as 1, $\frac{1}{3}$, $\frac{1}{5}$, ... and also f_3 and f_4 are separated from the other frequency components in the outputs by filters consistine of capacitively-couples parallel-tuned circuits. f_3 and f_4 can be considered alone.

The direction of phase-change in the 4.57 MHz carrier is reversed with respect to that of the 2.40 MHz carrier because of the converter modulation.

Figures B-4 and B-8 show detailed circuits.

(b) The converters. The aerial input signal is fed to a filter, to reject the image frequency of 9.37 MHz. The filter consisted of two parallel-resonant circuits capacitively-coupled. The individual bandwidth of each circuit was set to 0.3 MHz centered at 4.57 MHz. This gave the quality factor Q of the circuit, which with the coil inductance gave the parallel impedance. The input-link turns ratio was then set to present a nominal 75 ohms to the aerial.

The filtered 4.57 MHz carrier and the 6.97 MHz derived from the phase-lock mixer were mixed in an LM1496 balanced modulator. The 2.40 MHz sideband was obtained by filtering the output through a single parallel-resonant circuit. A link of nominal impedance 75 ohms fed this output to the Lynn receivers.

The cicuit board from this stage was designed by R. Borrell and I.M. Foster of this department as a general-purpose modulator board.

Overall 3-dB converter bandwidth, measured across a 75-ohm resistor at the output, was 100 KHz. At 4.57 MHz the output voltage to input voltage ratio was about 2. The image:signal output ratio at equal input levels was 1:100.

The circuit is shown in Fig. B-12.

(c) The relay system. The input to, and output from, the frequency converters was passed through Hamlin reed switches. These could be switched either manually or on computer command. These were used to allow reception of alternate pulses on 2.40 MHz and 4.57 MHz for sporadic-E experiments. The 20 dB 75 ohm resistive T-pad attenuator is inserted in the 2.40 MHz line so that the returned echo amplifiers for the two frequencies were of the same order of magnitude.

Figure B-10 shows the block diagram and Figure B-11 the circuit.

III. THE TRANSMITTERS

Parts I and II have described in outline how the carrier drives for both 2.40 MHz and 4.57 MHz are locked to the phase reference. Figure B-9 shows the circuit for the 4.57 MHz case. A 2N3643 transistor drives the 9.14 MHz carrier to the transmitter, and an SN72710 comparator restore signal levels to TTL level before division by two to 4.57 MHz.

The 2.40 MHz line-driving and receiving system was built by S.H. Krenek and the 2.40 MHz exciter by M.P. Lynn. The 4.57 MHz line-driving and receiving system was built by this author. The carrier waveforms were fed down separate coaxial lines, but the transmitter trigger line is common to both: thus both transmitters are pulsed together.

(1) Transmitter Characteristics

(a) 2.40 MHz

Peak power: 40 kW at final amplifier (Class C) anodes with PRF of 50 sec^{-1}.

Pulsewidth: 30 μsec - occasionally 50 μsec for sporadic-E experiments.

The transmitter feeds a broadband broadside array of four in-phase 3-wire antennas designed and built by S.H. Krenek. The dipole pairs run East-West.

(b) 4.57 MHz

Peak power: 17 kW at final amplifier (Class C) anodes with PRF of 50 sec^{-1}

Pulsewidth: 55 μsec.

The transmitter feeds a crossed four-wire array as described in Appendix A.

Mr J. de Voil of this department serviced and maintained both transmitters.

IV. EXPERIMENTAL PROCEDURE

(1) The Hardware

Hardware and timing is controlled by a Digital PDP-8e computer installed at Birdling's Flat field station. Control software is written in an assembler language, PAL-8, which is one of the assembler languages provided by Digital Equipment Corporation.

Experiment switching is implemented through a station control register. In the software a given number is sent to this register by first loading the number into the hardware accumulator. An IOT (accumulator input-output transfer command) sends the number to the register, the number value being decoded into a data part and bin address part. The data lines, which are sent to all bins, are individually set to TTL high or low levels. The clock pulse, sent only to the individual bin addressed, allows clocking of any flip flop present in that bin whose input is connected to a data line. In this way, COSINE or SINE receiver modes, 2.40 or 4.57 MHz reception, transmitter triggering, or various other functions, are controlled.

Analogue-to-digital conversion is accomplished by direct memory access. Registers for the number of words to be transferred, the starting core address of transfer, and the gating of sampling and analogue-to-digital conversion are set up. When the A-D converter is started, data held by the three sample-and-hold circuits (described in part I) is transferred

to consecutive locations in core memory. The sample-and-holds track for another gating period, when the analogue voltages are again held, converted to digital form and transferred to memory. This is continued until the word count is finished, upon which a flag comes up. The converted data is now all in core memory.

The A-D converter range is 0-10 volts in 1024 steps. Each step is 9.766 mV. The receiver no-signal levels are set to 5 volts to allow video output voltages above and below the mean to be measured. This offset must be subtracted in initial data processing.

Writing to standard magnetic tape is done in a similar way. Word count and current address registers have obvious functions. A magnetic tape command register and a magnetic tape status register allow software control and monitoring of magnetic tape functions. Data is written to a 7-track tape at density 800 B.P.I. on a Kennedy transport.

Timing is controlled by the machine cycle time of 1.2 microseconds, by a millisecond clock set and tested by the software, or by 2.5, 5.0 and 10.0 km markers derived from a computer clock.

Mr A.W. Black of this department serviced and maintained the computer and designed the interface.

(2) The Software

Assembler (Pal-8) programs to control the IOT's, timing, magnetic tape and equipment switching were written by this author. An amplitude-drifts data-collection program written by Dr. G.J. Fraser was the source of many concepts, techniques, and library routines, and its use is gratefully acknowledged. Mr. M.J. Smith kindly assisted in some of the writing and

testing of earlier versions of these computer programs.

(3) The Experiments Run

The main experiment run was: Total reflection phase-height/drifts on F-region at one frequency.

(a) The F-region experiment. This experiment is able to be run on either 2.40 MHz or 4.57 MHz. The flowchart is shown in Figure B-2. The program is derived from one which G.J. Fraser wrote for the drifts experiment.

The experiment is started by recording the height (or delay time) of the transmitter ground pulse with respect to the station control register transmitter trigger command. This command is actually sent to the transmitter at the first 10 km marker occurring after the control register command. The transmitter trigger pulse is then synchronized to the height markers. The delay through the transmitter is then subtacted from all subsequent echo heights.

The echo is then found on the A-scope. Seven heights are sampled, and their delay with respect to the transmitter trigger command is adjustable using the computer's switch register. The sampling is placed across the echo - with a 55 μsec pulse and group retardation the echo has a substantial amplitude over four or five of the middle heights.

Data is actually recorded in core only for height #4 of the seven heights taken. This was done to avoid redundant data for total reflection. Preliminary runs using the whole heights sequence indicated that the amplitude and phase of the echo for a given receiver, for the heights at which there was a substantial amplitude, behaved in a very similar way.

Correlation of data between those heights confirmed this. The wide 55 μsec pulse gives a satisfactory average echo.

After adjustment of the sampling height the experiment itself is started. A transmitter pulse is sent and A cos ϕ stored in a buffer for the seven heights and three receivers. Height #4 for the three receivers was kept for the magnetic tape data buffer. After eight milliseconds the A-D's measure the receiver output no-signal levels: these are added to COSINE sum and squared sum buffers for each receiver separately. This allows the mean and standard deviation of the no-signal level to be monitored. The receiver local oscillator is set to SINE output; then after two milliseconds the transmitter is again triggered and A sin ϕ for seven heights and three receivers obtained. Again only height #4 data is retained. Finally after eight milliseconds the receiver output no-signal levels for SINE are measured and added to SINE sum and squared sum buffers which are separate for each receiver.

This sequence is repeated at an interval of 256 msec between the COSINE scans of each group.

Every thirty seconds, heights #2 to #6 for receiver #1 had the echo amplitudes squared and added to a buffer with one double-precision word for each height. This was done for three groups of pulses, giving A^2 as a function of height across the echo. The maximum of this was then found: if the address of the maximum was not at height #4, the delay of the gate with respect to the transmitter trigger command was adjusted after the following pulse group. The amount of adjustment was recorded for later use.

This tracking procedure worked well for a total reflection which changed smoothly in height. Its effects did not seem to appear in the data, except occasionally as a phase jump in the phase-height data. The wide pulse seemed to average well. Tracking was not so successful for some daytime F-region echoes, which would become very weak, then disappear, and a few minutes later reappear at a group-height outside the test gate. In such cases, the computer switch register had to be used to readjust the gate delay, which again was recorded. Data was lost in these cases.

The software tracking routine always tracked the largest amplitude. When O- and X-modes crossed the larger-amplitude echo was followed. Ionograms for that day and time were subsequently referred to to see which mode it was.

When the buffer of height #4 receiver #1, #2, and #3 data for A cos ϕ and A sin ϕ was filled, it was written out to magnetic tape in a time less than that between pulse groups.

A Burroughs B6700 computer at the University of Canterbury read the magnetic tape block by block. After subtraction of the receiver no-signal levels the data was written out to three files:

(1) In A cos ϕ and A sin ϕ form

(2) In A, ϕ form

(3) Group-height adjustments by tracking and switch-register changes.

For files of type (1) and (2) there were three records per magnetic tape block. Each record corresponded to a given receiver at height #4, and had as many (A cos ϕ, A sin ϕ) or (A,ϕ) pairs as there were echo scans in that magnetic tape block.

V. CONCLUSIONS

In this appendix the hardware, operational, and programming aspects of the experiments have been described. Interpretation of the data and its relation to a theoretical model will be found in the main chapters.

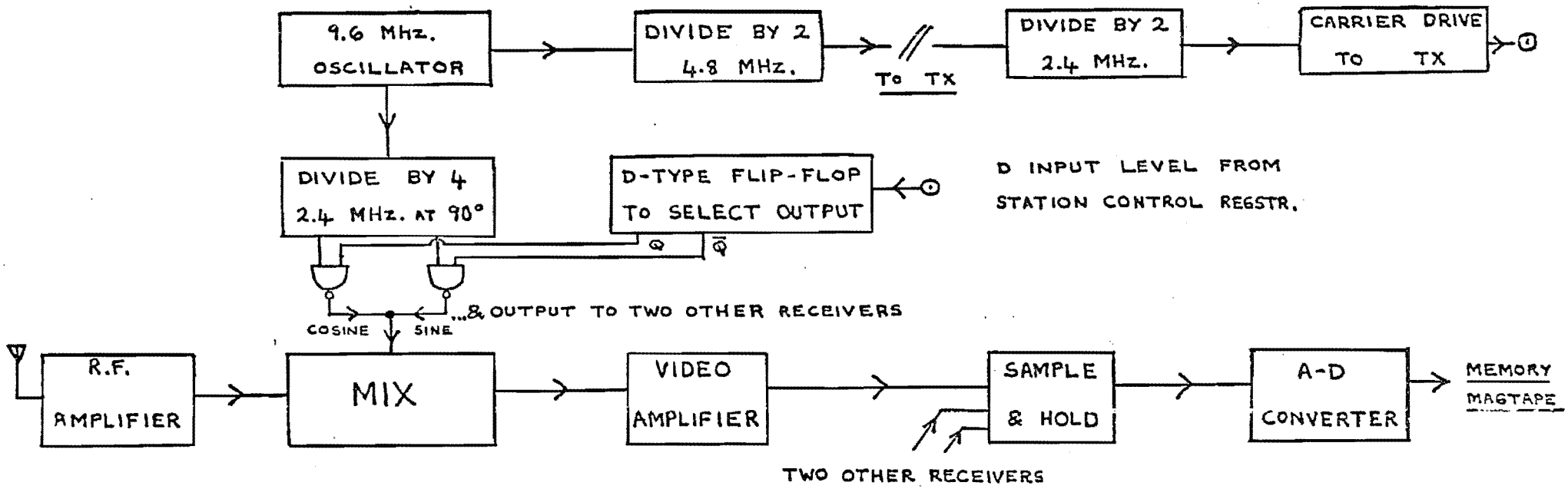

FIG. B-1:

M.P. LYNN PHASE-LOCK & RECEIVER SYSTEM:

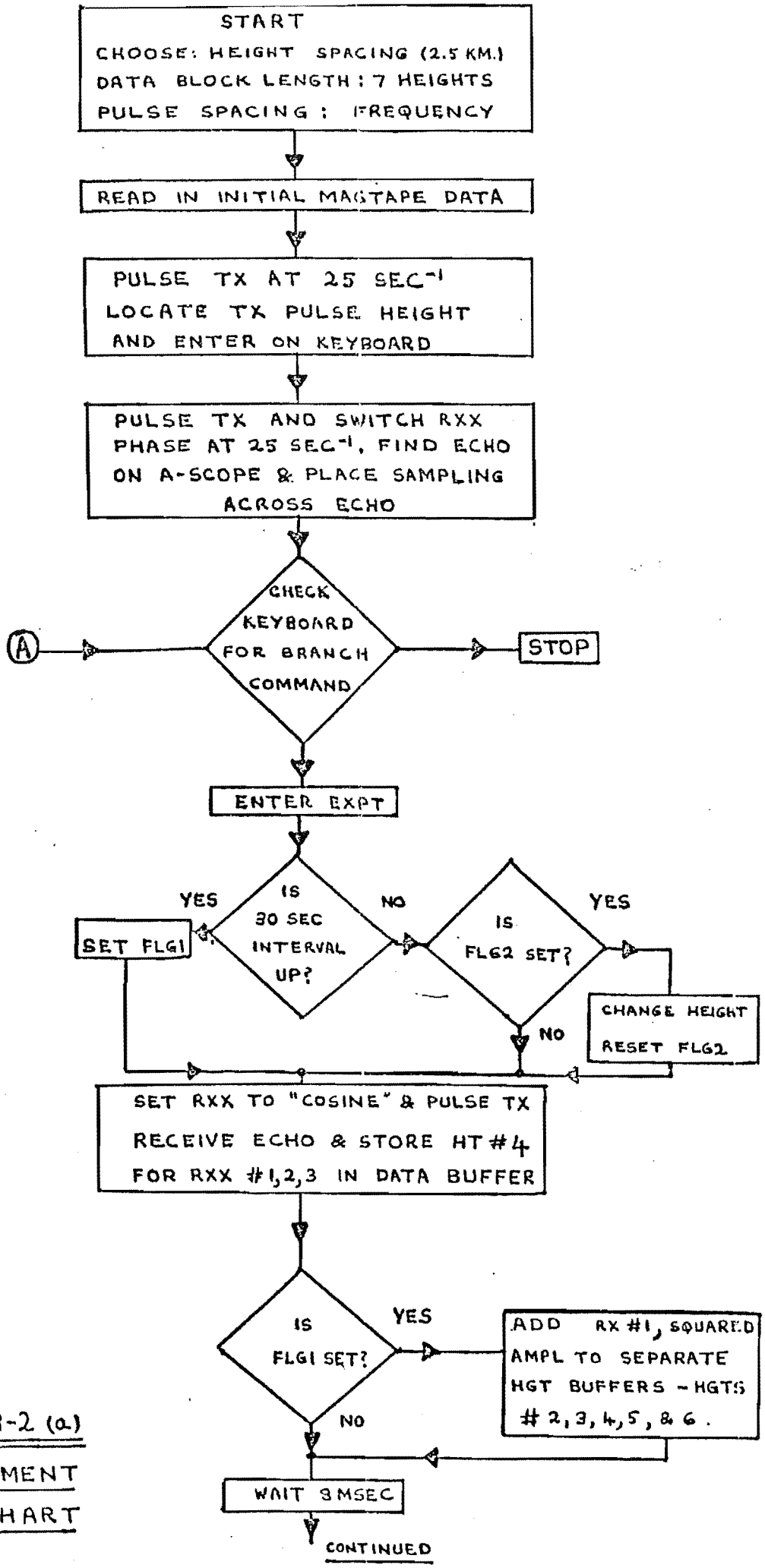

FIG. B-2 (a)

EXPERIMENT FLOWCHART

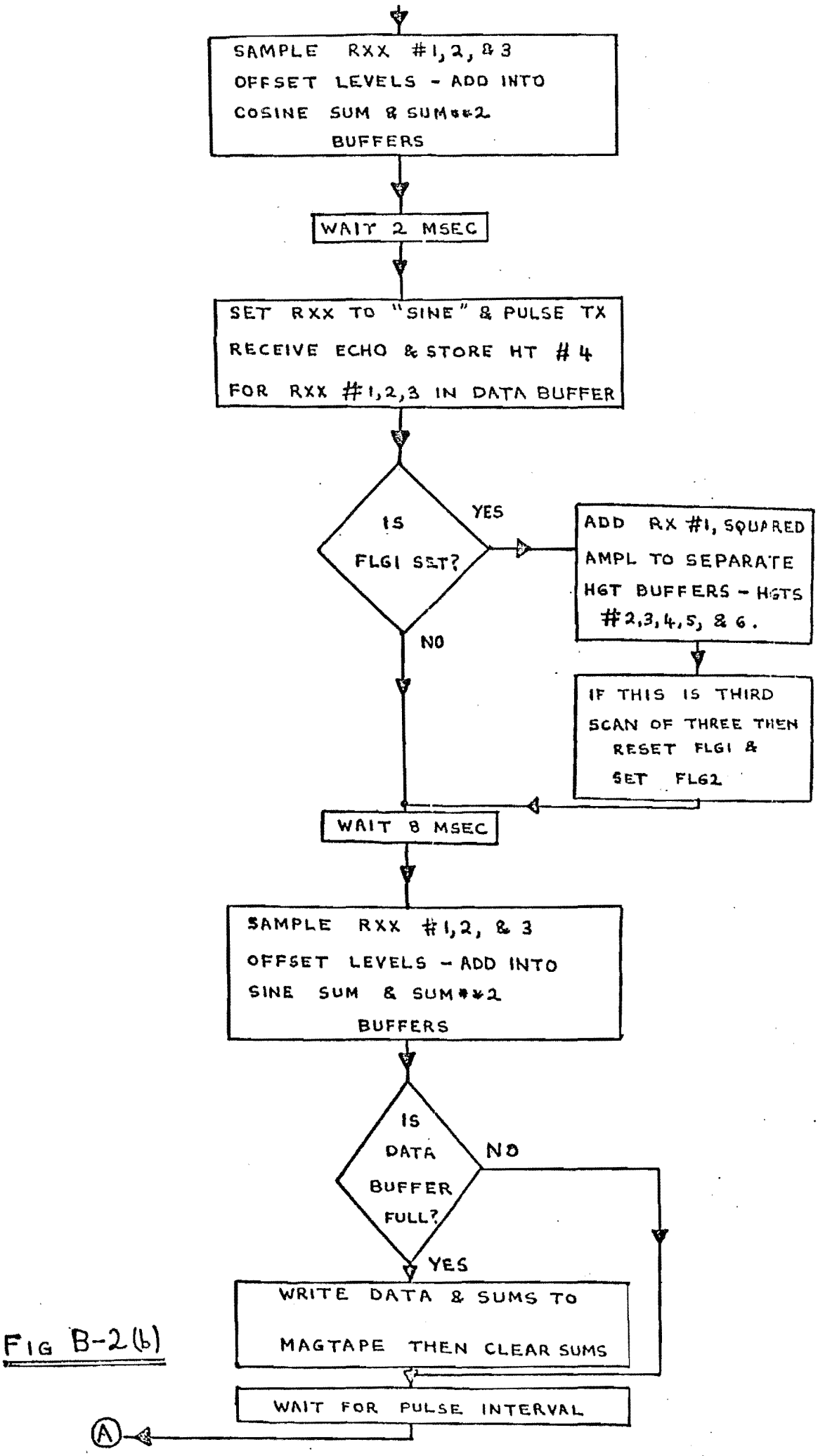
SAMPLE RXX #1,2,&3 OFFSET LEVELS - ADD INTO COSINE SUM & SUM**2 BUFFERS
WAIT 2 MSEC
SET RXX TO "SINE" & PULSE TX RECEIVE ECHO & STORE HT #4 FOR RXX #1,2,3 IN DATA BUFFER
IS FLG1 SET?
YES
NO
ADD RX #1, SQUARED AMPL TO SEPARATE HGT BUFFERS - HGTS #2,3,4,5, & 6.
IF THIS IS THIRD SCAN OF THREE THEN RESET FLG1 & SET FLG2
WAIT 8 MSEC
SAMPLE RXX #1,2, & 3 OFFSET LEVELS - ADD INTO SINE SUM & SUM**2 BUFFERS
IS DATA BUFFER FULL?
NO
YES
WRITE DATA & SUMS TO MAGTAPE THEN CLEAR SUMS
WAIT FOR PULSE INTERVAL
A

FIG B-2(b)

4.57 MHz. to 2.40 MHz Phase-Lock and Conversion System:

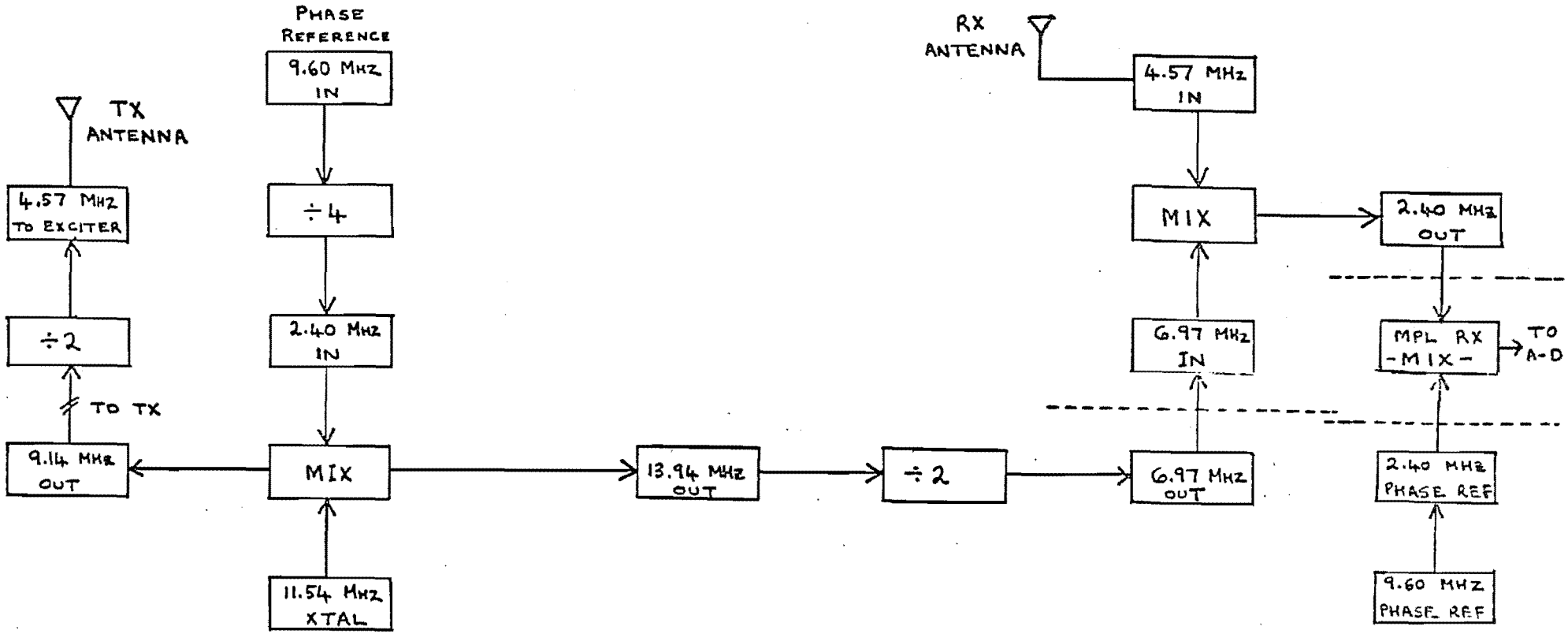

Fig. B-3

4.57 MHz. PHASE-LOCK MIXER:

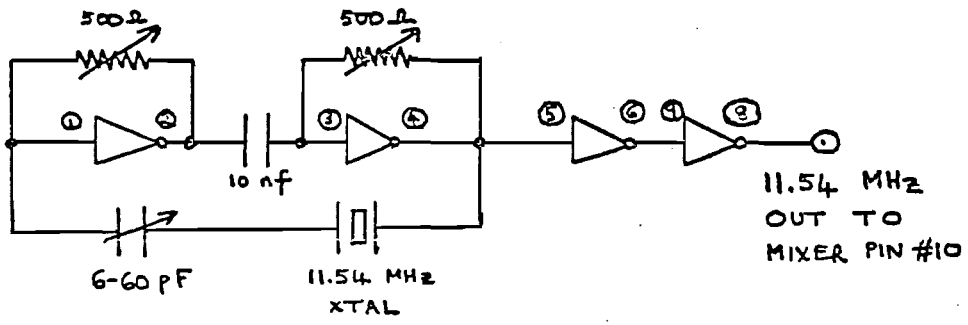

I.C. PACKAGE: SN 7404

B-4: LOGIC OSCILLATOR:

[CIRCUIT DUE TO H.A. VON BIEL]

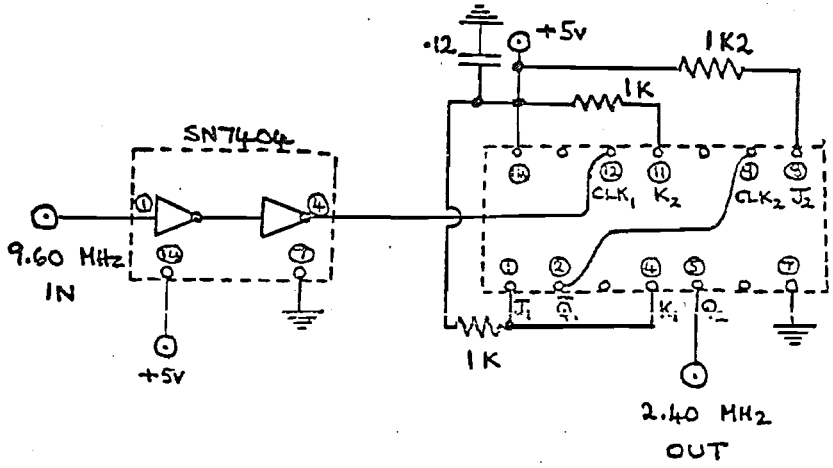

SN 74107

B-5: DIVIDE-BY-FOUR CIRCUIT:

4.57 MHz. PHASE-LOCK MIXER:

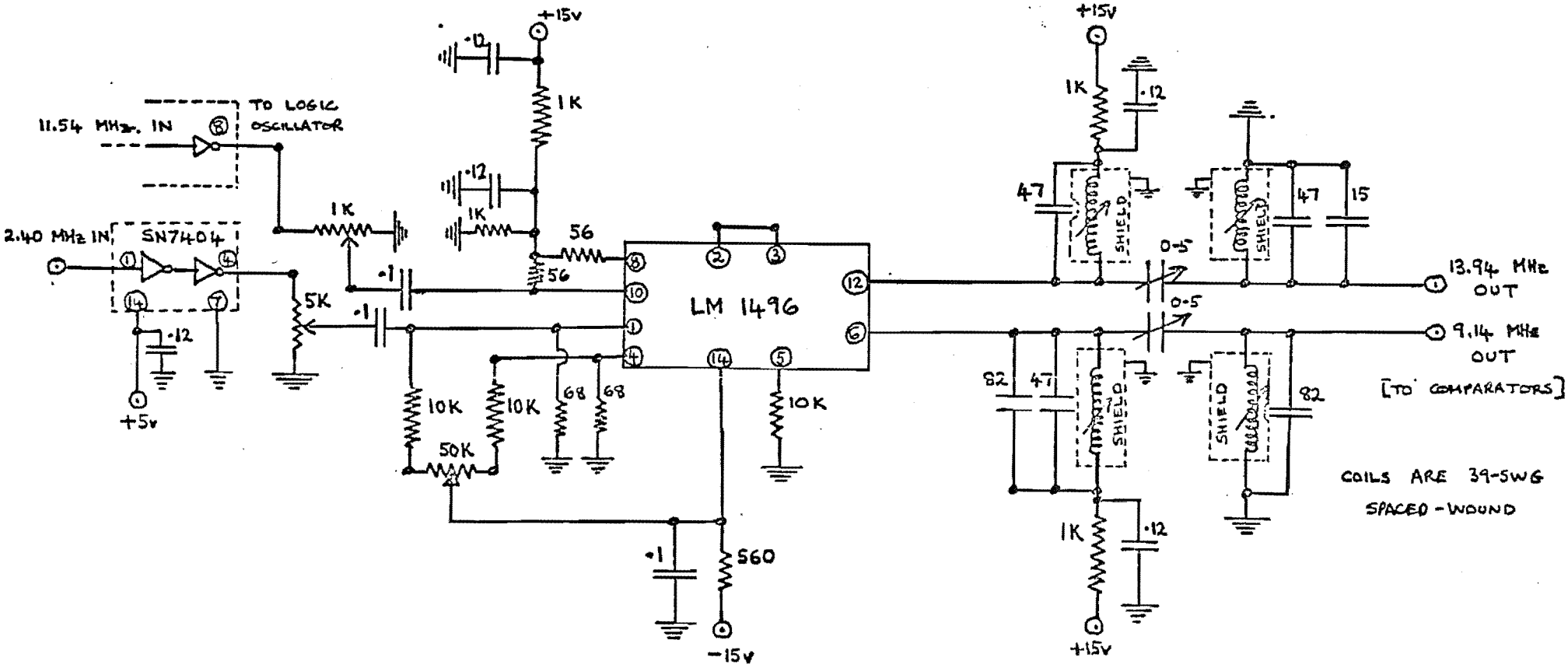

B-G: MIXER CIRCUIT:

[LM1496 BIASING CIRCUIT DUE TO I.M. FOSTER]

4.57 MHz. PHASE-LOCK MIXER:

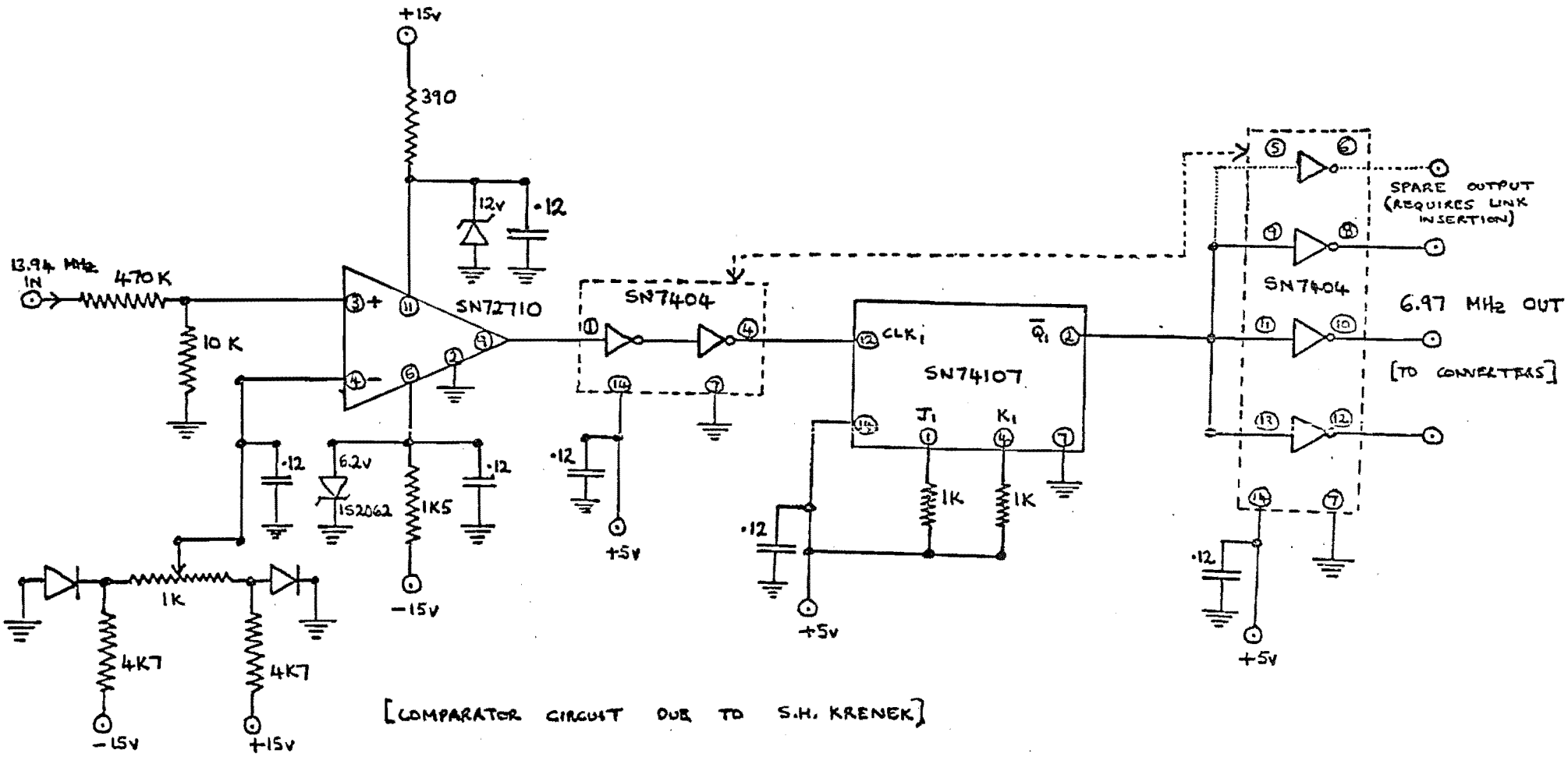

B-7: COMPARATOR, DIVIDER, AND BUFFERING CIRCUIT, FOR 6.97 MHz OUTPUT:

4.57 MHz. PHASE-LOCK MIXER:

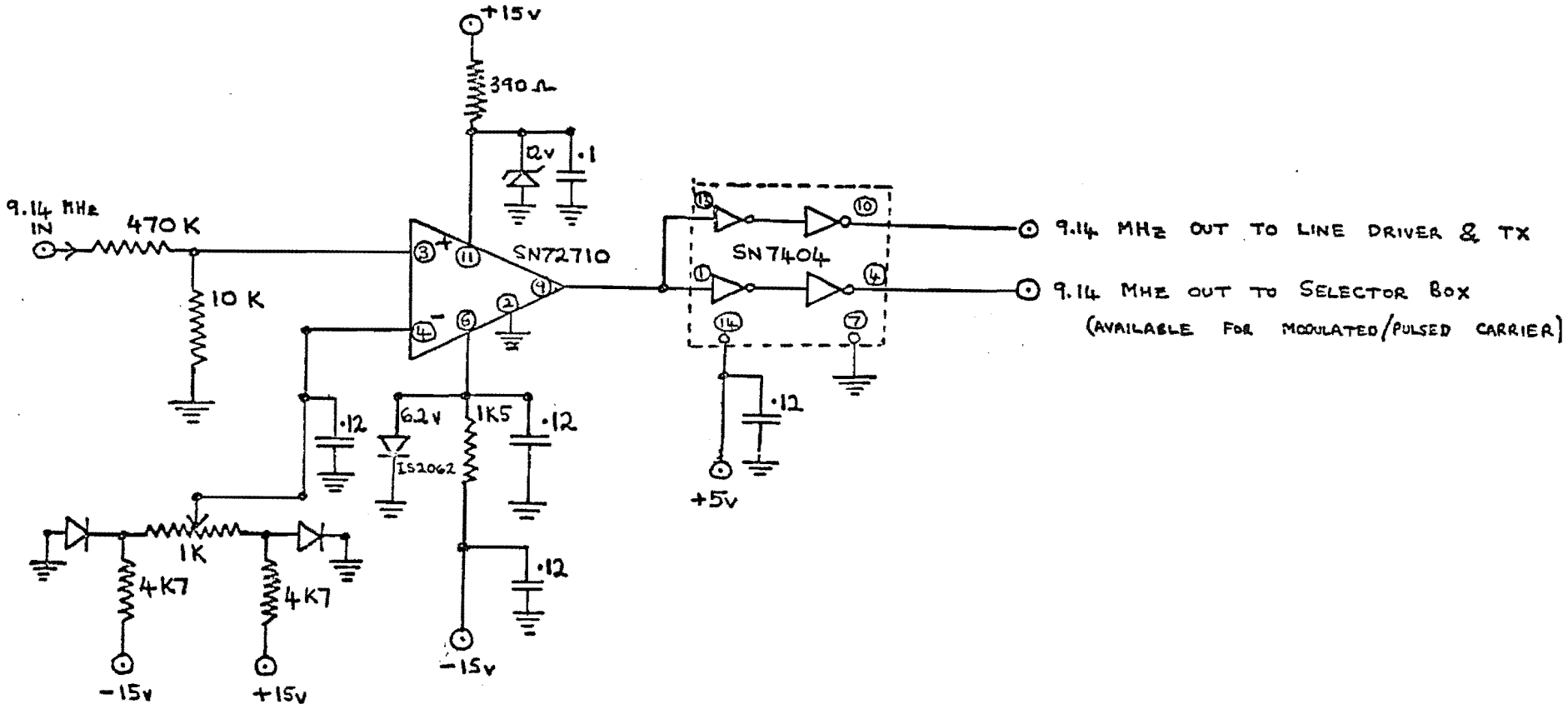

B-8: COMPARATOR AND BUFFERING CIRCUIT FOR 9.14 MHz. OUTPUT:

[COMPARATOR CIRCUIT DUE TO S.H. KRENEK]

4.57 MHz. Line driver & receiver:

Fig. B-9:

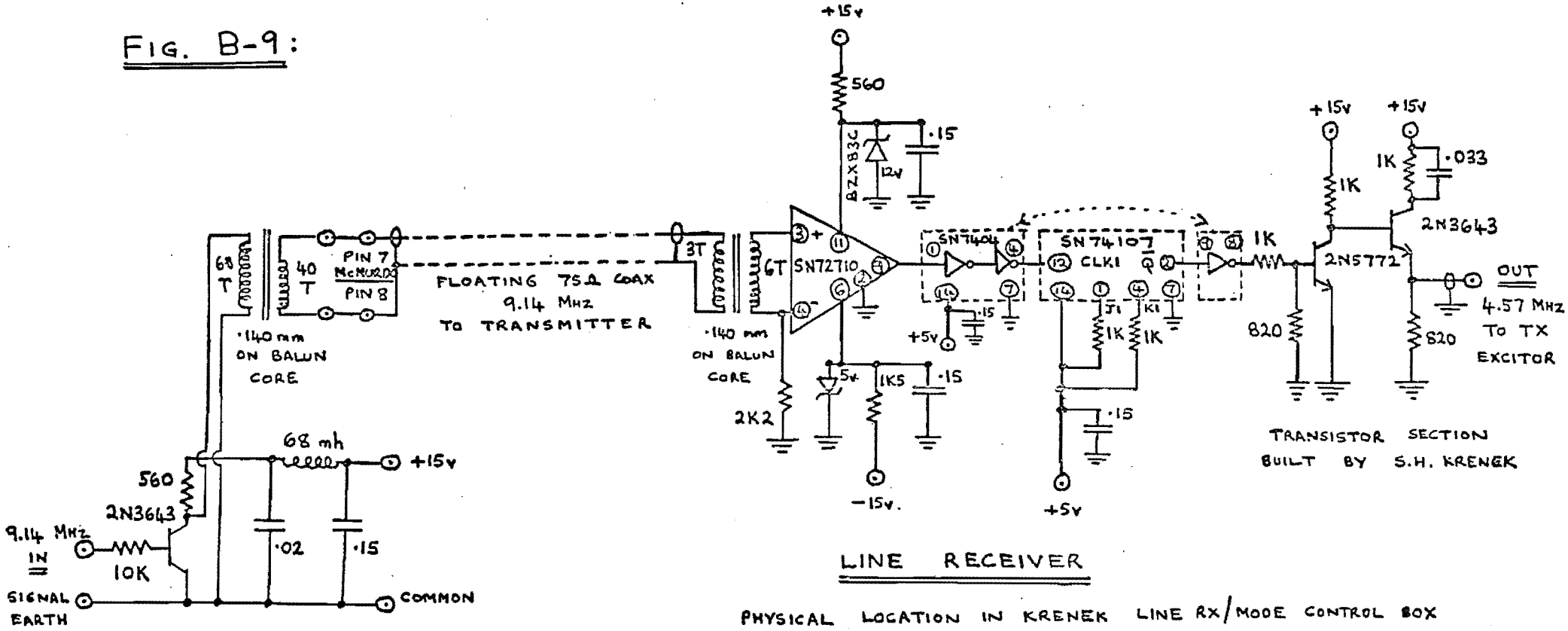

Line Driver

Bias circuit due to S.H. Krenek

Physical location in Cooper phase-lock mixer box

Line Receiver

Physical location in Krenek line RX/mode control box

Power supply colour codes:

	Krenek	Cooper
+5v	orange	orange
+15v	red	red
−15v	blue	black
Earth	black	green

SWITCHING RELAY BLOCK DIAGRAM:

FIG. B-10:

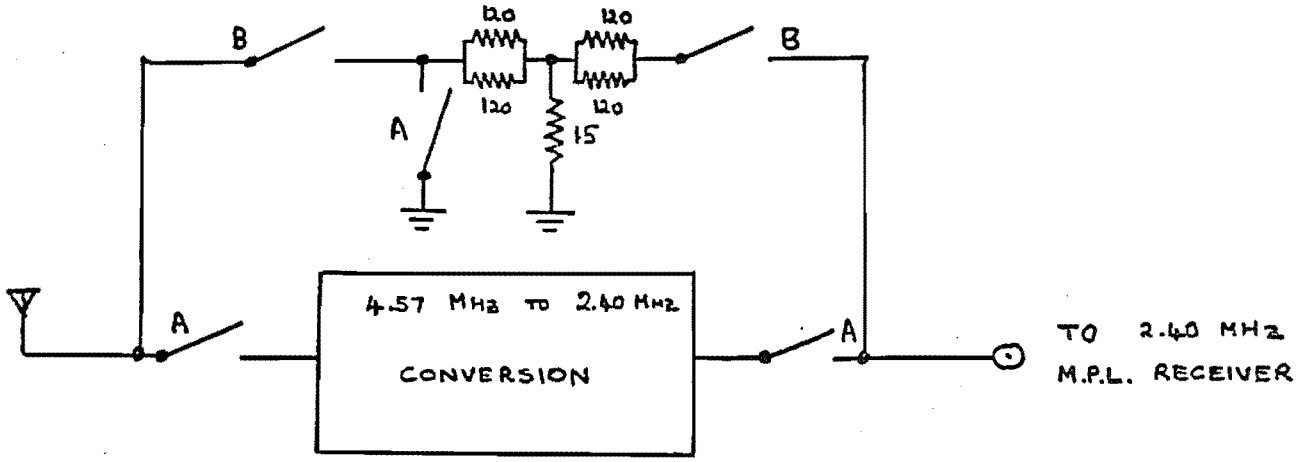

THE ATTENUATOR IS 20 dB AT 75 OHMS.

RELAYS A CLOSED AND RELAYS B OPEN FOR FREQUENCY CONVERSION

RELAYS B CLOSED AND RELAYS A OPEN FOR NO CONVERSION BUT 20 dB ATTENUATION

SWITCHING RELAY CONTROL:

FIG. B-11:

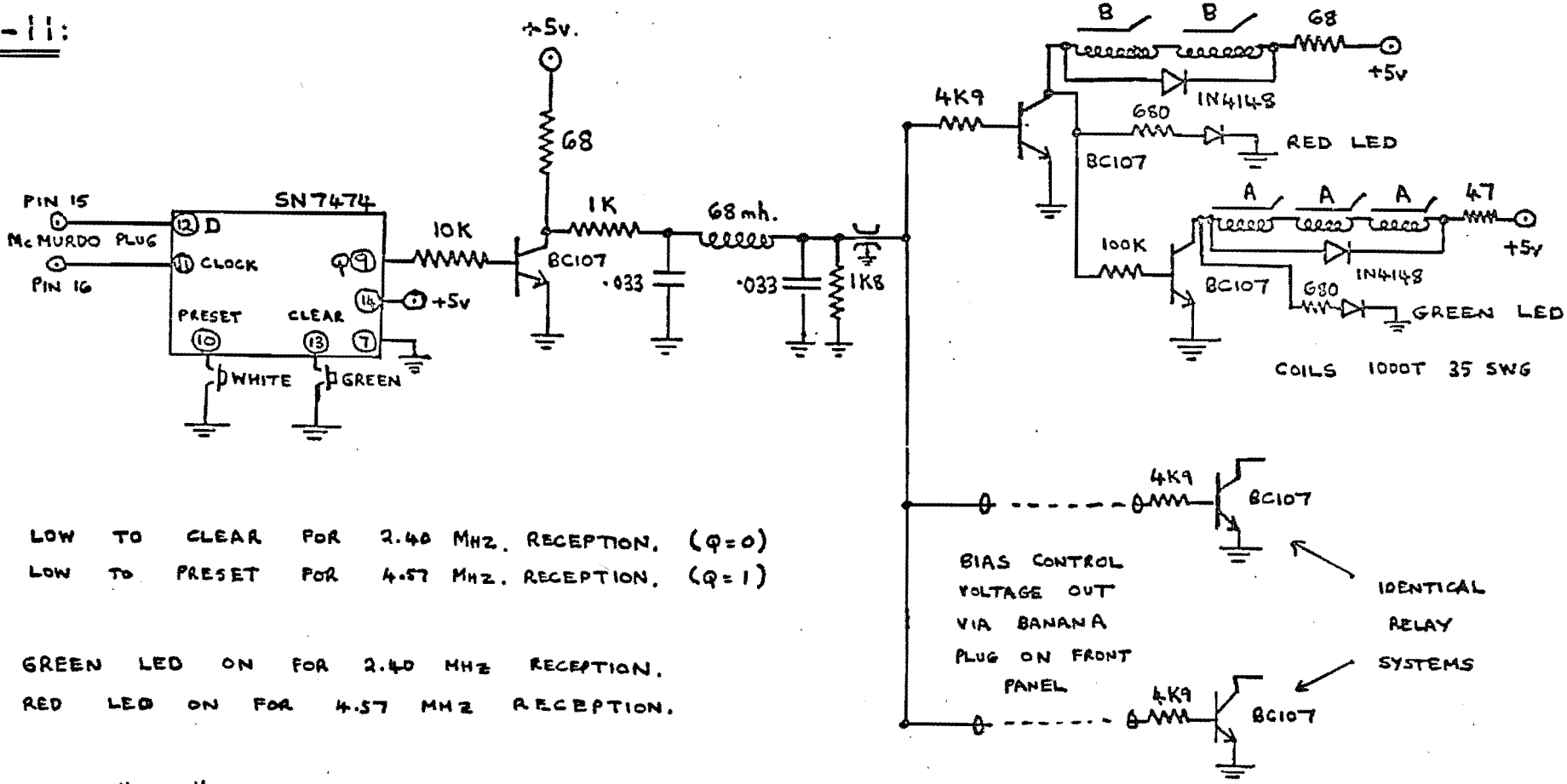

LOW TO CLEAR FOR 2.40 MHz. RECEPTION. (Q=0)
LOW TO PRESET FOR 4.57 MHz. RECEPTION. (Q=1)

GREEN LED ON FOR 2.40 MHz RECEPTION.
RED LED ON FOR 4.57 MHz RECEPTION.

BITS #6 – #11 OF STATION CONTROL REGISTER ARE DATA LINES. DATA VALUE =1 SETS PIN 15 AT LOW FOR 2.40 MHz. RECEPTION.

+5v. SUPPLY RUNS RELAYS ONLY.
ENTRY ON McMURDO PIN 8 – PIN 8 IS JOINED TO PIN 7 TO PASS SUPPLY TO NEXT BIN.

4.57 MHz. to 2.40 MHz. Frequency Converter:

Fig. B-12:

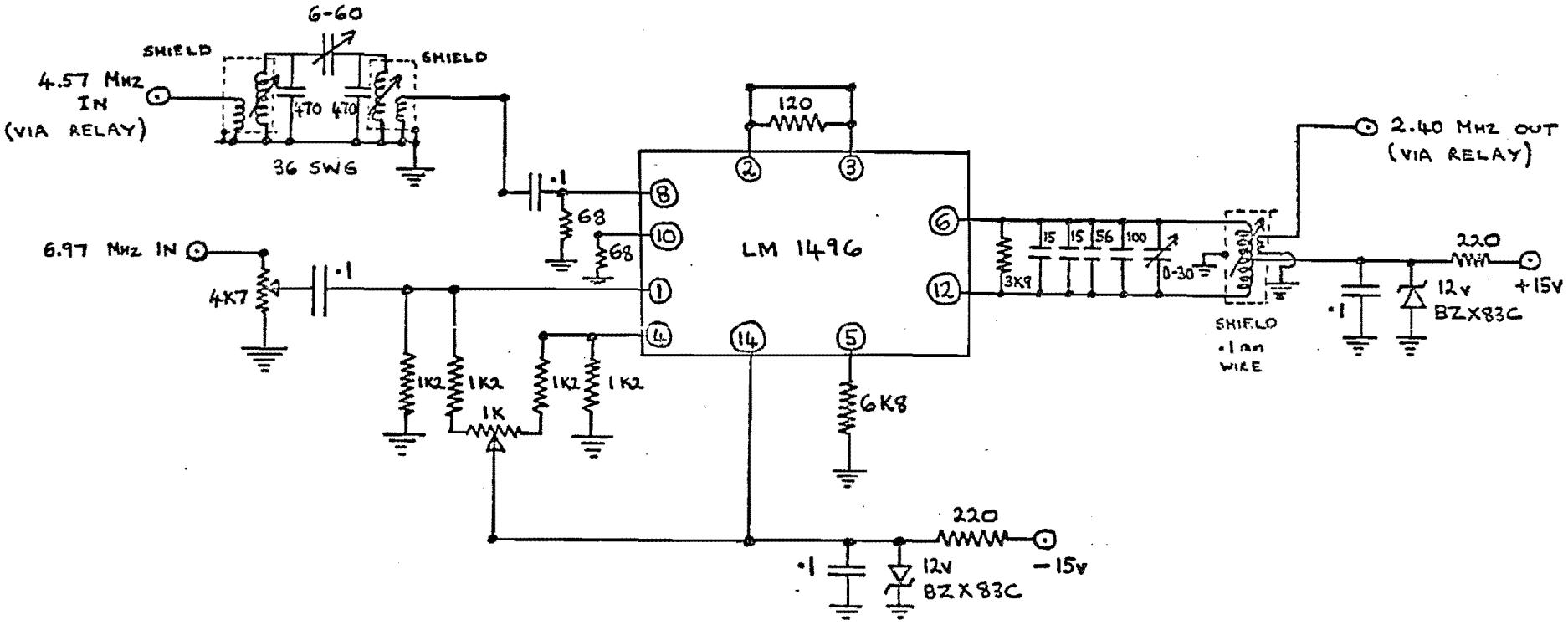

APPENDIX C

THE DETERMINATION OF POWER SPECTRA

1. INTRODUCTION

Power spectrum analysis is used extensively in Chapter 5 to obtain the periodicities in the phase-path variations. As noted there, the Maximum Entropy method is the principal method for obtaining power spectra, with Discrete Fourier Transform spectra being used as a checkback method.

In this appendix some details of the process of analysis are given. A measure is given of spectrum reliability, and comparisons of the results arising from different processing methods are made. The latter is particularly important in the case of overlapping spectra, when the significance of small period changes needs to be assessed.

An outline of the Maximum Entropy processing is given first, followed by a discussion and comparison with Discrete Fourier Transform spectra. This allows a decision to be made about useful spectra for use in data interpretation.

II. THE MAXIMUM ENTROPY METHOD

(1) General discussion of the method

The Maximum Entropy method (abbreviated as MEM here) is the newest Power Spectrum analysis method yet available. The method was originally proposed by Burg (1968, quoted by Ulrych and Bishop, 1975). Power spectra given by the method are characterized by a high resolution of spectral peaks, compared with those given by other methods under like

conditions. This has been noted by several authors, among them Radoski et al. (1976) who compared the MEM spectra of geomagnetic micropulsation data with those obtained by the older Blackman-Tukey (Blackman and Tukey, 1958) and Discrete Fourier Transform (Cooley and Tukey, 1965) methods.

The theory and methods of the MEM are given by many authors; a comprehensive review is given by Ulrych and Bishop (1975).

The MEM is theoretically based on the problem of finding spectra for random processes. It provides a spectrum estimate based on the input information, but which has minimum assumptions about unavailable data. The concept of the entropy of a time-series process is introduced; as in thermodynamics it is a measure of disorder in a system, or ignorance about a system (Ulrych and Bishop, 1975).

For a stationary Gaussian process there exists a relationship between the entropy H of the process and the power spectrum density S(f) of the process:

$$H \propto \int_{-f_{Nyq}}^{f_{Nyq}} \log S(f)\,df$$

which is Equation (1) of Ulrych and Bishop (1975) with f_{Nyq} the Nyquist frequency. The Maximum Entropy Spectral estimate for the process is that S(f) which maximizes H for the process: with the constraints that S(f) must be consistent with the known autocorrelations of the process. Details of procedures are found in, for example, Andersen (1974).

An important method of describing many statistical

processes is the autoregressive model of order m (for example, Jenkins and Watts, 1968). If X_t is the t-th term in such a process with μ the mean of the process, successive terms X_t are generated by

$$(X_t-\mu) = \alpha_1(X_{t-1}-\mu) + \alpha_2(X_{t-2}-\mu) + \cdots + \alpha_m(X_{t-m}-\mu)+Z_t$$

where Z_t is purely random. Such processes can be used to describe physical systems: an example cited by Jenkins and Watts (1968) is that of a second-order process with zero Z_t which describes a damped simple pendulum. Now work quoted by Ulrych and Bishop (1975) indicates that the determination of the MEM spectrum for an input process is equivalent to the fitting of an m'th order autoregressive process to the input process. The resulting spectrum thus depends on the order of autoregressive process fitted.

Associated with the fitting of an m'th order process are the m autoregressive coefficients $\alpha_1, \alpha_2, \ldots, \alpha_m$: they are required in the calculation of the spectrum at each frequency. The set $1, -\alpha_1, -\alpha_2, \ldots, -\alpha_m$ is an (m+1)- point prediction-error filter associated with the fitting of the m'th order autoregressive process: thus the choice of its length is equivalent to the specification of the order of the autoregressive process to be fitted.

The choice of autoregressive order is important in accurate determination of the spectrum. Experiments and comparisons are made with the phase-height data obtained: described below. It should be noted that MEM spectra presented here use the Burg method of obtaining the error-

predictor coefficients (Ulrych and Bishop, 1975). This has an improved resolution over the so-called Yule-Walker method of obtaining the coefficients.

The MEM approach contrasts with that of the Blackman-Tukey and Discrete Fourier Transform methods. The former estimates power spectra using autocorrelations of the data sample: but these estimated autocorrelations are calculated on the assumption that the data is zero outside the data segment taken. The latter takes the data sample as one period of an infinite, periodic waveform. The MEM method is claimed to make no assumptions concerning data outside the sample.

Uncertainties in the use of the method exist, and require awareness of their presence. The length of the prediction-error filter governs the resolution and number of peaks in the spectrum. It must be long enough for the spectrum estimate to resolve all peaks physically present, but excessive length introduces false spectral peaks which are entirely artefacts of the method.

For some data, removal of the mean and of trends can alter the spectrum estimate somewhat. It has been found that for some artificial sinusoidal time series, the number and position(s) of spectral peaks can differ depending on the length and initial phases of the data. Ulrych and Bishop (1975) quote work which allows a variance estimation of the spectrum estimate.

Each of these effects is discussed below and considers the possible effects on the spectrum estimates for the phase-height data. Because the MEM is a newer method, the

amount of experience with it on different types of timeseries is less than is the case for Blackman-Tukey spectra.

(2) MEM Spectrum Resolution

The fixing of predictor-error filter length is equivalent to fixing the order of the autoregressive process to which the data is to be fitted (Ulrych and Bishop, 1975). As mentioned previously, an overlong length will introduce non-physical spectral peaks; while too short a length will fail to resolve peaks which are physically present.

Several spectra were taken for a given set of phase-height data, with predictor-error order M increasing for successive spectra. The date used was for 19th February, 1978, 1256-1504, and consists of a set of 600 points, spread 12.8 seconds apart.

The spectra for increasing M show an increasing number of peaks; as expected and as found for other timeseries by other authors. The periods apparently present in the spectra are given in Table C-1. The values of M range from 80 to 280 which is 13% - 47% of the record length.

Periods to about 13 minutes (10% of record length) are quite stable, with the exception of the nominal 12-minute peak which decreases in period somewhat for spectra with M = 80 to 200. The nominal 25-minute peak varies by as much as ± 8%.

The question now arises of which predictor-error length to use. Akaike (quoted by Ulrych and Bishop, 1975) has given a Final Prediction Error (FPE) parameter which arises as an output of an autoregressive fit to a process. Ulrych and Bishop (1975) indicate the relation of the FPE to the

autoregressive process. The estimate of the FPE arising from an autoregressive fit is expected to be minimum if the order of the fit is correct.

Examination of the FPE value for different spectra showed it to vary only very slowly with changing predictor-error order M. The values very slowly rose for M ranging from 80 to 280, and no clear minimum was present. No examination for minimum FPE below M=80 was made.

The numerical experiments of Ulrych and Bishop (1975) do show the Burg-estimate FPE to vary only very slowly once the first minimum value of FPE is reached. A difficulty pointed out by Ulrych and Bishop (1975) is that a purely harmonic waveform does not generally have an autoregressive representation. Under some circumstances it can be preferable to take the spectrum corresponding to the predictor-error order giving the first minimum in FPE rather than at the absolute FPE minimum, but this can lead to degradation of resolution for more nearly periodic data.

It was decided finally not to use FPE as a measure of spectrum quality. For the phase-height data presented here, it was found better to compare the MEM spectrum found for different orders of predictor-error filter, with the spectrum found by the Discrete Fourier Transform method. The predictor-error order M for which the two spectrum agreed most closely (in number and frequency-values for spectral peaks) was taken to be the correct value.

Fig. C-1 compares three spectra for the data of 19th February, 1978: 1256-1504. The first spectrum is a log Discrete Fourier Transform spectrum (with Hamming window),

and the second and third spectra are log MEM spectra for prediction-error orders of M=200 and M=240 respectively.

It is seen that the M=240 MEM spectrum resolves all the peaks present in the DFT spectrum:
the 13-minute DFT spectrum peak is split into two peaks in the MEM spectrum. At M=200 the 13-minute peak is not split, but the peak at 20 minutes present in the DFT is then not resolved in the MEM spectrum.

Intermediate values of M between 200 and 240 indicated that the resolution of the 20-minute peak occurred when the 13-minute peak began to split.

It is concluded that the M=240 spectrum is closest to the DFT spectrum, at least for this data.

Phase-height data for 19th February, 1978, 1504-1712 have their spectrum periods tabulated in Table C-II. As before, the number of spectral peaks increases as M increases. The positions of the spectral peaks seem somewhat more stable than for the 1256-1504 run.

The consensus of opinion in the literature is that for optimum resolution, the number of predictor-error coefficients M should be between 20% and 50% of the record length. (For example, Courtillot et al., 1977; Ulrych and Bishop, 1975; Toman, 1976). However, some authors (Radoski et al., 1975, 1976) state that they have obtained stable and physically-meaningful spectra for values of M up to the number of points in the data sample. Radoski et al., (1976) and Toman (1976) found that as M was increased, the MEM spectrum approached an unsmoothed DFT spectrum.

(3) Trend Influence on MEM Spectra

Previous methods of spectrum analysis have required the mean and trends to be removed from data prior to analysis. If these low-frequency components were allowed to remain, the leakage arising from the finite length of data taken for analysis would introduce low-frequency power into higher-frequency components. The spectrum estimates for the higher frequencies are thus degraded.

In principle, trend removal should not be expected to affect an MEM spectrum, as the method should make no assumptions about the data beyond its defined interval. In practice some effects have been observed (Courtillot et al., 1977) and as a result it was felt necessary to test the phase-height data here.

It will be recalled that trend-removal for this data was done by digital convolution filtering over the entire data run. The two filters used had half-amplitude periods at 90 mins. and 45 mins. For a segment of the data run, segment mean must be removed separately.

Fig. C-2 shows a comparison of spectra for the phase-height data of 19th February, 1978: 1256-1504. M=240 here. Data for the first spectrum has had no filtering applied. The 90-minute and 45-minute half-power filters have been applied to the second and third spectra.

It is seen that the positions of spectrum peaks in frequency are very little affected. Application of a detrending filter increases the proportion of high-frequency power, as would be expected. A common feature of many MEM spectra obtained here is a peak at period about the length

of the record. The 45-minute filter removes this peak.

Overall the MEM method allows confidence in the position of spectral peaks, regardless of the detrending applied. This applies for a predictor-error filter order of 240: the one dound to agree best with a DFT spectrum.

Examination of detrending effects for lower filter orders (M=120,200, not shown) indicates that application of the 45-minute filter can cause either splitting or shifting of some low-frequency spectrum peaks of period a substantial proportion of the length of the record.

These latter conclusions agree with those of Courtillot et al., (1977), who studied the effects of trend removal on a timeseries consisting of 100 annual mean values of the aa magnetic activity index. Their Fig. 2 compares the MEM spectra of the timeseries, arising from raw data, data with mean removed, and different forms of detrending.

In broad terms, spectral peaks at or below 7 years (7% of the data length) were stable with respect to the absense, presence, and method of detrending. The 11-year and 22-year peaks in the spectra shifted in period by less than ±8% between detrending methods.

The very existence, and positions of peaks at periods over 50 years (50% of the data length) were very sensitive to the presence, absence and method of detrending.

Courtillot et al., (1977) conclude that spectral peaks at periods greater than one-third to one-half the record length cannot be relied upon. From their Fig. 2 it seems best not to detrend the data at all; not even to remove the mean.

The phase-height spectra presented here have the mean removed and a predictor-error filter of M=240 applied (40% of the data length). If the presence or absence of the longest (2-hour) peak is disregarded, the positions of spectrum peaks seem to be unchanged by the application, or not, of detrending.

(4) Line Shifting and Splitting of MEM Spectra

For synthetic sinusoid timeseries, a spectrum-line splitting/shifting effect has been observed under certain particular circumstances (Fougere et al., 1976; Fougere, 1977). This effect is different to that of the increase in number of spectral peaks with order of predictor-error filter.

Suppose a synthetic sinusoid is generated, and a small ($< 10^{-2}$) proportion of noise is added to it. The length of the signal to be taken is an odd number of quarter-cycles: 1.25 cycles, 3.25 cycles, and so on.

Fougere et al., (1976) found that for such input, MEM spectra obtained by the Burg method would give a varying number and peak position(s) of spectral peaks: depending upon the phase of the sinusoid at the beginning of the data sample. Synthetic signals an odd number of quarter cycles in length, with initial phase of 0^{o} or any multiple of 90^{o}, gave single-peak spectra at the correct frequency. At any other initial phase the spectrum peak split into a doublet or triplet: the splitting between the peaks being worst at initial phase an odd multiple of 45^{o}.

Later work (Fougere 1977) indicated that for a larger proportion of noise in the sinusoid the spectral peak would be shifted and not split.

These results are of relevance in the calculation of the time-varying spectra. It is possible that if a moving window is taken through predominately sinusoidal data, and spectra calculated; changes in the spectra could arise either from this effect or because there is a real time-change in the spectra of the data.

Fougere et al., (1976) looked for such an effect in the moving spectra of real data but found no such effect. Nevertheless, a similar test was made on the phase-height data to look for any such effect.

Table C-III indicates the results taken for the phase-height data of 19th February, 1978: 1256-1504. An examination is made for two orders of predictor-error filter: M=120, 220 The time-window is advanced through the data by 2.57 minutes per column: the first column for each order of M is for 1256-1504 exactly and may be identified with the appropriate column in Table C-I.

Examination of results for M=220 shows that the nominal 5.8-minute and 7.5-minute peaks are not affected. The nominal 24-minute peak and the nominal 13.6-minute peak both take shorter-period values for the third and subsequent spectra. The nominal 11.3-minute peak has a shorter period for the third and fourth spectra but returns to the initial value for the fifth and sixth spectra.

The following Table C-IV shows the phase-advance of a sinusoid at periods indicated:

TABLE C-IV PHASE ADVANCE OF SINUSOIDS

Nominal period	Number of cycles in run	Phase advance per spectrum	Splitting/shifting expected
8.8	14.5	106°	No: length is integral number of half-cycles
11.3	11.3	88°	No: phase shift is (nearly)a multiple of 90°.
13.6	9.4	73°	Yes, length is not quite an integral number of half-cycles and phase-shift not a multiple of 90°.
24	5.3	41°	Yes, length is (almost) an odd number of quarter-cycles. Every second phase-shift is an odd multiple of 45°.

The nominal 8.8-minute peak shows no shifts. However, the nominal 11.3-minute period peak definitely shows a period shift: not expected if the shifts arose from the changing value of waveform initial phase. The 24-minute peak should show a shift for every alternate spectrum.

In fact, the 11.3-minute, 13.6-minute, and 24-minute peaks all indicate a decrease in period for the third and fourth spectra; when differing effects would arise from changing waveform initial phase. For these reasons it is felt that the period changes seen are true changes in the data rather than artefacts of the MEM method. This allows confidence in obtaining overlapping spectra.

(5) Conclusions on MEM Spectra

For MEM spectra presented here, 600 points (128 minutes) of data were taken. A choice of predictor-error filter length of 240 (40% of the data length) was found to give a spectrum which was overall similar to a Hamming-windowed DFT spectrum. The Akaike FPE parameter was not found helpful in determining the optimum resolution.

For the optimum choice of predictor-error length, it was found that trend retention or removal had little effect on the periods of spectral peaks, with the exception of the peak at period the data length.

In contrast to the Fougere et al., (1976) results for synthetic waveforms, no splitting or shifting of spectral peaks due only to the MEM method were observed for this data. The alteration in frequency position for spectral peaks, as a window is moved through the data, is considered to exist within the data itself. This gives confidence in the reality of any changes to be indicated by moving spectra elsewhere.

Because the MEM spectrum is a spectrum estimate, it will have errors associated in the frequency position and amplitude of spectral peaks. The errors in frequency position given in the tables are merely those in fitting the positions of the peaks, and do not take into account any error inherent in the method itself. The error in power estimation of a spectral component is deferred until the discussion of DFT spectra below.

In conclusion, the overall resolution and stability of MEM gives confidence in its use of moving-spectrum studies.

III THE DISCRETE FOURIER TRANSFORM METHOD

(1) General Discussion of the Method

The direct way to find the spectrum of a segment of data is to find its Fourier Transform. The power spectrum at a given frequency is then the squared modulus of the Fourier Transform coefficient at that frequency.

If I(t) is a continuous, infinite-length stationary timeseries, its Fourier Transform F(f) is found from (Otnes and Enochson, 1972)

$$F(f) = \underset{T\to\infty}{\mathcal{L}t} \frac{1}{T} \int_{-T/2}^{T/2} I(t)\, \exp(2\pi i f t)\, dt \quad .$$

The practical case of the analysis of a finite segment of N data points, sampled at a uniform time spacing Δt, results in the Discrete Fourier Transform of the data set (Otnes and Enochson, 1972):

$$F(f) = \Delta t \sum_{k=0}^{N-1} I(k.\Delta t) \exp(2\pi i f . k\Delta t) \quad .$$

This is defined at any frequency f, but is periodic in f with period $\frac{1}{\Delta t}$ because of the sampling in time.

The discrete Fourier Transform is not usually calculated directly as defined above, but rather using the so-called Fast Fourier Transform algorithm (Cooley and Tukey, 1965) which allows very rapid computing speeds. Most versions of this algorithm require an input of length $N' = 2^{(\text{integer})}$ points and return the spectrum calculated at N' points spaced in frequency by $f = \frac{1}{N' \Delta T}$.

The sampling in frequency of a Discrete Fourier Transform effectively makes the time input waveform one period of an infinite, periodic waveform (Brault and White, 1971). Such implicit assumptions can bias the estimated spectrum unless steps are taken to minimize the bias.

Since the Discrete Fourier Transform (abbreviated as DFT) method has been used to assess the reliability of the MEM spectrum, as outlined previously, it is necessary to assess the biases and attempt to minimize them. Table C-V indicates an overall view of the steps taken to obtain DFT spectra, and a discussion of each step is given below.

(2) Leakage Reduction

The selection of a finite length of data for analysis is equivalent to the multiplication of an infinitely long timeseries by a window $W_1(t)$ which is unity for the data length and zero elsewhere. The spectrum estimate $\hat{S}(f)$ is then the convolution of the true transform with the transform $\bar{W}_1(f)$ of the window $W_1(t)$:

$$\hat{S}(f) = \frac{1}{T} \int_{f'=-\infty}^{\infty} S_{True}(f-f')\ \bar{W}_1(f')\,df'$$

The transform $\bar{W}_1(f)$ is of form $\frac{\sin(f)}{f}$ which has (for example, Otnes and Enochson, 1972) a number of sidelobes of substantial amplitude about the main lobe. Thus, as is well known, the convolution causes the spectrum estimate $\hat{S}(f)$ at a given frequency f_o to have contribution not only from the true spectrum at f_o but also at other frequencies f_1 displaced from f_o. The frequencies f_1 are those for which $\bar{W}_1(f)$ has

has substantial sidelobe amplitudes, when centered at f_o.

The power in strong apectral peaks can thus "leak into" and contaminate the spectrum estimate at other frequencies. For many spectra, there is predominant power in the low-frequency or trend components, and if leakage is not rectified the entire spectrum can be contaminated.

This is a well-known problem in practical data analysis, and standard techniques exist to improve the spectrum.

Removal of the data mean and of trends removes the very-low-frequency power and hence its leaked contribution to higher frequencies. This has been done for all DFT spectra presented here. The technique known as "pre-whitening" effectively flattens the spectrum, and reduces the leaked components arising from prominent spectral peaks. The final technique used here is to "window" the data. The data series $I(t_k)$ is multiplied by a set of weights, to generate on new input series $I'(t_k)$ as

$$I'(t_k) = I(t_k)W_2(t_k)$$

and in frequency domain the true transform is convolved with a different window $\bar{W}_2(f)$. The weights are set so that $\bar{W}_2(f)$ has sidelobes of very much smaller amplitude than those for $\bar{W}_1(f)$. Two popular windows are the Hanning and Hamming windows, with weights

$$\text{Hanning:} \quad W_2(t_k) = 0.50 - 0.50\cos\left(\frac{2\pi k}{N}\right)$$

$$\text{Hamming:} \quad W_3(t_k) = 0.54 - 0.46\cos\left(\frac{2\pi k}{N}\right)$$

for N points and k = 0,1,2,...,(N-1).

Fig. C-3 shows three spectra for the phase-height data of 19th February 1978: 1256-1504.

For all spectra, trend power was attenuated by the 90-minute filter. The segment mean of the 600 data points was removed. The window weights (if applicable) were applied to the 600 points, after which the data was extended by zeros to 2048 points for Fourier Transformation.

For the first spectrum, no window has been applied. A Hanning and a Hamming window, respectively, were applied to the second and third spectra.

The improvement in spectrum quality with windowing is immediately seen. This indicates that the residual low-frequency trend components allowed through by the 90-minute filter have enough amplitude to considerably contaminate the spectrum in the absence of windowing.

The spectrum is seen to have several well-defined peaks and a pre-whitening procedure was carried out to look for leakage from these peaks. The whitened series $I'(t_k)$ was obtained from

$$I'(t_k) = I(t_k) - 0.99\ I(t_{k-1}) \ .$$

The results (not shown) indicate spectrum peaks at the same periods as for the original data, although the relative amplitudes for periods greater than 20 minutes have been reduced.

Application of different windows shows very little difference in the position of spectrum peaks between Hanning and Hamming windows. The Hamming window results in considerably more relative power in the short-period

components: it should be recalled that the figure is of log spectra. This is probably because the sidelobe amplitudes of the Hanning and Hamming windows fall off as $1/f^6$ and $1/f^2$ respectively (Buckley, 1971), making the former window preferred for the suppression of long-range leakage.

Jenkins and Watts (1968) note that for many cases of spectrum estimation, the choice of window bandwidth is more important than that of window shape.

Fig. C-4 illustrates that for the data presented here, application of an effective window can remove the need for data detrending if the frequencies of spectral peaks are all that are of interest. Three spectra are compared: the data segment mean has been removed in all cases. The first spectrum has had no detrending: the second has had the 90-minute filter applied and third the 45-minute filter applied. The Hamming window was then applied to all data.

It is seen that the frequencies of spectral peaks do not change, although the spectrum peak resolution of the 90-minute filtered data is somewhat better than that for the un-detrended data. The proportional distribution of power among frequencies alters with the degree of detrending.

On the basis of results here, a Hamming window has been applied to all subsequent data as it appears to give the best resolution.

(3) Extension of the data set by zeros.

Since most versions of the FFT algorithm require the input length to be $N' = 2^{(\text{integer})}$ number of points, the original data set (after removal of the mean and windowing) must have a number of zero points added to make up the required length.

The frequency values for which the spectrum is calculated are now

$$f'_k = \frac{k}{N' \Delta t} \qquad k = 0,1,\ldots,(N'-1)$$

a finer spacing than the $\frac{1}{N\Delta t}$ spacing which would have arisen from the N original data points.

The effect of this on the spectrum will be discussed below, in the section on spectrum smoothing. A comparison in the *shape* of the spectrum, for the 600 data points extended to 2048 and 4096 points showed no visible difference between the two cases.

(4) Variance estimation and smoothing of the spectrum.

As with any statistical estimate, the sample spectrum $\hat{S}(f)$ has bias, consistency, and variance properties. Standard results obtained for Gaussian random processes do give some guide to the properties of a DFT spectrum, but need some care in use for peaky deterministic spectra.

The raw DFT spectrum for a random Gaussian process is very noisy. At the harmonic frequencies $f_k = \frac{k}{N\Delta t}$ the sample spectrum has the following properties (Jenkins and Watts, 1968: Otnes and Enochson, 1972):

(i) The spectrum estimate at $f = f_k$, $\hat{S}(f_k)$ has a standard deviation equal to its average:

$$S.D.[\hat{S}(f_k)] = \hat{S}(f_k) \quad .$$

Lengthening the input record for *random* signals does not decrease this error, and the sample spectrum does not converge to $S_{True}(f)$.

(ii) The spectrum estimate at f_k, $\hat{S}(f_k)$ is an unbiased estimator of the true spectrum value $S_{true}(f)$ (which for white noise is a constant at all frequencies) over several realizations of the white noise process:

$$E[\hat{S}(f_k)] = S_{true}(f_k) \quad .$$

(iii) The spectrum estimates at separate frequencies $\hat{S}(f_k)$ and $\hat{S}(f_j)$ are uncorrelated and independent.

(iv) The spectrum estimate at $f=f_k$, $\hat{S}(f_k)$ is distributed as a χ^2_2 random variable - with two degrees of freedom. (Two exceptions are $\hat{S}(f_k)$ for $f_k=0$ and $f_k=\frac{1}{2\Delta t}$ for which $\hat{S}(f_k)$ is distributed as χ^2_1).

The spectrum estimate for one realization of a noise process will give a very poor indication of the true (flat) spectrum.

An indication of error associated with the DFT spectra for the phase-height data can be obtained on the basis of the white-noise results.

For a raw DFT spectrum the bandwidth of analysis is the spacing between the frequency points $\frac{1}{T}$, with T the length of the data. This allows maximum resolution but also maximum spectrum variance (Otnes and Enochson, 1971).

With an extension by zeros the bandwidth of analysis is still $\frac{1}{T}$ where T is the length of the original data. However, the spectrum estimates are now spaced at $\frac{1}{N' \Delta t}$, so adjacent spectrum estimates are not independent. An indication of the smoothing can be seen in Fig. C-3. The effect on the variance of each estimate is to increase it by a factor $\frac{N'}{N}$ (Bloomfield 1976).

Smoothing and loss of resolution arises also from the application of a window. Although a window has sidelobes of very small amplitude, the main lobe is broadened, doubling (for Hanning and Hamming windows) the bandwidth of analysis again. Because data are altered, there is a loss in degrees of freedom and an increase in variance.

The final step in improving the reliability of a spectrum is to smooth adjacent (independent, if windowing or zero extension has been done) spectrum estimates. For a Gaussian normal process the M-point average spectrum estimate is distributed as χ^2_{2M}, and with the increased number of degrees of freedom the variance is reduced. This procedure will introduce bias in the spectrum except for perfect noise processes, and the bias will increase the smoother the spectrum.

No final smoothing has been done for the spectra here, as the correlation between spectral estimates introduced by the zero extension of the data seems to be sufficient smoothing without undue loss of resolution.

For display on the spectrum plots, a bandwidth calculation and a standard deviation calculation are made.

Bandwidth: Data length = 600 points x 12.8 second spacing
= 7680 seconds.

Reciprocal $\frac{1}{T} = 1.3 \times 10^{-4}$ Hz.

Bandwidth $\frac{2}{T} = 2.6 \times 10^{-4}$ Hz.

The resulting bandwidth is shown on the log FFT plots.

Standard Deviation:

On the basis of independent estimates, the standard deviation of an estimate is equal to the size of the estimate, approximately. This is if one spectrum estimate (with two degrees of freedom) appears within the bandwidth of the analysis.

For the case of window extension and smoothing:

Bandwidth of Analysis $= \frac{2}{T} = 2.6 \times 10^{-4}$ Hz.

Spacing of frequency $\Delta f = \frac{1}{2048.\Delta t} = 3.8 \times 10^{-5}$ Hz.

$\therefore$ Number of estimates within bandwidth = 7

and number of degrees of freedom = 14

ignoring the fact that the data are not now completely independent.

The statistic χ^2 is now used to calculate the error limits, as shown in the following table.

TABLE CVI PERCENTAGE CONFIDENCE INTERVAL

p = 95% $\alpha = 1 - p = .05$		
Coefficient	Value	Corrected* Value
$\frac{n}{\chi^2_{n;\frac{\alpha}{2}}}$	$\frac{14}{26.12} = 0.54$	0.43
$\frac{n}{\chi^2_{n;1-\frac{\alpha}{2}}}$	$\frac{14}{5.63} = 2.49$	3.1

The corrected value arises from two factors (Bloomfield 1976).

(i) The increase factor in standard deviation, $\sqrt{\frac{N'}{N}}$, arising from extension of N data points by zeros to form N′ data input points.

$$\sqrt{\frac{N'}{N}} = \sqrt{\frac{2048}{600}} = 1.8 \quad .$$

(ii) The formula in Bloomfield (1976, p.193) for the increase in variance arising from tapering. If the entire input time series is tapered with a cosine-bell taper, then the increase in standard deviation is

$$\sqrt{\tfrac{1}{2}\,\frac{(128-93.1)}{(8-5.1)^2}} = 1.4$$

The product of these factors is 2.58.

The χ^2 limits each way are adjusted by a factor of 1.25 each way to take the increase in standard deviation roughly into account. After conversion to logarithmic values, the 95% confidence interval is shown on the spectrum plots.

(5) Conclusions on DFT Spectra

For DFT spectra presented here, 600 points (128 minutes) of data were taken. Removal of the mean, application of a Hamming window, and extension by zeros to 2048 points without further smoothing gave stable and reliable spectra. A pre-whitening of some of the data indicated that no spurious spectrum peaks were present owing to leakage from true peaks.

Comparison with the MEM spectra showed good agreement with spectra with MEM predictor-error order of about 240. Although MEM spectra at this value may be slightly more

peaky at times than the corresponding DFT spectra, it is felt that overall best agreement is obtained under these conditions.

IV OVERALL CONCLUSION

For the daytime data of 19th February, 1978, MEM spectrum analysis with an error-predictor coefficient of 240 gave spectra which agreed with a Hamming-window Fourier Transform Spectrum. With the exception of peak the data length, spectrum peaks of interests down to 5 minutes appear reliable. For overlapping spectra, observed changes in spectrum peak periods appear to be real.

TABLE C-I MEM Spectra for Phase-Height : 19 February 1978 : 1256-1504 N.Z.S.T.

Data Filtered With 90-Minute Filter

Predictor-error Filter: order / Nominal period, mins	80	120	160	180	200	220	240	260	280
	-	48(±2)	51(±2)	40(±2)	42(±2)	42(±2)	42(±2)	42(±2)	43(±2)
	-	-	-	-	-	24(±1)	22(±1)	25(±1)	21(±1)
	-	-	-	-	-	13.6(±.5)	13.7(±.5)	13.7(±.5)	13.9(±.5)
	12.1(±.3)	12.3(±.3)	12.7(±.3)	12.2(±.3)	11.9(±.3)	11.3(±.3)	11.6(±.3)	11.6(±.3)	11.6(±.3)
	-	-	9.5(±.2)	8.9(±.2)	8.8(±.2)	8.8(±.2)	8.8(±.2)	8.9(±.2)	8.7(±.2)
	7.8(±.2)	7.7(±.2)	7.6(±.2)	7.4(±.2)	7.4(±.2)	7.5(±.2)	7.4(±.2)	7.4(±.2)	7.4(±.2)
	5.8(±.1)	6.0(±.1)	5.9(±.1)	6.0(±.2)	6.1(±.2)	6.1(±.2)	6.2(±.2)	6.2(±.2)	6.1(±.2)
	-	-	-	5.1(±.1)	5.4(±.1)	-	5.7(±.1)	5.7(±.1)	5.6(±.1)
	-	-	-	-	-	5.0(±.1)	5.0(±.1)	5.0(±.1)	5.0(±.1)
	-	-	4.8(±.1)	4.6(±.1)	4.7(±.1)	4.5(±.1)	4.5(±.1)	4.5(±.1)	4.5(±.1)

TABLE C-II MEM Spectra for Phase-Height : 19 February 1978 : 1504-1712 N.Z.S.T.

Data Filtered With 90-Minute Filter

Predictor-error Filter: order / Nominal Period, mins	80	120	160	180	200	220	240	260	280
	-	26(±1)	28(±1)	29(±2)	31(±2)	32(±2)	32(±2)	32(±2)	32(±2)
	-	-	-	17(±1)	20(±1)	22(±1)	22(±1)	22(±1)	22(±1)
	-	13.4(±.5)	15.3(±.5)	13.9(±.5)	13.9(±.5)	15.3(±.5)	15.6(±.5)	15.7(±.5)	15.4(±.5)
	-	-	12.1(±.3)	11.0(±.3)	11.3(±.3)	12.5(±.3)	12.6(±.3)	12.5(±.3)	12.3(±.3)
	-	-	-	-	-	10.5(±.2)	10.4(±.2)	10.4(±.2)	10.4(±.2)
	9.3(±.2)	8.2(±.2)	8.0(±.2)	7.9(±.2)	8.0(±.2)	8.0(±.2)	8.1(±.2)	8.1(±.2)	8.1(±.2)
	5.8(±.1)	5.8(±.1)	5.9(±.2)	6.1(±.2)	6.0(±.2)	6.0(±.2)	6.0(±.2)	5.9(±.2)	5.9(±.2)
	-	-	5.4(±.1)	5.6(±.1)	5.4(±.1)	5.3(±.1)	5.4(±.1)	5.3(±.1)	5.3(±.1)
	-	-	-	5.1(±.1)	4.7(±.1)	4.8(±.1)	4.8(±.1)	4.8(±.1)	4.8(±.1)
	-	-	-	4.4(±.1)	4.4(±.1)	4.4(±.1)	4.4(±.1)	4.4(±.1)	4.4(±.1)

TABLE C-III MEM Spectra for Phase-Height : 19 February 1978. First Spectrum 1256 - 1504 N.Z.S.T.
Data Filtered with 90-Minute Filter

Predictor error order / Nominal period, min	120	120	120	120	120	120	220	220	220	220	220	220
	48 (±2)	48 (±2)	-	-	-	-	42 (±2)	41 (±2)	35 (±2)	32 (±2)	29 (±2)	28 (±2)
							24 (±1)	23 (±1)	19 (± 1)	19 (±1)	21 (±1)	20 (±1)
							13.6 (±.3)	13.6 (±.3)	12.8 (±.3)	12.9 (±.3)	12.8 (±.3)	12.7 (±.3)
	12.3 (±.3)	12.4 (±.3)	12.2 (±.2)	11.4 (±.3)	12.1 (±.3)	12.0 (±.3)	11.3 (±.3)	11.2 (±.2)	10.5 (±.2)	10.6 (±.2)	11.1 (±.2)	11.3 (±.2)
							8.8 (±.2)	8.8 (±.2)	8.9 (±.2)	8.8 (±.2)	8.8 (±.2)	8.9 (±.2)
	7.7 (±.2)	7.7 (±.2)	7.8 (±.2)	7.9 (±.2)	7.9 (±.2)	8.1 (±.2)	7.5 (±.2)	7.5 (±.2)	7.4 (±.2)	7.5 (±.2)	7.4 (±.2)	7.4 (±.2)

Each spectrum is over a time-period of 128 minutes, starting later by 2 min 34 sec.

TABLE C-V Calculation of Spectra Using Discrete Fourier Theorem

PROCESS	ACTION	PARAMETERS
Raw data to tracked phase-height data.	1 (Amplitude, Phase) point every 0.256 seconds at one height only for total reflection. Track phase values through $2n\pi$.	1 receiver 1 height Total reflection.
Decimation of data.	Decimate by 50 for points at 12.8 second spacing.	
Detrending of data.	Linear convolution filter with 201 weights removes trends: half-power at 90-minute period.	201 weights.
Selection of data.	Select a segment of data for spectral analysis $I(t_0), I(t_1), \ldots, I(t_{N-1})$ the phase-height values.	Usually 600 points = 128 minutes. Point spacing = 12.8 seconds.
Leakage reduction.	Subtrace sample mean from each point. Multiply each point by window, to obtain $I'(t_k) = W(t_k)I(t_k)$.	Hamming window or Hanning window usually used.
Extension of zeros.	Add $N'-N$ zeros to make data length $N' = 2^{(\text{integer})}$.	$N' = 1024$, 2048, or 4096 usually.
Apply the transform.	Application of the transform to N' complex (amplitude, tracked phase) points. The real transform of the tracked phase alone is recovered.	N' frequency values obtained. For real data only $\frac{N'}{2}$ are independent.
Smooth the spectrum.	Average a number of adjacent (independent) spectrum components to obtain a smoothed spectrum, with decreased variance.	Not done, as extension by zeros and window has smoothed spectrum enough.

LOG FFT SPECTRUM 19 FEB 1978 1256-1504 90-MIN FILTER

600 POINTS 2048 DFT POINTS HAMMING WINDOW

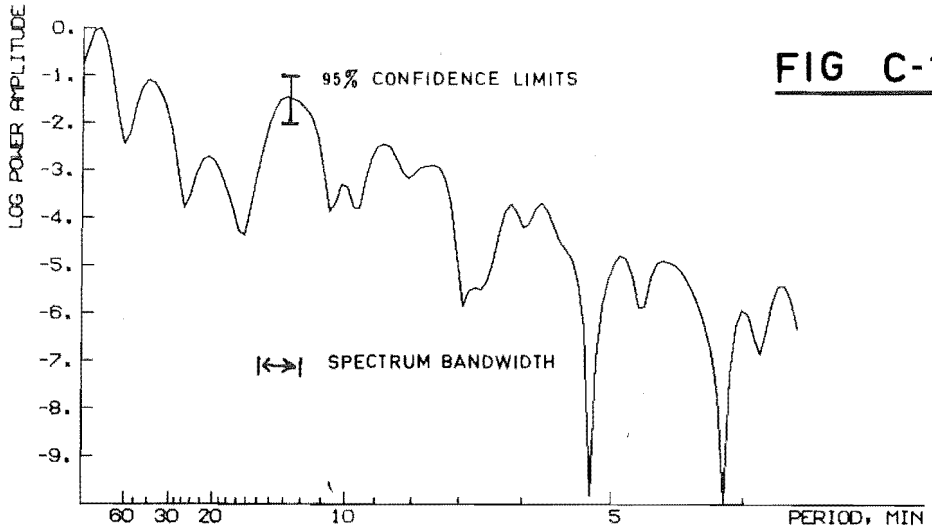

FIG C-1

LOG MEM SPECTRUM 19 FEB 1978 1256-1504 90-MIN FILTER

600 POINTS LOG FPE 18.14071 ORDER OF PREDICT-ER FILTER 200

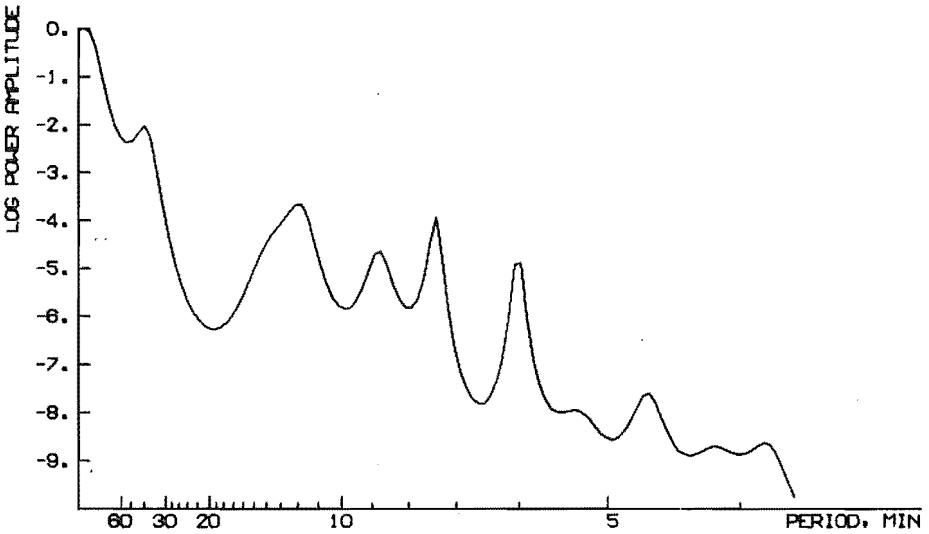

LOG MEM SPECTRUM 19 FEB 1978 1256-1504 90-MIN FILTER

600 POINTS LOG FPE 17.84012 ORDER OF PREDICT-ER FILTER 240

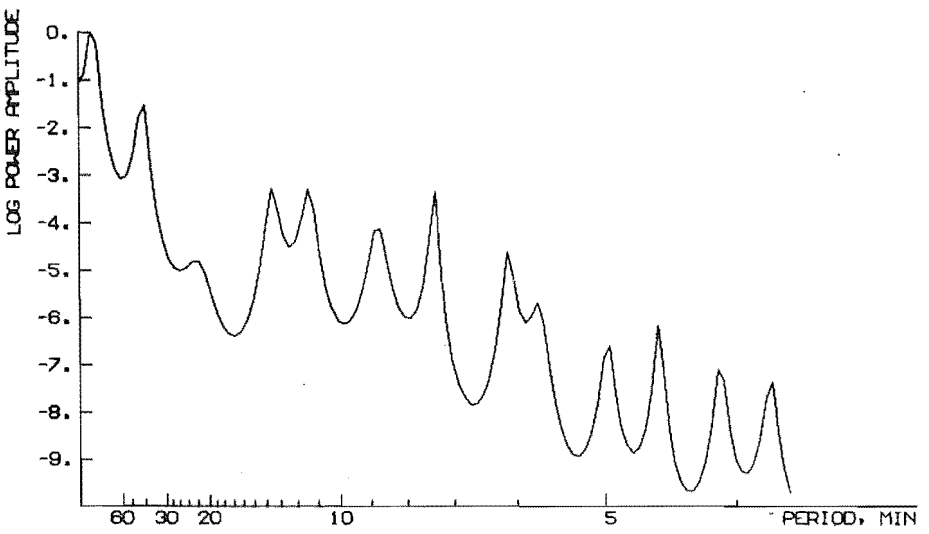

LOG MEM SPECTRUM 19 FEB 1978 1256-1504 NO FILTER

600 POINTS LOG FPE 17.98449 ORDER OF PREDICT-ER FILTER 240

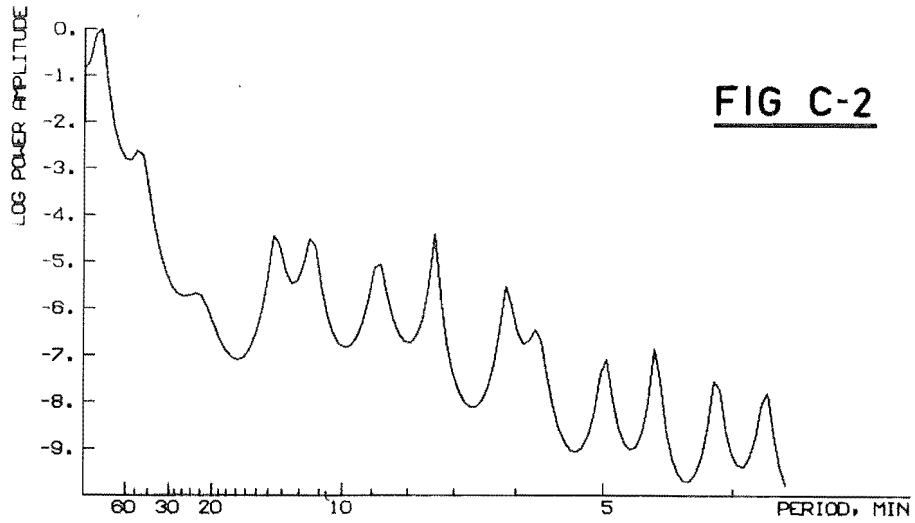

FIG C-2

LOG MEM SPECTRUM 19 FEB 1978 1256-1504 90-MIN FILTER

600 POINTS LOG FPE 17.84012 ORDER OF PREDICT-ER FILTER 240

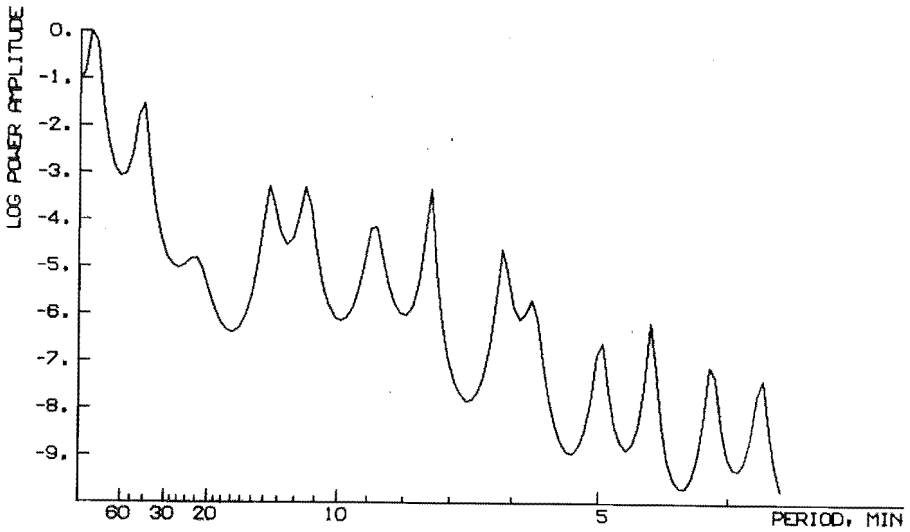

LOG MEM SPECTRUM 19 FEB 1978 1256-1504 45-MIN FILTER

600 POINTS LOG FPE 17.58615 ORDER OF PREDICT-ER FILTER 240

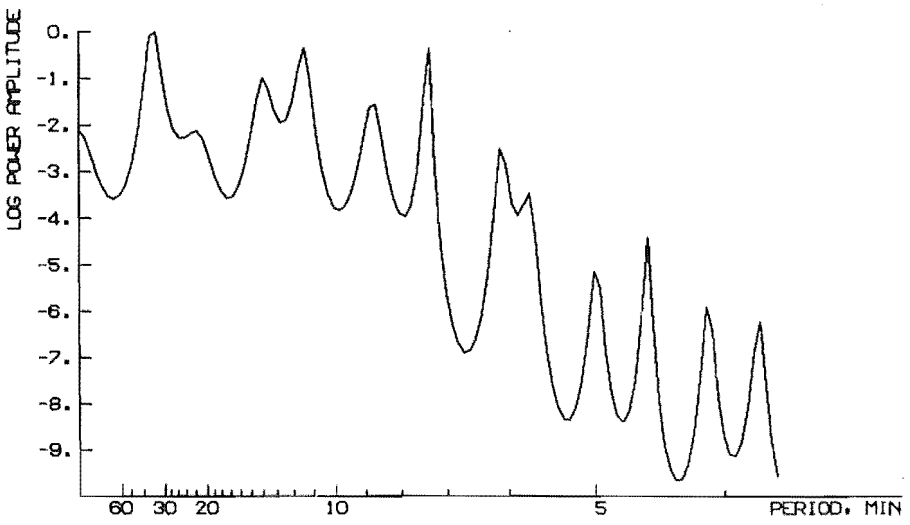

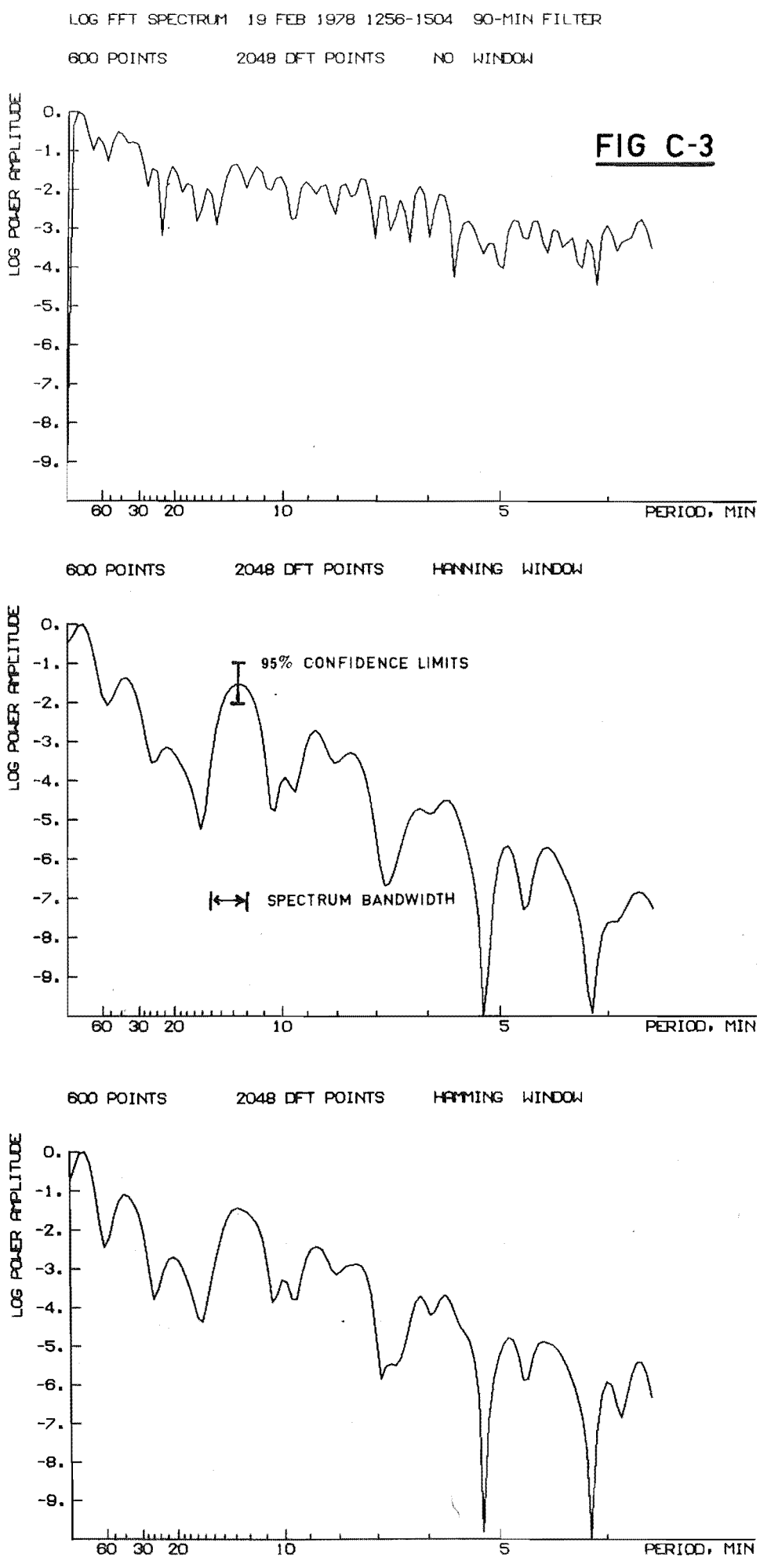
LOG FFT SPECTRUM 19 FEB 1978 1256-1504 90-MIN FILTER
600 POINTS 2048 DFT POINTS NO WINDOW
LOG POWER AMPLITUDE
0.
-1.
-2.
-3.
-4.
-5.
-6.
-7.
-8.
-9.
60 30 20 10 5
PERIOD, MIN
600 POINTS 2048 DFT POINTS HANNING WINDOW
95% CONFIDENCE LIMITS
SPECTRUM BANDWIDTH
600 POINTS 2048 DFT POINTS HAMMING WINDOW

FIG C-3

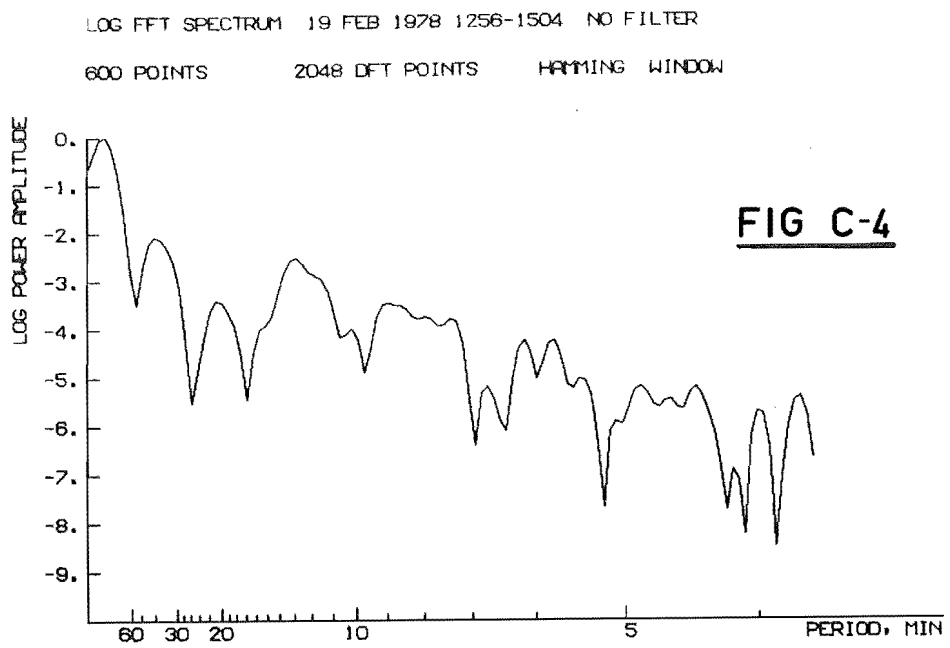
LOG FFT SPECTRUM 19 FEB 1978 1256-1504 NO FILTER
600 POINTS 2048 DFT POINTS HAMMING WINDOW
LOG POWER AMPLITUDE
0.
-1.
-2.
-3.
-4.
-5.
-6.
-7.
-8.
-9.
60 30 20 10 5
PERIOD, MIN

FIG C-4

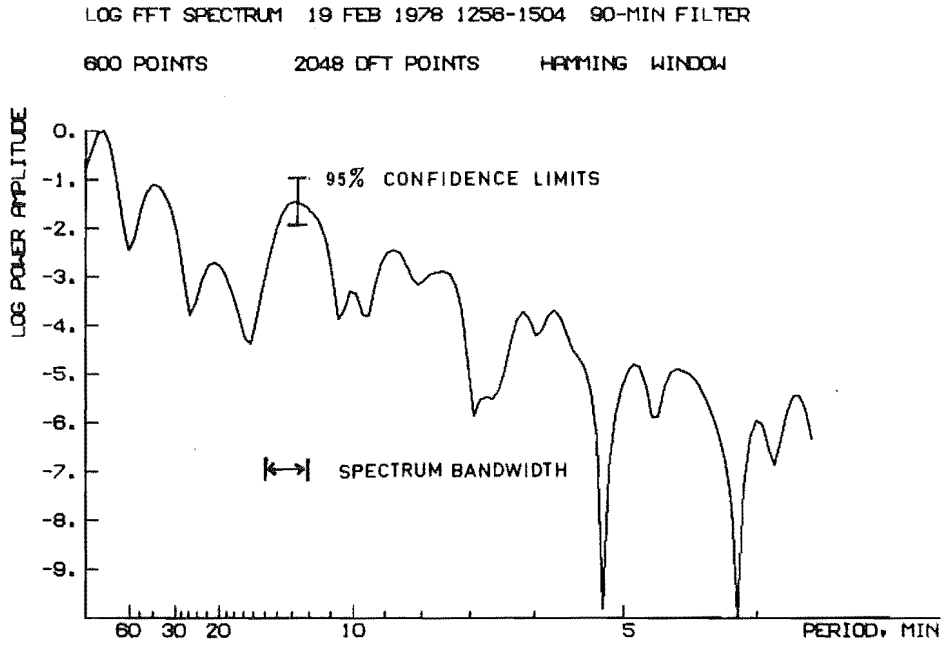
LOG FFT SPECTRUM 19 FEB 1978 1256-1504 90-MIN FILTER
600 POINTS 2048 DFT POINTS HAMMING WINDOW
LOG POWER AMPLITUDE
95% CONFIDENCE LIMITS
SPECTRUM BANDWIDTH
0.
-1.
-2.
-3.
-4.
-5.
-6.
-7.
-8.
-9.
60 30 20 10 5
PERIOD, MIN

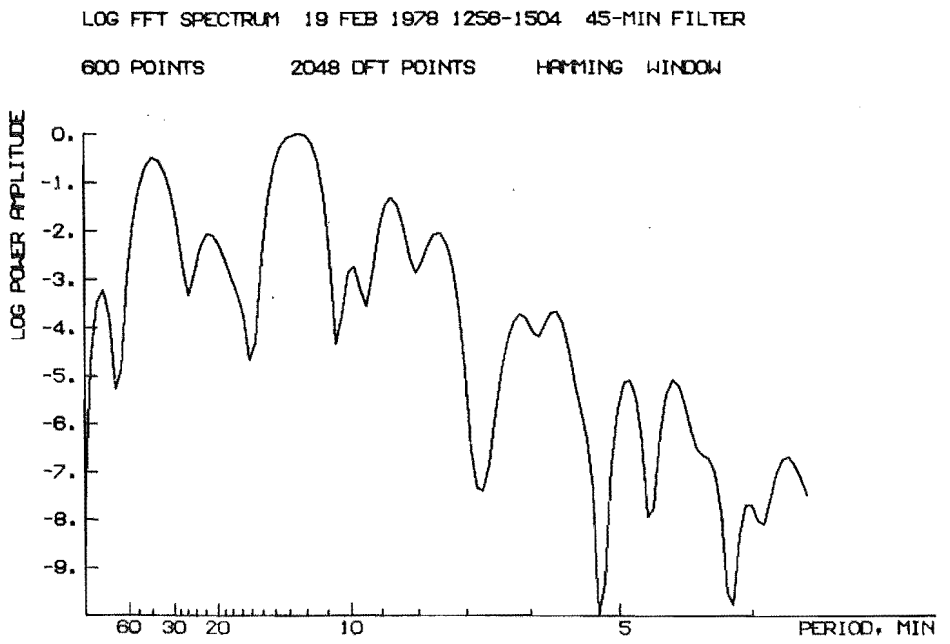
LOG FFT SPECTRUM 19 FEB 1978 1256-1504 45-MIN FILTER
600 POINTS 2048 DFT POINTS HAMMING WINDOW
LOG POWER AMPLITUDE
0.
-1.
-2.
-3.
-4.
-5.
-6.
-7.
-8.
-9.
60 30 20 10 5
PERIOD, MIN

APPENDIX D

THE TREATMENT OF SIGN IN THE FOURIER-TRANSFORM MODELLING OF DIFFRACTION

In general treatments, an incoming plane wave is taken as modified in amplitude and phase by an infinite diffracting screen situated in the X-Y plane (Ratcliffe, 1956, P.191) (Mercier, 1959, P.764). The emerging complex amplitude is

$$\underline{f}(X,Y) = A(X,Y)\ \exp\{i\phi(X,Y)\}$$

and the numerical treatment in this thesis keeps the amplitude A constant and varies only the phase $\phi(X,Y)$.

For numerical calculations it must be clear what the sign of ϕ means physically. The screen model eventually to be taken will, of course, be a reflecting screen which reflects a plane wave travelling to it from the ground.

I. MODEL OF THE PHASE SCREEN.

Given a sinusoidal mirror-like reflector of wavelength λ_{scr}

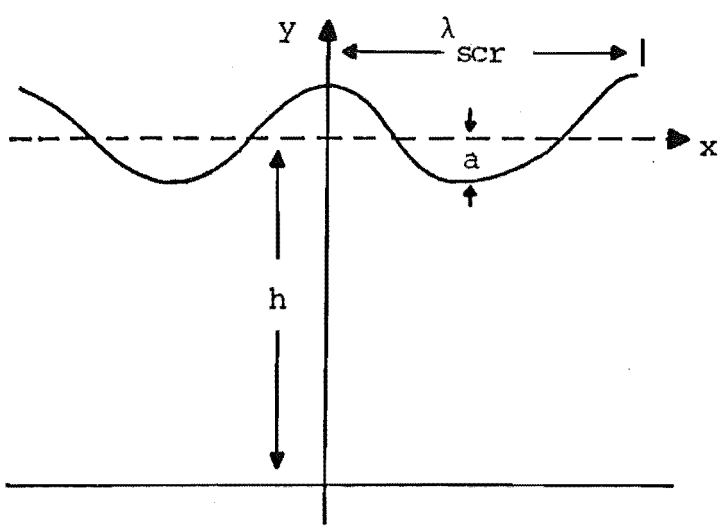

then $y = h + a \cos\left(\frac{2\pi x}{\lambda_{scr}}\right)$

and for a plane wave incident from below, a reflection from points

$$y_{max} = h+a$$

will have a phase behind reflections from points

$$y_{min} = h-a$$

in time.

II. CHOICE OF WAVE DIRECTION

For the diffracted fields, waves travelling in the positive Z-direction are of interest. These are waves like cos $(kZ-\omega t)$ or $\cos(\omega t-kZ)$: we choose $\cos(kZ-\omega t)$ with Z in standard units.

For a phase shift Φ, the wave becomes $\cos\{kZ-\omega t+\Phi\}$. This is illustrated in the diagram immediately below, which is a plot of $\cos(kZ-\omega t)$ and $\cos(kZ-\omega t+\Phi)$. The middle axis is that of the total wave phase $(kZ-\omega t)$, which remains constant for a given part of the wave moving along the positive Z-axis with time t at phase velocity $V_\phi = \frac{\omega}{k}$. The effect of adding a constant phase Φ to the phase $(kZ-\omega t)$ can be seen.

The bottom axis is that of distance for fixed time, and is a time shapshot of the spatial variation of the wave. The top axis is that of time at a fixed distance or place - note its reversal in direction compared to the other two axes, which is necessary for the total phase $(kZ-\omega t)$ to keep the right values.

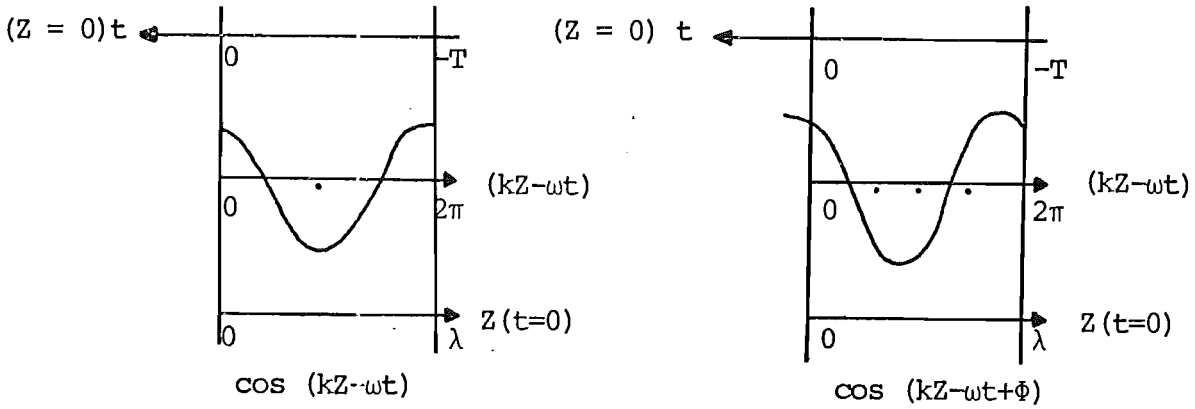

It is seen from the diagram that for Φ positive:

(1) For fixed Z, the wave-crest occurs at a later time.

(2) For fixed t, the crest occurs at a shorter distance from the origin.

Taking waves travelling in the positive direction as $\cos(kZ-\omega t)$, then positive Φ is associated with reflection points y_{max} of the reflecting screen.

III. THE SIGN OF THE EXPONENT IN THE FOURIER TRANSFORM

Ratcliffe (1956, P.191) considers a single plane wave travelling at an angle Θ to the positive Z direction. The complex amplitude $\underline{A}(\Theta)$ is the initial amplitude and phase of the wave at the screen at time zero. The wave is

$$\underline{A}(\Theta)\, d\Theta \exp[2\pi i\{(X \sin\Theta + Z\cos\Theta)/\lambda - nt\}]$$

or

$$\underline{K}(\Theta) \exp\{i\chi(\Theta)\} \exp[2\pi i\{(X \sin\Theta + Z\cos\Theta)/\lambda - nt\}]$$

where

$\underline{A}(\Theta) = K(\Theta) \exp\{i\chi(\Theta)\}$ explicitly and $2\pi n = \omega$.

Along the distance path, which passes through the points (0,0) and (X,Z), then $\chi(\Theta)$ positive has the effect of Φ positive, as in II above.

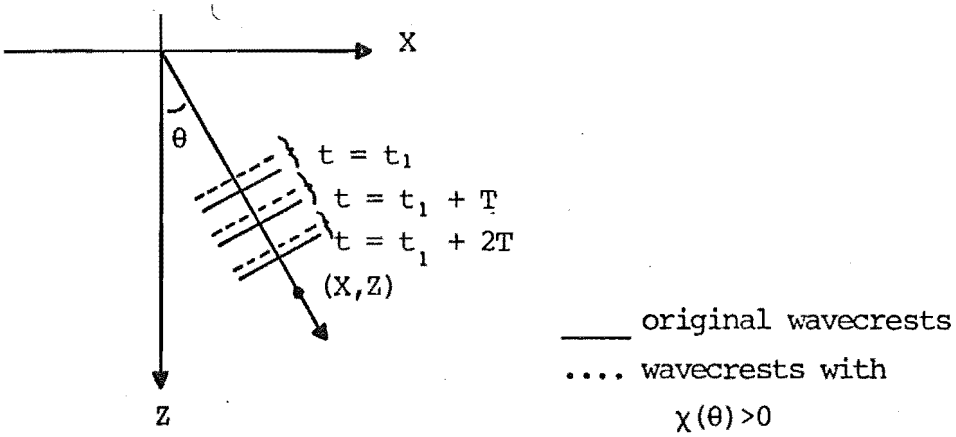

(1) Summation of Angular Spectrum Components to Obtain the Total Field

The X-component of the total field is (Ratcliffe, 1956, Eq. 1)

$$\underline{f}(x,z)\exp(-2\pi int) = \int_{\Theta=-\pi/2}^{\pi/2} K(\Theta)\exp\{iX(\Theta)\}.\cos\Theta \cdot \exp[2\pi i(x\sin\Theta + z\cos\Theta)-nt]$$

retaining the explicit separation of $\underline{A}(\Theta)$ and using wavelength units $x = \frac{X}{\lambda}$ and $z = \frac{Z}{\lambda}$, which becomes, using $S = \sin\Theta$, Ratcliffe's Eq. 2:

$$\underline{f}(x,z)\exp(-2\pi int) = \int_{S=-1}^{1} U(S)\exp\{i\Omega(S)\}\exp[2\pi i(Sx+Cz)-nt]dS$$

with $\underline{A}(\Theta) = K(\Theta)\exp\{iX(\Theta)\} = \underline{F}(S) = U(S)\exp\{i\Omega(S)\}$.

At the screen, $z = 0$, thus, including evanescent waves,

$$\underline{f}(x,0)\exp(-2\pi int) = \int_{S=-\infty}^{\infty} U(S)\exp\{i\Omega(S)\}\exp[2\pi i(Sx-nt)]dS$$

so

$$\underline{f}(x,0) = \int_{S=-\infty}^{\infty} U(S)\exp\{i\Omega(S)\}\exp(2\pi iSx)\,dS$$

and the complex Fourier (or angular spectrum) coefficient is

$$U(S)\exp\{i\Omega(S)\} = \int_{x=-\infty}^{\infty} \underline{f}(x,0)\exp(-2\pi iSx)\,dx$$

or

$$U(S)\exp\{i\Omega(S)\} = \int_{x=-\infty}^{\infty} a(x)\exp\{i\phi(x)\}\exp(-2\pi iSx)\,dx$$

with explicit separation of $\underline{f}(x,0)$ into amplitude and phase parts $a(x)$ and $\phi(x)$.

The full field

$$\underline{f}(x,z)\exp(-2\pi int) = a(x,z)\exp\{i\phi(x,z)\}\exp(-2\pi int)$$

is not itself a plane wave but is a sum of plane waves: but it is travelling in the positive z-direction. Positive ϕ indicates a phase or time delay with respect to the $\phi=0$ case. To represent $\underline{f}(x,0)$ by a complex number with positive ϕ corresponds physically to the maximum height of a reflecting screen, equivalent to having a transmission screen imposing positive ϕ on the wave at that point x.

IV. SOME ELEMENTARY CHECKS

(1) The slit

A slit extending $-a \leq x \leq +a$ in unit amplitude has a Fourier transform

$$\underline{F}(S) = 2a \frac{\sin(2\pi Sa)}{2\pi Sa} + j0$$

An angular component at angle S has a phase gain of $\pi z_0 S^2$ over the normal component at angle S in the small-angle approximation: this is expressed as

$$\exp[2\pi i(Sx+Cz)] = \exp[2\pi i(Sx+z_0 - \frac{z_0 S^2}{2})]$$

recalling that negative Φ implies a phase gain with waves $\exp[i(kz-\omega t)]$.

The field at an observation plane is the sum of such components, thus at x=0 and taking just the significant components of magnitude near 1 around S=0, the summed field should have a phase gain over $2\pi i z_0$. This is so (Fig. 3-7, Chapter 3) - the value of the phase is of course negative. This agrees with the cornu spiral slit result, with the $\frac{\pi}{4}$ Kirchoff correction for phase applied.

(2) The Phase Screen

(a) Focussing. Parallel light incident on a spherical mirror is focussed back through the focal point, (Jenkins and White, 1957, Ch.6), and the focal length of the mirror is half the radius of curvature of the mirror for paraxial rays. Thus one expects focussing with an increase in intensity for mirrors concave with respect to the incoming plane waves: and defocussing with an intensity decrease for convex mirrors.

The radius of curvature for a curve y = y(x) is given by (Love and Rainville, 1967, P.188)

$$\rho = \frac{[1+(y')^2]^{3/2}}{|y''|}$$

which for a curve $y(x) = \frac{\Delta\phi}{4\pi} \cos\left(\frac{2\pi x}{\lambda_{scr}}\right)$

becomes for $x = 0 \quad \rho(x=0) = \frac{\lambda^2_{scr}}{\pi.\Delta\phi}$

so the focal distance z_F is $\frac{\lambda^2_{scr}}{2\pi.\Delta\phi}$ in radio wavelength units.

Because of diffractive effects the amplitude maximum occurs at a distance z somewhat greater than z_F, but the position x on the observation screen of the focussing coincides with the position x of a concave mirror on the diffracting screen - that is, where ϕ is greatest positive: the position of greatest phase lag. This is what one would expect. (See, for example, Fig. 3-5, Chapter 3).

(b) Direct Use of Angular Spectrum Components. For a shallow screen, with $\Delta\phi \leq 0.1$, there are angular spectrum components

$$\underline{f}(x) = 1 + \frac{i\Delta\phi}{2} \exp\left(\frac{2\pi i x}{\lambda_{scr}}\right) + \frac{i\Delta\phi}{2} \exp\left(-\frac{2\pi i x}{\lambda_{scr}}\right)$$

where with waves $(kz-\omega t)$ the i represents a time-lag. The side-waves travel at a greater speed than the main wave. In their travel to a plane at distance z_0 they gain in phase by $\pi z_0 s^2$ (Ratcliffe, 1956, Fig. 44). Thus at a plane distant

$$z_0 = \frac{\lambda^2_{scr}}{2}$$

the side-waves and main wave are in phase and the wavefront is amplitude-modulated. Following Ratcliffe (1956, Eq. 54)

$$\underline{f}(x,z_0) = 1 + \Delta\phi \cos\left(\frac{2\pi x}{\lambda_{scr}}\right)$$

and at $z_0 = \lambda^2_{scr}$ pure phase modulation leads to

$$\underline{f}(x,z_0) = 1 - i\Delta\phi \cos\left(\frac{2\pi x}{\lambda_{scr}}\right)$$

arising from the phase lag $\frac{\pi}{2}$ and the phase gain $\pi z_0 S^2 = \pi$ to give a net phase lead of $\frac{\pi}{2}$.

From the $z_0 = \frac{\lambda^2_{scr}}{2}$ case an amplitude of $1+\Delta\phi$ is expected at x=0. This is shown in Fig. D-1 for $\Delta\phi = 1.0$. In fact, because at $\Delta\phi = 1$ the screen is comparatively deep, the peak amplitude is 1.4 not 2. Also, Fig. D-1 shows, for $z_o=\lambda^2_{scr}$, a modulation of peak value $\Delta\phi = 1.0$ radians about the mean value of phase arising from the distance z_0 travelled. Again, the phase lead at x = 0 appears as a negative perturbation because of the sign (kz-ωt) chosen for the wave.

The sign of

$$f\left(x, z_0 = \frac{\lambda^2_{scr}}{2}\right) = 1 + \Delta\phi \cos\left(\frac{2\pi x}{\lambda_{scr}}\right)$$

does not agree with that of Ratcliffe's equation (54) because he takes positive phase angle to imply a phase lead. This is apparent from his Figure 5(a) and (b), where at x=0 the time-rotating vector exp(-2πint), which rotates anticlockwise, has its clockwise angle increased by $\Delta\phi$ at x=0. The amplitude-modulated curve presented here for $z_0 = \frac{\lambda^2_{scr}}{2} = \frac{d^2}{2}$ is the negative of that in Ratcliffe's Fig. 13(a) for that reason.

V. USE OF THE FOURIER TRANSFORM IN ENSURING CORRECT SIGN

Since

$$\underline{F}(S) = \int_{x=-\infty}^{\infty} \underline{f}(x) \exp(-2\pi i S x) dx$$

and the transform package used gives for the forward transform

$$\underline{F}(S) = \int_{x=-\infty}^{\infty} \underline{f}(x) \exp(+2\pi i S x) dx$$

the correct sign for angular spectra and observation fields is obtained by using the inverse and forward transforms respectively, and adjusting the scaling to ensure agreement with that arising from a Discrete Fourier transform.

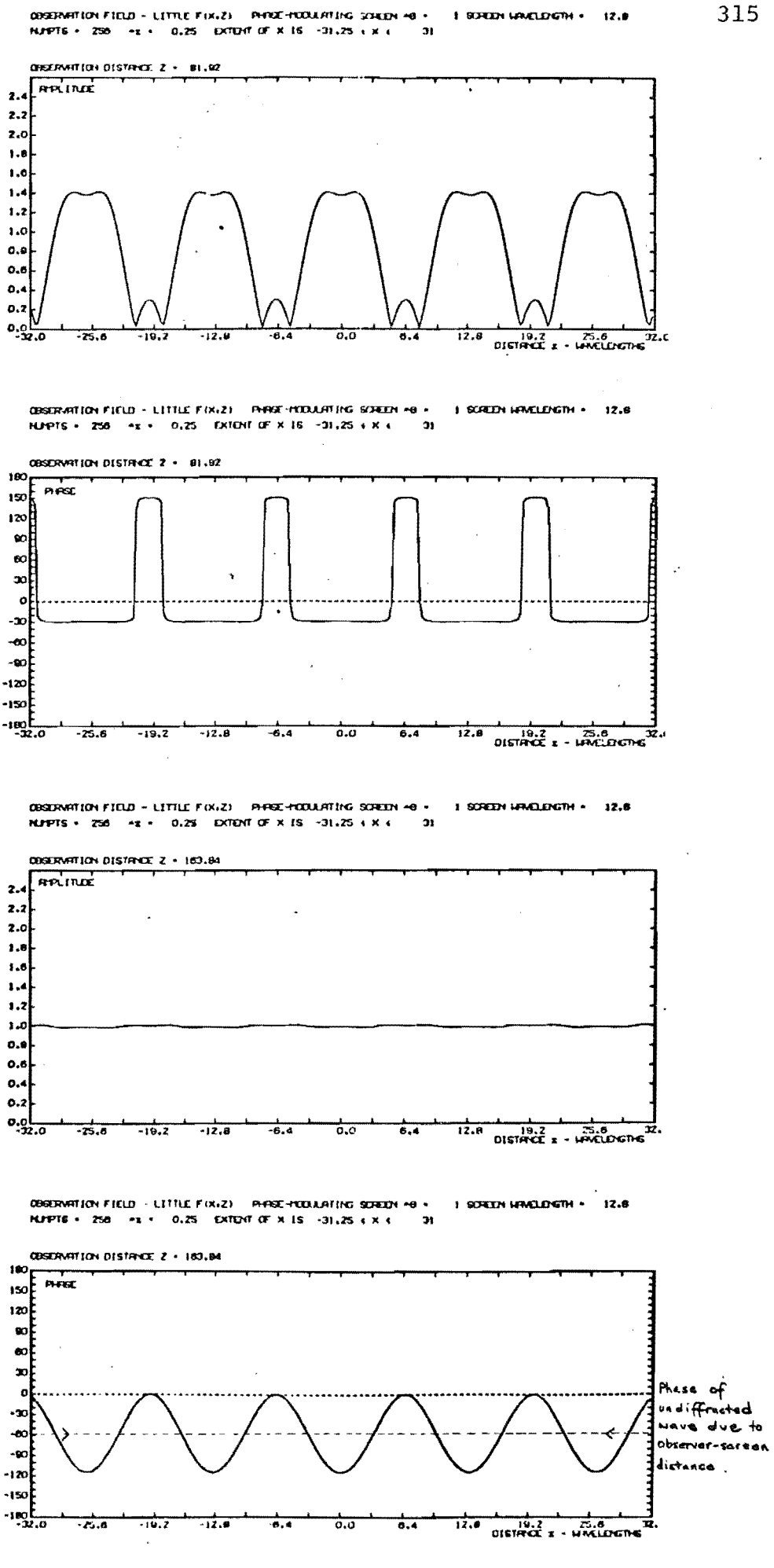

FIG D-1 FIELD AMPL. & PHASE MODULATION

APPENDIX E.

PHASE TIME-SHIFTS BETWEEN ANTENNAS

In this appendix the details of antenna arrangement, and the method of finding the direction of arrival of the radio wave are given.

The arrangement of antennas used for F-region work at 4.57 MHz are in Fig. E-1.

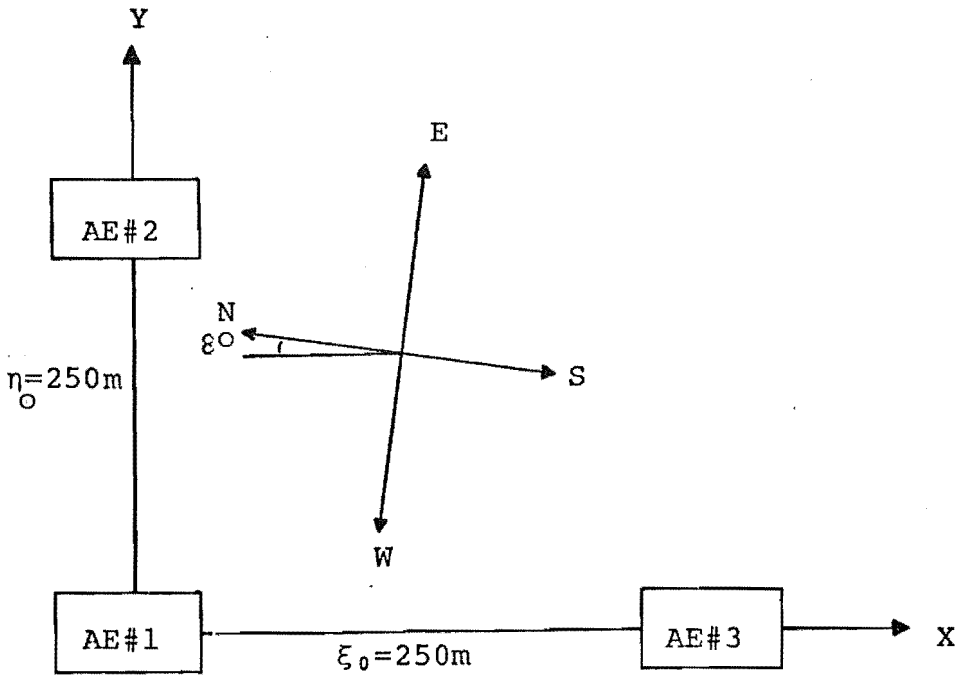

Figure E-1

The numbers given to the aerials are those used in operational work.

It is convenient to refer to the right-hand system of axes, and this is most easily done by dropping the operational numbers and switching the numbering of antennas #1 and #3. The data is easily re-arranged to do this, and the amended numbering is shown in Fig. E-2.

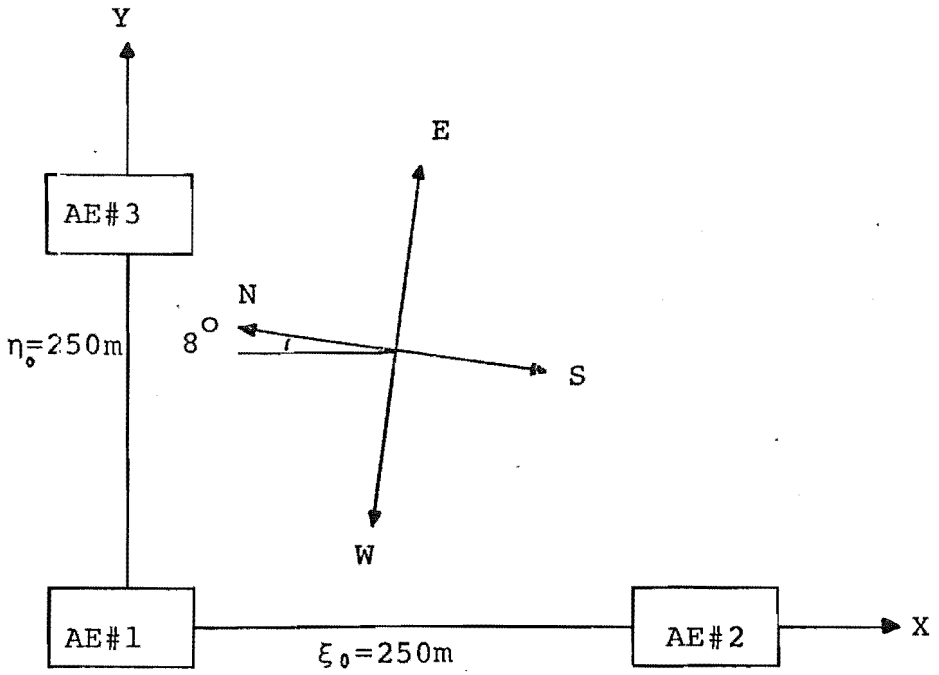

Figure E-2

An attempt was made to cross-correlate phase-height maxima from the three aerials, thence to obtain apparent velocities, and finally a direction of motion.

This was found to be unsuccessful. The associated uncertainties were of the order of the results themselves, making the results meaningless. The aerial separation, in comparison with the structure sizes of the phase height, was so small that time-differences of the phase-height signals between aerials were very small.

An an alternative the phase of the complex cross-correlation of the signal was used to obtain an angle-of-arrival and an echo location.

Given two timeseries

$$\underline{f}_1(t) = A_1(t)e^{i\phi_1(t)}$$

and $$\underline{f}_2(t) = A_2(t)e^{i\phi_2(t)} ,$$

the complex cross-correlation is

$$\underline{\rho}_{f_1 f_2}(\tau) = \frac{\langle(\underline{f}_1^*(t) - \langle\underline{f}_1^*(t)\rangle)(\underline{f}_2(t+\tau) - \langle\underline{f}_2(t)\rangle)\rangle}{\langle(\underline{f}_1^*(t) - \langle\underline{f}_1^*(t)\rangle)(\underline{f}_2(t) - \langle\underline{f}_2(t)\rangle)\rangle}$$

with averages taken over the time period of the measurement.

Let the phases of $\underline{f}_1(t)$ and $\underline{f}_2(t)$ be constants ϕ_1 and ϕ_2 independent of time. Then the value of the complex cross-correlation at zero lag, $\underline{\rho}_{f_1 f_2}(0)$ is, for unit variance,

$$\underline{\rho}_{f_1 f_2}(0) = \langle(\underline{f}_1^*(t) - \langle\underline{f}_1^*(t)\rangle)(f_2(t) - \langle f_2(t)\rangle)\rangle$$

$$= \langle(A_1(t) - \langle A_1(t)\rangle)(A_2(t) - \langle A_2(t)\rangle)\rangle e^{-i(\phi_1-\phi_2)}$$

It is seen that the phase of the complex cross-correlation at zero lag is the negative of the phase difference $(\phi_1-\phi_2)$ between the signals, for the time over which the correlation is taken.

In general (Paul, Wright and Fedor 1974) the argument of the complex cross-correlation coefficient at zero lag is the (negative) mean weighted phase difference between the timeseries $\underline{f}_1(t)$ and $\underline{f}_2(t)$, $-\langle\phi_1(t) - \phi_2(t)\rangle$. (It should be noted that their definition of complex correlation differs in the function which is conjugated, from that used here: their definition is that of Ratcliffe, 1956).

The complex correlation technique is used here to obtain phase differences between aerial pairs:

ϕ_{12} between aerial pair 1 and 2

ϕ_{13} between aerial pair 1 and 3

from which the angle of arrival of the wavefront may be found. We have

$$\phi_{12} = - \text{Arg}(\underline{\rho}_{12}(0))$$

$$\phi_{13} = - \text{Arg}(\underline{\rho}_{13}(0))$$

Using the co-ordinate of Fig. E-2, the phase angle ϕ_{ij} is taken as positive if the (assumed plane) wavefront strikes aerial i before aerial j (see Fig. E-3).

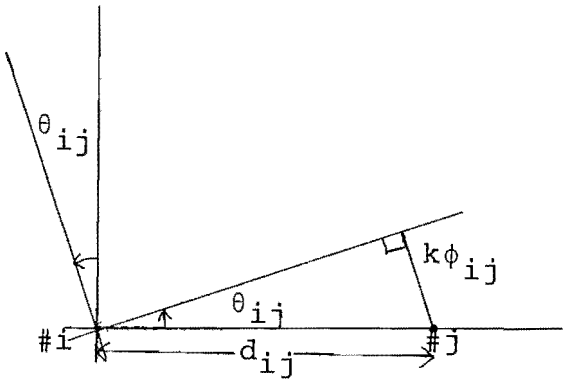

Figure E-3

The corresponding angle of the wavefront to the vertical, θ_{ij}, is taken positive under these circumstances also,

$$\theta_{ij} = \sin^{-1}\left(\frac{\phi_{ij}}{kd_{ij}}\right)$$

with d_{ij} the distance between antenna i and antenna j and $k = \frac{2\pi}{\lambda_{rad}}$.

With phase differences ϕ_{12} and ϕ_{13} available, the direction of arrival of the (plane) wavefront onto the aerial array is required.

(e1) Determination of the Echo location

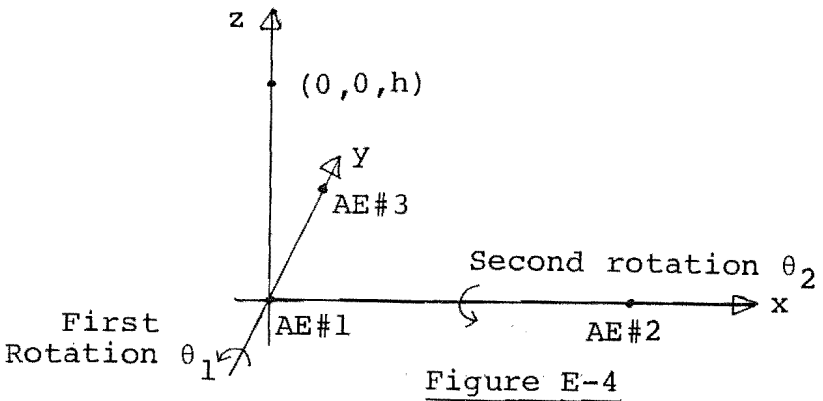

Figure E-4

Fig. E-4 shows the aerials of Fig. E-2 on an XYZ system of axes. The location of the reflection point on the ground (X-Y) plane is of interest. It will be found by rotating the point (0,0,h) through the angles θ_{12} and θ_{13}.

A general point (x_1,y_1,z_1) will have new co-ordinates (x_2,y_2,z_2) given by

$$\begin{pmatrix} x_1 \\ y_1 \\ z_1 \end{pmatrix} = \begin{pmatrix} \cos\theta_1 & 0 & \sin\theta_1 \\ 0 & 1 & 0 \\ -\sin\theta_1 & 0 & \cos\theta_1 \end{pmatrix} \begin{pmatrix} x_2 \\ y_2 \\ z_2 \end{pmatrix}$$

if the point is rotated by angle θ_1 (anticlockwise positive) in the Z-X plane. Further rotation of the point by angle θ_2 in the Z-Y plane gives the point new co-ordinates (x_3,y_3,z_3) given by

$$\begin{pmatrix} x_2 \\ y_2 \\ z_2 \end{pmatrix} = \begin{pmatrix} 1 & 0 & 0 \\ 0 & \cos\theta_2 & \sin\theta_2 \\ 0 & -\sin\theta_2 & \cos\theta_2 \end{pmatrix} \begin{pmatrix} x_3 \\ y_3 \\ z_3 \end{pmatrix}$$

from which

$$\begin{pmatrix} x_1 \\ y_1 \\ z_1 \end{pmatrix} = \begin{pmatrix} \cos\theta_1 & -\sin\theta_1\sin\theta_2 & \sin\theta_1\cos\theta_2 \\ 0 & \cos\theta_2 & \sin\theta_2 \\ -\sin\theta_1 & -\cos\theta_1\sin\theta_2 & \cos\theta_1\cos\theta_2 \end{pmatrix} \begin{pmatrix} x_3 \\ y_3 \\ z_3 \end{pmatrix}$$

or

$$\begin{pmatrix} x_3 \\ y_3 \\ z_3 \end{pmatrix} = \begin{pmatrix} \cos\theta_1 & 0 & -\sin\theta_1 \\ -\sin\theta_1\sin\theta_2 & \cos\theta_2 & -\cos\theta_1\sin\theta_2 \\ \sin\theta_1\cos\theta_2 & \sin\theta_2 & \cos\theta_1\cos\theta_2 \end{pmatrix} \begin{pmatrix} x_1 \\ y_1 \\ z_1 \end{pmatrix}$$

Thus rotation of a point $(x_1,y_1,z_1) = (0,0,h)$ by θ_1 round the Y-axis and θ_2 round the X-axis gives new coordinates (x_3,y_3,z_3) given by:

$$\begin{pmatrix} x_3 \\ y_3 \\ z_3 \end{pmatrix} = \begin{pmatrix} (-\sin\theta_1).h \\ (-\cos\theta_1\sin\theta_2).h \\ (\cos\theta_1\cos\theta_2).h \end{pmatrix}$$

The height of the reflection point, z_3, is reduced from h by a factor $(\cos\theta_1\cos\theta_2)$ by the rotation. On average, it will be at height h at all times, so finally

$$\begin{pmatrix} x_3 \\ y_3 \\ z_3 \end{pmatrix} = \begin{pmatrix} \left(\frac{-\sin\theta_1}{\cos\theta_1\cos\theta_2}\right).h \\ (-\tan\theta_2).h \\ h \end{pmatrix}$$

with (x_3,y_3) the co-ordinates of the reflection point on the ground.

The determination of the echo location (x_3,y_3) from the measured phase-differences ϕ_{12} and ϕ_{13} is as given above.

Systematic errors in the values of ϕ_{12} and ϕ_{13} arise from relative phase-shifts between receiver channels. These can arise from phase-shifts between the individual receivers themselves, phase-shifts in the feeding networks arising from differences in matching curcuits, and phase-shifts resulting from differing feeder-line lengths.

As stated in Appendix A, the receiver/antenna system was never calibrated for relative phase. It will be assumed here that relative phase-shifts between receiver channels arise only from the electrical lengths of the feeder systems from each antenna array to the receiver hut.

Differences in electrical length (assuming a velocity factor of 0.975 for open-wire line) are such that at 4.57 MHz,

$$\phi_{12}\ \text{(corrected)} = \phi_{12}\ \text{(raw)} + 2.98\ \text{radians}$$
$$\phi_{13}\ \text{(corrected)} = \phi_{13}\ \text{(raw)} + 2.51\ \text{radians}$$

and the corrected values are used to obtain angles of arrival.